Novel Therapeutic Strategies Against *Pseudomonas aeruginosa*: Dual Inhibitors of LecA and LasB and Lectin-Targeted Liposomal Drug Delivery

Dissertation
zur Erlangung des Grades
des Doktors der Naturwissenschaften
der Naturwissenschaftlich-Technischen Fakultät
der Universität des Saarlandes

von
Dipl.-Chem. Olga Metelkina

Saarbrücken
2025

Tag des Kolloquiums:	05.11.2025
Dekan:	Prof. Dr.-Ing. Dirk Bähre
Berichterstatter:	Prof. Dr. Alexander Titz Prof. Dr. Claus-Michael Lehr
Akad. Mitglied:	Dr. Jörg Haupenthal
Vorsitz:	Prof. Dr. Marc Schneider

"I would rather have questions that can't be answered than answers that can't be questioned."
– Richard Feynman

Acknowledgments

First and foremost, I would like to express my deepest gratitude to my supervisor, Prof. Dr. Alexander Titz, for his invaluable guidance, continuous support, and encouragement throughout this research. His expertise, insightful suggestions, and critical perspective have profoundly shaped the direction and depth of this thesis.

I am sincerely grateful to all the members of the Chemical Biology of Carbohydrates group for creating such a warm, supportive, and motivating atmosphere. In particular, I would like to thank Marta Czekańska, Dr. Eva Zahorska, Dr. Eike Siebs, Dr. Joscha Meiers, Mario Fares, Lisa Marie Denig, Dr. Ghamdan Beshr and Dr. Stefanie Wagner for making daily life in the lab and beyond not only productive but genuinely enjoyable. Special thanks go to Dirk Hauck for his reliable lab support, thoughtful input, and exceptional technical expertise.

I would like to sincerely thank Prof. Dr. Claus-Michael Lehr for his valuable guidance throughout my research, and the entire DDEL group for their support. I am also grateful to Prof. Dr. Anna Hirsch and the DDOP group for their insightful discussions and collaborative spirit throughout this project. I would like to thank Dr. Marcus Koch from the Leibniz Institute for New Materials and Dr. Mathias Müsken from the Helmholtz Centre for Infection Research for their highly valuable support with microscopy analysis. I also thank Prof. Dr. Andreas Manz and Dr. Jonathan O'Connor from the Korea Institute of Science and Technology Europe for their expert assistance in the development of the microfluidic assay.

A heartfelt thank you goes to my parents for their unwavering patience, encouragement, and understanding during this journey. I am especially grateful to my husband for his constant support and belief in me, which kept me motivated during the most challenging times.

Finally, I dedicate this work to everyone who inspired me to pursue scientific research and supported me along the way, especially my chemistry teachers and former supervisors, whose guidance ignited and nurtured my passion for science.

Curriculum Vitae

Mrs. Olga Metelkina

Work and research experience

August 2024 – present	*Associate Director* at BioNTech SE, Formulation Functionalization
February 2022 - July 2024	*Scientist* at BioNTech SE, Formulation Functionalization
August 2018 - January 2022	*PhD student* at Helmholtz Institute for Pharmaceutical Research Saarland, Germany
2016-2017	*Intern* at the University of Nottingham, United Kingdom

Education

Graduated in June 2018	*Specialist degree* at Department of Chemistry, Lomonosov Moscow State University, Russia *Diploma with Honours*

Publications

- **O. Metelkina**, J. Konstantinović, A. Klein, R. Shafiei, M. Fares, A. Alhayek, S. Yahiaoui, W.A.M. Elgaher, J. Haupenthal, A. Titz, A.K.H. Hirsch, "Dual inhibitors of Pseudomonas aeruginosavirulence factors LecA and LasB", *Chemical Science*, 2024, 15, 13333-13342.

- **O. Metelkina**, B. Huck, J. O'Connor, M. Koch, A. Manz, C.-M. Lehr, A. Titz, "Targeting extracellular lectins of Pseudomonas aeruginosa with glycomimetic liposomes," Journal of Materials Chemistry B, 2022, 10, 537-548

- B. Huck, D. Thiyagarajan, A. Bali, A. Boese, K. Besecke, C. Hozsa, R. Gieseler, M. Furch, C. Carvalho, F. Waldow, D. Schwudke, **O. Metelkina**, A. Titz, H. Huwer, K. Schwarzkopf, J. Hoppstädter, M. Koch, B. Loretz*, C.-M. Lehr, "Nano-in-Microparticles for Aerosol Delivery of Antibiotic-loaded, Fucose-derivatized and Macrophage-targeted Liposomes to Combat Mycobacterial Infections: In Vitro deposition, Pulmonary Barrier Interactions and Targeted Delivery," *submitted*, 2021.

- A.R. Iliasov, T.R. Nizamov, V.A. Naumenko, A.S. Garanina, S.S. Vodopyanov, A.A. Nikitin, A.G. Pershina, A.A. Chernysheva, Y. Kan, P.S. Mogilnikov, **O.N. Metelkina**, I.V. Schetinin, A.G. Savchenko, A.G. Majouga, M.A. Abakumov, "Non-magnetic shell coating of magnetic nanoparticles as key factor of toxicity for cancer cells in a low frequency alternating magnetic field," *Colloids and Surfaces B: Biointerfaces*, 2021, 206.

- **O. Metelkina**, R. Lodge, P. Rudakovskaya, V. Gerasimov, C. Lucas, I. Grebennikov, I. Shchetinin, A. Savchenko, G. Pavlovskaya, G. Rance, M. Gimenez-Lopez, A. Khlobystov, A. Majouga, "Nanoscale Engineering of Hybrid Magnetite-Carbon Nanofibre Materials for Magnetic Resonance Imaging Contrast Agents," *Journal of Materials Chemistry C*, 2017, 5, 2167-2174.

- P.G. Rudakovskaya, V.M. Gerasimov, **O.N. Metelkina**, E.K. Beloglazkina, N.V. Zyk, A.G. Savchenko, I.V. Shchetinin, S.V. Salikhov, M.A. Abakumov, N.L. Klyachko, Yu.I. Golovin and A.G. Mazhuga, "Synthesis and characterization of peg-silane functionalized iron oxide (II, III) nanoparticles for biomedical application," *Nanotechnologies in Russia*, 2015, 10, 896-903.

Summary

The first part of the thesis focuses on the development of novel dual-function inhibitors that simultaneously target *P. aeruginosa* virulence factors LecA and LasB. These compounds demonstrated significantly improved binding affinity and in vitro biological activities compared to their individual counterparts. In particular, dual inhibitor **12** showed superior efficacy in reducing LecA-promoted bacterial adhesion relative to the single-target inhibitors.

In the second part of the research, glycomimetic ligands of LecA and LecB were conjugated to phospholipids and incorporated into liposomes to create glycosylated nanocarriers. These targeted liposomes showed high binding specificity and affinity toward their respective lectins, and were evaluated for their ability to encapsulate therapeutic molecules, including antibiotics and pathoblockers. Among the tested compounds, colistin and HIPS2050 demonstrated the most favorable release profiles, supporting their potential for further investigation in targeted liposomal drug delivery.

This thesis highlights the potential for further development of dual inhibitors and targeted liposomes as novel therapeutic strategies against *P. aeruginosa* biofilm infections.

Zusammenfassung

Der erste Teil der Arbeit konzentriert sich auf die Entwicklung neuartiger Dual-Inhibitoren, die gleichzeitig auf die Virulenzfaktoren LecA und LasB von *P. aeruginosa* abzielen. Diese Verbindungen zeigten im Vergleich zu ihren Einzelsubstanzen eine deutlich verbesserte Bindungsaffinität sowie gesteigerte biologische Aktivität in vitro. Insbesondere der Dual-Inhibitor 12 erwies sich als besonders wirksam bei der Reduktion der durch LecA geförderten bakteriellen Adhäsion im Vergleich zu Einzelliganden.

Im zweiten Teil der Arbeit wurden Glykomimetika von LecA und LecB an Phospholipide gekoppelt und in Liposomen eingebaut, um glycosylierte Nanocarrier zu erzeugen. Diese zielgerichteten Liposomen zeigten eine hohe Bindungsspezifität und -affinität gegenüber ihren jeweiligen Lektinen und wurden hinsichtlich ihrer Fähigkeit untersucht, therapeutische Moleküle wie Antibiotika und Pathoblocker zu enkapsulieren. Unter den getesteten Wirkstoffen wiesen Colistin und HIPS2050 die günstigsten Freisetzungsprofile auf, was ihr Potenzial für weitere Untersuchungen im Bereich des liposomalen Wirkstofftransports unterstreicht.

Diese Dissertation zeigt das Potenzial für die weiterführende Entwicklung von Dual-Inhibitoren und zielgerichteten Liposomen als neuartige therapeutische Strategien gegen Biofilminfektionen durch *P. aeruginosa* auf.

List of abbreviations

ApoE – apolipoprotein E

ASGPR – asialoglycoprotein receptor

BDQ – bedaquiline

CFU – Colony-forming unit

CLRs – C-type lectin receptors

ConA – Concanavalin A

CRDs – carbohydrate recognition domains

DC-SIGN – Dendritic cell-specific ICAM-3-grabbing nonintegrin

DCs – Dendritic cells

DNA – Deoxyribonucleic acid

DPPE – 1,2-dipalmitoyl-sn-glycero-3-phosphoethanolamine

DSPC – 1,2-distearoyl-sn-glycero-3-phosphocholine

DSPE – 1,2-distearoyl-sn-glycero-3-phosphoethanolamine

GalNAc – N-Acetylgalactosamine

GFP – green fluorescent protein

HPLC – High-performance liquid chromatography

HUVEC – human umbilical vein endothelial cells

i.m. – intramuscular

LCs – Langerhans cells

LC MS – Liquid chromatography with tandem mass spectrometry

LDL – low-density lipoprotein

LeX – Lewis X

LN – lipid nanoparticles

LPX – Lipoplexes

LPS – Lipopolysaccharide

LSECs – liver sinusoidal endothelial cells

LVX – levofloxacin

MGL – macrophage galactose-type C-type lectin

MR – Mannose receptor

MRSA – Methicillin-resistant *Staphylococcus aureus*

NSCLC – human non-small cell lung cancer

NTA – Nanoparticle Tracking Analysis

P. aeruginosa – Pseudomonas aeruginosa

PBMCs – Peripheral blood mononuclear cells

PdI – Polydispersity index

PEG – polyethylene glycol

RNA – Ribonucleic acid

RP-18 – Reversed-phase column with C18 chains bonded to a silica support

siRNA – small interfering RNA

SPR – Surface plasmon resonance

UV – Ultraviolet

Table of Contents

Introduction. Recent advances in lectin-targeted drug delivery with glycosylated lipid-based nanocarriers

Manuscript in preparation

Olga Metelkina and Prof. Dr. Alexander Titz*
Helmholtz Institute for Pharmaceutical Research Saarland (HIPS)
Helmholtz Centre for Infection Research (HZI) Campus E8.1, 66123 Saarbrücken (Germany),
Deutsches Zentrum für Infektionsforschung (DZIF), Standort Hannover-Braunschweig, 38124 Braunschweig, Germany
and
Department of Chemistry, Saarland University, 66123 Saarbrücken, Germany
E-mail: alexander.titz@helmholtz-hips.de

Introduction

Lipid-based nanocarriers represent one of the most advanced and potent platform for effective drug delivery approved by FDA and EMA.[1–4] In recent years, these nanocarriers have demonstrated remarkable potential in the ability to encapsulate and deliver a wide range of therapeutic agents, including small molecules, nucleic acids, and peptides.[5–8] The exceptional properties of lipid-based nanocarriers, such as low toxicity, high bioavailability, enhanced potency, prolonged physical stability, reproducibility, and scalability contribute to their efficacy as a potent delivery system.[9–12]

Nevertheless, achieving optimal biodistribution of lipid nanocarriers and enhancing delivery efficacy impose challenges.[13–16] Targeted delivery offers a potential solution to these challenges by enhancing the uptake of nanoparticles by specific cell types.[17–20]

Lectins are carbohydrate-binding proteins, that possess the ability to selectively recognize and bind to specific carbohydrate structures. These proteins play a pivotal role in various biological processes, including cell-cell adhesion, cell signaling, and host-pathogen interactions.[21] Specificity in carbohydrate binding renders cell-surface exposed lectins promising candidates for targeting specific cells or tissues, thereby increasing the precision of drug delivery and potentially reducing off-target effects. For example, some lectins have been identified as receptors on mammalian immune cells such as dendritic cells, Langerhans cells and

macrophages. Important members of the lectin family include the mannose receptor (CD206), Langerin (CD207), DC-SIGN (CD209), and macrophage galactose-type C-type lectin (MGL, CLEC10A, CD301).[22–24] Notably, the asialoglycoprotein receptor (ASGPR), abundantly expressed on hepatocytes, serves as the prime example of a mammalian lectin for drug targeting already in clinical use.[25–28] Moreover, soluble bacterial lectins are known to play a critical role in infections promoting bacterial dissemination along with biofilm formation.[29,30]

Multivalent presentation of lectin ligands such as carbohydrates and glycomimetics has proven to be an effective strategy for targeting lectins, as it leads to a significant increase in binding affinity.[31–37] Lipid based nanoparticles are frequently employed as platforms for carbohydrate multivalency. These carriers provide a highly tunable and controllable system for the presentation of multiple ligands, allowing for modulation of ligand density and spatial arrangement.

Types of nanocarriers

Encapsulation of a drug into a carrier helps to improve its physico-chemical properties, including stability, solubility and release kinetics, protecting it from degradation and premature clearance.[38,39] Common types of lipid-based nanocarriers include lipid nanoemulsions, liposomes and lipoplexes, lipid nanoparticles, solid lipid nanoparticles, and nanostructured lipid carriers.[8,40] The choice of lipid-based nanoparticle type depends on the specific requirements of the therapeutic agent and the desired delivery strategy. FDA-approved examples of the lipid-based nanoparticles include encapsulation of small molecules like doxorubicin in Doxil as well as nucleic acids such as mRNA in Comirnaty. The ability to easily incorporate targeted ligands into the lipid-based nanoparticles make them well-suited for achieving targeted delivery to specific cells or tissues.

Targeted drug delivery

Targeted drug delivery aims to improve the therapeutic efficacy of conventional formulations while minimizing adverse effects associated with systemic drug administration.[43–45] This approach involves delivery of therapeutic agents to specific disease sites or target cells, by utilizing molecular targets expressed on diseased cells or tissue, thereby enhancing drug accumulation and therapeutic response.

Physico-chemical properties of the carrier, such as size, zeta-potential, surface chemistry and nanoparticle composition in total, strongly affect its biodistribution leading to accumulation of the drug in certain organs or tissues.[46–48] But although adjusting carrier properties can

influence its localization in the body, it has only a limited effect on organ-specific accumulation. Active targeted drug delivery using functionalized carriers with high specificity for receptors expressed on certain cell types can further improve drug biodistribution, increase the local concentration of the active substance and thereby maximizing therapeutic efficacy.
Despite its potential advantages, targeted drug delivery also faces challenges and limitations. Achieving specific and efficient targeting can be complex, requiring the identification and validation of suitable targetable molecules and appropriate delivery systems. Furthermore, limitations in the penetration of deep tissues or the tumor microenvironment may hinder effective drug delivery. Nonetheless, ongoing advancements in nanotechnology and molecular targeting strategies hold promise for overcoming these challenges and further advancing targeted drug delivery as a valuable approach in modern therapeutics.

Carbohydrates and glycomimetics as targeting ligands

Carbohydrate-based ligands, such as monosaccharides and oligosaccharides, can selectively recognize and bind to carbohydrate-binding proteins or lectins that are expressed on the surface of cells or within specific tissue. Carbohydrates possess structural diversity, stemming from variations in monosaccharide stereochemistry and composition, linkage, and branching patterns, which provide a wide range of options for ligand design resulting in carbohydrate-based ligands with different binding affinity and selectivity, enabling targeted drug delivery systems to be precisely tailored for specific receptors. Despite the mentioned advantages of carbohydrate-based therapeutic molecules, there is also a number of their drawbacks linked with poor selectivity, hydrophilicity, which limits oral uptake, and potential degradation by glycosidases resulting in short circulation half-life.[49] To address these limitations, modifications can be made to the chemical structures of native carbohydrates to enhance their drug-like properties, resulting in the molecules called glycomimetics. Clinically approved examples of such molecules include miglustat, a glucosylceramide synthase inhibitor used to treat Gaucher disease; acarbose, an α-glucosidase inhibitor used as an anti-diabetic drug; and oseltamivir, a neuraminidase inhibitor for influenza treatment, among others.[33] Potential modifications in the design of glycomimetic structures include the replacement of hydroxyl groups, substitution of endocyclic oxygen, alterations in the O-glycosidic linkage, and the incorporation of hydrophobic fragments.[33]
For example, Medve *et al.* developed a mannose-based glycomimetic able to selectively bind DC-SIGN but not Langerin receptor allowing to precisely select the target and avoid unspecific interactions.[50] Richichi *et al.* synthesized a fucose-based inhibitor highly potent against lectin

Bambl from *B. ambifaria* but not active in case of another bacterial lectin LecB from *P. aeruginosa*.[51] Another example of great potential for carbohydrates as selective ligands was showed by Zahorska *et al.* where divalent galactose-based inhibitor possess excellent activity in nanomolar range for bacterial LecA without an off-target effect against human galectin-1.[34] Furthermore, the use of carbohydrates as targeting ligands offers benefits in terms of biocompatibility and biodegradability. Carbohydrates are naturally occurring biomolecules that are generally well-tolerated by the human body. They can exhibit low immunogenicity and toxicity, making them suitable for use in drug delivery systems.[52,53] Additionally, carbohydrates can undergo enzymatic degradation within the body, ensuring the safe clearance of the targeting ligands after drug delivery and reducing the risk of long-term accumulation and potential side effects.

Carbohydrate multivalency

Carbohydrate multivalency is a concept that has garnered significant attention in the field of molecular recognition and targeted drug delivery.[54–56] It involves presenting multiple carbohydrate ligands on a scaffold or carrier system, leading to enhanced binding interactions with carbohydrate-binding proteins, such as lectins, which often possess two or more carbohydrate recognition domains (CRDs). Several phenomena can lead to an enhanced binding affinity in case of multivalent carbohydrate presentation, namely a chelate effect, clustering of the receptor on cell surface, local increase of the ligand density at the binding epitopes (statistical effect) and subsite binding.[57]

Such a multivalent approach enables stronger and more stable interactions with carbohydrate-binding proteins, as the simultaneous engagement of multiple ligands can compensate for weaker individual binding affinities. Moreover, carbohydrate multivalency can enhance binding selectivity, as the arrangement and spatial organization of ligands are able to mimic the natural presentation of carbohydrates on cell surfaces or extracellular matrices designed to interact with the lectins of interest. Both of these features, allow the design of highly efficient and selective therapeutic agents, with potential applications in areas such as cancer therapy, vaccine development, and combating infectious diseases.

Lectins

Lectins represent a large family of soluble and transmembrane proteins capable of binding carbohydrates without exhibiting any enzymatic activity towards them, present in all species, including plants, animals, bacteria and fungi.[58] Lectins play pivotal role in molecular

recognition processes interacting with various carbohydrate epitopes including, for example, the glycocalyx on mammalian cells or carbohydrate components (e.g, Lipopolysaccharide) of bacterial cell walls, as well as glycoproteins and glycolipids of different origins. They are known to be associated with the development or cancer and autoimmune diseases, and are also engaged in the proliferation of viral, parasitic, bacterial and fungal infections. All the lectins contain one or several carbohydrate recognition domains, but vary in overall structure, carbohydrate specificity, function and spatial localization. Interaction of lectins with monosaccharides is very often characterized by K_D in the millimolar range and an increase in the corresponding affinity can be achieved via multivalent representation of the carbohydrate moieties.

Utilization of lectins as targets for drug delivery enables to access additional internalization pathways, e.g., clathrin-mediated endocytosis in case of transmembrane lectins expressed on antigen presenting cells, hepatocytes or to interact with bacterial lectins, co-localized with the site of infection and biofilm formation, therefore concentrating the therapeutic agent in that area.

Below are the most recent examples of lipid-based nanoparticles targeted towards human and bacterial lectins with a perspective to apply them for targeted drug delivery.

Mannose receptor (MR, CD206)

The mannose receptor, also known as CD206, is a C-type lectin receptor that plays a critical role in various physiological and pathological processes. It is primarily expressed on antigen-presenting cells, including macrophages, dendritic cells, and certain subsets of endothelial cells.[59–62] CD206 is able to bind carbohydrates containing terminal mannose, fucose, or N-acetylglucosamine residues.[63] CD206-mediated endocytosis and internalization of ligands occur through clathrin-coated pits and subsequent trafficking to endosomal compartments. This interaction is dependent on the carbohydrate recognition domains of CD206, which engage with glycosylated ligands present in the extracellular environment. Upon internalization, CD206 directs the ligands to lysosomal degradation or delivers them to intracellular compartments for antigen processing and presentation, thereby contributing to the immune response.

The recognition of mannosylated proteins and mannan-coated cell walls of pathogens, e.g., *Mycobacterium tuberculosis* and *Candida* species, by CD206 contributes to the efficient clearance of disease-causing agents.[64–66] By capturing and internalizing these pathogens, CD206 facilitates their degradation and elimination. Furthermore, CD206 has also been

associated with several diseases, including cancer, and inflammatory disorders, where its expression and activity can influence disease progression and therapeutic outcomes.

The introduction of mannose moieties onto the nanoparticle surface can facilitate the targeted interaction between nanocarriers and mannose receptor increasing cellular uptake. Hagimori *et al.* developed mannose-grafted lipids for targeted delivery of liposomes to macrophages.[67] DSPC-based lipids comprising 5 to 10 repeating serine-glycine units were synthesized using solid-phase peptide synthesis. The resulting mannosylated conjugates were incorporated into PEGylated liposomes through post-insertion techniques, resulting in formulations with varying concentrations of the mannosylated lipid (3, 6, and 9 mol%). Since PEG can act as a barrier, reducing the exposure of mannose ligands and thereby diminishing their interaction with the receptor, serine-glycine peptides were used as linkers to enhance interaction with receptor-presenting cells. Liposomes containing 9% of Man-$(SG)_5$ exhibited a significant enhancement in interaction with peritoneal macrophages compared to the ungrafted liposomes (Figure 2 A). In contrast, liposomes in which mannose was conjugated through a PEG linker (Man-PEG_{2000}/PEGylated liposomes), demonstrated lower efficiency in interaction with macrophages. It was shown that only the targeted liposomes were localized within lysosomes, presumably through mannose receptor-mediated endocytosis. Inhibition of this interaction with mannan significantly reduced the uptake of the Man-$(SG)_5$ liposomes, indicating the involvement of the mannose receptor in the cellular uptake process.

Goswami *et al.* assessed the impact of mannose functionalization on lipid nanoparticles (LNPs) for RNA-based vaccines.[68] The effect of mannosylation of LNPs composed of Dlin DMA:DSPC:Chol:DMG-PEG_{2000} (40:10:48:2) on the enhancement of IgG titers was investigated in mice after intramuscular (i.m.) and intradermal (i.d.) administration. Four different mannan ligands conjugated to cholesterol-amine were incorporated into the LNPs at a concentration of 15 mol%, replacing the cholesterol component in the formulation (Figure 2B). It was revealed that formulation containing 2% trimannoside M3 demonstrated better recognition by Concanavalin A (ConA) compared to the Man1 and Man2 ligands. Moreover, LNPs containing only 0.3% of DMG-PEG_{2000}, instead of 2% in a classical formulation, showed significantly enhanced recognition by ConA. Mannosylation led to an increase of IgG1 isotypes in vivo, while the levels of IgG2 were comparable for all formulations after i.m. administration.

Moku *et al.* aimed at targeting the mannose receptor on dendritic cells using mannose-mimicking analogues di-shikimoyl (DSG) and di-quinoyl (DQG) with two hydrophobic tails incorporated into LNPs[69] as non-viral carriers for DNA vaccines. LNPs with DSG/GFP

complex exhibited 16-fold increase in transfection efficiency compared to the control LNPs. Preincubation of dendritic cells with mannan resulted in a significant decrease in the transfection efficacies of LNPs containing DSG and DQG due to the blocking of mannose receptor. The enhanced transfection efficacy was translated to mice, where number of GFP-positive cells isolated from the inguinal lymph nodes was increased for targeted LNPs after 24 h subcutaneous administration (Figure 2C).

Xiao *et al.* used mannose receptor-targeted LNPs for the delivery of siRNA to downregulate pro-inflammatory factors.[70] DoGo lipids were functionalized with mannose and incorporated into LNPs to facilitate interaction with the mannose receptor on microglial cells. In a BV2 cellular uptake assay, formulations containing 5-15% of D-DvMa with mannose were compared to formulations containing D-DvGlu with glucuronic acid as a negative control. A decrease in cellular uptake at 4 °C was observed compared to 37 °C, which suggested that an energy-dependent mechanism of cellular uptake is playing a significant role for the interaction between mannosylated LNPs and BV2 cells (Figure 2D). A competitive blocking experiment with mannan demonstrated a dose-dependent inhibition of cellular uptake of mannosylated LNPs, while no inhibition was observed in control experiments using dextran or zymosan.

In their study, Catania *et al.* explored the targeted delivery of membrane-impermeable antibiotics to the mannose receptor using mannose-decorated liposomes as nanocarriers.[71] They synthesized a series of glycolipids with both monovalent and oligovalent presentation of mannose moieties linked with cholesterol (Figure 2E). The liposomes containing 10% of Chol-Man_1 did not lead to the aggregation with ConA and at least 1% of Chol-Man_{10} was required to initiate the aggregation of the liposomes. The highest degree of aggregation was observed in formulations containing 10% Chol-Man_{10} or Chol-Man_{20}. Investigation of the mannosylated LNPs in vitro in RAW 264.7 macrophages actively expressing CD206 receptor,[72,73] showed a clear advantage of the particles bearing highly mannosylated lipids at 10 and 20 mol% - L-(Chol-Man_{10})$_{10\%}$ and L-(Chol-Man_{20})$_{10\%}$, over LNPs with a mannose mono-ligand L-(Chol-Man_1)$_{10\%}$ did not show any significant difference compared to the non-targeted control (Fig. 8). Moreover, mannosylated liposomes L-(Chol-Man_{20})$_{10\%}$ exhibited an enhanced macrophage association in transgenic zebrafish embryos.

Mannose-cholesterol conjugates were employed for the synthesis of glycofunctionalized liposomes containing encapsulated messenger RNA (MPn-LPX) in order to assess their capacity for dendritic cell targeting through interaction with the mannose receptor.[74] A comparative analysis was performed on three distinct polyethylene glycol linkers – PEG_{100},

PEG_{1000}, and PEG_{2000} (Figure 3A), with PEG_{1000} identified as an optimal choice, providing both high transfection efficacy and good RNA integrity. Lipoplexes (LPX) were prepared using the thin-film hydration method, incorporating 5 mol% of the respective mannose conjugates. It was shown that MP1000-LPX formulation was particularly effective in promoting cellular uptake and transfection compared to other MPn-LPX formulations. Efficient cellular uptake of MP_{1000}-LPX by dendritic cells confirmed the involvement of a receptor-mediated mechanism in the interaction between LPX and DCs.

Mousavifar *et al.* presented novel neoglycolipids, wherein a single mannose residue is conjugated to an aromatic scaffold through a hydrophobic linker, and two lipid tails with varying chain lengths are incorporated (Figure 3B).[75] A self-assembly process using the ethanol injection method were employed for particle preparation,[76] incorporating the glycolipids, containing lipid tails of varying lengths (C_8, C_{10}, C_{12}, C_{14}, and C_{16}). It was observed that liposomes formed with C_{14} lipids exhibited the optimal physico-chemical properties and displayed the highest degree of CoA-mediated agglutination. In vitro study of C_{14}-based liposomes in murine JAWSII dendritic cells and J774A.1 macrophages demonstrated increased uptake of the mannosylated liposomes.

Kim *et al.* developed LNPs targeted to different types of liver cells by incorporating mannose-containing lipids (Figure 3C).[77] An increase of PEGylated lipids from 1.5 to 5.0% in the formulation lead to reduced adsorption of serum apolipoprotein E (ApoE) on the nanoparticle surface and consequently diminished uptake via interaction with low-density lipoprotein (LDL) receptors.[78] The LNP distribution between hepatocytes, liver sinusoidal endothelial cells (LSECs) and Kupffer cells was investigated *in vivo*. LNPs containing 3% of PEG-lipid and 2.5% mannose-PEG lipid demonstrated significant reduction of ApoE adsorption resulting in their internalization by mannose-mediated pathway. Expression of the mannose receptor (CD206) by liver sinusoidal endothelial cells (LSECs) facilitated the retargeting of mannosylated LNPs, leading to a reduction in their uptake by hepatocytes. The difference between targeted and untargeted LNPs, both containing 1.5% total PEG-lipid, was less pronounced and attributed to higher adsorption of ApoE uptake through the ApoE/ LDL-receptor pathway.

As an alternative to mannosylation, Duran *et al.* developed fucosylated TargoSphere liposomes encapsulating levofloxacin[79] and analyzed their cellular internalization in vitro. Consequently, PBMCs, monocytes, and dendritic cells expressing CD206 and CD209 exhibited highest uptake of fucosylated carriers, which was reduced when the cells were preincubated with 1 mM L-fucose.

Huck *et al.* loaded TargoSpheres with the antibiotics bedaquiline (BDQ) or levofloxacin (LVX) and studied uptake in THP-1 cells.[80] Binding of fucosylated BDQ-loaded nanocarriers to LecB immobilized in a glass chamber. Only fucosylated fluorescently labeled nanocarriers were capable of interacting with the lectin within the chamber, resulting in a fluorescent signal. Nevertheless, upon pre-incubation of the chamber with free L-fucose, no interaction between the targeted liposomes and the lectin was observed, as the binding pocket became fully occupied with the competitive binder.[81] Moreover, incubation of fucosylated liposomes with dTHP-1 cells or monocyte-derived macrophages *in vitro* led to a 20% increase in cellular uptake compared to plain liposomes. This enhanced uptake effect was counteracted by preincubation of the cells with 10 mM L-fucose, highlighting the receptor-specific interaction of fucosylated particles with cells.

Langerin (CD207)

Another important C-type lectin receptor is Langerin (CD207) primarily expressed on Langerhans cells (LCs). Langerin plays a crucial role in the process of endocytosis and cross-presentation of antigens to T cells.[82,83] Among the various ligands recognized by Langerin, the most notable ones include mannosides, specifically mannose oligosaccharides, as well as fucose and GlcNAc.[84] The specific recognition of these carbohydrates by Langerin contributes to the effective capture and presentation of antigens by Langerhans cells, affecting immune responses and triggering adaptive immunity.

Wamhoff *et al.* identified a selective ligand for Langerin and applied its lipid conjugate to formulate targeted liposomes (Figure 3D)[85] and demonstrate high specificity of the ligand towards the Langerin lectin in comparison to DC-SIGN and Dectin-1. Targeted formulations containing DSPE-PEG-GlcNTosyl demonstrated a strong ability to bind Langerhans cells, while cells incubated with non-targeted formulations showed no fluorescent signal, indicating a lack of specific binding.

Schulze *et al.* further investigated the potential of targeting Langerin-expressing cells (LCs) using GlcNTosyl-functionalized liposomes (Figure 3D).[86] Targeted liposomes containing 4.5 mol% DSPE-PEG-GlcNTosyl[85] were tested in vitro in human epidermal cell suspension and demonstrated a 3-fold increase in signal intensity in LCs for the targeted formulations compared to CD45- cells or non-targeted liposomes.

DC-SIGN (CD209)

Dendritic cell-specific ICAM-3-grabbing nonintegrin (DC-SIGN, CD209) is a highly significant representative of the C-type lectin receptor family. DC-SIGN exhibits the capability to bind to mannose, N-linked mannose oligosaccharides, and fucosides.[87] It is primarily expressed on the surface of dendritic cells and macrophages, playing a crucial role in coordinating immune responses against bacterial infections through the recognition and binding of highly mannosylated glycans present on the surface of microorganisms. This interaction triggers downstream signaling events, leading to the activation of immune cells and the production of pro-inflammatory cytokines.[24]

Wawrzinek *et al.* studied the allosteric regulation of DC-SIGN using a heteromultivalent targeting approach to selectively interact with CD209+ cells while avoiding binding to Langerin-expressing cells.[88] Liposomes incorporating 3.75 mol% of a lipid conjugate with a natural ligand, such as mannose, fucose, or Lewis X (LeX), and 0.36 mol% of a glycomimetic derivative exhibited cooperative interaction with higher efficacy in DC-SIGN+ cells compared to homomultivalent liposomes functionalized with 4.75 mol% of mannosylated lipid. The highest binding efficacy was achieved for formulations with equimolar concentrations of the natural ligand and the glycomimetic. The enhancement of liposomal binding *in vitro* was demonstrated by the increased binding of the targeted liposomes to the DC-SIGN receptor on the THP-1 cells.

E-selectin (CD62E)

An adhesion receptor E-selectin is prominently expressed on the surface of endothelial cells and serves a critical function in mediating the inflammatory response. Recognizing the significance of E-selectin in inflammation, Glycomimetics Inc. embarked on designing novel ligands specifically targeting E-selectin. These ligands were subsequently synthesized and conjugated with phospholipids to formulate E-selectin targeted formulations (Figure 3E) aiming to modulate E-selectin-mediated inflammatory processes.[89] For the preparation of targeted liposomes, 5 mol% of Compound 3 was incorporated into the liposomal formulation consisting of HSPC/Cholesterol/Compound 3 in a ratio of 55:40:5. As a control, liposomes were prepared using DSPE instead of the ligand conjugate. High affinity of targeted liposomes towards E-selectin was demonstrated by SPR and a fluorescence-based assay with E-selectin immobilized on a plate and incubated with fluorescently labelled liposomes either containing Compound 3 or DSPE. It was demonstrated that targeted liposomes not only were able to bind

E-selectin expressed on the surface of activated HUVEC cells in vitro, but also specifically accumulate in the NSCLC tumor in vivo.

Asialoglycoprotein receptor (ASGPR)

Asialoglycoprotein receptor is a Ca^{2+}-dependent C-type lectin predominantly expressed on the surface of mammalian hepatocytes. Its primary role is the recycling of glycoproteins with terminal galactose or GalNAc residues, facilitating their endocytosis and subsequent lysosomal degradation. ASGPR relevance for therapeutic application became prominent in 2019, when givosiran (Givlaari), the first GalNAc siRNA conjugate, got approved for the treatment of acute hepatic porphyria, followed by lumasiran (Oxlumo), inclisiran (Leqvio), vutrisiran (Amvuttra), nedosiran (Rivfloza).[25–28,90] Furthermore, fitusiran, a prophylactic therapy for hemophilia, lowering antitrombin level, can be the next ASGPR-targeted siRNA-based drug.[91] In all cases, trivalent GalNAc ligands (Figure 4) are conjugated with siRNA molecules to enable its efficient delivery to the liver. Another example of successful delivery via ASGPR targeting is eplontersen, a conjugate of GalNAc with an antisense oligonucleotide, for the treatment of polyneuropathy approved by FDA in 2023.[92]

Verve Therapeutics has two drugs in their pipeline utilizing delivery with GalNAc-functionalized LNP.[93] Recently Phase 1b trials were initiated for Verve-102 to investigate the gene-editing system for PCSK9 gene inactivation, aimed at reducing low-density lipoprotein cholesterol (LDL-C) levels for the treatment of cardiovascular disease.[94] Another Phase1b trial for Verve-201, an in vivo CRISPR editing system targeting ANGPTL3 gene to lower LDL-C and triglyceride levels, is planned to be started soon.[95]

Bacterial lectins

Bacterial lectins have emerged as a highly promising target for targeted drug delivery in the treatment of microbial infections. These lectins predominantly exist as extracellular or membrane proteins, rendering them readily accessible for interactions with ligands without the necessity of crossing the bacterial cell wall. Functioning as adhesins, bacterial lectins facilitate crucial interactions between bacteria and host cells, as well as mediate inter-bacterial interactions through binding with the glycocalyx present on the bacterial cell wall.[58,96] Moreover, bacterial lectins play a pivotal role in biofilm formation and subsequent attachment to surfaces, further underscoring their significance in microbial pathogenesis. Therefore prevention of these lectin-carbohydrate interactions can lead to the development of innovative

therapeutic strategies aimed at disrupting bacterial adhesion, biofilm formation, and infection progression.[97,98]

Metelkina *et al.* developed glycosylated liposomes specifically designed to target the lectins LecA and LecB in *P. aeruginosa*.[81] LecA (PA-IL) and LecB (PA-IIL) are extracellular proteins known to play vital roles in the structure and formation of biofilms.[29,30] LecA exhibits binding affinity towards galactosides, whereas LecB demonstrates a strong affinity for mannosides and fucosides.[32,99–103] Due to their extracellular localization, these lectins can readily interact with targeted formulations without the need to traverse the bacterial outer membrane.[98,104,105] To create the glycosylated liposomes, the researchers incorporated conjugates of DPPE with thiogalactoside and C-fucoside, specifically designed to target LecA and LecB (Figure 3F), respectively, into liposomes with a diameter of 200 nm. The conjugates were incorporated at concentrations of either 1 or 15 mol%. The efficacy of lectin binding was assessed using several techniques, including a fluorescence polarization-based competitive binding assay, a fluorescence-based flow assay, SPR, and a lectin aggregation assay. All the methods consistently demonstrated the targeted specificity of the functionalized liposomes, revealing a direct correlation between the degree of enhancement in binding efficacy and the increased percentage of incorporated glycolipids. These findings can be applied in further development of glycosylated liposomes as a targeted delivery system for combating *P. aeruginosa* infections.

Staphylococcus aureus **lectins**

Aiello *et al.* conducted a study exploring the targeted delivery of resveratrol, a quorum sensing inhibitor, using glycosylated liposomes for the treatment of methicillin-resistant Staphylococcus aureus (MRSA) biofilms.[106] Trans-resveratrol (RSV) was encapsulated within the phospholipid bilayer liposomes composed of DOPC/cholesterol, incorporating cationic glycosylated amphiphiles to enhance the interaction with the MRSA biofilm via both electrostatic attraction to the negatively charged biofilm and specific carbohydrate-lectin interactions of adhesins present in the biofilm.[107,108] Mannosylated and galactosylated formulations were shown to effectively eradicate MRSA biofilm matrix, with the highest efficacy observed for the galactosylated formulations, which achieved biofilm demolition at an RSV concentration of 0.019 mM — 60-fold lower than its MIC of 1.2 mM.

Conclusions

While conventional lipid-based nanoparticles have already demonstrated their high efficacy in drug delivery and are represented by several approved products on the market, lectin-targeted formulations are in the early phases of clinical trials but have already shown the promising initial results in the priclinical studies.

The exploration of combinatorial approaches, such as co-delivery of various types of cargo using lectin-targeted nanoparticles, holds great potential for synergistic therapeutic effects. Furthermore, the translation of lectin-targeted nanoparticles into a broader range of clinical applications requires the advancement of their safety profiles, pharmacokinetics, and immunogenicity. Addressing these aspects through rigorous preclinical studies and clinical trials will be crucial for the successful translation of lectin-targeted nanoparticle therapeutics into commercial products.

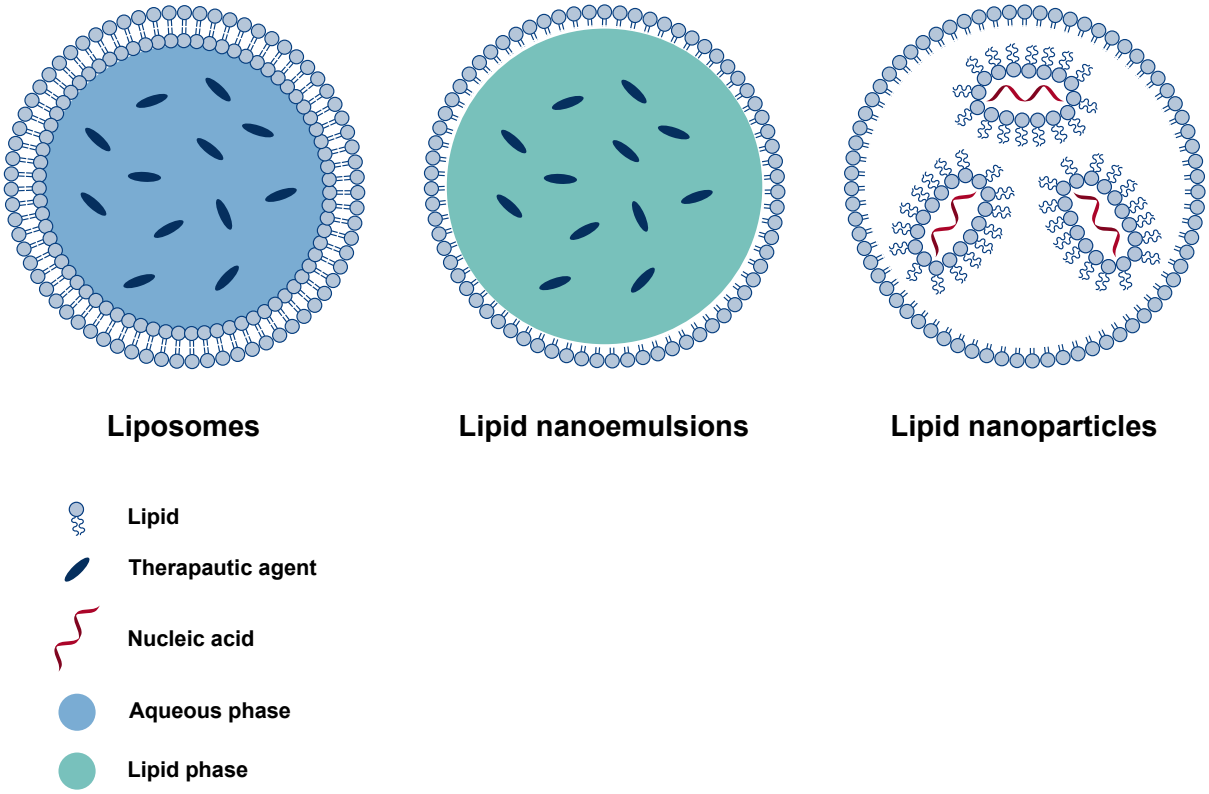

Figure 1. Schematic representation of various lipid-based carriers for drug delivery.

A

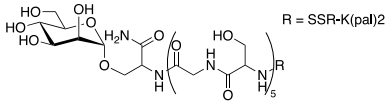

Man-(SG)5-R

B

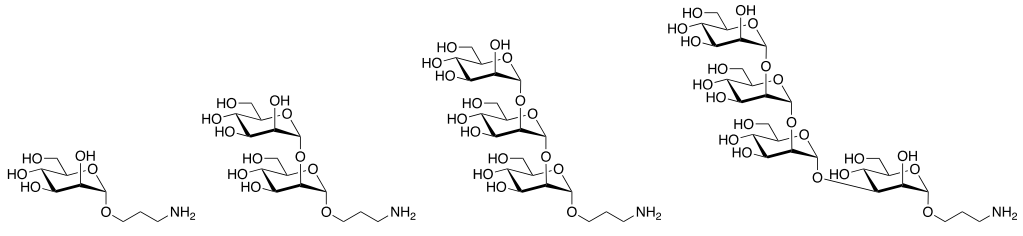

Man1 **Man2** **Man3** **Man4**

Man1-4 Cholesterolamine

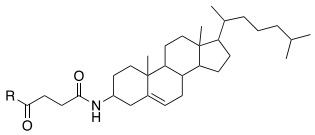

R = Man1-4

C

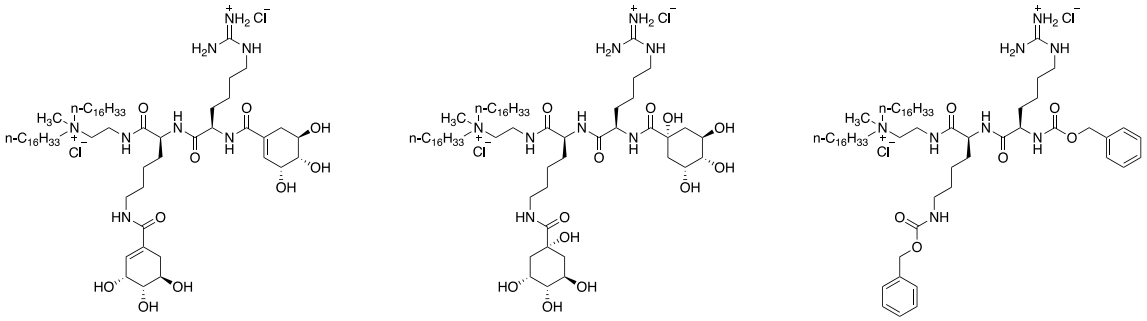

DSG **DQG** **BBG**

D

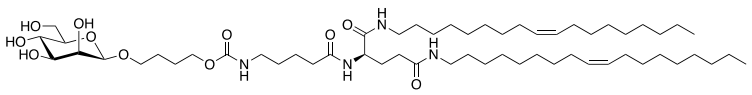

D-DvMa

E

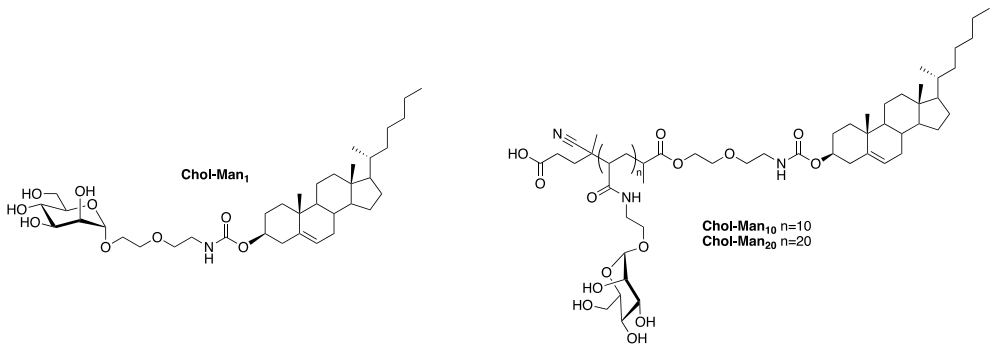

Figure 2. A) Mannose conjugate with serine-glycine pentapeptide by Hagimori *et al.*;[67] B) Mannan conjugates with cholesterolamine by Goswami *et al.*;[68] C) Mannose-mimetics conjugates of di-shikimoyl (DSG) and di-quinoyl (DQG) by Moku *et al.*;[69] D) Mannose conjugated with DoGo lipid by Xiao *et al.*;[70] E) Cholesterol-linked mannose moieties by Catania *et al.*;[71] F) PEGylated mannose-based cholesterol derivatives by Wang *et al.*;[74] G) Mannose-based lipids with aromatic scaffold by Mousavifar *et al.*;[75] H) DSPE-PEG-Mannose lipid by Kim *et al.*;[77] I) DSPE-PEG-GlcNTosyl, mannose-based lipid by Wamhoff *et al.*[85] and DSPE-PEG-mannoside lipid by Schulze *et al.*;[86] J) E-selectin ligand by Glycomimetics Inc.;[89] K) Galactose- and fucose-based lipid conjugates by Metelkina *et al.*[81]

A

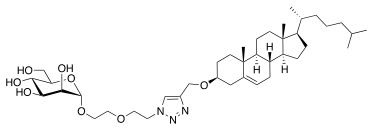

MP_{100}-CH

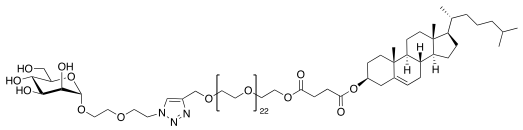

MP_{1000}-CH

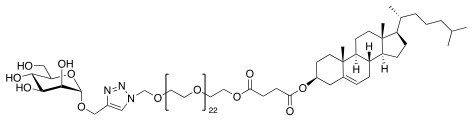

MP_{2000}-CH

B

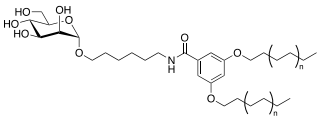

n = 2 - 6

C

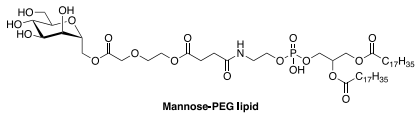

Mannose-PEG lipid

D

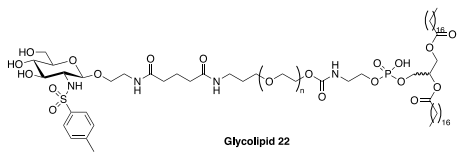

Glycolipid 22

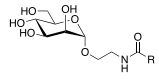

Glycolipid 23 or Man-Lip

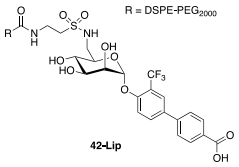

42-Lip

E

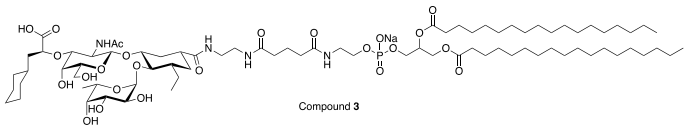

Compound 3

F

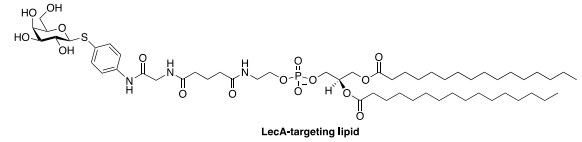

LecA-targeting lipid

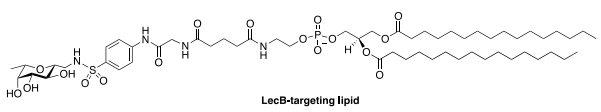

LecB-targeting lipid

Figure 3. A) PEGylated mannose-based cholesterol derivatives by Wang *et al.*;[74] B) Mannose-based lipids with aromatic scaffold by Mousavifar *et al.*;[75] C) DSPE-PEG-Mannose lipid by Kim *et al.*;[77] D) DSPE-PEG-GlcNTosyl, mannose-based lipid by Wamhoff *et al.*[85] and DSPE-PEG-mannoside lipid by Schulze *et al.*;[86] E) E-selectin ligand by Glycomimetics Inc.;[89] F) Galactose- and fucose-based lipid conjugates by Metelkina *et al.*[81]

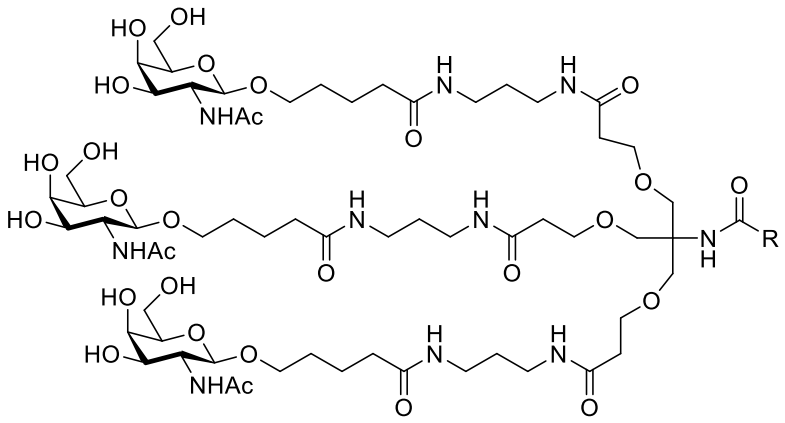

Figure 4. Trivalent GalNAc ligand developed by Alnylam Pharmaceuticals.

References

[1] T. T. H. Thi, E. J. A. Suys, J. S. Lee, D. H. Nguyen, K. D. Park, N. P. Truong, *Vaccines (Basel)* **2021**, *9*, DOI 10.3390/vaccines9040359.
[2] H. Daraee, A. Etemadi, M. Kouhi, S. Alimirzalu, A. Akbarzadeh, *Artificial Cells, Nanomedicine, and Biotechnology* **2016**, *44*, 381–391.
[3] J. A. Kulkarni, D. Witzigmann, S. Chen, P. R. Cullis, R. van der Meel, *Acc. Chem. Res.* **2019**, *52*, 2435–2444.
[4] J. A. Kulkarni, P. R. Cullis, R. van der Meel, *Nucleic Acid Therapeutics* **2018**, *28*, 146–157.
[5] B. Chatin, M. Mével, J. Devallière, L. Dallet, T. Haudebourg, P. Peuziat, T. Colombani, M. Berchel, O. Lambert, A. Edelman, B. Pitard, *Molecular Therapy - Nucleic Acids* **2015**, *4*, DOI 10.1038/mtna.2015.17.
[6] S. Kube, N. Hersch, E. Naumovska, T. Gensch, J. Hendriks, A. Franzen, L. Landvogt, J.-P. Siebrasse, U. Kubitscheck, B. Hoffmann, R. Merkel, A. Csiszár, *Langmuir* **2017**, *33*, 1051–1059.
[7] X. Hou, T. Zaks, R. Langer, Y. Dong, *Nature Reviews Materials* **2021**, *6*, 1078–1094.
[8] R. Tenchov, R. Bird, A. E. Curtze, Q. Zhou, *ACS Nano* **2021**, *15*, 16982–17015.
[9] N. M. Patro, K. Devi, R. S. Pai, S. Suresh, *Journal of Nanoparticle Research* **2013**, *15*, 2124.
[10] K. M. Laginha, E. H. Moase, N. Yu, A. Huang, T. M. Allen, *J Drug Target* **2008**, *16*, 605–610.
[11] M. H. Y. Cheng, J. Leung, Y. Zhang, C. Strong, G. Basha, A. Momeni, Y. Chen, E. Jan, A. Abdolahzadeh, X. Wang, J. A. Kulkarni, D. Witzigmann, P. R. Cullis, *Advanced Materials* **2023**, *35*, 2303370.
[12] C. Webb, S. Ip, N. V. Bathula, P. Popova, S. K. V. Soriano, H. H. Ly, B. Eryilmaz, V. A. Nguyen Huu, R. Broadhead, M. Rabel, I. Villamagna, S. Abraham, V. Raeesi, A. Thomas, S. Clarke, E. C. Ramsay, Y. Perrie, A. K. Blakney, *Mol. Pharmaceutics* **2022**, *19*, 1047–1058.
[13] C. Guéguen, T. Ben Chimol, M. Briand, K. Renaud, M. Seiler, M. Ziesel, P. Erbacher, M. Hellal, *European Journal of Pharmaceutics and Biopharmaceutics* **2023**, DOI 10.1016/j.ejpb.2023.08.002.
[14] R. Pattipeiluhu, G. Arias-Alpizar, G. Basha, K. Y. T. Chan, J. Bussmann, T. H. Sharp, M.-A. Moradi, N. Sommerdijk, E. N. Harris, P. R. Cullis, A. Kros, D. Witzigmann, F. Campbell, *Advanced Materials* **2022**, *34*, 2201095.
[15] J. Di, Z. Du, K. Wu, S. Jin, X. Wang, T. Li, Y. Xu, *Pharm Res* **2022**, *39*, 105–114.
[16] F. Campbell, F. L. Bos, S. Sieber, G. Arias-Alpizar, B. E. Koch, J. Huwyler, A. Kros, J. Bussmann, *ACS Nano* **2018**, *12*, 2138–2150.
[17] V. Makwana, J. Karanjia, T. Haselhorst, S. Anoopkumar-Dukie, S. Rudrawar, *International Journal of Pharmaceutics* **2021**, *593*, 120117.
[18] H. Bardania, S. Tarvirdipour, F. Dorkoosh, *Artificial Cells, Nanomedicine, and Biotechnology* **2017**, *45*, 1478–1489.
[19] J. A. Katakowski, G. Mukherjee, S. E. Wilner, K. E. Maier, M. T. Harrison, T. P. DiLorenzo, M. Levy, D. Palliser, *Molecular Therapy* **2016**, *24*, 146–155.
[20] P. Stoitzner, N. Romani, C. Rademacher, H. C. Probst, K. Mahnke, *European Journal of Immunology* **2022**, *52*, 1909–1924.
[21] Varki A, Cummings RD, Esko JD, et al., editors., in *Essentials of Glycobiology. 4th Edition.*, Cold Spring Harbor (NY): Cold Spring Harbor Laboratory Press, **2022**.
[22] E. P. McGreal, J. L. Miller, S. Gordon, *Curr Opin Immunol* **2005**, *17*, 18–24.

[23] G. D. Brown, J. A. Willment, L. Whitehead, *Nature Reviews Immunology* **2018**, *18*, 374–389.
[24] U. Svajger, M. Anderluh, M. Jeras, N. Obermajer, *Cell Signal* **2010**, *22*, 1397–1405.
[25] *Givlaari*, European Medicines Agency, **2020**.
[26] *Oxlumo*, European Medicines Agency, **2020**.
[27] *Amvuttra*, European Medicines Agency, **2022**.
[28] *Leqvio*, European Medicines Agency, **2021**.
[29] D. Tielker, S. Hacker, R. Loris, M. Strathmann, J. Wingender, S. Wilhelm, F. Rosenau, K.-E. Jaeger, *Microbiology* **2005**, *151*, 1313–1323.
[30] S. P. Diggle, R. E. Stacey, C. Dodd, M. Cámara, P. Williams, K. Winzer, *Environmental Microbiology* **2006**, *8*, 1095–1104.
[31] C. W. Cairo, J. E. Gestwicki, M. Kanai, L. L. Kiessling, *J. Am. Chem. Soc.* **2002**, *124*, 1615–1619.
[32] E. Zahorska, F. Rosato, K. Stober, S. Kuhaudomlarp, J. Meiers, D. Hauck, D. Reith, E. Gillon, K. Rox, A. Imberty, W. Römer, A. Titz, *Angewandte Chemie International Edition* **2023**, *62*, e202215535.
[33] S. Leusmann, P. Ménová, E. Shanin, A. Titz, C. Rademacher, *Chem. Soc. Rev.* **2023**, *52*, 3663–3740.
[34] E. Zahorska, S. Kuhaudomlarp, S. Minervini, S. Yousaf, M. Lepsik, T. Kinsinger, A. K. H. Hirsch, A. Imberty, A. Titz, *Chem. Commun.* **2020**, *56*, 8822–8825.
[35] B. Lepenies, J. Lee, S. Sonkaria, *Advanced Drug Delivery Reviews* **2013**, *65*, 1271–1281.
[36] J. Meiers, E. Siebs, E. Zahorska, A. Titz, *Current Opinion in Chemical Biology* **2019**, *53*, 51–67.
[37] S. Cecioni, A. Imberty, S. Vidal, *Chem. Rev.* **2015**, *115*, 525–561.
[38] F. Yamashita, M. Hashida, *Advanced Drug Delivery Reviews* **2013**, *65*, 139–147.
[39] Y.-H. Cheng, C. He, J. E. Riviere, N. A. Monteiro-Riviere, Z. Lin, *ACS Nano* **2020**, *14*, 3075–3095.
[40] M. L. Guevara, F. Persano, S. Persano, *Front Chem* **2020**, *8*, 589959.
[41] M. K. Riaz, M. A. Riaz, X. Zhang, C. Lin, K. H. Wong, X. Chen, G. Zhang, A. Lu, Z. Yang, *Int J Mol Sci* **2018**, *19*, DOI 10.3390/ijms19010195.
[42] Y. Xu, T. Fourniols, Y. Labrak, V. Préat, A. Beloqui, A. des Rieux, *ACS Nano* **2022**, *16*, 7168–7196.
[43] M. T. Manzari, Y. Shamay, H. Kiguchi, N. Rosen, M. Scaltriti, D. A. Heller, *Nature Reviews Materials* **2021**, *6*, 351–370.
[44] B. S. Pattni, V. P. Torchilin, in *Targeted Drug Delivery : Concepts and Design* (Eds.: P.V. Devarajan, S. Jain), Springer International Publishing, Cham, **2015**, pp. 3–38.
[45] D. Rosenblum, N. Joshi, W. Tao, J. M. Karp, D. Peer, *Nature Communications* **2018**, *9*, 1410.
[46] S. T. LoPresti, M. L. Arral, N. Chaudhary, K. A. Whitehead, *Journal of Controlled Release* **2022**, *345*, 819–831.
[47] S.-D. Li, L. Huang, *Mol. Pharmaceutics* **2008**, *5*, 496–504.
[48] C. Oussoren, J. Zuidema, D. J. A. Crommelin, G. Storm, *Biochimica et Biophysica Acta (BBA) - Biomembranes* **1997**, *1328*, 261–272.
[49] B. Ernst, J. L. Magnani, *Nature Reviews Drug Discovery* **2009**, *8*, 661–677.
[50] L. Medve, S. Achilli, J. Guzman-Caldentey, M. Thépaut, L. Senaldi, A. Le Roy, S. Sattin, C. Ebel, C. Vivès, S. Martin-Santamaria, A. Bernardi, F. Fieschi, *Chemistry – A European Journal* **2019**, *25*, 14659–14668.
[51] B. Richichi, A. Imberty, E. Gillon, R. Bosco, I. Sutkeviciute, F. Fieschi, C. Nativi, *Org. Biomol. Chem.* **2013**, *11*, 4086–4094.

[52] R. D. Astronomo, D. R. Burton, *Nature Reviews Drug Discovery* **2010**, *9*, 308–324.
[53] S. Nishat, P. R. Andreana, *Vaccines (Basel)* **2016**, *4*, DOI 10.3390/vaccines4020019.
[54] C. Müller, G. Despras, T. K. Lindhorst, *Chem. Soc. Rev.* **2016**, *45*, 3275–3302.
[55] M. Martínez-Bailén, J. Rojo, J. Ramos-Soriano, *Chem. Soc. Rev.* **2023**, *52*, 536–572.
[56] M. Duca, D. Haksar, J. van Neer, D. M. E. Thies-Weesie, D. Martínez-Alarcón, H. de Cock, A. Varrot, R. J. Pieters, *ACS Chem. Biol.* **2022**, *17*, 3515–3526.
[57] L. L. Kiessling, J. E. Gestwicki, L. E. Strong, *Current Opinion in Chemical Biology* **2000**, *4*, 696–703.
[58] N. Sharon, H. Lis, *Science* **1989**, *246*, 227–234.
[59] M. R. Lennartz, F. S. Cole, P. D. Stahl, *J Biol Chem* **1989**, *264*, 2385–2390.
[60] L. Cochand, P. Isler, F. Songeon, L. P. Nicod, *Am J Respir Cell Mol Biol* **1999**, *21*, 547–554.
[61] M. Gröger, W. Holnthoner, D. Maurer, S. Lechleitner, K. Wolff, B. B. Mayr, W. Lubitz, P. Petzelbauer, *J. Immunol.* **2000**, *165*, 5428.
[62] K. Elvevold, J. Simon-Santamaria, H. Hasvold, P. McCourt, B. Smedsrød, K. K. Sørensen, *Hepatology* **2008**, *48*, 2007–2015.
[63] P. D. Stahl, R. A. Ezekowitz, *Curr Opin Immunol* **1998**, *10*, 50–55.
[64] P. B. Kang, A. K. Azad, J. B. Torrelles, T. M. Kaufman, A. Beharka, E. Tibesar, L. E. DesJardin, L. S. Schlesinger, *J Exp Med* **2005**, *202*, 987–999.
[65] J. D. Ernst, *Infect Immun* **1998**, *66*, 1277–1281.
[66] I. Porcaro, M. Vidal, S. Jouvert, P. D. Stahl, J. Giaimis, *J Leukoc Biol* **2003**, *74*, 206–215.
[67] M. Hagimori, Y. Chinda, T. Suga, K. Yamanami, N. Kato, T. Inamine, Y. Fuchigami, S. Kawakami, *European Journal of Pharmaceutical Sciences* **2018**, *123*, 153–161.
[68] R. Goswami, D. T. O'Hagan, R. Adamo, B. C. Baudner, *Pharmaceutics* **2021**, *13*, DOI 10.3390/pharmaceutics13020240.
[69] G. Moku, S. Vangala, S. K. Gulla, V. Yakati, *Chembiochem* **2021**, *22*, 523–531.
[70] H. Xiao, S. Han, H. Baigude, *RSC Adv.* **2021**, *11*, 32549–32558.
[71] R. Catania, F. Mastrotto, C. J. Moore, C. Bosquillon, F. H. Falcone, A. Huett, G. Mantovani, S. Stolnik, *Advanced Therapeutics* **2021**, *4*, 2100168.
[72] M. Stein, S. Keshav, N. Harris, S. Gordon, *J Exp Med* **1992**, *176*, 287–292.
[73] L. Martinez-Pomares, *J Leukoc Biol* **2012**, *92*, 1177–1186.
[74] F. Wang, W. Xiao, M. A. Elbahnasawy, X. Bao, Q. Zheng, L. Gong, Y. Zhou, S. Yang, A. Fang, M. M. S. Farag, J. Wu, X. Song, *Frontiers in Pharmacology* **2018**, *9*.
[75] L. Mousavifar, J. D. Lewicky, A. Taponard, R. Bagul, M. Rivat, S. Abdullayev, A. L. Martel, N. L. Fraleigh, A. Nakamura, F. J. Veyrier, H.-T. Le, R. Roy, *Pharmaceutics* **2022**, *14*, DOI 10.3390/pharmaceutics14112300.
[76] A. Wagner, K. Vorauer-Uhl, H. Katinger, *European Journal of Pharmaceutics and Biopharmaceutics* **2002**, *54*, 213–219.
[77] M. Kim, M. Jeong, S. Hur, Y. Cho, J. Park, H. Jung, Y. Seo, H. A. Woo, K. T. Nam, K. Lee, H. Lee, *Sci Adv* **2021**, *7*, DOI 10.1126/sciadv.abf4398.
[78] A. Akinc, W. Querbes, S. De, J. Qin, M. Frank-Kamenetsky, K. N. Jayaprakash, M. Jayaraman, K. G. Rajeev, W. L. Cantley, J. R. Dorkin, J. S. Butler, L. Qin, T. Racie, A. Sprague, E. Fava, A. Zeigerer, M. J. Hope, M. Zerial, D. W. Sah, K. Fitzgerald, M. A. Tracy, M. Manoharan, V. Koteliansky, A. de Fougerolles, M. A. Maier, *Molecular Therapy* **2010**, *18*, 1357–1364.
[79] V. Durán, E. Grabski, C. Hozsa, J. Becker, H. Yasar, J. T. Monteiro, B. Costa, N. Koller, Y. Lueder, B. Wiegmann, G. Brandes, V. Kaever, C.-M. Lehr, B. Lepenies, R. Tampé, R. Förster, B. Bošnjak, M. Furch, T. Graalmann, U. Kalinke, *Journal of Controlled Release* **2021**, *334*, 201–212.

[80] B. C. Huck, D. Thiyagarajan, A. Bali, A. Boese, K. F. W. Besecke, C. Hozsa, R. K. Gieseler, M. Furch, C. Carvalho-Wodarz, F. Waldow, D. Schwudke, O. Metelkina, A. Titz, H. Huwer, K. Schwarzkopf, J. Hoppstädter, A. K. Kiemer, M. Koch, B. Loretz, C.-M. Lehr, *Advanced Healthcare Materials* **2022**, *11*, 2102117.
[81] O. Metelkina, B. Huck, J. S. O'Connor, M. Koch, A. Manz, C.-M. Lehr, A. Titz, *J. Mater. Chem. B* **2022**, *10*, 537–548.
[82] J. Valladeau, O. Ravel, C. Dezutter-Dambuyant, K. Moore, M. Kleijmeer, Y. Liu, V. Duvert-Frances, C. Vincent, D. Schmitt, J. Davoust, C. Caux, S. Lebecque, S. Saeland, *Immunity* **2000**, *12*, 71–81.
[83] C. M. Fehres, H. Kalay, S. C. M. Bruijns, S. A. M. Musaafir, M. Ambrosini, L. van Bloois, S. J. van Vliet, G. Storm, J. J. Garcia-Vallejo, Y. van Kooyk, *Journal of Controlled Release* **2015**, *203*, 67–76.
[84] H. Feinberg, A. S. Powlesland, M. E. Taylor, W. I. Weis, *Journal of Biological Chemistry* **2010**, *285*, 13285–13293.
[85] E.-C. Wamhoff, J. Schulze, L. Bellmann, M. Rentzsch, G. Bachem, F. F. Fuchsberger, J. Rademacher, M. Hermann, B. Del Frari, R. van Dalen, D. Hartmann, N. M. van Sorge, O. Seitz, P. Stoitzner, C. Rademacher, *ACS Cent. Sci.* **2019**, *5*, 808–820.
[86] J. Schulze, M. Rentzsch, D. Kim, L. Bellmann, P. Stoitzner, C. Rademacher, *Biochemistry* **2019**, *58*, 2576–2580.
[87] Jeroen Geurtsen, Nicole N. Driessen, Ben J. Appelmelk, *Microbial Glycobiology* **2010**, 673–695.
[88] R. Wawrzinek, E.-C. Wamhoff, J. Lefebre, M. Rentzsch, G. Bachem, G. Domeniconi, J. Schulze, F. F. Fuchsberger, H. Zhang, C. Modenutti, L. Schnirch, M. A. Marti, O. Schwardt, M. Bräutigam, M. Guberman, D. Hauck, P. H. Seeberger, O. Seitz, A. Titz, B. Ernst, C. Rademacher, *J. Am. Chem. Soc.* **2021**, *143*, 18977–18988.
[89] Magnani, John L., Peterson, John M., Fogler, William E., Baek, Myung-Gi, *E-Selectin Targeting Agents*, **n.d.**, WO2022061168A1.
[90] Y. Y. Syed, *Drugs* **2023**, *83*, 1729–1733.
[91] G. Young, A. Srivastava, K. Kavakli, C. Ross, J. Sathar, C.-W. You, H. Tran, J. Sun, R. Wu, S. Poloskey, Z. Qiu, S. Kichou, S. Andersson, B. Mei, S. Rangarajan, *The Lancet* **2023**, *401*, 1427–1437.
[92] T. Coelho, W. Marques Jr, N. R. Dasgupta, C.-C. Chao, Y. Parman, M. C. França Jr, Y.-C. Guo, J. Wixner, L.-S. Ro, C. R. Calandra, P. A. Kowacs, J. L. Berk, L. Obici, F. A. Barroso, M. Weiler, I. Conceição, S. W. Jung, G. Buchele, M. Brambatti, J. Chen, S. G. Hughes, E. Schneider, N. J. Viney, A. Masri, M. R. Gertz, Y. Ando, J. D. Gillmore, S. Khella, P. J. B. Dyck, M. Waddington Cruz, NEURO-TTRansform Investigators, *JAMA* **2023**, *330*, 1448–1458.
[93] L. N. Kasiewicz, S. Biswas, A. Beach, H. Ren, C. Dutta, A. M. Mazzola, E. Rohde, A. Chadwick, C. Cheng, S. P. Garcia, S. Iyer, Y. Matsumoto, A. V. Khera, K. Musunuru, S. Kathiresan, P. Malyala, K. G. Rajeev, A. M. Bellinger, *Nature Communications* **2023**, *14*, 2776.
[94] *A Study of VERVE-102 in Patients With Familial Hypercholesterolemia or Premature Coronary Artery Disease*, **2024**.
[95] Lee Richard, Denizio Jamie, Dutta Chaitali, Hsu Hui-Ting, Garrity Ryan, Pacheco Alline, Rohde Ellen, Jayaram Hari, Kathiresan Sekar, Bellinger Andrew, Khera Amit V., *Journal of the American College of Cardiology* **2023**, *81*, 1115–1115.
[96] N. Gilboa-Garber, K. D. Zinger-Yosovich, D. Sudakevitz, B. Lerrer, A. Imberty, M. Wimmerova, A. M. Wu, N. C. Garber, in *The Molecular Immunology of Complex Carbohydrates-3* (Ed.: A.M. Wu), Springer US, Boston, MA, **2011**, pp. 155–211.

[97] D. Passos da Silva, M. L. Matwichuk, D. O. Townsend, C. Reichhardt, D. Lamba, D. J. Wozniak, M. R. Parsek, *Nature Communications* **2019**, *10*, 2183.
[98] S. Wagner, D. Hauck, M. Hoffmann, R. Sommer, I. Joachim, R. Müller, A. Imberty, A. Varrot, A. Titz, *Angewandte Chemie International Edition* **2017**, *56*, 16559–16564.
[99] N. Garber, U. Guempel, A. Belz, N. Gilboa-Garber, R. J. Doyle, *Biochimica et Biophysica Acta (BBA) - General Subjects* **1992**, *1116*, 331–333.
[100] N. Garber, U. Guempel, N. Gilboa-Garber, R. J. Royle, *FEMS Microbiology Letters* **1987**, *48*, 331–334.
[101] R. Sommer, K. Rox, S. Wagner, D. Hauck, S. S. Henrikus, S. Newsad, T. Arnold, T. Ryckmans, M. Brönstrup, A. Imberty, A. Varrot, R. W. Hartmann, A. Titz, *J. Med. Chem.* **2019**, *62*, 9201–9216.
[102] R. Sommer, S. Wagner, K. Rox, A. Varrot, D. Hauck, E.-C. Wamhoff, J. Schreiber, T. Ryckmans, T. Brunner, C. Rademacher, R. W. Hartmann, M. Brönstrup, A. Imberty, A. Titz, *J. Am. Chem. Soc.* **2018**, *140*, 2537–2545.
[103] R. Sommer, S. Wagner, A. Varrot, C. M. Nycholat, A. Khaledi, S. Häussler, J. C. Paulson, A. Imberty, A. Titz, *Chem. Sci.* **2016**, *7*, 4990–5001.
[104] J. Meiers, E. Zahorska, T. Röhrig, D. Hauck, S. Wagner, A. Titz, *J. Med. Chem.* **2020**, *63*, 11707–11724.
[105] J. Meiers, K. Rox, A. Titz, *J. Med. Chem.* **2022**, *65*, 13988–14014.
[106] S. Aiello, L. Pagano, F. Ceccacci, B. Simonis, S. Sennato, F. Bugli, C. Martini, R. Torelli, M. Sanguinetti, A. Ciogli, C. Bombelli, G. Mancini, *Colloids and Surfaces A: Physicochemical and Engineering Aspects* **2021**, *617*, 126321.
[107] R. A. Harper, G. H. Carpenter, G. B. Proctor, R. D. Harvey, R. J. Gambogi, A. R. Geonnotti, R. Hider, S. A. Jones, *Colloids and Surfaces B: Biointerfaces* **2019**, *173*, 392–399.
[108] I. Ofek, D. L. Hasty, N. Sharon, *FEMS Immunology & Medical Microbiology* **2003**, *38*, 181–191.

Chemical Science

Chapter 1.

ROYAL SOCIETY OF CHEMISTRY

EDGE ARTICLE

View Article Online
View Journal | View Issue

Cite this: *Chem. Sci.*, 2024, **15**, 13333

All publication charges for this article have been paid for by the Royal Society of Chemistry

Received 23rd April 2024
Accepted 11th July 2024

DOI: 10.1039/d4sc02703e

rsc.li/chemical-science

Dual inhibitors of *Pseudomonas aeruginosa* virulence factors LecA and LasB†

Olga Metelkina, ‡[abc] Jelena Konstantinović, ‡[a] Andreas Klein,[ad] Roya Shafiei,[ad] Mario Fares,[abc] Alaa Alhayek,[a] Samir Yahiaoui,[a] Walid A. M. Elgaher,[a] Jörg Haupenthal,[a] Alexander Titz *[abc] and Anna K. H. Hirsch *[abd]

Dual inhibitors of two key virulence factors of *Pseudomonas aeruginosa*, the lectin LecA and the protease LasB, open up an opportunity in the current antimicrobial-resistance crisis. A molecular hybridization approach enabled the discovery of potent, selective, and non-toxic thiol-based inhibitors, which simultaneously inhibit these two major extracellular virulence factors and therefore synergistically interfere with virulence. We further demonstrated that the dimerization of these monovalent dual inhibitors under physiological conditions affords divalent inhibitors of LecA with a 200-fold increase in binding affinity. The bifunctional LecA/LasB-blocker **12** showed superiority for the inhibition of virulence mediated by both targets over the individual inhibitors or combinations thereof *in vitro*. Our study sets the stage for a systematic exploration of dual inhibitors as pathoblockers for a more effective treatment of *P. aeruginosa* infections and the concept can certainly be extended to other targets and pathogens.

Introduction

Bacterial resistance to antibiotics is a growing global health problem that urgently requires a solution.[1] Disarming pathogens by targeting bacterial virulence factors has emerged as a new approach to fighting drug-resistant infections.[2–5] Bacterial virulence factors such as toxins, adhesins, invasins, and quorum-sensing molecules play crucial roles in host colonization and infection promotion by suppressing the host immune defense.[6,7] Reducing bacterial virulence *via* the inhibition of these factors also decreases the host's susceptibility to infection and allows the immune system to eliminate bacteria. Moreover, the inhibition of bacterial virulence factors mechanistically reduces the selection pressure for resistant mutants due to the ability of pathoblockers to disarm the pathogens without direct killing.[3,4]

Pseudomonas aeruginosa is a Gram-negative bacterium that is classified as critical on the WHO pathogen priority list and currently, numerous avenues of research are being explored in parallel to identify new therapeutics against this pathogen.[8,9]

Extracellular elastase LasB is a zinc-metalloprotease produced by *P. aeruginosa* and one of its pivotal virulence factors. Its importance for the overall pathogenicity of *P. aeruginosa* has been established and it is considered a valid drug target.[10] The role of LasB in degrading the components of the connective tissue such as elastin and extracellular matrix components (ECMs, *e.g.*, collagen and laminin) facilitates host colonization.[11,12] Besides this, LasB plays an important role in disrupting the host immune system through the degradation of immunoglobulins, cytokines and other immune factors.[13,14] LasB is also known for hydrolyzing blood proteins, such as transferrin and lactoferrin, consequently leading to free-radical-induced cytotoxicity.[15,16] In addition to the host substrates, LasB participates in the processing and activation of other bacterial components (LasA, leucine aminopeptidase, lysine endopeptidase and others), promoting the inflammation process.[17–19]

Another virulence factor, lectin LecA (PA-IL), is an extracellular galactophilic carbohydrate-binding protein expressed by *P. aeruginosa*, which mediates biofilm matrix formation and host colonization.[20,21] It is responsible for bacterial adhesion interacting with the glycocalyx of mammalian cells.[22,23] LecA also attenuates ciliary beating in human airways, preventing mucus clearance and inhibiting the growth of respiratory epithelial cells.[21,24,25] On a molecular level, this lectin was shown to mediate bacterial uptake in a lipid zipper mechanism by binding to host glycolipids presented on its cell surfaces.[26] Additionally, LecA enhances host cellular absorption of another virulence factor, exotoxin A, inducing a pathogenic effect on the intestinal epithelium and it increases the injury of the alveolar capillary barrier.[20,27] It has been demonstrated that the

[a]*Helmholtz Institute for Pharmaceutical Research Saarland (HIPS), Helmholtz Centre for Infection Research (HZI), Campus E8.1, 66123 Saarbrücken, Germany. E-mail: alexander.titz@helmholtz-hips.de; anna.hirsch@helmholtz-hips.de*

[b]*Deutsches Zentrum für Infektionsforschung (DZIF), Standort Hannover – Braunschweig, 38124 Braunschweig, Germany*

[c]*Department of Chemistry, Saarland University, 66123 Saarbrücken, Germany*

[d]*Department of Pharmacy, Saarland University, 66123 Saarbrücken, Germany*

† Electronic supplementary information (ESI) available. See DOI: https://doi.org/10.1039/d4sc02703e

‡ These authors contributed equally.

inhibition of LecA reduces biofilm formation and the overall virulence of *P. aeruginosa*.[20] Glycomimetics have the potential to act as promising pathoblockers.[28] To increase the efficacy of LecA inhibition and overcome its moderate micromolar affinity to galactosides caused by a shallow binding pocket, multivalent ligands are often utilized.[29–33]

The crucial effects of these two proteins on the infection progress make them validated and attractive therapeutic targets. Simultaneously targeting both LasB and LecA is compelling for multiple reasons. The extracellular co-localization of LasB and LecA overcomes the major hurdle for many therapeutic molecules to penetrate the Gram-negative cell wall. Furthermore, the dual inhibitors can increase drug efficacy in comparison to combination therapy when the two separate therapeutic molecules are applied together.[34] It is expected that a single drug acting on multiple targets possesses more predictable pharmacokinetic and safety profiles, lowers the probability of resistance development and avoids undesirable drug–drug interactions.[34]

In this work, we have chosen established inhibitors of LasB and LecA based on α-isobutyl/benzyl-*N*-aryl-mercaptoacetamide and phenyl β-D-galactoside, respectively, and merged them into one molecule that blocked LecA and LasB with moderate to high potency.[9,35–37,41] In addition, by utilizing the inherently limited chemical stability of thiols and their tendency to form disulfides in an extracellular environment, highly potent divalent LecA-inhibitors were obtained. These disulfides are likely to be formed in the infection setting after saturating LasB *in situ*, yielding highly potent inhibitors of the second virulence factor LecA.

Results and discussion

Design of dual inhibitors

To develop dual inhibitors against *P. aeruginosa* virulence factors LasB and LecA, we selected previously developed thiol-based LasB ligands, which demonstrated high potency but also limited chemical stability due to their tendency to dimerize to disulfides under physiological conditions.[37] It is known that the moderate micromolar potency of galactosides as LecA inhibitors can be significantly improved by utilizing divalent ligands, where two carbohydrate molecules are bridged with a linker to simultaneously bind to two sites in the LecA tetramer.[29,31,33,38] Taking these facts into account, we combined nitrophenyl β-D-thiogalactoside **1** as a LecA inhibitor with the *N*-aryl-mercaptoacetamide-based LasB inhibitors **2** and **3** by merging their aryl moieties into dual inhibitors **11**, **12**, **17**, **18**, **24** and **25** (Fig. 1).[37,39–41] The resulting compounds should be capable of efficiently inhibiting LasB in the initial thiol form, while the dimerization of excess ligand under physiological conditions at the infection site transforms them from moderately monovalent into more potent divalent LecA inhibitors.

Our previously reported crystal structure of thiol **3** in complex with LasB suggested potential for further elongation of the molecule in the direction of the aniline ring (Fig. 2A).[37] At the same time, the co-crystal structure of LecA with **1** showed the opportunity to modify the nitro group in the *para*-position of the phenyl ring without disturbing the crucial interaction of the sugar moiety in the binding pocket (Fig. 2B),[45] which is backed by reported structure–activity relationships.[36,40,42,43] In our hybridized molecules, the thiol group should maintain its crucial coordination to the zinc ion in the active site of LasB, while the galactoside will conserve the calcium(II) chelation with its 3- and 4-hydroxy groups and the T-shaped CH–π interactions between the phenyl aglycon and His50 in the binding site of LecA.[40,44]

Further, we have shown that *N*-arylmercaptoacetamides have moderate redox stability and tend to oxidize to disulfides under physiological conditions.[46] This drawback may offer a significant advantage for the inhibition of LecA, that is, multivalent interactions are among the most efficient ways invented by nature to enhance the lectin–carbohydrate interaction.[47,48] Therefore, we speculated that the designed compounds will first inhibit LasB as thiols, while their excess at the site of infection inevitably dimerizes to give divalent galactosides with an enhancement in LecA binding affinity.

Synthesis of dual LecA/LasB inhibitors

As a first step, we synthesized glycomimetic thiols **11** and **12** in the form of diastereomeric mixtures (Scheme 1A). 4-Nitrothiophenol was glycosylated with β-D-galactose pentaacetate (**4**) using triflic acid as a catalyst to give β-thioglycoside **5** in 66% yield. The reduction of the nitro group to aniline derivative **6** using Pd/C-catalyzed hydrogenation was followed by amide coupling with racemic 2-bromo-4-methylpentanoic acid or 2-bromo-3-phenylpropanoic acid, which afforded compounds **7** and **8** in 86% and 74% yield, respectively. Bromides **7** and **8** were converted into thioacetates **9** and **10** *via* nucleophilic substitution with potassium thioacetate in good yields. The subsequent deprotection under Zemplén conditions with sodium methoxide in methanol furnished thiols **11** and **12** in 43% and 60% yield, respectively.

To investigate whether stereochemistry has an impact on the activity, we synthesized two pairs of diastereomers, utilizing enantiomerically pure starting materials (Scheme 1B). In the case of compounds **17**, **18** and **24**, the corresponding α-bromo carboxylic acids with inverse stereochemistry were used. In the case of **25**, the synthesis started from D-leucine affording (*R*)-2-bromo-4-methylpentanoic acid (**19′**) in quantitative yield, based on the work of Izumiya and Nagamatsu.[49–51] The four derivatives were obtained following the procedures described for the diastereomeric mixtures (Scheme 1).

For the α-benzyl derivatives **17** and **24**, the high degree of diastereomeric purity has been conserved during the three-step reaction cascade, as evidenced by the comparison of the NMR signals corresponding to the anomeric carbon atoms in the ^{13}C NMR spectra of the diastereomeric mixture **11** and the separate diastereomers. Diastereomeric mixture **11** showed two signals at 88.27 and 88.23 ppm, corresponding to the anomeric carbon atoms of the two diastereomers, while **17** and **24** demonstrated one single signal each with a 0.04 ppm difference in chemical shifts (ESI†). The anomeric carbon atom in diastereomeric mixture **12** and in both isomers **18** and **25** appears as a single

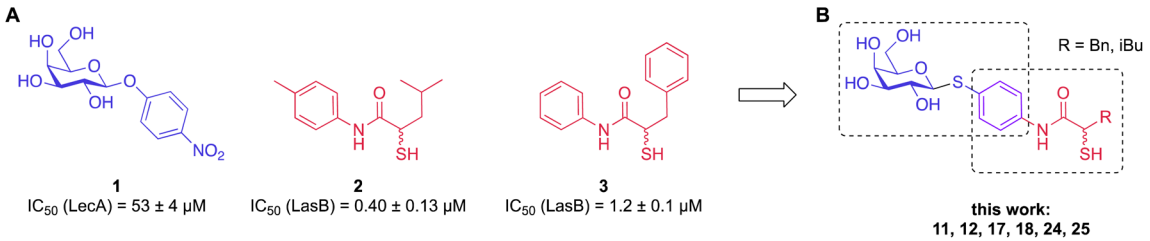

Fig. 1 (A) Reported LecA and LasB inhibitors **1–3** and (B) their combination into dual inhibitors.

signal at 88.3 ppm, due to the smaller and/or more flexible isobutyl substituent (ESI†).

The tendency of thiols to form disulfides in an oxidative environment suggests that our monovalent inhibitors will dimerize *in situ* over time, forming structures that can serve as divalent LecA inhibitors with enhanced potency against LecA. Disulfide formation in the presence of *P. aeruginosa* culture supernatant was studied for the two inhibitors **11** and **12** and analyzed by liquid chromatography-mass spectrometry (LC-MS) (Fig. 3B). Disulfides **26** and **27** were synthesized *via* oxidation with H_2O_2 in DMSO/H_2O and used as reference compounds for the stability assay (Fig. 3A). For both, **26** (Bn) and **27** (*i*Bu), we observed two closely eluting substances with identical mass by LC-MS, suggesting that different diastereomers were formed. The separation of those two peaks of the benzylated derivative **26** using preparative HPLC gave **26a** and **26b** (*m*/*z* of 901.28, Fig. S1†).

In the presence of the bacterial culture supernatant of *P. aeruginosa*, the conversion of thiols **11** and **12** into the corresponding disulfides **26** and **27** was monitored at 37 °C and thiol half-lives of 48 min for **11** and 70 min for **12** were determined (Fig. 3B). The kinetics to convert the thiols to the corresponding disulfides allows **11** and **12** to first act as LecA and LasB dual inhibitors and to transform over time into more potent divalent inhibitors of LecA, **26** and **27** (Fig. 3).

Activity against antivirulence targets LecA and LasB

We next evaluated the six synthesized thiol derivatives **11**, **12**, **17**, **18**, **24** and **25** for their inhibitory activity against both LecA and LasB. In addition, we determined the inhibitory activity of disulfides **26** and **27** on LecA but not on LasB as the essential thiol for coordination to the zinc ion is absent, leading to an expected loss in inhibitory activity.

The LasB activity of the thiol derivatives **11**, **12**, **17**, **18**, **24** and **25** was tested using a functional FRET-based *in vitro* proteolysis assay (Fig. 4A). Both α-isobutyl and α-benzyl derivatives demonstrated inhibitory activity against LasB in the same range as the previously observed activities of compounds **2** and **3** (IC_{50} = 0.40 and 1.2 μM, respectively).[37,41] Interestingly, α-benzyl derivative **11** (IC_{50} = 0.30 μM) showed a four-fold improvement in activity compared to **3**. α-Isobutyl derivative **12** (IC_{50} = 0.80 μM) proved to be somewhat less potent than the α-benzyl **11**, and its diastereomer with (*R*)-configuration on the right-hand side of molecule **18** showed a slightly lower IC_{50} of 0.51 μM compared to its (*S*)-isomer (**25**, IC_{50} = 0.77 μM). On the other hand, the (*S*)-isomer **24** (IC_{50} = 0.22 μM) proved to be three-fold more potent compared to the (*R*)-isomer **17** (IC_{50} = 0.73 μM) among the α-benzylated series.

The four thiols **17**, **18**, **24** and **25** as well as three disulfides **26a**, **26b** and **27** were then evaluated for their activity against LecA using a competitive binding assay based on fluorescence polarization (Fig. 4B). The IC_{50} values obtained for LecA inhibition suggested that the addition of the LasB-inhibiting moiety has a positive effect on the affinity towards LecA, decreasing the IC_{50} more than two-fold, from 52.5 μM for **1** to 18.1 μM and 19.8 μM for **11** and **12**, respectively. The substitution of the isobutyl residue with a benzyl group did not affect the affinity of disulfides in the LecA assay (IC_{50} = 4.7 μM and 3.0 μM for **26a** and **26b**, respectively, and IC_{50} = 5.7 μM for **27**), but had an impact

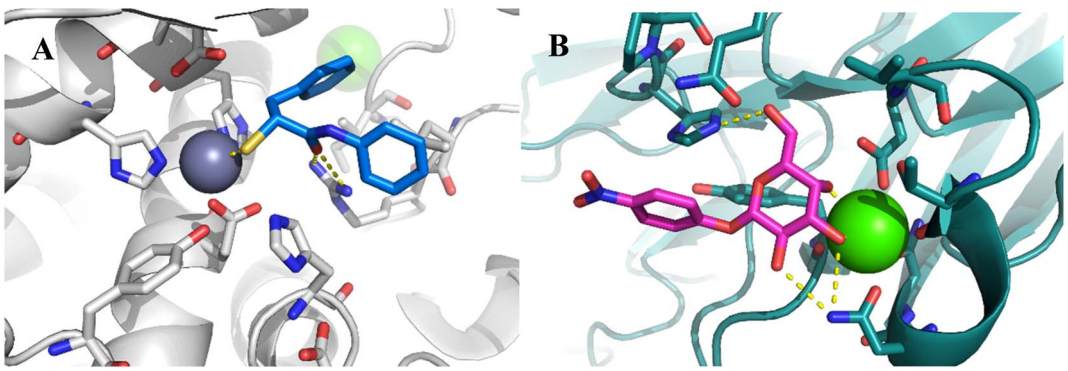

Fig. 2 A) Crystal structure of LasB (gray) in complex with **3** (cyan) (PDB code: 7OC7);[37] (B) crystal structure of LecA (petrol) in complex with **1** (magenta) (PDB code: 3ZYF).[45]

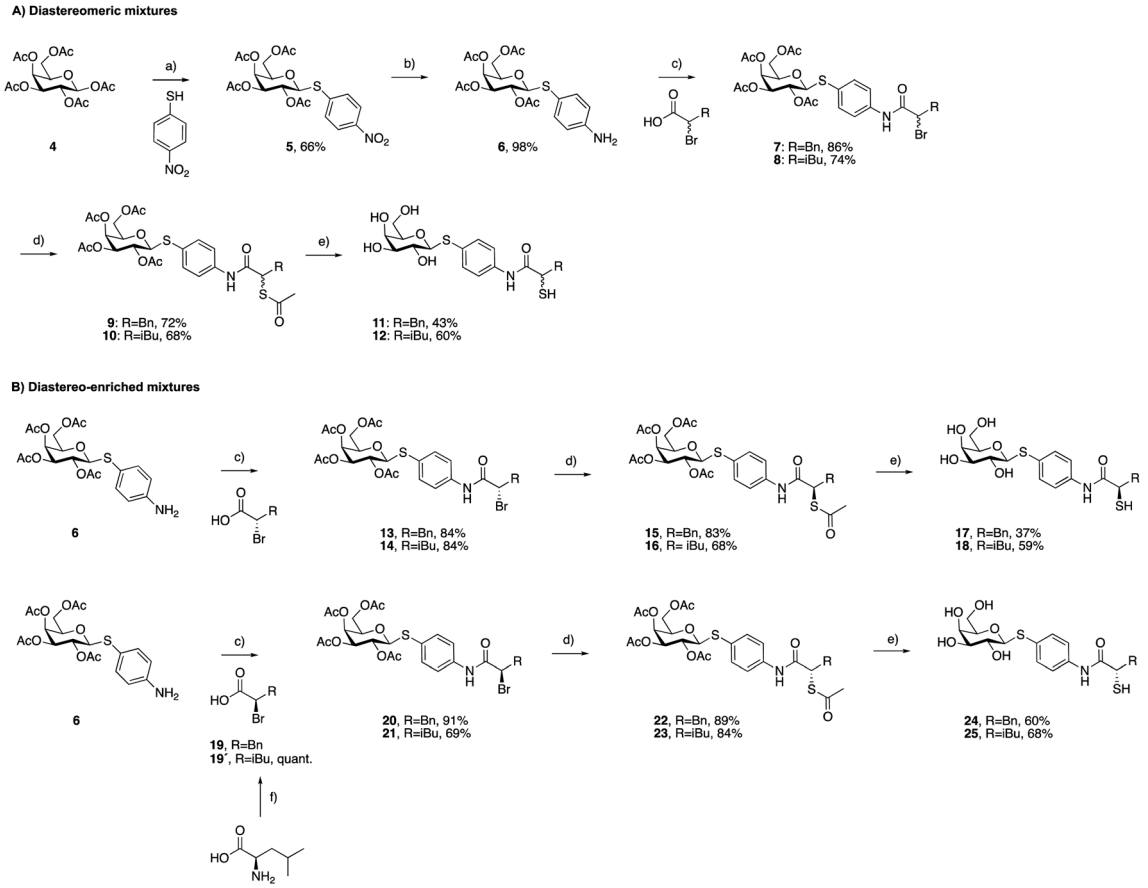

Scheme 1 Synthesis of LecA/LasB dual inhibitors. (a) TfOH, MS 3 Å, DCM, 0 °C, 30 min; (b) H_2, Pd/C, DCM, r.t., 18 h; (c) EDC*x*HCl, DCM, r.t., 4 h; (d) KSAc, acetone, r.t., 2 h; (e) NaOMe, MeOH, r.t., 45 min; (f) $NaNO_2$, 48% HBr, H_2O, 0 °C to r.t, 3 h.

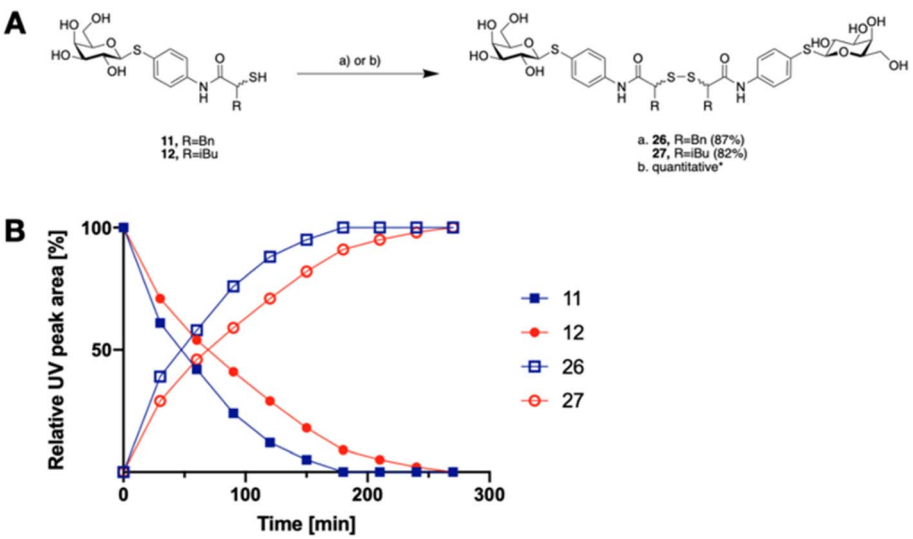

Fig. 3 A) Oxidative dimerization of thiols **11** and **12** into disulfides **26** and **27** using (a) H_2O_2, DMSO/H_2O or (b) *P. aeruginosa* culture supernatant (yield based on LC-MS); (B) dimerization kinetics of thiols **11** or **12** in the presence of *P. aeruginosa* culture supernatant into disulfides **26** or **27** analyzed by LC-MS.

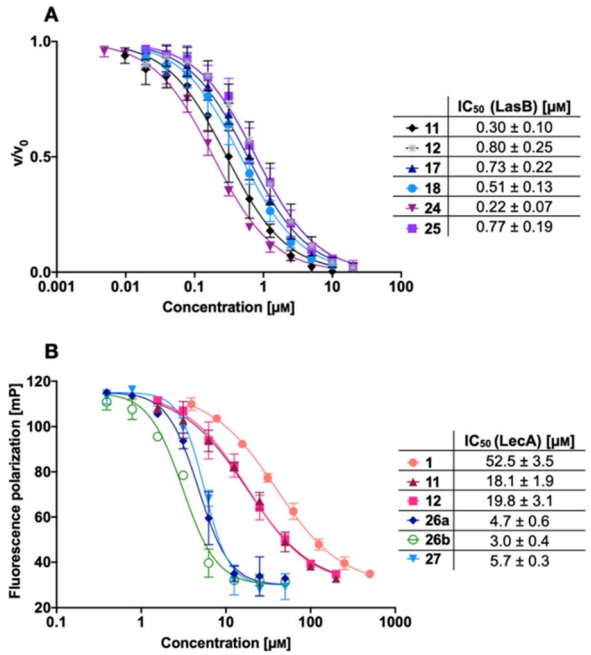

Fig. 4 A) Evaluation of LecA/LasB dual inhibitors by a FRET-based *in vitro* LasB inhibition assay; (B) evaluation of monomeric LecA/LasB inhibitors **11** and **12** and divalent LecA inhibitors **26a**, **26b** and **27** and comparison to the control pNP-Gal (**1**) by a competitive binding assay for LecA based on fluorescence polarization. IC_{50} values were calculated from at least three independent experiments performed in triplicate.

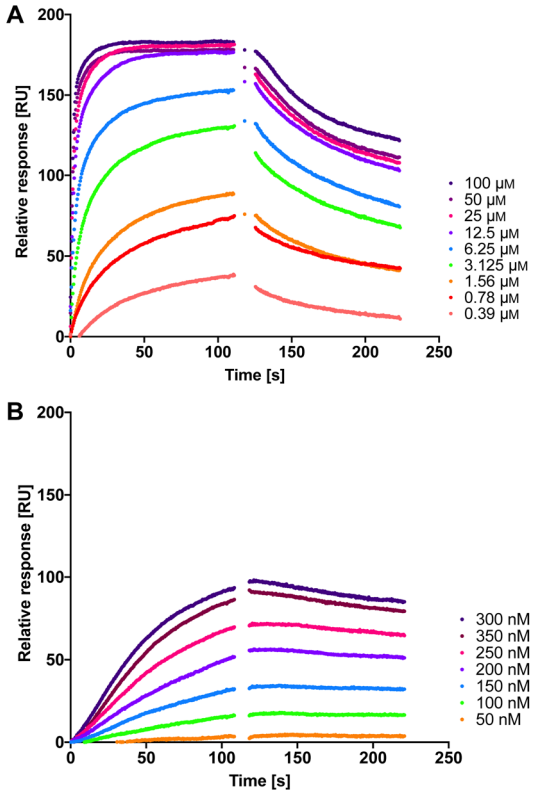

Fig. 5 The interaction of dual inhibitors thiol **17** (A) and disulfide **26a** (B) with LecA studied using SPR.

on the solubility of the corresponding disulfide. While isobutyl disulfide **27** showed a kinetic solubility >600 μM in 10 mm PBS with 2% DMSO at 37 °C, both benzyls **26a** and **26b** had a kinetic solubility of only 300 μM under the same conditions.

In this competitive binding assay, the observed affinity of the divalent LecA-inhibitors **26a**, **26b** and **27** increased more than three-fold compared to the corresponding thiols **11** and **12** (Fig. 4B). Considering the steep Hill slopes >2 of the fitted curves (Fig. 4B), we suspected that both divalent compounds approached the lower limit of the assay as observed before for inhibitors with significantly increased binding strength compared to the fluorescent primary ligand.[31,33]

Therefore, we measured the LecA affinity of thiol derivatives **17**, **18**, **24** and **25** and disulfides **26a**, **26b** and **27** using surface plasmon resonance (SPR) with LecA covalently immobilized on a sensor chip *via* amide coupling (Fig. 5 and Table 1). The data demonstrate a significant increase in the affinity of the divalent compounds for LecA. Based on the fitting of the kinetic binding curves, divalent compounds displayed an up to 200-fold increase in activity (K_D = 7.4 nM and 6.6 nM for **26a** and **26b**, respectively, and K_D = 4.5 nM for **27**) compared to their monovalent thiol analogues (K_D values = 1300 nM, 630 nM, 840 nM and 1000 nM for **17**, **18**, **24** and **25**, respectively), shifting K_D values from the low-micromolar to the single-digit nanomolar range (Fig. 5 and S3†). Thiols **17**, **18**, **24** and **25** reached equilibrium binding within 60 s of interaction with immobilized LecA, followed by their dissociation with moderate off-rates. In contrast, the disulfides demonstrated very slow association rates with an approximately 10-fold increase of k_a compared to the value for **1** (Table 1).[52] Due to the very small off-rates for **26a**, **26b** and **27**, these values have been calculated based on the response at 350 nm of the injected compound and monitoring their dissociation for 30 min (Fig. S2†). The observed very tight binding to immobilized LecA required optimization of the protein surface regeneration procedure. Effective conditions were identified as one injection of 50 mm isopropyl β-D-thiogalactoside in the running buffer, followed by one injection of 20 mm EDTA disodium salt in water. The

Table 1 Kinetic analysis of LecA/LasB inhibitors binding to immobilized LecA using SPR[a]

Compound	k_a [$\times 10^4$ M^{-1} s^{-1}]	k_d [$\times 10^{-4}$ s^{-1}]	K_D [nM]
1	0.40 ± 0.05	1000 ± 330	21 000 ± 4600
17	0.71 ± 0.14	86 ± 20	1300 ± 540
18	1.41 ± 0.47	82 ± 11	630 ± 290
24	0.88 ± 0.23	72 ± 5	840 ± 160
25	0.90 ± 0.31	85 ± 2	1000 ± 590
26a	3.8 ± 0.8	2.8 ± 0.3	7.4 ± 1.4
26b	4.6 ± 0.7	3.0 ± 1.2	6.6 ± 2.4
27	5.2 ± 0.6	2.2 ± 0.3	4.5 ± 0.4

[a] Mean values and standard deviations are from at least three independent experiments.

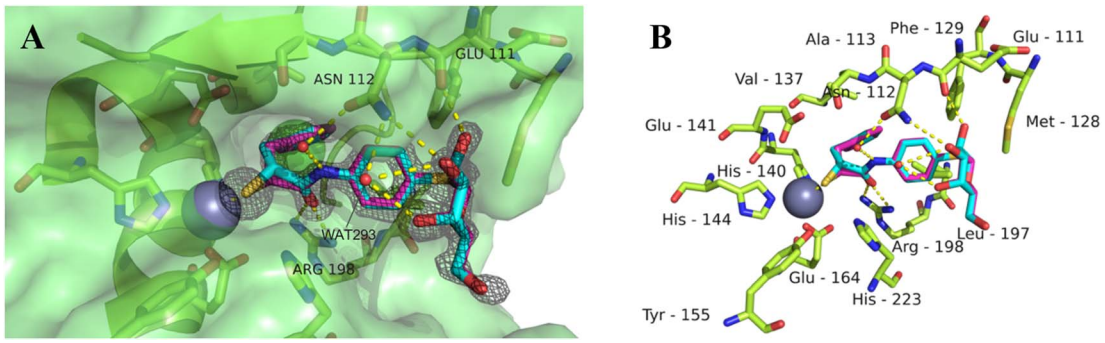

Fig. 6 Crystal structure of **11** in complex with LasB (PDB: 7Z68). (A) Cartoon representation of LasB with a transparent surface (green) and ligated **11** (cyan (*R*), pink (*S*)). The amino acids of LasB forming the binding site are represented as sticks. The gray isomesh represents the polder map of **11** contoured at 3σ. (B) Stick representation of the LasB binding site with bound **11**. Polar interactions between LasB and **11** are highlighted by dashed lines (color code: oxygen = red, nitrogen = blue, sulfur = yellow, and red spheres = water).

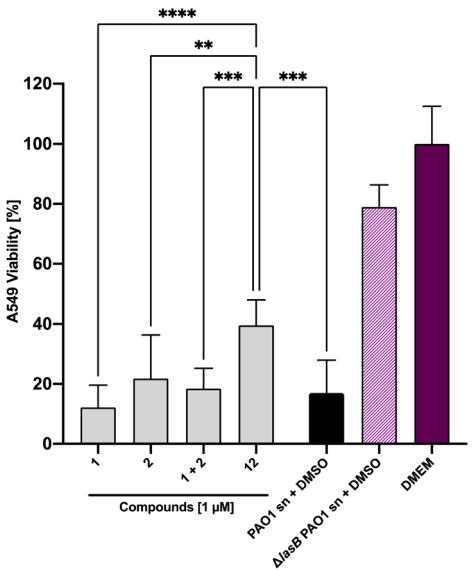

Fig. 7 Inhibition of the LasB-dependent cytotoxicity of *P. aeruginosa* PAO1 culture supernatant on human A549 cells. Effect of PAO1 supernatant in the absence (black bar) or presence (grey) of compounds **1**, **2**, **1** + **2** or **12**. The culture supernatant of the *lasB* knockout mutant (Δ*lasB* PAO1) was applied as a positive control (light purple). The viability of cells that were untreated (DMEM) served as a negative control and are shown in dark violet. The graphs represent the means of three independent experiments ± SD. One-way ANOVA statistical analysis was performed following Dunnett's multiple comparisons test, comparing the mean value of each concentration to the mean value of PAO1 without any treatment with compounds (***$p \leq 0.001$, **$p \leq 0.01$, and *$p \leq 0.05$).

regenerated chip surface was controlled using an injection of **1** to ensure that the activity of LecA was maintained.

Selectivity and toxicity profile of thiols 11 and 12

Given that the novel inhibitors contain a free thiol as a strong zinc binding group, we analyzed the selectivity of the diastereomeric mixtures **11** and **12** on six human matrix metalloproteases (MMPs) as putative off-targets.[53] The data obtained demonstrate selectivity of both compounds for the two intended targets over all six off-targets tested since less than 20% inhibition was observed at 100 μM (Table S1†). Furthermore, we tested the impact of **11** and **12** on bacterial viability to ensure that these compounds are antivirulence agents and not antibiotics. No antimicrobial activity was detected up to 100 μM (Table S2†). Finally, we evaluated the cytotoxicity of compounds **11** and **12** against three human cell lines, HepG2, HEK293, and A549, revealing no detectable cytotoxicity at 100 μM (Table S3†).

Having established the inhibitors' high potency on both antivirulence targets and outstanding toxicity and selectivity properties, we set off to determine the modes of interaction with their targets LecA and LasB at the molecular level. Unfortunately, crystals could not be obtained for LecA with the observable electron density of thiols or the very potent disulfides. The crystal structures of multivalent ligands with multivalent LecA are intrinsically difficult to obtain and only one example has been reported to date, which also displays only incomplete electron density of the ligand.[54]

Co-crystallization of thiol 11 with LasB

To get better insights into the binding mode and to understand the potency of the new inhibitors, we performed co-crystallization experiments with LasB, using the diastereomeric mixture of the α-benzylated analog **11**.

The LasB–**11** complex crystallized in the space group $P12_11$, and crystals diffracted to 1.5 Å resolution (Fig. 6 and Table S4†). The obtained electron density of the ligand in the active site of LasB suggests that the enzyme accommodates both (*R*)- and (*S*)-isomers of compound **11**. These data therefore explain why there is no stronger difference in the activities of the two isomers in the *in vitro* LasB assay ((*R*)-isomer **17** ($IC_{50} = 0.73$ μM) and (*S*)-isomer **24** ($IC_{50} = 0.22$ μM)).

As observed for previous crystal structures of thiols with LasB,[37,46] also here the thiol of **11** displaces the water molecule in the tetrahedral coordination sphere of the zinc ion in the binding site, leading to a sulfur–zinc distance of 2.3 Å. The carbonyl oxygen of **11** forms a hydrogen bond with the side chain of Arg198 (3.1 Å) in the active site, stabilizing the binding of the compound in the core region. The benzyl ring is placed in

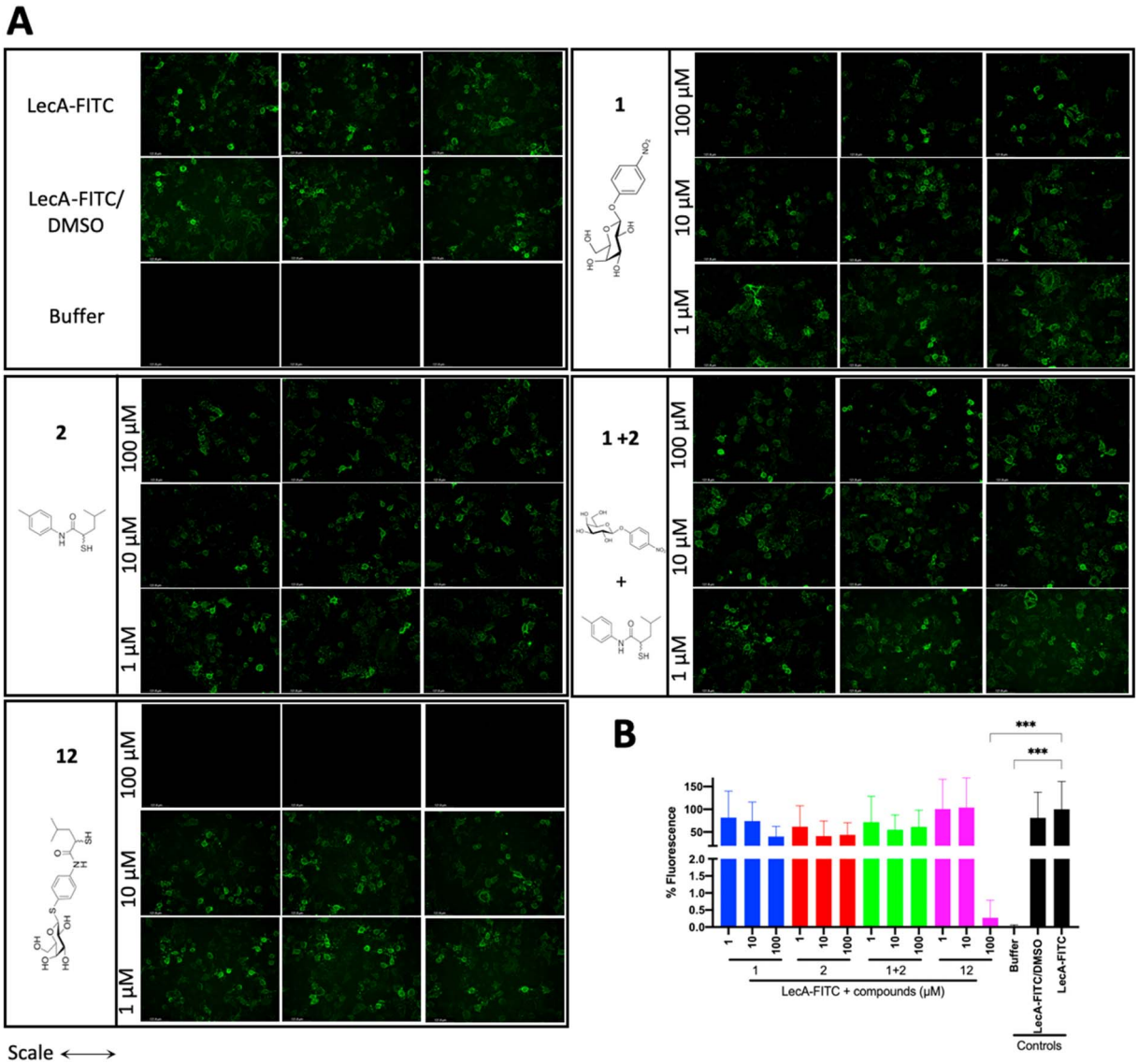

Fig. 8 Analysis of the inhibitory activity of **1**, **2**, a combination of **1** + **2** and **12** on the adhesion of fluorescein-labelled LecA to human A549 cells by fluorescence microscopy. (A) Three representative fluorescence images of one biological replicate of LecA-FITC bound to A549 cells in the presence of the different compounds and under different concentrations (scale bar corresponds to 250 µM). (B) Quantification of mean image fluorescence intensities with the averages and standard deviations for 3 biological replicates ((A), S7A and B†). Intensities are normalized with LecA-FITC in the absence of inhibitors to 100% and in the absence of FITC-LecA to 0%. One-way ANOVA statistical analysis was performed following Dunnett's multiple comparisons test, comparing the mean value of each condition to the mean value of the LecA-FITC positive control (***$p \leq 0.001$, all other data have no statistical significance compared to the LecA-FITC positive control).

the lipophilic S2′ pocket, thereby increasing the binding affinity *via* hydrophobic interactions. The galactose moiety is further stabilized by hydrogen bonds between its 2-hydroxy group (2-OH) and the backbone carbonyl of Glu111, two water-mediated hydrogen bonds *via* the same water (WAT293) between galactose 3-OH and 4-OH and the side chain of Asn112 and a second water-mediated hydrogen bond of 3-OH and the same side chain of Asn112. Thus, the side chain of Asn112 is heavily involved in coordinating through its amide-NH_2 to the ligand's carbohydrate moiety with two water-mediated hydrogen bonds and its amide-oxygen forming a hydrogen bond with the ligand's amide NH. An interesting observation is the unexpected folding of the aglycon, which leads to an intramolecular spatial proximity of hydroxyl 4-OH with its phenyl aglycon. Distances as close as 4.5 Å between 4-OH oxygen and the aryl carbon atom connected to the sulfur indicate attractive intramolecular ROH-π bonding.

In vitro antivirulence evaluation of 1, 2 and 12 on A549 cells

Next, we set out to analyze the ability of the dual inhibitor **12** and the individual treatment or combination of galactoside **1** and thiol **2** to reduce LasB-dependent cytotoxicity from *P. aeruginosa* PAO1 culture supernatant on A549 cells. None of the investigated compounds influenced A549 cell viability at 100

μM in the absence of bacterial culture supernatant (Fig. S4†). When A549 cells were exposed to *P. aeruginosa* PAO1 culture supernatant, both 100 μM and 10 μM of **12** led to an increase in cell viability compared to the combination of the individual LasB (**2**) and LecA (**1**) inhibitors at the corresponding concentrations (Fig. S5†). At 100 μM of **12**, the cytotoxicity of PAO1 culture supernatant reached that of the LasB-deficient strain, which served as the control (Fig. S5†). At 1 μM, only the dual inhibitor **12** had a statistically significant beneficial effect on cell viability, whereas neither **1** nor **2** nor their combination had any effect (Fig. 7 and S5†). These data demonstrate the enhanced potency of the dual inhibitor against the secreted *P. aeruginosa* virulence factors.

Evaluation of the dual inhibitors in LecA adhesion to A549 cells

LecA-mediated cell adhesion is crucial for the initial infection and host-cell invasion of *P. aeruginosa*. Therefore, compounds **1** and **2**, a combination of **1**+**2** and the dual inhibitor **12** were assessed for their ability to inhibit LecA-binding to human A549 cells. 10 μM of LecA-FITC and different concentrations of the respective compounds were incubated at 4 °C for 30 min with confluent A549 cells. After extensive washing, the analysis of the cells *via* fluorescence microscopy revealed that only the dual inhibitor **12** at 100 μM significantly inhibited the binding of LecA-FITC to A549 cells to the background level. No visible fluorescence signal was observed, which was comparable to the negative control of A549 cells in the absence of labeled LecA (Fig. 8). All other compounds and concentrations tested did not show a noticeable reduction in the fluorescence signal compared to the positive control consisting of A549 cells and LecA-FITC (Fig. 8 and S7†). The observation that the dual inhibitor showed high inhibition of LecA cell adhesion, while compounds **1** and **2** alone or in combination failed to do so, further highlights the superiority of **12**.

Conclusions

We report the first dual inhibitors of the major virulence factors LecA and LasB from the WHO priority I pathogen *P. aeruginosa*. Quite remarkably, our dual inhibitors displayed improved inhibitory activity and affinity for both targets down to 220 nM for LasB and 18 μM for LecA, compared to the individual predecessors of 400 nM and 53 μM, respectively. Implied by design, the divalent disulfide derivatives are formed *in situ*, which resulted in a 200-fold increase reaching single-digit nanomolar LecA activity determined using SPR (K_Ds 4.5–7.4 nM). We anticipate that the observed conversion rates of thiols into disulfides in the presence of the bacterial culture supernatant of *P. aeruginosa* are beneficial to ensure the initial saturation of LasB with the thiol and allow the subsequent inhibition of LecA with the potent bivalent disulfides. The crystal structure of the dual inhibitor **11** in complex with LasB confirmed the interaction at the atomic level. To further assess the potential of these merged inhibitors as candidates for therapeutic applications at this early stage, we evaluated their selectivity and toxicity profiles. Importantly, the compounds did not show any inhibition of a panel of six human MMPs as potential off-targets and cytotoxicity was not observed. Finally, we demonstrated a reduction of the cytotoxicity of *P. aeruginosa* culture supernatant by the dual inhibitor **12** on A549 cells *in vitro*, which primarily originates from secreted LasB, as well as an efficient inhibition of LecA adhesion to A549 cells. Both inhibitory effects were observed only for the dual inhibitor **12**, but were absent for single or combination treatments with LecA- or LasB inhibitors **1** and **2**, respectively.

Disarming highly pathogenic *P. aeruginosa* by interfering with its major pathogenicity factors offers a promising new option for therapeutics. Future research will focus on infection models using more complex *in vivo* systems, to support the importance of the presented dual inhibitors and their translation into practical applications.

Experimental section

Experimental details, materials, methods, chemical syntheses and transcripts of ^{1}H and ^{13}C NMR spectra can be found in the ESI.†

Data availability

The datasets supporting this article have been uploaded as part of the ESI.† The crystal structure dataset has been deposited at the Protein Database under code 7Z68, **https://www.rcsb.org/structure/7Z68**.

Author contributions

O. M. and J. K. contributed equally. All authors discussed the results and commented on the manuscript. Design of the study: O. M., J. K., S. Y., A. T., A. K. H. H.; project management A. T., A. K. H. H.; acquisition of funding: A. T., A. K. H. H.; project supervision: A. T., A. K. H. H.; design and chemical synthesis: O. M., J. K., S. Y.; evaluation of oxidative dimerization of thiols by LC-MS: O. M.; evaluation of LasB activity by *in vitro* inhibition assay: J. K.; evaluation of LecA binding by fluorescence polarization assay and SPR: O. M.; cytotoxicity and selectivity profile: J. H.; X-ray: A. K.; *in vitro* antivirulence evaluation: A. A., R. S.; LecA adhesion to A549 cells *in vitro*: R. S., M. F.; writing original draft: O. M., J. K.; writing – review and editing: O. M., J. K., A. T., A. K. H. H., with a contribution of all authors.

Conflicts of interest

The authors declare no competing financial interest.

Acknowledgements

A. T. thanks the European Research Council for funding part of this work (ERC starting grant 716311). A. K. H. H. gratefully acknowledges funding from the European Research Council (ERC starting grant 757913) and the Helmholtz-Association's Initiative and Networking Fund. J. K. acknowledges funding by

the Alexander von Humboldt Foundation. We are indebted to Dr Asfandyar Sikandar and Sebastian Adam (HIPS) for helpful suggestions with structure determination. Furthermore, we are grateful to Dr Joscha Meiers (HIPS), Annabelle Varrot and Anne Imberty (CERMAV) for attempts to crystallize LecA with thiols and disulfides. Dr Anne Imberty is further acknowledged for providing pET25-pail for LecA expression. We thank Nico Dankbar (Xantec) for the invaluable tips for SPR. The authors would like to thank Selina Wolter, Simone Amann, Jeannine Jung and Dennis Jener (HIPS) for technical assistance with LasB *in vitro* inhibition, selectivity and toxicity assays.

References

1 M. Miethke, M. Pieroni, T. Weber, M. Brönstrup, P. Hammann, L. Halby, P. B. Arimondo, P. Glaser, B. Aigle, H. B. Bode, R. Moreira, Y. Li, A. Luzhetskyy, M. H. Medema, J.-L. Pernodet, M. Stadler, J. R. Tormo, O. Genilloud, A. W. Truman, K. J. Weissman, E. Takano, S. Sabatini, E. Stegmann, H. Brötz-Oesterhelt, W. Wohlleben, M. Seemann, M. Empting, A. K. H. Hirsch, B. Loretz, C.-M. Lehr, A. Titz, J. Herrmann, T. Jaeger, S. Alt, T. Hesterkamp, M. Winterhalter, A. Schiefer, K. Pfarr, A. Hoerauf, H. Graz, M. Graz, M. Lindvall, S. Ramurthy, A. Karlén, M. van Dongen, H. Petkovic, A. Keller, F. Peyrane, S. Donadio, L. Fraisse, L. J. V. Piddock, I. H. Gilbert, H. E. Moser and R. Müller, *Nat. Rev. Chem*, 2021, **5**, 726–749.
2 M. Totsika, *Future Med. Chem.*, 2017, **9**, 267–269.
3 M. B. Calvert, V. R. Jumde and A. Titz, *Beilstein J. Org. Chem.*, 2018, **14**, 2607–2617.
4 A. E. Clatworthy, E. Pierson and D. T. Hung, *Nat. Chem. Biol.*, 2007, **3**, 541–548.
5 S. Walesch, J. Birkelbach, G. Jézéquel, F. P. J. Haeckl, J. D. Hegemann, T. Hesterkamp, A. K. H. Hirsch, P. Hammann and R. Müller, *EMBO Rep.*, 2023, **24**, e56033.
6 L. G. Rahme, E. J. Stevens, S. F. Wolfort, J. Shao, R. G. Tompkins and F. M. Ausubel, *Science*, 1995, **268**, 1899–1902.
7 L. Chen, J. Yang, J. Yu, Z. Yao, L. Sun, Y. Shen and Q. Jin, *Nucleic Acids Res.*, 2005, **33**, D325–D328.
8 S. B. Olivia Lawe Davies, *WHO publishes list of bacteria for which new antibiotics are urgently needed*, 2017, **https://www.who.int/news/item/27-02-2017-who-publishes-list-of-bacteria-for-which-new-antibiotics-are-urgently-needed**.
9 S. Wagner, R. Sommer, S. Hinsberger, C. Lu, R. W. Hartmann, M. Empting and A. Titz, *J. Med. Chem.*, 2016, **59**, 5929–5969.
10 M. J. Everett and D. T. Davies, *Drug Discov Today*, 2021, **26**, 2108–2123.
11 C. Wolz, E. Hellstern, M. Haug, D. R. Galloway, M. L. Vasil and G. Döring, *Mol. Microbiol.*, 1991, **5**, 2125–2131.
12 D. Leduc, N. Beaufort, S. de Bentzmann, J.-C. Rousselle, A. Namane, M. Chignard and D. Pidard, *Infect. Immun.*, 2007, **75**, 3848–3858.
13 J. Sun, D. L. LaRock, E. A. Skowronski, J. M. Kimmey, J. Olson, Z. Jiang, A. J. O'Donoghue, V. Nizet and C. N. LaRock, *EBioMedicine*, 2020, **60**, 102984.
14 M. Parmely, A. Gale, M. Clabaugh, R. Horvat and W. W. Zhou, *Infect. Immun.*, 1990, **58**, 3009–3014.
15 B. E. Britigan, M. B. Hayek, B. N. Doebbeling and R. B. J. Fick, *Infect. Immun.*, 1993, **61**, 5049–5055.
16 R. A. Miller, G. T. Rasmussen, C. D. Cox and B. E. Britigan, *Infect. Immun.*, 1996, **64**, 182–188.
17 E. Kessler, M. Safrin, J. K. Gustin and D. E. Ohman, *J. Biol. Chem.*, 1998, **273**, 30225–30231.
18 R. Sarnovsky, J. Rea, M. Makowski, R. Hertle, C. Kelly, A. Antignani, D. V. Pastrana and D. J. Fitzgerald, *J. Biol. Chem.*, 2009, **284**, 10243–10253.
19 J. Oh, X.-H. Li, S.-K. Kim and J.-H. Lee, *Sci. Rep.*, 2017, **7**, 4416.
20 C. Chemani, A. Imberty, S. de Bentzmann, M. Pierre, M. Wimmerova, B. P. Guery and K. Faure, *Infect. Immun.*, 2009, **77**, 11.
21 S. P. Diggle, R. E. Stacey, C. Dodd, M. Cámara, P. Williams and K. Winzer, *Environ. Microbiol*, 2006, **8**, 1095–1104.
22 A. Audfray, A. Varrot and A. Imberty, *C. R. Chim.*, 2013, **16**, 482–490.
23 J. Tiralongo and A. P. Moran, in *Microbial Glycobiology*, ed. O. Holst, P. J. Brennan, M. von Itzstein and A. P. Moran, Academic Press, San Diego, 2010, pp. 549–565.
24 M. Mewe, D. Tielker, R. Schönberg, M. Schachner, K.-E. Jaeger and U. Schumacher, *J. Laryngol. Otol.*, 2005, **119**, 595–599.
25 O. Bajolet-Laudinat, S. Girod-de Bentzmann, J. M. Tournier, C. Madoulet, M. C. Plotkowski, C. Chippaux and E. Puchelle, *Infect. Immun.*, 1994, **62**, 4481–4487.
26 T. Eierhoff, B. Bastian, R. Thuenauer, J. Madl, A. Audfray, S. Aigal, S. Juillot, G. E. Rydell, S. Müller, S. de Bentzmann, A. Imberty, C. Fleck and W. Römer, *Proc. Natl. Acad. Sci. U.S.A.*, 2014, **111**, 12895.
27 R. S. Laughlin, M. W. Musch, C. J. Hollbrook, F. M. Rocha, E. B. Chang and J. C. Alverdy, *Ann. Surg.*, 2000, **232**, 133–142.
28 S. Leusmann, P. Ménová, E. Shanin, A. Titz and C. Rademacher, *Chem. Soc. Rev.*, 2023, **52**, 3663–3740.
29 F. Pertici and R. J. Pieters, *Chem. Commun.*, 2012, **48**, 4008–4010.
30 B. Blanchard, A. Nurisso, E. Hollville, C. Tétaud, J. Wiels, M. Pokorná, M. Wimmerová, A. Varrot and A. Imberty, *J. Mol. Biol.*, 2008, **383**, 837–853.
31 E. Zahorska, S. Kuhaudomlarp, S. Minervini, S. Yousaf, M. Lepsik, T. Kinsinger, A. K. H. Hirsch, A. Imberty and A. Titz, *Chem. Commun.*, 2020, **56**, 8822–8825.
32 M. Bergmann, G. Michaud, R. Visini, X. Jin, E. Gillon, A. Stocker, A. Imberty, T. Darbre and J.-L. Reymond, *Org. Biomol. Chem.*, 2016, **14**, 138–148.
33 E. Zahorska, F. Rosato, K. Stober, S. Kuhaudomlarp, J. Meiers, D. Hauck, D. Reith, E. Gillon, K. Rox, A. Imberty, W. Römer and A. Titz, *Angew. Chem., Int. Ed.*, 2023, **62**, e202215535.
34 A. Anighoro, J. Bajorath and G. Rastelli, *J. Med. Chem.*, 2014, **57**, 7874–7887.
35 C. Kaya, I. Walter, A. Alhayek, R. Shafiei, G. Jézéquel, A. Andreas, J. Konstantinović, E. Schönauer, A. Sikandar,

J. Haupenthal, R. Müller, H. Brandstetter, R. W. Hartmann and A. K. H. Hirsch, *ACS Infect. Dis.*, 2022, **8**, 1010–1021.
36 I. Joachim, S. Rikker, D. Hauck, D. Ponader, S. Boden, R. Sommer, L. Hartmann and A. Titz, *Org. Biomol. Chem.*, 2016, **14**, 7933–7948.
37 C. Kaya, I. Walter, S. Yahiaoui, A. Sikandar, A. Alhayek, J. Konstantinović, A. M. Kany, J. Haupenthal, J. Köhnke, R. W. Hartmann and A. K. H. Hirsch, *Angew Chem. Int. Ed. Engl.*, 2002, **61**(5), e202112295, DOI: **10.1002/anie.202112295**.
38 V. Wittmann and R. J. Pieters, *Chem. Soc. Rev.*, 2013, **42**, 4492–4503.
39 F. Casoni, L. Dupin, G. Vergoten, A. Meyer, C. Ligeour, T. Géhin, O. Vidal, E. Souteyrand, J.-J. Vasseur, Y. Chevolot and F. Morvan, *Org. Biomol. Chem.*, 2014, **12**, 9166–9179.
40 R. U. Kadam, D. Garg, J. Schwartz, R. Visini, M. Sattler, A. Stocker, T. Darbre and J.-L. Reymond, *ACS Chem. Biol.*, 2013, **8**, 1925–1930.
41 K. Voos, S. Yahiaoui, J. Konstantinović, E. Schönauer, A. Alhayek, A. Sikandar, K. S. Chaib, T. Ramspoth, K. Rox, J. Haupenthal, J. Köhnke, H. Brandstetter, C. Ducho and A. K. H. Hirsch, *ChemRxiv*, 2022, DOI: **10.26434/chemrxiv-2022-fjrqr**.
42 E. Siebs, E. Shanina, S. Kuhaudomlarp, P. da Silva Figueiredo Celestino Gomes, C. Fortin, P. H. Seeberger, D. Rognan, C. Rademacher, A. Imberty and A. Titz, *Chembiochem*, 2022, **23**, e202100563.
43 J. Rodrigue, G. Ganne, B. Blanchard, C. Saucier, D. Giguère, T. C. Shiao, A. Varrot, A. Imberty and R. Roy, *Org. Biomol. Chem.*, 2013, **11**, 6906–6918.
44 V. Camberlein, G. Jézéquel, J. Haupenthal and A. K. H. Hirsch, *Antibiotics*, 2022, **11**(8), 1060, DOI: **10.3390/antibiotics11081060**.
45 R. U. Kadam, M. Bergmann, M. Hurley, D. Garg, M. Cacciarini, M. A. Swiderska, C. Nativi, M. Sattler, A. R. Smyth, P. Williams, M. Cámara, A. Stocker, T. Darbre and J.-L. Reymond, *Angew. Chem., Int. Ed.*, 2011, **50**, 10631–10635.
46 A. M. Kany, A. Sikandar, J. Haupenthal, S. Yahiaoui, C. K. Maurer, E. Proschak, J. Köhnke and R. W. Hartmann, *ACS Infect. Dis.*, 2018, **4**, 988–997.
47 L. L. Kiessling, *Bioorg. Med. Chem.*, 2018, **26**, 5229–5238.
48 W. I. Weis and K. Drickamer, *Annu. Rev. Biochem.*, 1996, **65**, 441–473.
49 N. Izumiya and A. Nagamatsu, *Bull. Chem. Soc. Jpn.*, 1952, **25**, 265–267.
50 N. Tka, J. Kraïem and B. B. Hassine, *Synth. Commun.*, 2013, **43**, 735–743.
51 E. R. Samuels and I. F. Sevrioukova, *Tetrahedron Lett.*, 2018, **59**, 1140–1142.
52 O. Metelkina, B. Huck, J. S. O'Connor, M. Koch, A. Manz, C.-M. Lehr and A. Titz, *J. Mater. Chem. B*, 2022, **10**, 537–548.
53 H. Laronha and J. Caldeira, *Cells*, 2020, **9**(5), 1076, DOI: **10.3390/cells9051076**.
54 R. Visini, X. Jin, M. Bergmann, G. Michaud, F. Pertici, O. Fu, A. Pukin, T. R. Branson, D. M. E. Thies-Weesie, J. Kemmink, E. Gillon, A. Imberty, A. Stocker, T. Darbre, R. J. Pieters and J.-L. Reymond, *ACS Chem. Biol.*, 2015, **10**, 2455–2462.

Journal of Materials Chemistry B

Chapter 2.

ROYAL SOCIETY OF CHEMISTRY

PAPER

View Article Online
View Journal | View Issue

Cite this: J. Mater. Chem. B, 2022, 10, 537

Targeting extracellular lectins of *Pseudomonas aeruginosa* with glycomimetic liposomes†

Olga Metelkina,[abc] Benedikt Huck,[de] Jonathan S. O'Connor,[fg] Marcus Koch,[h] Andreas Manz,[fg] Claus-Michael Lehr[de] and Alexander Titz *[abc]

Received 23rd September 2021,
Accepted 17th December 2021

DOI: 10.1039/d1tb02086b

rsc.li/materials-b

The antimicrobial resistance crisis requires novel approaches for the therapy of infections especially with Gram-negative pathogens. *Pseudomonas aeruginosa* is defined as priority 1 pathogen by the WHO and thus of particular interest. Its drug resistance is primarily associated with biofilm formation and essential constituents of its extracellular biofilm matrix are the two lectins, LecA and LecB. Here, we report microbial lectin-specific targeted nanovehicles based on liposomes. LecA- and LecB-targeted phospholipids were synthesized and used for the preparation of liposomes. These liposomes with varying surface ligand density were then analyzed for their competitive and direct lectin binding activity. We have further developed a microfluidic device that allowed the optical detection of the targeting process to the bacterial lectins. Our data showed that the targeted liposomes are specifically binding to their respective lectin and remain firmly attached to surfaces containing these lectins. This synthetic and biophysical study provides the basis for future application in targeted antibiotic delivery to overcome antimicrobial resistance.

Introduction

Resistance to antimicrobials is rising and expected to lead to more deaths from infections than from cancer in 2050 as stated by the WHO.[1] *Pseudomonas aeruginosa* are particularly problematic Gram-negative bacteria belonging to the ESKAPE pathogens, the major etiological agents of drug-resistant nosocomial infections. The main difficulty for treating *P. aeruginosa* infections is associated with its ability to form biofilms, a social lifestyle where the bacteria are embedded in a self-produced, resistance-conferring matrix.[2] This biofilm increases antimicrobial resistance against antibiotics by a factor of 10–1000 and thereby renders these drugs ineffective.[3] Therefore, the identification and development of new drugs and delivery strategies is a highly active research field.[2]

The formulation of antibiotics as nanomedicines[4–7] has been widely studied to overcome the different limitations of the free drugs, such as toxicity, solubility and bioavailability associated with sustained drug release,[8] efficient mucus penetration[9] and the ability of some formulations, *e.g.* liposomes, to fuse with the bacterial cell envelopes.[10,11] Especially the liposomes have evolved as potent nanovehicles for antimicrobials.[6] Arikayce (Insmed, Inc.), the liposomal formulation of amikacin, has been recently approved by the FDA for the treatment of *Mycobacterium avium* complex (MAC) lung infections.

Liposomes are hollow microscopic spherical lipid-based nanoparticles.[12] They can be produced using various types of phospholipids to form lipid bilayers and supplementation with cholesterol changes fluidity and rigidity of the liposomal membrane. The advantage of liposomes responsible for their high popularity is the fact that diverse drugs covering a broad physicochemical property range can be encapsulated within liposomes. Relatively large amounts can be loaded into the inner sphere to overcome low drug solubility and provide stability under physiological conditions.

Moreover, the precise routing of a drug to the site of the disease can further improve the drug's availability at the diseased tissue and thereby increase pharmacodynamic efficacy. Thus, targeted drug delivery plays an important role in modern medicine for numerous diseases, such as tumors, infections and others. The increased local concentration of a targeted drug enables a decrease of total dosage and consequently a reduction of side effects.[13,14]

[a] Chemical Biology of Carbohydrates, Helmholtz Institute for Pharmaceutical Research Saarland, Helmholtz Centre for Infection Research, 66123 Saarbrücken, Germany. E-mail: alexander.titz@helmholtz-hzi.de
[b] Deutsches Zentrum für Infektionsforschung (DZIF), Standort Hannover-Braunschweig, 38124 Braunschweig, Germany
[c] Department of Chemistry, Saarland University, 66123 Saarbrücken, Germany
[d] Drug Delivery, Helmholtz Institute for Pharmaceutical Research Saarland, Helmholtz Centre for Infection Research, 66123 Saarbrücken, Germany
[e] Department of Pharmacy, Saarland University, 66123 Saarbrücken, Germany
[f] KIST Europe, 66123 Saarbrücken, Germany
[g] Department of Systems Engineering, Saarland University, 66123 Saarbrücken, Germany
[h] INM – Leibniz Institute for New Materials, 66123 Saarbrücken, Germany

† Electronic supplementary information (ESI) available. See DOI: 10.1039/d1tb02086b

Targeting of therapeutic molecules generally follows two approaches: covalent conjugation of drug and targeting ligand[15] or non-covalent drug encapsulation in surface-modified nanovehicles. The presence of a covalent bond between drug and targeting ligand has the advantage that fast dissociation and release of the untargeted drug is avoided. Careful conjugate design is important since the covalent modification of the drug can, on the other hand, also result in a loss of therapeutic activity. Prominent examples are antibody–drug conjugates used primarily in cancer and the recently approved cefiderocol, a cephalosporin antibiotic conjugated to a substrate for the bacterial cell uptake machinery. A comprehensive overview on conjugates of antimicrobials has recently been provided by Brönstrup and Klahn.[16]

Non-covalent drug encapsulation overcomes this hurdle since the targeting ligand is attached to the vehicle and the cargo remains unchanged. The widely used liposomes have another unique advantage due to their accessibility for chemical functionalization at the molecular level. Production of liposomes using varying ratios of targeted and untargeted lipids then allows the defined modification of the liposomal surface with targeting moieties.[17] It was demonstrated that functionalization of the liposomal surface with carbohydrate moieties is a powerful approach allowing to target certain types of human cells, such as hepatocytes[18,19] and various immune cells.[20,21] Rademacher *et al.* reported the delivery of vaccines to dermal Langerhans cells using a targeted liposome decorated with a glycomimetic ligand for binding to their surface receptor Langerin.[22] Additionally, the opportunity to use carbohydrate-decorated liposomes as vaccines against infections and cancer have been extensively studied in the last decade.[23–26] The high potency and efficacy of the liposomes functionalized with carbohydrate moieties in inhibiting corresponding lectins is provided by their multivalent interaction with the proteins, similar to those observed for other multivalent systems.[27] Rademacher *et al.* have further reported on heteromultivalent liposomes that enable efficient co-targeting of the same protein, *i.e.* DC-SIGN, through synergistic allosteric activation resulting in efficient binding to its carbohydrate recognition site.[28]

The targeting of antibiotics to biofilm-associated infections of *P. aeruginosa* is an active field of research. Extracellular and biofilm-associated proteins are the first potential targets encountered by an antimicrobial drug. Among many other biomolecules, *P. aeruginosa* expresses two extracellular lectins, LecA (PA-IL) and LecB (PA-IIL), that are crucial for establishing a mature biofilm structure.[29,30] These proteins are carbohydrate-binding agents with LecA recognizing galactosides and LecB binding firmly to mannosides and fucosides. Both lectins are secreted homotetrameric proteins, a property which allows to efficiently bind and cross-link numerous glycoconjugates, *e.g.* host cell surface glycans, bacterial surface polysaccharides and the various exopolysaccharides secreted by *P. aeruginosa*. In addition to the biofilm-deficient phenotypes of the individual genetic LecA or LecB mutants, the localization of LecB towards the surface of the biofilm has been experimentally demonstrated.[29–31] The resulting crosslinks between lectins and glycoconjugates are believed to be responsible for the stabilization of the biofilm matrix.[32] We and others have therefore previously used these lectins as targets for antibiofilm agents.[2,33–37] Our group has developed diverse glycomimetic inhibitors for LecA ranging from various galactosides to catechols[38–40] and for LecB originating from modified mannosides[35,41,42] and evolving into *C*-glycosidic sulfonamides.[35,36,43] Furthermore, we have shown that a LecA-directed fluorescein-conjugate of a covalently binding epoxygalactoheptose moiety can be used to image bacterial biofilms *in vitro*.[44]

These results and the current lack of new antibiotics encouraged us to further develop these glycomimetics into targeting moieties for antibiotic delivery. In a first work reported in 2020, we have covalently attached either galactosides targeting LecA or *C*-fucosides targeting LecB to the widely used antibiotic ciprofloxacin.[33] While we showed that these conjugates bind to the respective lectins, retain activity on their target bacterial gyrase, and are enriched at a biofilm compared to the parent antibiotic, their antibacterial activity has been reduced. This reduction is a consequence of the covalent modification of the drug that results in a decreased cellular uptake, and thus a reduced availability of the drug.

Here, we circumvented the covalent modification of the drug to be routed to the site of infection by developing new shuttles based on LecA- and LecB-targeted liposomes. These liposomes possess several copies of the targeting ligands on their surfaces which results in a multivalent presentation of these lectin ligands, leading to an increased affinity to their respective lectins.

Conventional methods to investigate the interactions between lectins and carbohydrates usually include fluorescence polarization assay (FP), enzyme-linked lectin assay (ELLA) and isothermal titration calorimetry (ITC).[27] Although all these methods demonstrated their reliability for quantifying the affinity of monovalent ligands, the possible aggregation of multivalent lectins in presence of multivalent ligands may affect the assay readout and therefore such results should be carefully interpreted. On the other hand, surface plasmon resonance (SPR) avoids aggregation and precipitation, but data evaluation and quantification can be cumbersome as a result of the various interaction models.[45]

Microfluidics has been an important tool for the development of *in vitro* systems surrounding biofilm formation, analysis and drug treatments, especially for those concerning the circulatory system.[46–48] The majority of the human circulatory system presents a laminar flow at a relaxed heart rate, in accordance to the low Reynolds number resulting from the small diameters of blood vessels.[49] Medium sized arteries range from 0.8 mm to 1.8 mm in diameter and experience a blood flow rate of 3 mL min^{-1} at a relaxed heart rate, whilst corresponding veins experience 1.2 mL min^{-1} at a relaxed heart rate.[50] Such diameters and flow rates compute to Reynolds numbers that should only reach around 2000 during mild exercise, which represents the transitional phase in a perfect undeformed channel. As such, microfluidic systems are ideal for mimicking the laminar flow within blood vessels at flow rates similar to a relaxed heart rate.[51,52]

We therefore developed a microfluidic system as a reductionistic model for a biofilm infection and intravenous liposome administration. We demonstrated that the targeted liposomes are specifically retained on a lectin-coated surface from a passing liquid stream. The loading of unmodified antibiotics into these targeted liposomes will further avoid the previously observed reduction of their pharmacodynamic effects, which was induced by the previous covalent conjugation.

Results and discussion

Synthesis of phospholipid–lectin ligand conjugates

Phospholipids are the main building blocks of liposomes. To obtain lectin-targeted phospholipids, we developed a synthetic route for the covalent conjugation of phospholipids with lectin ligands. Here, the two designed lectin-targeting groups were based on our previous reports on lectin inhibitors:[35,36,39] the LecA-targeted ligand **8** (Scheme 1) consists of a β-linked galactoside carrying an aromatic aglycon and a thioglycosidic linkage for increased stability, while the LecB targeting ligand **15** (Scheme 2) is based on a hybrid-molecule between the two LecB ligands, mannose and fucose, and is further modified with a phenylsulfonamide substituent. For both cases, the aryl moiety is substituted in its *para*-position where the phospholipid can later be attached *via* amide bond formation (Scheme 3).

For the synthesis of the LecA–ligand **8** (Scheme 1) β-D-galactose pentaacetate was reacted with 4-nitrothiophenol in a triflic acid-mediated glycosylation in 66% yield. The nitro group in **2** was then reduced using Pd/C and hydrogen to give aniline **3** quantitatively. Bromoacetylation of the per-*O*-acetylated aniline, followed by nucleophilic substitution of the bromide with sodium azide gave **6** in 73% yield over two steps. The latter compound was then hydrogenolytically reduced to amine **7** which was finally deacetylated under Zemplén conditions to provide LecA–ligand **8** in near quantitative yields.

Sulfonamide derivatives of *C*-fucosides demonstrate high affinity to LecB[35,36] and they were therefore chosen as suitable ligands for targeting liposomes. Starting from L-fucose, the *C*-glycoside was installed *via* a Henry[43,53] reaction with nitromethane to give **9** in 49% yield (Scheme 2). Catalytic hydrogenation of the nitro group gave amine **10** which was then transformed into sulfonamide **11** with 4-nitrophenylsulfonyl chloride and triethylamine. A second hydrogenation step yielded aniline **12** which was directly bromoacetylated. Crude **13** was

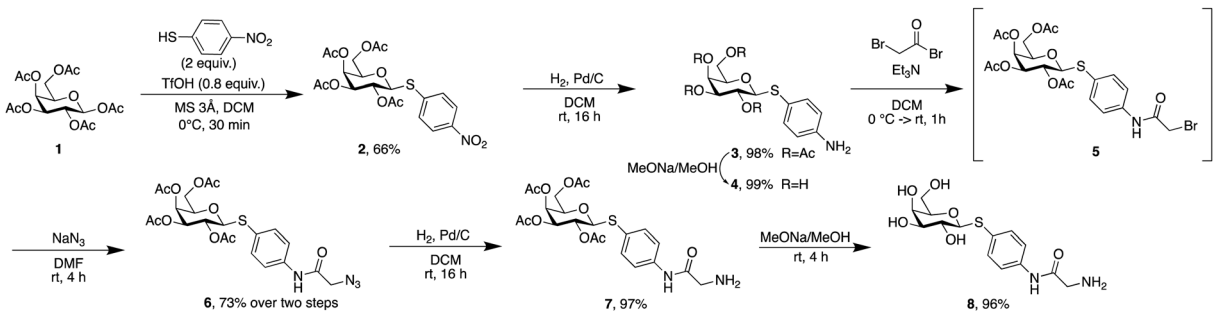

Scheme 1 Synthesis of the LecA-targeting ligand thiogalactoside **8**.

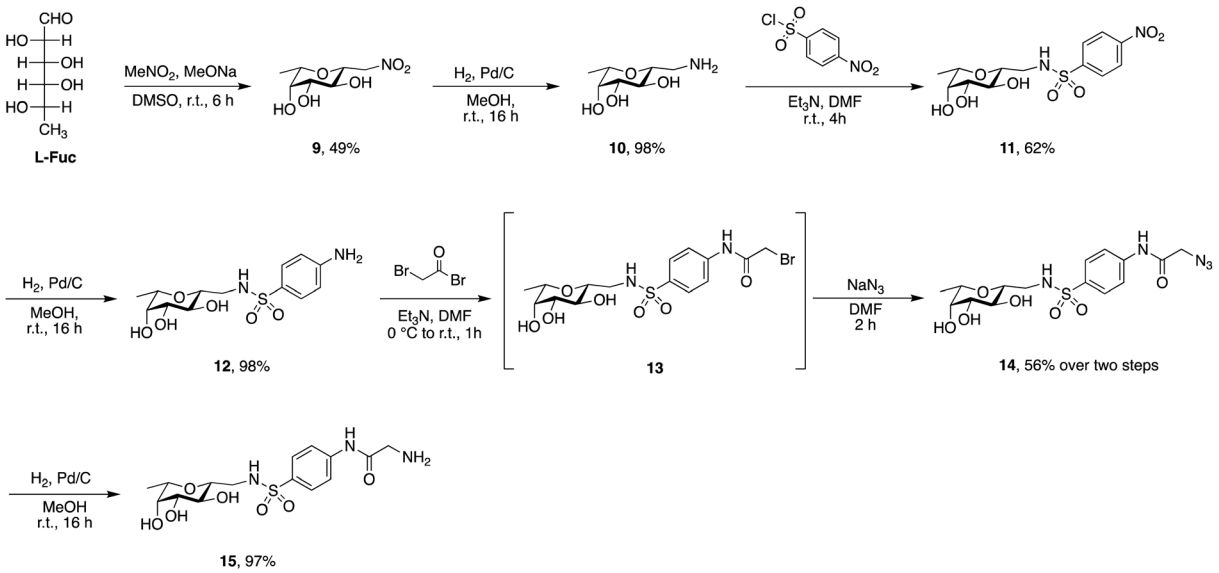

Scheme 2 Synthesis of the LecB-targeting ligand *C*-fucoside **15**.

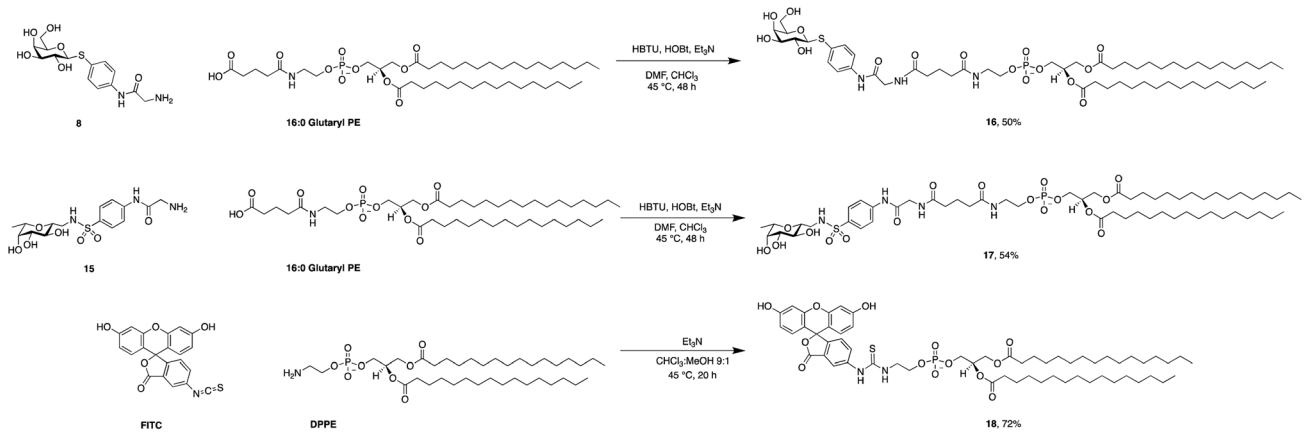

Scheme 3 Synthesis of phospholipid conjugates: lectin-targeted lipids **16** and **17** and fluorescein-labelled lipid **18**.

subjected to a nucleophilic substitution with sodium azide to give *C*-fucosylated azide **14** in 56% yield over two steps. A third catalytic hydrogenation yielded amine **15** quantitatively.

Then, both carbohydrate-based targeting ligands, **8** and **15**, were coupled to phospholipids in order to graft the targeting ligands onto the surfaces of the liposomes. The chosen lipid for conjugation was 1,2-dipalmitoyl-*sn-glycero*-3-phosphoethanolamine (16 : 0 PE) which was modified as an amide with glutaric acid. This 16 : 0 glutaryl phosphoethanolamine (16 : 0 glutaryl PE) offers one carboxylic acid available for conjugation with the targeting ligands. The amide bond between this carboxylic acid and the amine of the corresponding glycomimetics **8** and **15** was established using HBTU/HOBt to give conjugates **16** and **17**. Optimization of the reaction conditions revealed a mixture of chloroform and dimethylformamide (ratio 2 : 1) as an optimal solvent for this reaction. The use of HOBt is crucial for the success of the reaction since the intermediate active ester of the phospholipid ensures complete solubility. Purification of **16** and **17** was successful when performed under reverse phase chromatography using a C18-column and a gradient of the solvents isopropanol/water/MeOH (ratio 5 : 4 : 1) and isopropanol, both supplemented with 0.2% formic acid. Furthermore, fluorescein isothiocyanate was conjugated with 16 : 0 PE in compound **18** as a tool to produce fluorescently labelled liposomes.

Preparation and characterization of lectin-targeted liposomes

With the various lipids in hand, an array of liposomes was produced using DSPC/cholesterol and various ratios of targeting ligands **16** and **17** and incorporation of fluorescein-containing lipid **18** (Table 1). All liposomes were prepared by mixing the corresponding lipids at the indicated ratios followed by their self-assembly *via* thin-film hydration and extrusion. In general, the sizes of all liposomes were comparable at approx. 200 nm (range 176–208 nm) (Fig. S1, ESI†) with a rather low polydispersity index ranging from 0.077 to 0.158. All liposomes showed a negative zeta potential in the range of −20 to −52 mV.

With the liposomes in hand, we first studied their binding to the lectins LecA or LecB in established competitive binding assays[39–41] (Fig. 1). The specificity of the LecA-targeted liposomes carrying glycolipid **16** for LecA and the LecB-targeted liposomes carrying glycolipid **17** for LecB was established, untargeted plain liposomes were added at comparable DSPC/Chol concentrations and showed no sign of inhibition. Monovalent non-lipidated controls **4** and **12** have further been included for referencing the increase in affinity due to their multivalent presentation on the liposomal surface. Furthermore, the impact of the targeting ligand's surface density on target binding was also studied using liposomes with 1% or 15% (w/w) of the phospholipids carrying the lectin-targeted ligand. In all cases, a concentration-dependent

Table 1 Characterization of various liposomes with different lipid composition. All fluorescently labelled liposomes contain 1% phospholipid **18**. Chol = cholesterol, DSPC = 1,2-distearoyl-*sn-glycero*-3-phosphocholine

Type	Formulation	Mass ratio	Size (nm)	PdI	Zeta (mV)	Particle concentration (particles per mL)
Plain	DSPC : Chol	2 : 1	207 ± 4	0.133 ± 0.024	−20 ± 0.5	
Plain, fluorescent	DSPC : **18** : Chol	2 : 0.02 : 1	208 ± 2	0.077 ± 0.018	−43 ± 0.2	$1.55 \times 10^8 \pm 7.90 \times 10^6$
LecA-targeted, 1% **16**	DSPC : **16** : Chol	1.98 : 0.02 : 1	203 ± 3	0.158 ± 0.008	−29 ± 1	
LecA-targeted, 15% **16**	DSPC : **16** : Chol	1.7 : 0.3 : 1	194 ± 6	0.149 ± 0.011	−51 ± 2	
LecA-targeted, 1% **16**, fluorescent	DSPC : **16** : **18** : Chol	1.96 : 0.02 : 0.02 : 1	182 ± 2	0.149 ± 0.015	−32 ± 0.2	
LecA-targeted, 15% **16**, fluorescent	DSPC : **16** : **18** : Chol	1.68 : 0.3 : 0.02 : 1	186 ± 2	0.097 ± 0.044	−46 ± 2	$7.35 \times 10^8 \pm 4.38 \times 10^7$
LecB-targeted, 1% **17**	DSPC : **17** : Chol	1.98 : 0.02 : 1	202 ± 2	0.131 ± 0.022	−31 ± 2	
LecB-targeted, 15% **17**	DSPC : **17** : Chol	1.7 : 0.3 : 1	208 ± 1	0.102 ± 0.004	−49 ± 3	
LecB-targeted, 1% **17**, fluorescent	DSPC : **17** : **18** : Chol	1.96 : 0.02 : 0.02 : 1	176 ± 1	0.111 ± 0.02	−40 ± 2	
LecB-targeted, 15% **17**, fluorescent	DSPC : **17** : **18** : Chol	1.68 : 0.3 : 0.02 : 1	204 ± 1	0.099 ± 0.035	−52 ± 1	$5.65 \times 10^8 \pm 7.60 \times 10^7$

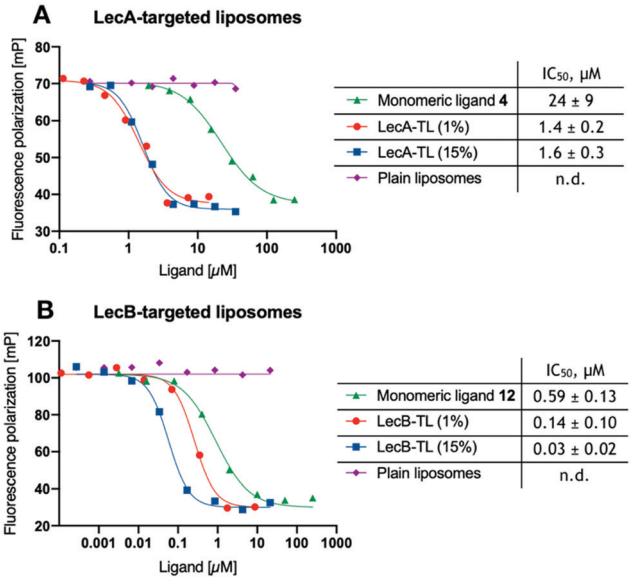

Fig. 1 Competitive binding of lectin-targeted liposomes to LecA (A) or LecB (B). Plain liposomes do not contain targeting ligand and have therefore been used at total lipid concentrations comparable to the targeted liposomes (TL). IC_{50}s for liposomes are normalized and depicted per targeting group, *i.e.* the affinity of a liposome carrying several copies of the targeting ligand is much higher. Averages and standard deviations from at least 3 independent experiments of technical triplicates each.

inhibition curve was obtained for the targeting liposomes or the controls **4** and **12** with their corresponding lectins (Fig. 1).

To obtain comparable IC_{50} values after curve fitting, those values of the targeted liposomes were normalized to the molar concentration of lectin-targeted phospholipids **16** and **17**. The concentration of the targeting ligands was quantified by LC-MS using a calibration curve for **16** and **17**. The inhibition of both lectins with the targeted lipids displayed multivalently in the liposomes showed a significant boost compared to the free monomeric ligands **4** or **12**. While the increase in relative potency was over 15-fold for LecA, it reached a nearly 20-fold increase for LecB. Surprisingly, varying the ligand density from 1% to 15% LecA-targeted lipid **16** did not change the molar inhibition, which could be an intrinsic trait of these liposomes or a result of having possibly reached the assay wall of these very potent multivalent systems. In contrast the increase of LecB-targeting lipid **17** from 1% to 15% in the resulting liposomes led to a further increase in normalized affinity.

The interaction of multivalent ligands with multivalent receptors often leads to oligomerization induced aggregation. In the present case, the targeted liposomes constitute a highly multivalent ligand system interacting with tetravalent lectins. To analyze the effect of aggregation the liposomal solutions were studied in presence of the corresponding lectins using dynamic light scattering (DLS) and with fluorescently labelled liposomes by nanoparticle tracking analysis (NTA) or fluorescence microscopy.

Liposomes containing 0, 1 or 15% LecA- or LecB-targeted phospholipids at a total lipid concentration of 800 μg mL^{-1} in aqueous buffer were incubated with LecA or LecB at varying concentrations (Fig. 2). Subsequently, these mixtures were diluted 1 : 10 with buffer and analyzed by DLS to determine *Z*-average size and polydispersity index (PdI) of the particle solution. The average size of plain liposomes did not change with increasing lectin concentration, while the observed average sizes of lectin-targeted liposomes increased from 200 nm to larger than 1 μm with increasing LecA concentrations as a consequence of multivalency-induced aggregation. Finally, aggregates became colloidally unstable and precipitated.

For further analysis of the liposome/lectin interaction, we produced LecA-, LecB-, and untargeted liposomes spiked with 1% of the fluorescent lipid **18**. The aggregation of targeted

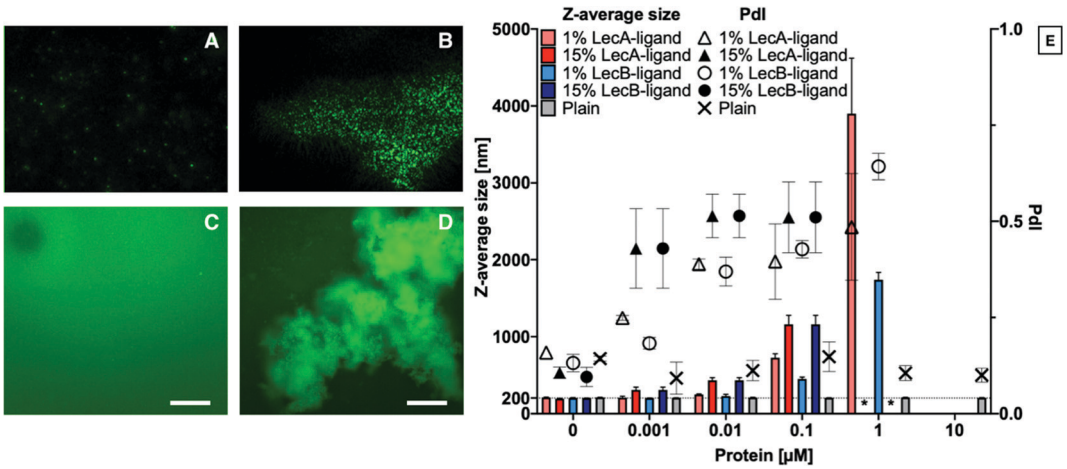

Fig. 2 Lectin-targeted liposomes are specifically aggregated with lectins in solution. (A) Plain liposomes and (B) LecB-targeted liposomes preincubated with LecB for 30 min, protein to targeting ligand molar ratio of 2 : 1 – images taken with a NTA camera; (C) plain liposomes and (D) LecA targeted-liposomes incubated with LecA for 15 min – images were taken by fluorescence microscope; (E) correlation of *Z*-average size and polydispersity index (PdI) of LecA- or LecB-targeted and plain liposomes and the concentration of the corresponding lectin. Increase of the protein concentration led to liposomal aggregation. * – sample precipitated, in case of 10 μM lectin concentration all lectin-targeted samples precipitated. Averaged values from 2 independent experiments with 6–12 technical replicates, error bars correspond to standard deviation. For C and D: scale bar corresponds to 200 μm.

liposomes with their lectins in solution was studied using fluorescence detection methods, such as NTA and fluorescence microscopy. The clearly observable aggregation for the system LecA/LecA-targeted liposomes analyzed by DLS (Fig. 2E), could be confirmed using NTA analysis where no aggregation of the fluorescently spiked plain liposomes was observed whereas the LecA-targeted analogs showed aggregation (Fig. 2A and B). Due to the related tetrameric structure of LecB, a similar tendency of LecB-targeted liposomes to aggregate in presence of LecB was observed using fluorescence microscopy while plain liposomes remained stably dispersed and were not aggregated by either of the lectins (Fig. 2A and C–E).

The lectin-targeted liposomes are designed to attach to the biofilm of *P. aeruginosa* in the infected patient and release their antibiotic cargo at the site of the infection. Clearance mechanisms are enhanced by the dynamic flow of body fluids, *e.g.* in the vascular system. To analyze the successful targeting of liposomes under flow, we developed a model system where the lectins LecA or LecB have been immobilized onto an abiotic surface and the specific retention of the liposomes onto this surface was analyzed under flow conditions *in vitro*.

For this purpose, we engineered a polydimethylsiloxane (PDMS)–glass microfluidic device system that consisted of four flow cells upon the same hydrogel-coated support as shown in Fig. 3. 3D printing was implemented in the production of the devices to allow for rapid prototyping of different architectures of devices at a vastly reduced cost compared to other methods. Only the PDMS was plasma treated to avoid damaging the hydrogel prior to experimentation. This treatment resulted in weaker bonding between the glass and PDMS, which was mitigated by using epoxy sealant around the flow cell. We chose multiple cells on the same support to allow for simultaneous experiments and comparison between the cells without needing to compensate for hydrogel variation between different devices. Separation of the four cells also eliminated any opportunity of cross contamination between experiments and interfering illumination from neighbouring cells. PDMS was chosen due to its optical transparency (Fig. S3, ESI†) and chemical inertness to the liposomes and other capillary treatments within this work, thus removing the possibility of residual liposome adsorption hence eliminating background noise. Flow cells channel dimensions were designed to be approximately 5.75 × 1 × 0.5 mm (length × width × depth), with a corresponding volume of 2.82 μL (Fig. S2, ESI†). These dimensions were chosen to mimic medium to small arteries/veins found *in vivo*. Flow cells ruptured with flow rates above 2.4 mL min^{-1}. Laminar flow was observed throughout all experimentation, with flow rates up to 500 μL min^{-1}. Therefore; the fabricated devices were suitable for modeling flow through similar sized veins at low flow rates.

The obtained flow channels were subsequently coated with the lectins LecA or LecB *via* covalent amide coupling to the *N*-hydroxysuccinimide ester activated glass slide surface. After thorough equilibration of the lectin-coated surfaces with buffer to remove blocking agent and unbound proteins, fluorescent LecA-, LecB- or untargeted liposomes were injected and the flow cell was imaged by confocal fluorescence microscopy (Fig. 4 and 5).

Surface targeting-ligand density can be an important factor for targeted nanomaterials and their interaction with their receptors. Since the targeted lectins are multivalent, varying ligand density may affect binding and thus targeting efficiency. For the above described competitive binding assay (Fig. 1), aggregation induced by the multivalent ligand/receptor system is also likely to occur as demonstrated by DLS and fluorescence detection in solution (Fig. 2). Because the lectins are covalently bound to the surface in the microfluidics system, aggregation induced precipitation from the solution is reduced and the observed bound fluorescence intensity directly correlates to the strength of the targeting efficiency which allows to study the influence of the targeting ligand density.

With the appropriately coated microfluidics device in hand, we studied the targeting effects of the various fluorescent liposomes with different targeting ligand densities, *i.e.* 1% or 15% of the targeted phospholipids **16** and **17** (Fig. 4 and 5). To assess the carbohydrate-dependency of the targeting process, the competitive inhibition of their interaction with the lectin-coated

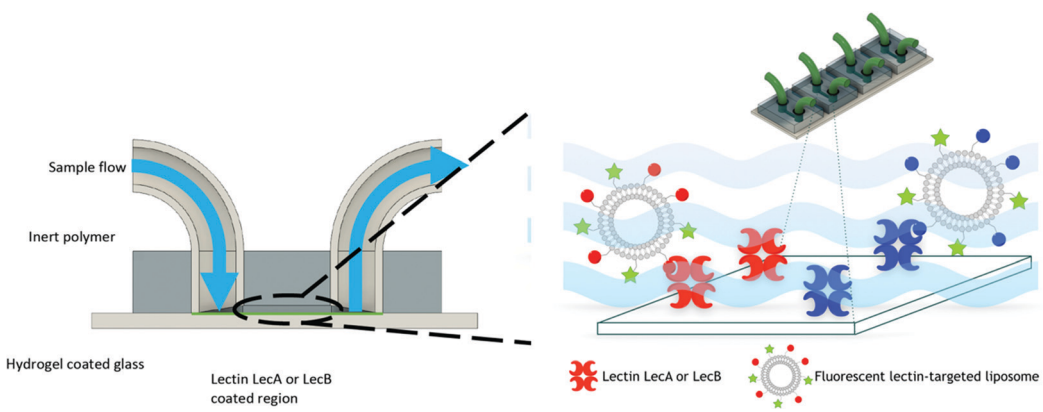

Fig. 3 Concept of the *in vitro* microfluidic device. Fluorescent lectin-targeted liposomes interact with the proteins LecA or LecB that have been covalently immobilized on the glass surface. The liposomes are retained on the surface due to their specific ligand–lectin interaction and targeting was quantified by microscopy.

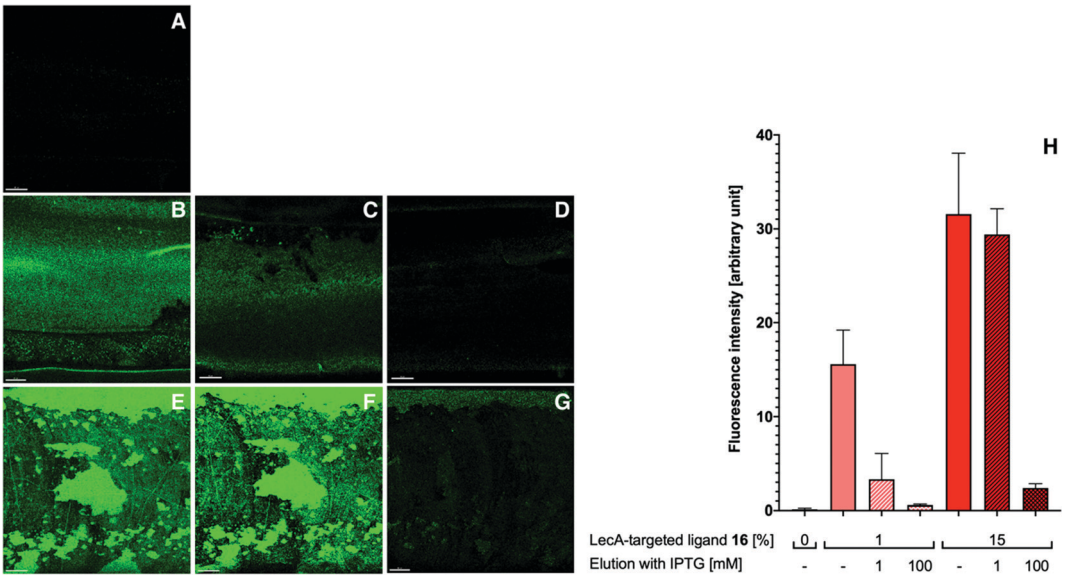

Fig. 4 Targeting liposomes to a LecA-coated surface under flow. Injection of liposomes (5 min) and analysis by confocal microscopy after washing out unbound liposomes with buffer (5 min): Fluorescent liposomes without targeting ligand (A); fluorescent liposomes with 1% LecA-targeted phospholipid **16** (B); fluorescent liposomes with 1% LecA-targeted phospholipid **16** eluted with 1 mM IPTG (C) and 100 mM IPTG (D); fluorescent liposomes with 15% LecA-targeted phospholipid **16** (E); fluorescent liposomes with 15% LecA-targeted phospholipid **16** after elution with 1 mM IPTG (F) and 100 mM IPTG (G); quantification of the interaction between LecA-targeted liposomes with LecA-modified surface under flow conditions. Averages from 3 independent experiments with 9–12 technical replicates, error bars correspond to standard deviation. For A–G: scale bar = 50 μm.

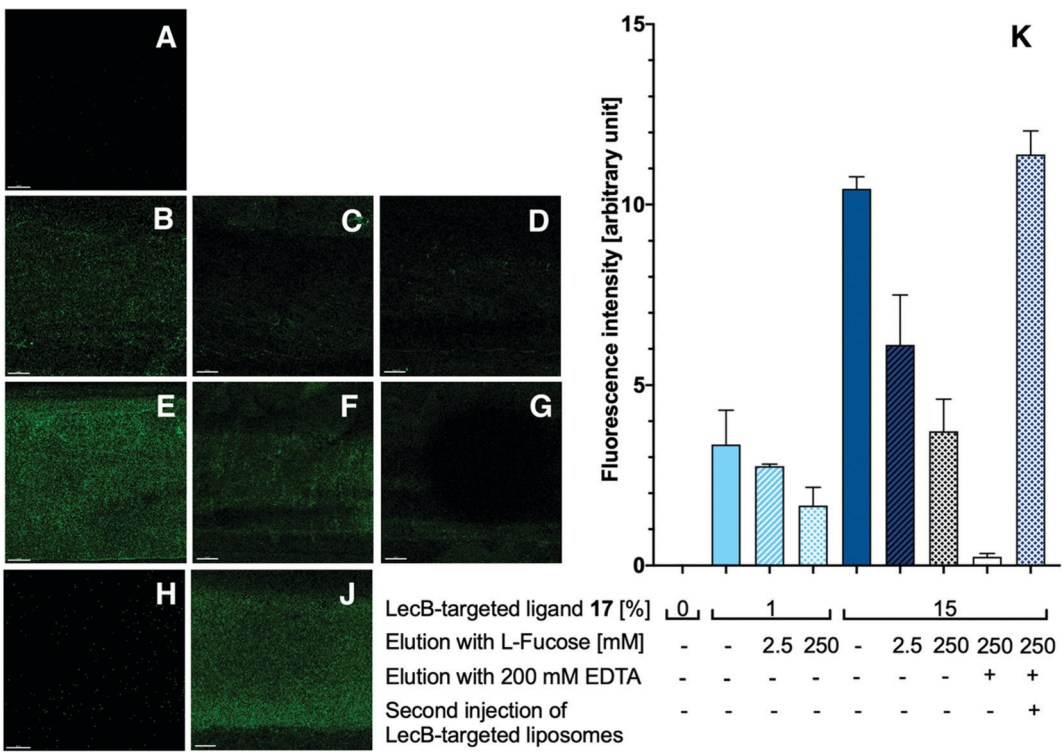

Fig. 5 Targeting liposomes to a LecB-coated surface under flow. Injection of liposomes (5 min) and analysis by confocal microscopy after washing out unbound liposomes with buffer (5 min): Fluorescent liposomes without targeting ligand (A); fluorescent liposomes with 1% LecB-targeted phospholipid **17** (B); fluorescent liposomes with 1% LecB-targeted phospholipid **17** eluted with 2.5 mM L-fucose (C) and 250 mM L-fucose (D); fluorescent liposomes with 15% LecB-targeted phospholipid **17** (E); fluorescent liposomes with 15% LecB-targeted phospholipid **17** after elution with 250 mM L-fucose for 5 min (F) and 10 min (G); fluorescent liposomes with 15% LecB-targeted phospholipid **17** eluted with 200 mM EDTA to regenerate the glass surface (H); regenerated chamber after equilibration with PBS/Ca for 10 min and repeated injection of the liposomes with 15% LecB-targeted phospholipid **17** (J); quantification of the fluorescence image analyses to assess the interaction between LecB-targeted liposomes with LecB-coated surface using the microfluidic device (K). Averages from 3 independent experiments with 9–12 technical replicates, error bars correspond to standard deviation. Scale bars correspond to 50 μm.

surfaces was studied after addition of isopropyl β-D-thiogalactoside (IPTG) for LecA or L-fucose for LecB. Fluorescence intensities of all recorded images were further measured and the effects could be quantified.

Drastic differences in fluorescence intensities were measured between targeted and plain liposomes for the respective lectins. In case of the glycomimetic-functionalized liposomes, the targeting to lectin-coated surfaces was highly stable under flow conditions as detected by the remaining strong fluorescence signal even after continuous washing with buffer for 1 h. In contrast, plain liposomes were fully removed indicating that the interaction between liposomes and the coated surfaces is carbohydrate-dependent.

In both cases, an increase in targeting ligand density from 1% to 15% significantly increased the detected fluorescence signal. This observation suggests that liposomes containing 15% of the targeting ligand are more efficient in both cases. Furthermore, a tendency to also form aggregates on the lectin-coated surface was observed for the more densely decorated LecA-targeted liposomes in particular. The latter corresponded to the increased efficacy of the multivalent interaction for LecA when compared to the monovalent ligand in the competitive binding assay. In case of LecB, differences in fluorescence intensity between 1% and 15% targeted liposomes could be observed, but the aggregation was significantly lower than for LecA and a more homogenous distribution of the liposomes along the entire channel was observed. Apart from the unknown quantity of immobilized lectin, one explanation for this phenomenon is the different spatial orientation of binding sites in the LecB tetramer which disfavors simultaneous binding compared to LecA where the sites are adjacent and optimally oriented for the multivalent binding to a surface localized pair of ligands.

The carbohydrate specificity of the interaction between lectin-targeted liposomes and surface-attached lectins was confirmed by the efficient removal of LecA-targeted liposomes after injection of IPTG or LecB-targeted liposomes after injection of L-fucose (Fig. 4G and 5G). The displacement of LecB-targeted liposomes was difficult and required increased amounts of competitive inhibitor L-fucose (>250 mM) compared to an efficient displacement of the LecA-targeted system and its competitor IPTG (100 mM), which is in agreement with the increased binding affinity of LecB towards its ligands compared to LecA. Regeneration of the lectin-coated microfluidics channels was achieved washing with 200 mM aqueous EDTA and after re-equilibration with calcium(II)-containing buffer, the system could be reused for analysis (Fig. 5J and K).

With the data from the competitive binding assay and the microfluidic flow assay with optical detection, we clearly observed a specific binding of the targeted liposomes to their lectin targets and a good retention under flow conditions. Both of these observations indicate our targeted liposome's potential for applications.

However, in both of these assays, we could not quantify the binding affinity of the targeted liposomes for their lectins, since it is likely that the lower assay limit was reached for the competitive binding assay (Fig. 1). Therefore, we established a surface-plasmon resonance experiment with LecA-targeted liposomes and surface-immobilized LecA. Carboxylic acids present on hydrophilic SPR chips were activated and LecA was immobilized at high density through amide coupling. To validate the system, the monovalent LecA ligand *para*-nitrophenyl β-D-galactoside (pNP-Gal) was injected in a multicycle experiment at concentrations ranging from 1.56 to 400 μM (Fig. 6A and B). Fast association (k_{on} = 4.32 × 10^3 M^{-1} s^{-1}) and dissociation kinetics (k_{off} = 0.0831 s^{-1}) were determined and equilibrium analysis revealed a K_d of 17.9 μM which is in agreement with literature reports (ITC: K_d = 14.1 μM, competitive binding assay IC_{50} = 19.0 μM).[39,54,55]

Subsequently, we tested LecA-targeted liposomes decorated with 15% of targeting ligand **16** on the same SPR chip (Fig. 6C and D). The LecA-targeted liposomes were injected at a calculated concentration of **16** ranging from 2 to 250 μM in a multicycle experiment. Strongly different sensorgrams were obtained indicating a slow association and a virtually absent dissociation from immobilized LecA. In fact, regeneration of the chip surface required the use of EDTA and the presence of a detergent for

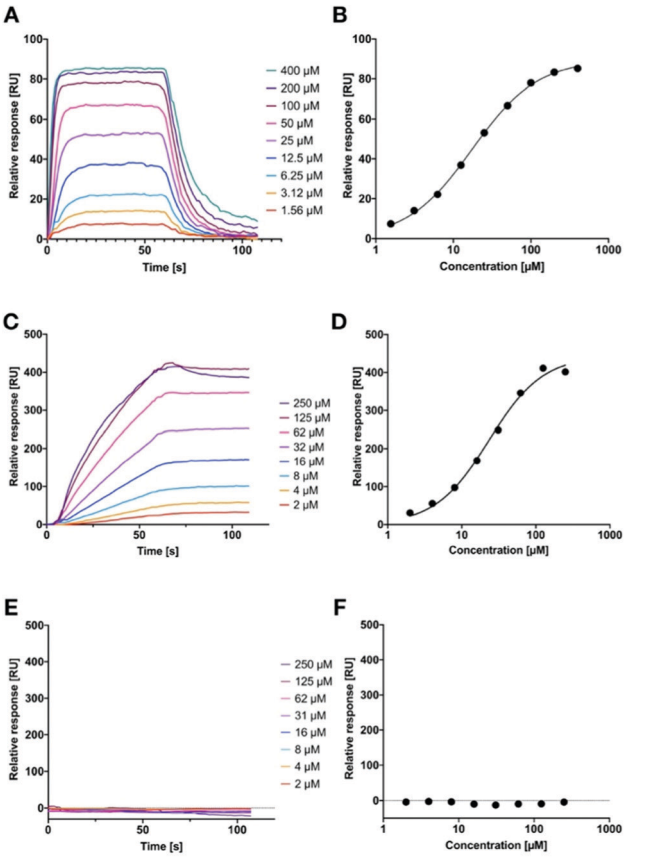

Fig. 6 Surface plasmon resonance analysis of the interaction of surface-immobilized LecA with pNP-Gal (A and B) or 15% LecA-targeted liposomes alone (C and D) and in presence of 50 mM IPTG in the running buffer as competitor (E and F). SPR sensorgrams are shown in (A), (C) and (E); indicated concentrations correspond to the monovalent pNP-Gal in (A and B), and the targeted phospholipid in (C–F); maximal obtained response for the different concentrations is plotted for affinity analysis in (B), (D), and (F).

efficient liposome removal. The association of the liposomes with the surface was so slow that it did not reach a saturation within 60 seconds of injection time, and further extension of the association phase to 120 seconds did also not lead to saturation (120 s data not shown). We also studied binding kinetics at a higher flow rate of 100 μL min^{-1} and did not observe mass transport effects impacting the binding of the liposomes with immobilized LecA (Fig. S5A, ESI†).[45] Thus, the affinity analysis was performed on the highest response obtained and indicated a comparable affinity per molecule of targeting ligand to pNP-Gal. However, these fitting data must be considered with care as no saturation was achieved and they also contradict the approx. 20-fold higher potency of inhibition in the competitive binding assay. It can nevertheless be generalized, that these LecA-targeted liposomes are very potent binders, which once trapped at their surface-exposed target LecA will not detach again for very long time spans (Fig. S5B, ESI†). This fact can be assigned to their highly multivalent binding and provides an excellent basis for future use of the liposomes for targeted antibiotic delivery and furthermore for infection imaging experiments.

Since we could not reach saturation with the targeted liposomes, we tested the specificity of their binding to the surface in presence of a small galactoside as inhibitor of the LecA binding sites. The chip was now equilibrated with running buffer containing 50 mM IPTG and the injection of the liposomes was repeated as before (Fig. 6E and F). In presence of IPTG, the LecA-targeted liposomes did not bind to the LecA-surface in the SPR experiment. In addition, the LecB-targeted liposomes were also tested on the LecA-chip and no binding was detected (Fig. S4, ESI†). Both observations are further corroborating the high carbohydrate specificity of binding.

Conclusions

In conclusion, we have developed highly specific and highly potent nanovehicles for the targeting of biofilm associated lectins of *P. aeruginosa*, LecA and LecB. After coupling synthetic glycomimetics to phospholipids, a set of LecA- and LecB-targeted liposomes with varying lipid composition have been produced and characterized. These targeted liposomes showed high specificity to their respective targets and exhibited very strong carbohydrate-dependent binding to surfaces coated with these lectins. Microscopic analysis of targeted fluorescent liposomes in a microfluidic device demonstrated their potential for imaging applications. Future work will address the use of these targeted delivery systems for antibiotic delivery to break antimicrobial resistance and reduce toxicity of untargeted drugs.

Materials and methods

General methods, chemical synthesis and NMR spectra can be found in the ESI.†

Preparation and characterization of liposomes

For liposome preparation 20 mg phospholipids and 10 mg cholesterol were dissolved in a 5 mL mixture of chloroform/methanol 2 : 1. Targeting lipids **16** or **17** and/or fluorescein labelled lipid **18** were added at the indicated ratios. After complete removal of organic solvents using a rotary evaporator under reduced pressure at 70 °C, the obtained thin lipid film was hydrated with 5 mL PBS/Ca buffer (20 mM Tris, 137 mM NaCl, 2.6 mM KCl at pH 7.4 supplemented with 1 mM $CaCl_2$), under rotation for 1 h at 65 °C followed by sonication for 30 sec at 65 °C. The resulting colloidal solution was extruded 10 times through a 0.2 μm pore size polycarbonate membrane (Polycarbonate track-etched membrane, Sartorius, Germany) at 70 °C *via* a Lipofast L-50 extruder (Avestin, Germany). For DLS analysis, the obtained liposomes were diluted 100-fold in MilliQ water to determine the *Z*-average size and polydispersity index (PdI) by dynamic light scattering (DLS) and measure the ζ-potential by electrophoretic light scattering using a Zetasizer Nano ZS (Malvern Panalytical Ltd, UK). Data are presented in Table 1. To measure the exact concentration of the LecA- or LecB-targeting ligands in the obtained solutions, liposomes were diluted 100-fold in MeOH and analyzed by LC-MS using the solvent system A: iPrOH/MeOH/H_2O (5 : 4 : 1) + 0.05% HCOOH, B: iPrOH + 0.05% HCOOH and a gradient of 5–40% B.

Imaging of liposomes using cryo transmission electron microscopy

Cryo-TEM imaging of the obtained liposomal solutions was conducted by placing a 3 μL droplet of the liposomal solution onto a S147-4 holey carbon film (Plano, Germany) before blotting the sample to a thin liquid film for 2 s and plunging into liquid ethane at T = 108 K using a Gatan (Pleasonton, USA) CP3 cryo plunge system. The vitrified sample was transferred under liquid nitrogen to a Gatan model 914 cryo-TEM holder and visualized at T = 100 K using a JEOL (Akishima, Japan) JEM-2100 LaB6 TEM operating at an accelerating voltage of 200 kV at low-dose conditions. Images are shown in Fig. S1 (ESI†).

Quantification of nanoparticle concentration and stability

Sizes and concentrations of the fluorescent liposomes were determined by nanoparticle tracking analysis (NTA, LM-10, Malvern, UK). Samples at a total phospholipid concentration of 4 mg mL^{-1} were diluted 1 : 10.000 in PBS/Ca, 200 μL aliquots were injected into a chamber illuminated by a laser beam at 532 nm and three 30 sec long videos were recorded. The data were processed and analyzed using NanoSight 3.1 software.

Additionally, LecB-targeted fluorescent liposomes (15% phospholipid **17**) in PBS/Ca were incubated with LecB (molar ratio ligand/protein 1 : 1, corresponds to 50 μM), for 1 h at 37 °C and the obtained mixture was diluted 1 : 10.000 in PBS/Ca and studied by NTA as described above (Fig. 2A and B).

Competitive binding assay

The procedure for fluorescence polarisation-based competitive binding assays for both lectins, LecA and LecB, was adopted

form Joachim *et al.* for LecA and Sommer *et al.* for LecB.[39,56] The assay was performed in PBS/Ca^{2+} buffer (20 mM Tris, 137 mM NaCl, 2.6 mM KCl at pH 7.4 supplemented with 1 mM $CaCl_2$). The final protein concentrations in the assays were 1 μM for LecA or 20 nM for LecB. Fluorescence intensities were recorded on a PheraStar FS plate reader (BMG Labtech GmbH, Germany) and polarization was calculated and plotted. IC_{50} values were obtained from a four-parameter curve fitting procedure. Averages and standard deviations were calculated from at least three independent experiments of technical triplicates each. pNP-Gal was used as a positive control and the obtained IC_{50} was 21 ± 6 μM, which agrees with literature data.[39]

Microfluidics device preparation

The design and dimensions of the microfluidic device is shown in Fig S2 (ESI†). Instrumentation: 3D computer aided drawings were drawn on Autodesk Fusion 360 (Autodesk, California, USA), exported as .STL files and sliced into GCode by Ultimaker Cura (Ultimaker, Utrecht, Netherlands) and printed using a fused filament 3D printer (Ultimaker2 Extended+, Ultimaker, Utrecht, Netherlands). All molds were printed with a 0.25 mm nozzle. The print speed was 20 mm s^{-1}, layer height was 0.1 mm, print temperature was 210 °C, bed temperature was set to 60 °C. A PICO low pressure plasma system (Diener Electronic GmbH & Co. KG, Ebhausen, Germany) was used for the plasma treatment of PDMS. Device fabrication: Molds were fabricated by the direct 3D printing of PLA onto cleaned microscope slides. The print height of the first layer on the glass slide was adjusted by the height of the microscope slide used, typically 100 μm plus 10 μm for nozzle clearance. The total print time of the mold was two hours and 29 minutes. PDMS was prepared in a 10 : 1 ratio (polymer : crosslinker) by weight. The PLA-glass mold was then sealed with hot glue and then filled with PDMS. The PDMS was left to cure overnight at 40 °C. The PDMS was then removed from the mold and was cleaned with isopropanol and deionized water. The PDMS was then plasma treated with oxygen, 350 W for 1 minute and immediately brought into contact with the NHS-activated glass slide (SL HCX, XanTec bioanalytics GmbH, Düsseldorf, Germany). The PDMS–glass device was then placed under a 2 kg mass and baked for 2 hours. Epoxy glue was applied to the PDMS–glass edge to help secure and avoid the peeling off of the PDMS. Silicone tubing was then inserted into the inlets/outlets and sealed in place with black PDMS and left to cure at 40 °C for 1 hour or longer if not cured. Devices were sterilized with ethanol and dried before use.

In vitro flow assay preparation

The microfluidics device was assembled as described above. For rehydration of the hydrogel surface, each channel was rinsed with MilliQ H_2O (500 μL min^{-1}, 10 min). Then, the channel was loaded with LecA or LecB (140 μM) in 10 mM sodium acetate buffer pH 4.5 and incubated for 90 min at room temperature. The channels were consequently treated with 1 M ethanolamine hydrochloride at pH 8.5 in MilliQ water (500 μL min^{-1}, 15 min) followed by reequilibration of the channels with PBS/Ca buffer (500 μL min^{-1}, 45 min).

For the experiments with fluorescently labelled liposomes, the corresponding channel was flushed with a solution of targeted or plain fluorescein-labelled liposomes (total phospholipid concentration = 70 μg mL^{-1}) in PBS/Ca buffer (500 μL min^{-1}, 5 min) followed by elution of unbound material with PBS/Ca buffer (500 μL min^{-1}, 10 min). To test for carbohydrate-dependent elution, a channel with bound targeted liposomes was additionally rinsed with a solution of the respective competitive inhibitor (IPTG for LecA or L-fucose for LecB) dissolved at the indicated concentrations in PBS/Ca buffer (500 μL min^{-1}, 10 min).

Confocal fluorescence microscopy

Fluorescence images were acquired immediately after eluting unbound material from the channel with PBS–Ca^{2+}-buffer with a Leica DMi8 Confocal Fluorescence Microscope (Leica Microsystems, Germany) equipped with a 25× water immersion objective. Fluorescein was excited with a 488 nm laser. Images were acquired at the bottom of the channels. Images were background corrected based on the blank control and the mean fluorescence intensity was measured using ImageJ (2.1.0/1.53c) software.[57] The obtained mean values were plotted using GraphPad Prism 6 (GraphPad Software Inc., San Diego, CA).

Inverted fluorescence microscopy

To study the stability of liposomes in presence of LecA, plain (1% of lipid **18**) and LecA-targeted (15% of lipid **16**, 1% of lipid **18**) fluorescent liposomes in PBS/Ca (40 μg mL^{-1} total phospholipid concentration) were preincubated with 14 μM LecA for 15 min in PDMS channels at static conditions. The channels were subsequently investigated with an inverted fluorescence microscope (Nikon Eclipse Ti-S) equipped with a Nikon Intensilight 130 W mercury lamp and 10× plan Nikon objective with a numerical aperture of 0.25. Images were acquired with the attached Orca R2 monochrome 1.3 MP CCD camera (Hamamatsu, Japan) at a resolution of 1024 × 1024 with 0.547 μm per pixel. Images were processed using ImageJ for background correction (Fig. 2C and D).

Surface plasmon resonance

SPR experiments were performed on a Reichert 2-channel SPR SR7500DC (Reichert Technologies Life Sciences, Buffalo, NY, USA) at 25 °C. For LecA immobilization, the surface of a HC1000M sensor chip (XanTec bioanalytics GmbH, Düsseldorf, Germany) was equilibrated with borate elution buffer (1 M NaCl, 0.1 M sodium borate pH 9.0), followed by activation of the carboxylic acids with 0.2 M *N*-hydroxysuccinimide (NHS) and 0.4 M 1-ethyl-3-(3-dimethylaminopropyl)carbodiimide hydrochloride (EDC*HCl) in MilliQ water channel 1 and 2 (contact time of 480 s, flow rate 10 μL min^{-1}) until the binding response reached 800 RU. LecA (100 μg mL^{-1}) in 10 mM sodium acetate pH 3.6 was then injected to the activated chip surface on channel 2 (contact time 660 s, flow rate 10 μL min^{-1}) and 5500 RU of LecA were immobilized. Remaining NHS esters in both channels were quenched with 1 M ethanolamine hydrochloride in MilliQ water pH 8.5 (contact time 360 s,

flow rate 10 μL min^{-1}). Liposome stock solutions (at 500 μM of targeted phospholipid in PBS/Ca) were subsequently diluted in running buffer (10 mM phosphate buffer pH 7.4, 2.7 mM KCl, 137 mM NaCl, 100 μM $CaCl_2$). Liposomes were injected (contact time of 60 s and dissociation time of 60 s, flow rate 50 μL min^{-1}) at a concentration of the targeted phospholipid of 2, 4, 8, 16, 31, 62, 125 and 250 μM. The chip surface was regenerated after each liposome injection by 3 injections of 1% CHAPS and 100 mM EDTA in MilliQ water followed by 4 injections of the running buffer (contact time of 120 s, flow rate 50 μL min^{-1}). 100 μM pNP-Gal in running buffer was injected before and after each analyte to monitor chip regeneration and protein activity.

Affinity/equilibrium analysis was performed for pNP-Gal on the same chip. A pNP-Gal stock solution (10 mM in PBS/Ca) was prepared, then diluted to the required concentrations in running buffer and injected at 1.56, 3.125, 6.25, 12.5, 25, 50, 100, 200 and 400 μM (injection time of 60 s, flow rate 50 μL min^{-1}) without regeneration steps. Data analysis was performed using Scrubber 2.0 software (Biologic Software Pty Ltd) using a 1 : 1 binding model to fit the experimental data.

Conflicts of interest

The authors declare no conflicts of interests.

Acknowledgements

A. T. acknowledges funding from the European Research Council for an ERC Starting Grant (Sweetbullets, 716311). We further thank Dr Jelena Konstantinovic and Dr Andreas Kany (HIPS) for HRMS measurements.

References

1 J. O'Neill, *Tackling drug-resistant infections globally: final report and recommendations*, Government of the United Kingdom, 2016.
2 S. Wagner, R. Sommer, S. Hinsberger, C. Lu, R. W. Hartmann, M. Empting and A. Titz, *J. Med. Chem.*, 2016, **59**, 5929–5969.
3 D. Monroe, *PLoS Biol.*, 2007, **5**, e307.
4 A. Gonzalez Gomez and Z. Hosseinidoust, *ACS Infect. Dis.*, 2020, **6**, 896–908.
5 M. J. Mitchell, M. M. Billingsley, R. M. Haley, M. E. Wechsler, N. A. Peppas and R. Langer, *Nat. Rev. Drug Discovery*, 2021, **20**, 101–124.
6 K. Forier, K. Raemdonck, S. C. De Smedt, J. Demeester, T. Coenye and K. Braeckmans, *J. Controlled Release*, 2014, **190**, 607–623.
7 W. Gao, S. Thamphiwatana, P. Angsantikul and L. Zhang, *Wiley Interdiscip. Rev.: Nanomed. Nanobiotechnol.*, 2014, **6**, 532–547.
8 S. B. Lim, A. Banerjee and H. Önyüksel, *J. Controlled Release*, 2012, **163**, 34–45.
9 T. Yu, K. W. Y. Chan, A. Anonuevo, X. Song, B. S. Schuster, S. Chattopadhyay, Q. Xu, N. Oskolkov, H. Patel, L. M. Ensign, P. C. M. van Zjil, M. T. McMahon and J. Hanes, *Nanomedicine*, 2015, **11**, 401–405.
10 R. E. W. Hancock and F. S. L. Brinkman, *Annu. Rev. Microbiol.*, 2002, **56**, 17–38.
11 Z. Drulis-Kawa, A. Dorotkiewicz-Jach, J. Gubernator, G. Gula, T. Bocer and W. Doroszkiewicz, *Int. J. Pharm.*, 2009, **367**, 211–219.
12 V. P. Torchilin, *Nat. Rev. Drug Discovery*, 2005, **4**, 145–160.
13 Y.-C. Yeh, T.-H. Huang, S.-C. Yang, C.-C. Chen and J.-Y. Fang, *Front. Chem.*, 2020, **8**, 286.
14 W. Gao, Y. Chen, Y. Zhang, Q. Zhang and L. Zhang, *Adv. Drug Delivery Rev.*, 2018, **127**, 46–57.
15 M. Srinivasarao and P. S. Low, *Chem. Rev.*, 2017, **117**, 12133–12164.
16 P. Klahn and M. Brönstrup, *Nat. Prod. Rep.*, 2017, **34**, 832–885.
17 A. A. Khan, K. S. Allemailem, S. A. Almatroodi, A. Almatroudi and A. H. Rahmani, *3 Biotech.*, 2020, **10**, 163.
18 G. J. L. Bernardes, R. Kikkeri, M. Maglinao, P. Laurino, M. Collot, S. Y. Hong, B. Lepenies and P. H. Seeberger, *Org. Biomol. Chem.*, 2010, **8**, 4987–4996.
19 S. Kawakami and M. Hashida, *J. Controlled Release*, 2014, **190**, 542–555.
20 P.-L. Jiang, H.-J. Lin, H.-W. Wang, W.-Y. Tsai, S.-F. Lin, M.-Y. Chien, P.-H. Liang, Y.-Y. Huang and D.-Z. Liu, *Acta Biomater.*, 2015, **11**, 356–367.
21 C. M. Nycholat, S. Duan, E. Knuplez, C. Worth, M. Elich, A. Yao, J. O'Sullivan, R. McBride, Y. Wei, S. M. Fernandes, Z. Zhu, R. L. Schnaar, B. S. Bochner and J. C. Paulson, *J. Am. Chem. Soc.*, 2019, **141**, 14032–14037.
22 E.-C. Wamhoff, J. Schulze, L. Bellmann, M. Rentzsch, G. Bachem, F. F. Fuchsberger, J. Rademacher, M. Hermann, B. Del Frari, R. van Dalen, D. Hartmann, N. M. van Sorge, O. Seitz, P. Stoitzner and C. Rademacher, *ACS Cent. Sci.*, 2019, **5**, 808–820.
23 S. Deng, L. Bai, R. Reboulet, R. Matthew, D. A. Engler, L. Teyton, A. Bendelac and P. B. Savage, *Chem. Sci.*, 2014, **5**, 1437–1441.
24 F. Broecker, S. Götze, J. Hudon, D. C. K. Rathwell, C. L. Pereira, P. Stallforth, C. Anish and P. H. Seeberger, *J. Med. Chem.*, 2018, **61**, 4918–4927.
25 G. Liao, Z. Zhou, S. Suryawanshi, M. A. Mondal and Z. Guo, *ACS Cent. Sci.*, 2016, **2**, 210–218.
26 D. Fayolle, N. Berthet, B. Doumeche, O. Renaudet, P. Strazewski and M. Fiore, *Beilstein J. Org. Chem.*, 2019, **15**, 937–946.
27 S. Cecioni, A. Imberty and S. Vidal, *Chem. Rev.*, 2015, **115**, 525–561.
28 R. Wawrzinek, E.-C. Wamhoff, J. Lefebre, M. Rentzsch, G. Bachem, G. Domeniconi, J. Schulze, F. F. Fuchsberger, H. Zhang, C. Modenutti, L. Schnirch, M. A. Marti, O. Schwardt, M. Bräutigam, M. Guberman, D. Hauck, P. H. Seeberger, O. Seitz, A. Titz, B. Ernst and C. Rademacher, *J. Am. Chem. Soc.*, 2021, **143**, 18977–18988.
29 S. P. Diggle, R. E. Stacey, C. Dodd, M. Cámara, P. Williams and K. Winzer, *Environ. Microbiol.*, 2006, **8**, 1095–1104.
30 D. Tielker, S. Hacker, R. Loris, M. Strathmann, J. Wingender, S. Wilhelm, F. Rosenau and K.-E. Jaeger, *Microbiology*, 2005, **151**, 1313–1323.

31 D. Passos da Silva, M. L. Matwichuk, D. O. Townsend, C. Reichhardt, D. Lamba, D. J. Wozniak and M. R. Parsek, *Nat. Commun.*, 2019, **10**, 2183.
32 J. Meiers, E. Siebs, E. Zahorska and A. Titz, *Curr. Opin. Chem. Biol.*, 2019, **53**, 51–67.
33 J. Meiers, E. Zahorska, T. Röhrig, D. Hauck, S. Wagner and A. Titz, *J. Med. Chem.*, 2020, **63**, 11707–11724.
34 M. B. Calvert, V. R. Jumde and A. Titz, *Beilstein J. Org. Chem.*, 2018, **14**, 2607–2617.
35 R. Sommer, K. Rox, S. Wagner, D. Hauck, S. S. Henrikus, S. Newsad, T. Arnold, T. Ryckmans, M. Brönstrup, A. Imberty, A. Varrot, R. W. Hartmann and A. Titz, *J. Med. Chem.*, 2019, **62**, 9201–9216.
36 R. Sommer, S. Wagner, K. Rox, A. Varrot, D. Hauck, E.-C. Wamhoff, J. Schreiber, T. Ryckmans, T. Brunner, C. Rademacher, R. W. Hartmann, M. Brönstrup, A. Imberty and A. Titz, *J. Am. Chem. Soc.*, 2018, **140**, 2537–2545.
37 V. Wittmann and R. J. Pieters, *Chem. Soc. Rev.*, 2013, **42**, 4492–4503.
38 E. Zahorska, S. Kuhaudomlarp, S. Minervini, S. Yousaf, M. Lepsik, T. Kinsinger, A. K. H. Hirsch, A. Imberty and A. Titz, *Chem. Commun.*, 2020, **56**, 8822–8825.
39 I. Joachim, S. Rikker, D. Hauck, D. Ponader, S. Boden, R. Sommer, L. Hartmann and A. Titz, *Org. Biomol. Chem.*, 2016, **14**, 7933–7948.
40 S. Kuhaudomlarp, E. Siebs, E. Shanina, J. Topin, I. Joachim, P. da Silva Figueiredo Celestino Gomes, A. Varrot, D. Rognan, C. Rademacher, A. Imberty and A. Titz, *Angew. Chem., Int. Ed.*, 2021, **60**, 8104–8114.
41 D. Hauck, I. Joachim, B. Frommeyer, A. Varrot, B. Philipp, H. M. Möller, A. Imberty, T. E. Exner and A. Titz, *ACS Chem. Biol.*, 2013, **8**, 1775–1784.
42 R. Sommer, D. Hauck, A. Varrot, S. Wagner, A. Audfray, A. Prestel, H. M. Möller, A. Imberty and A. Titz, *ChemistryOpen*, 2015, **4**, 756–767.
43 R. Sommer, T. E. Exner and A. Titz, *PLoS One*, 2014, **9**, e112822.
44 S. Wagner, D. Hauck, M. Hoffmann, R. Sommer, I. Joachim, R. Müller, A. Imberty, A. Varrot and A. Titz, *Angew. Chem., Int. Ed.*, 2017, **56**, 16559–16564.
45 E. M. Munoz, J. Correa, R. Riguera and E. Fernandez-Megia, *J. Am. Chem. Soc.*, 2013, **135**, 5966–5969.
46 M. T. Meyer, V. Roy, W. E. Bentley and R. Ghodssi, *J. Micromech. Microeng.*, 2011, **21**, 10.
47 A. Thomas, S. Wang, S. Sohrabi, C. Orr, R. He, W. Shi and Y. Liu, *Biomicrofluidics*, 2017, **11**, 024102.
48 M. Ejiugwo, Y. Rochev, G. Gethin and G. O'Connor, *Tissue Eng., Part C*, 2021, **27**, 77–88.
49 E. P. Helps and D. A. McDonald, *J. Physiol.*, 1954, **124**, 631–639.
50 M. Klarhöfer, B. Csapo, C. Balassy, J. C. Szeles and E. Moser, *Magn. Reson. Med.*, 2001, **45**, 716–719.
51 B. Majhy, P. Priyadarshini and A. K. Sen, *RSC Adv.*, 2021, **11**, 15467–15476.
52 V. M. Dominical, D. M. Vital, F. O'Dowd, S. T. O. Saad, F. F. Costa and N. Conran, *Exp. Hematol.*, 2015, **43**, 223–228.
53 D. Hauck, V. R. Jumde, C. J. Crawford and A. Titz, in *Carbohydrate Chemistry: Proven Synthetic Methods*, ed. P. Kosma, T. Wrodnigg and A. Stütz, CRC Press, Boca Raton, FL, 1st edn, 2021, vol. 5, pp. 17–22.
54 R. U. Kadam, D. Garg, J. Schwartz, R. Visini, M. Sattler, A. Stocker, T. Darbre and J.-L. Reymond, *ACS Chem. Biol.*, 2013, **8**, 1925–1930.
55 S. Kuhaudomlarp, E. Gillon, A. Varrot and A. Imberty, in *Lectin Purification and Analysis: Methods and Protocols*, ed. J. Hirabayashi, Springer US, New York, NY, 2020, pp. 257–266.
56 R. Sommer, S. Wagner, A. Varrot, C. M. Nycholat, A. Khaledi, S. Häussler, J. C. Paulson, A. Imberty and A. Titz, *Chem. Sci.*, 2016, **7**, 4990–5001.
57 C. T. Rueden, J. Schindelin, M. C. Hiner, B. E. DeZonia, A. E. Walter, E. T. Arena and K. W. Eliceiri, *BMC Bioinf.*, 2017, **18**, 529.

Chapter 3. Liposomal drug encapsulation and release

1. Introduction

Infections, caused by various pathogenic microorganisms, continue to be a global health challenge, requiring the constant evolution of antimicrobial therapeutics. Antibiotics are medications used to prevent and treat infectious diseases by either killing bacteria – bactericidal, or slowing down their growth — bacteriostatic.[1] The emergence of drug-resistant bacterial strains[2] requires a constant investigation of new antibiotics[3] or, alternatively, new formulations of already known drugs capable of delivering more efficient treatment with higher efficacy.[4]

In this context, liposomes have emerged as a promising nanocarrier for antibiotics, holding great potential for the improvement of antimicrobial therapy. Liposomes are lipid vesicles containing one or more lipid bilayers composed of phospholipids and/or cholesterol, mimicking the natural structure of cell membranes.[5] The properties of liposomes, such as size, ζ-potential, fluidity and stability, can be modulated by altering the structure and composition of lipids used for liposome preparation. It has been shown that saturated phospholipids result in bilayers with higher rigidity and lower permeability compared to the unsaturated analogues.[5] Furthermore, the presence of steroids, such as cholesterol, in the liposomal composition improves the stability of liposomes and reduces the fluidity of the lipid bilayer.[6]

The presence of both a hydrophobic membrane and a hydrophilic core makes liposomes suitable carriers for delivering drug substances with a wide range of physicochemical properties. This characteristic helps to overcome issues such as limited antibiotic solubility and stability, for example, by protecting drug substances from exposure to enzymes, e.g. staphylococcal β-lactamases.[7–9] Moreover, liposomal encapsulation of antibiotics helps to improve pharmacokinetic and pharmacodynamic profiles of antibiotics.[10] Another advantage of the liposomal formulations is linked with their ability to simultaneously encapsulate multiple therapeutic agents, allowing combination therapy with different antibiotics or therapeutic agents, e.g. β-lactamase inhibitors or efflux pumps inhibitors. The main mechanism through which liposomes can interact with bacterial cells is the fusion of the liposomal lipid bilayer with the bacterial cell wall. In particular, liposomes formulated with fusogenic phospholipids containing phosphoethanolamine head groups can enhance this interaction by disturbing the bacterial membrane structure, thereby increasing its permeability and promoting antibiotic uptake.[10,11] As a result of the alteration in the interaction between bacterial cells and

liposomes, liposomal formulations can prevent the development of resistance mechanisms used by bacterial pathogens.[12]

1.1 Liposomal drug encapsulation and release

Modifying the liposomal composition, such as type of phospholipids and their amount, as well as cholesterol presence, allows for the optimization of drug encapsulation efficiency and release,[6] and also enables the alteration of biodistribution by affecting the physicochemical properties of the nanocarriers.[13,14] For example, ζ-potential plays a crucial role in the interaction with active substances loaded into liposome. Positively charged liposomes are particularly efficient for encapsulating DNA or RNA, as they from lipoplexes through Coulombic interactions with the negatively charged backbone of nucleic acids.[15,16] Another important characteristic of the liposomes is their lamellarity. Depending on the preparation method liposomes can be unilamellar and have only one lipid bilayer or multilamellar and possess multiple lipid bilayers. Depending on the application of the formulation, the specific molecule being encapsulated, and the desired release profile, a particular type of vesicle may be preferred.[17]

Given the advantages of liposomal antibiotic formulations, it was decided to investigate the applicability of various antimicrobials for treating *Pseudomonas aeruginosa* infections. We selected several antibiotics whose release rates from liposomes were suitable for potential in vitro assessments aimed at evaluating the feasibility of using glycofunctionalized liposomes for drug encapsulation.

1.2 Ciprofloxacin

The antibiotic ciprofloxacin is a member of the fluoroquinolone class and is widely used in the clinical setting for the treatment of bacterial infections. Its mechanism of action includes the inhibition of DNA gyrase and topoisomerase IV, pivotal enzymes involved in DNA replication and repair within bacterial cells.[18]

Although highly effective, the clinical use of ciprofloxacin is associated with several challenges. First and foremost, an increasing number of bacteria are developing resistance to ciprofloxacin via diverse mechanisms, such as mutations in DNA gyrase genes (gyrA/gyrB) and topoisomerase IV (parC/parE), decreased level of expression of porin in the outer membrane (cfxB), and increased expression of efflux pumps (nfxB).[19,20] *P. aeruginosa* is one of the pathogens for which the number of ciprofloxacin-resistant isolates is increasing very rapidly requiring a better therapy approaches to sustain the efficacy of the treatment.[21–24]

Another difficulty associated with ciprofloxacin treatment is its high toxicity, which limits the maximum tolerable dose of the antibiotic. Animal studies demonstrated that one of potential approaches to overcome this issue could be encapsulation of ciprofloxacin into PEGylated liposomes, providing elongated blood circulation time and sustained release.[25] This leads to better tolerability of relatively high doses of ciprofloxacin without necessitating more frequent administration.

1.3 Tobramycin

Tobramycin belongs to the class of aminoglycoside antibiotics and holds a prominent role in the array of antimicrobial agents being active against both Gram-positive and Gram-negative bacteria.[26] Its mechanism of action centers on inhibiting bacterial protein synthesis by binding irreversibly to the 30S ribosomal subunit and therefore preventing the formation of 70S complex disabling translation of mRNA and resulting in bacteria death.[27]

Tobramycin is also used in therapy of *P. aeruginosa* infections in cystic fibrosis patients when applied via inhalation.[28,29] Despite its high efficacy, the treatment is often limited by the side effects, such as nephrotoxicity and ototoxicity.[30,31] One of the potential solutions to improve the efficacy of tobramycin, particularly treatment for pulmonary infections of *P. aeruginosa* via intratracheal administration, can be liposomal formulation of the antibiotic. It demonstrated a three-fold higher reduction, with observed levels below 10^3 CFU of *P. aeruginosa* (corresponding to >99.9% kill) compared to the conventional formulation.[32] This increase in treatment efficacy is associated with several phenomena, such as lowering a rate constant of absorption, longer distributional and elimination half-life as well as significantly enhanced pulmonary exposure for the liposomal tobramycin.

1.4 Colistin

Colistin, or polymyxin E, is a polycationic peptide antibiotic, used as a last resort treatment for infections caused by Gram negative bacteria, including *P. aeruginosa*. Its mechanism of action is linked with the ability of colistin to work as a detergent of cell membrane. Due to its positive charge, colistin interacts with negatively charged phosphate group of bacterial LPS, followed by displacement of divalent cations Ca^{2+} and Mg^{2+} therefore affecting the LPS structure and as a result membrane permeability. Additionally, it has been reported that polymyxins are able to precipitate cytoplasmic components.[33,34] Due to its high toxicity, the use of colistin is limited and primarily applicable for treating pulmonary infections caused by multidrug-resistant bacteria.

1.5 Pathoblokers

Pathoblockers are small therapeutic molecules that selectively inhibit the harmful properties of bacteria without killing them. Unlike antibiotics, which eliminate bacteria, pathoblockers work by disarming microorganisms, preventing them from damaging their host without affecting bacterial survival. One example of this mechanism is the inhibition of bacterial quorum sensing (QS), an intercellular communication system that enable bacteria like *P. aeruginosa* to coordinate behavior through the production and detection of signaling molecules. Inhibiting QS reduces bacterial pathogenicity by impairing their ability to coordinate biofilm formation.[35]

2. Results and Discussion

2.1 Ciprofloxacin

Ciprofloxacin hydrochloride was selected as a model compound to assess both encapsulation efficiency and drug release in both untargeted and lectin-targeted liposomes. One of the methods to increase the efficacy of ciprofloxacin loading into the liposomes is a transmembrane $(NH_4)_2SO_4$ gradient, where the concentration of ammonium sulfate inside the liposome is higher than in the outside leads to the active loading of drugs which are weak amphipathic bases, e.g., doxorubicin or ciprofloxacin, into an aqueous core of the liposomes.[8,36] Such a loading strategy allows to achieve >90% drug encapsulation efficiency. Formulation of liposomes via hydration with $(NH_4)_2SO_4$ leads to the presence of ammonium sulfate in extra- and intraliposomal aqueous phases. Elimination of ammonium sulfate from the extraliposomal phase results in a high concentration gradient. Followed by proton exchange with the ammonium ions, drug is actively loaded into the aqueous core of the liposome (Figure 1).

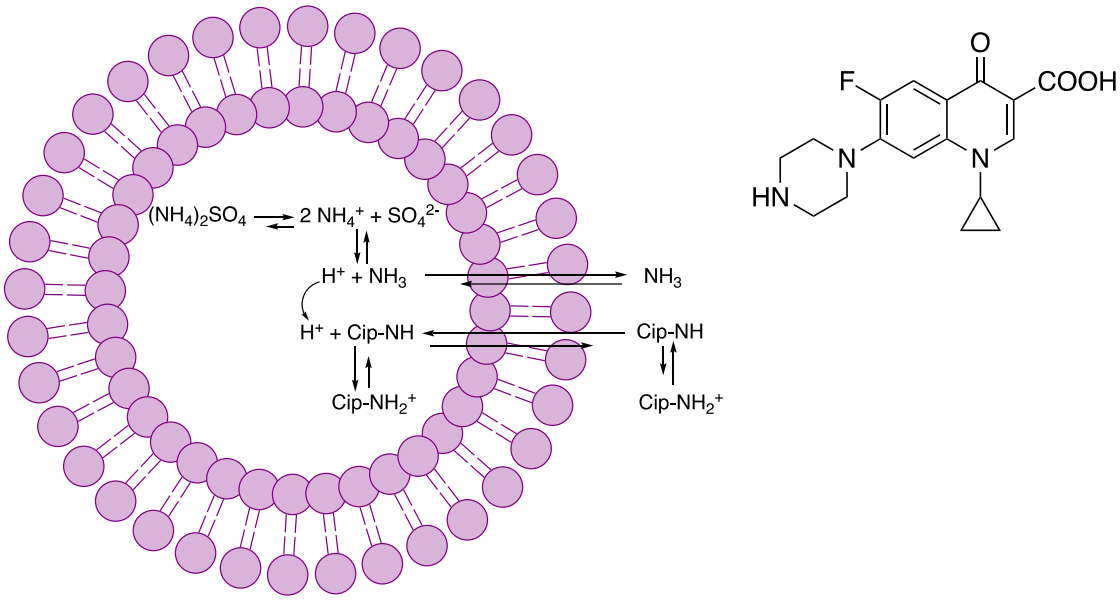

Figure 1. Schematic representation of transmembrane ammonium sulfate gradient in liposomes[36] and the structure of ciprofloxacin molecule.

Encapsulation of ciprofloxacin into glyco-functionalized liposomes was performed using the thin-film hydration method with an ammonium sulfate gradient and a ciprofloxacin hydrochloride stock solution at a concentration near its solubility limit 35 mg/mL (Table 1). Although the obtained samples demonstrated EE values above 70%, the data revealed fast drug release, with less than 40% of the drug retained within the liposomes after 1 h, decreasing further to less than 20% after 4 hours (Table 1).

The rapid release profile of ciprofloxacin is plausibly attributed to its presence in a balanced zwitterionic state when dissolved in 10 mM sodium phosphate buffer pH 7.4, in which release studies were conducted. Ciprofloxacin is characterized by two acid dissociation constants: $pK_{a1} = 6.09$ and $pK_{a2} = 8.62$ and the calculated isoelectronic point, obtained by averaging these values, is pI = 7.14.[37] Consequently, the drug molecule maintains a minimal net electrical charge under physiological pH, thereby preventing the possibility of Coulombic attraction between ciprofloxacin and negatively charged liposomes.

Table 1. Characteristics of targeted liposomal formulations of ciprofloxacin.

	D, nm	PdI	ζ-potential, mV	C loaded ciprofloxacin, mg/mL	Encapsulation efficiency	Drug retained after 4 h
LecA-targeted liposomes	232±6	0.254±0.01	-41±5	23.5	78%	15%
LecB-targeted liposomes	231±2	0.131±0.05	-18±7	23.0	77%	20%
untargeted liposomes	202±1	0.090±0.01	-33±9	21.5	72%	16%

Considering the unsuitability of the kinetic profile for further research utilizing drug-loaded liposomes, a decision was made to replace the encapsulated antibiotic with one that exhibits a slower release pattern.

2.2 Tobramycin

Untargeted liposomes for tobramycin (Figure 2) encapsulation were prepared using an 8 mg/mL stock solution of tobramycin sulfate, resulting in a final liposomal tobramycin concentration of 5.3 mg/mL and a drug-to-DSPC molar ratio of 2:1. The obtained liposomes had an average diameter (D_h) of 192±3 nm and a ζ-potential of -32±1 mV.

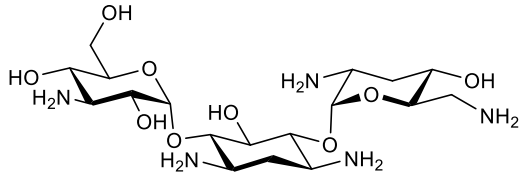

Figure 2. Structure of tobramycin.

EE was determined to be 66% and investigation of tobramycin release at 37 °C over 24 hours demonstrated that only about 10% of the encapsulated tobramycin remained in the liposomes after 4 hours (Figure 3A). This rapid drug release indicated low suitability of tobramycin for the current study; and therefore, further experiments with tobramycin were not conducted.

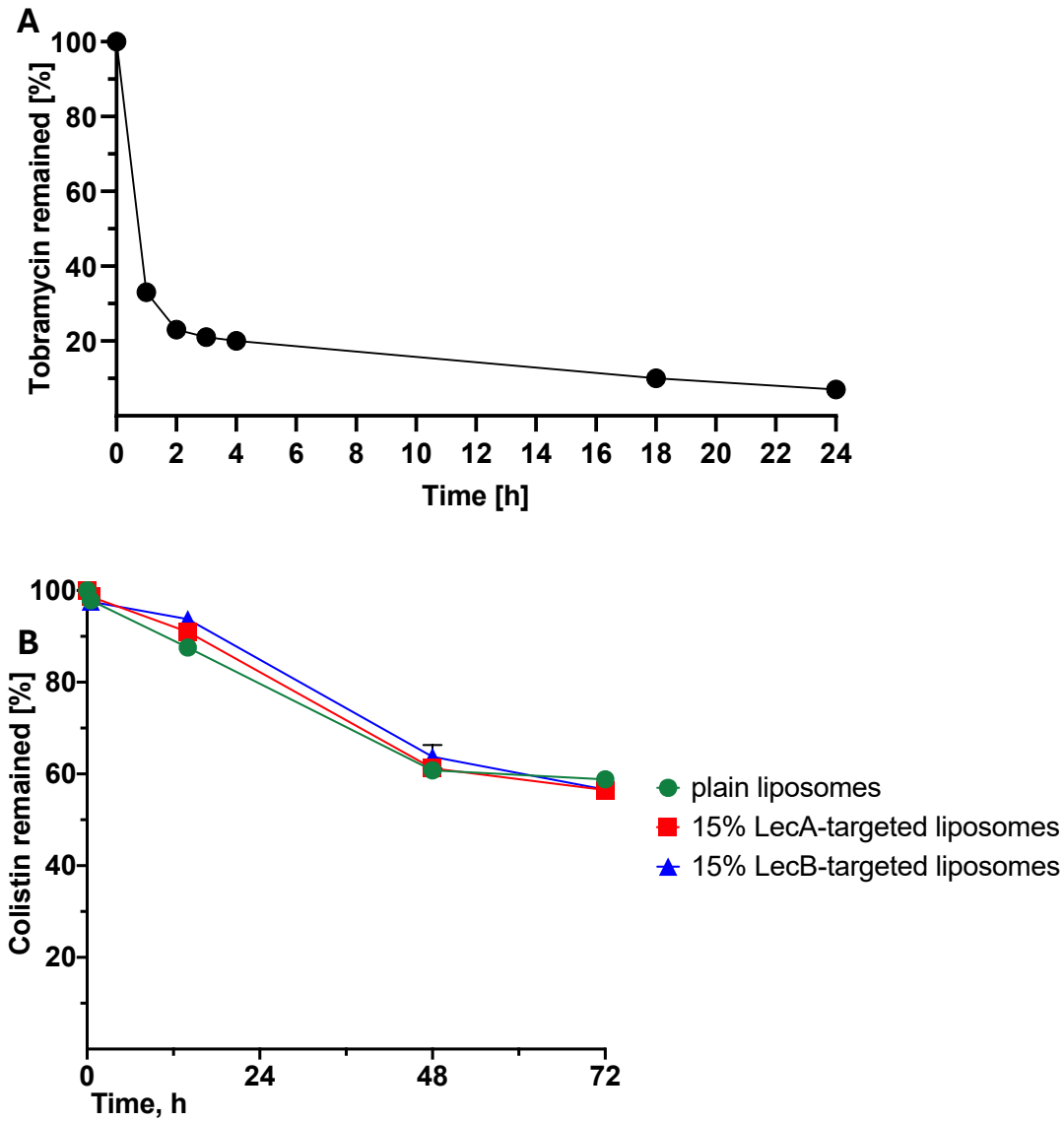

Figure 3. A) Tobramycin retained in liposomes after incubation in 10 mM sodium phosphate buffer at 37 °C, 300 rpm; B) Colistin retained in liposomes after incubation in 10 mM sodium phosphate buffer at 37 °C, 300 rpm.

2.3 Colistin

For colistin (Figure 4) encapsulation, a comparison between targeted and untargeted liposomes showed no significant differences in size or ζ-potential between the formulations. The assessment of colistin-loaded untargeted and targeted liposomes demonstrated high drug encapsulation efficiency (Table 2), with approximately 60% retention over 72 hours.

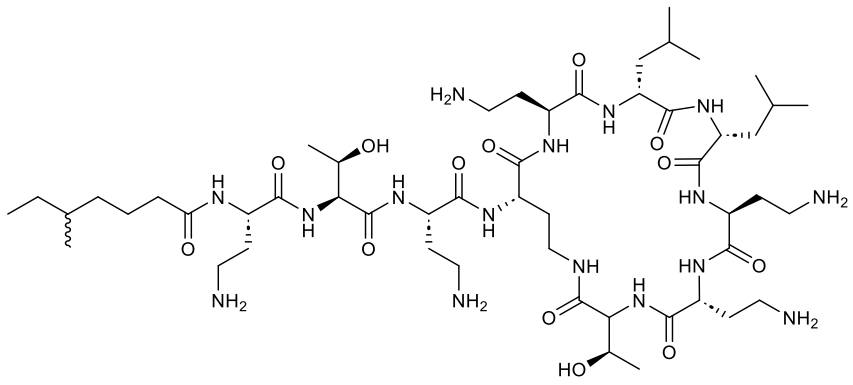

Figure 4. Structure of colistin.

The presence of carbohydrate moieties had no effect on drug retention (Figure 3B), suggesting that colistin is a suitable therapeutic molecule for further liposomal formulation experiments with potential applications in *P. aeruginosa* treatment.

Table 2. Characteristics of targeted liposomal formulations of colistin.

Liposomes	D, nm	PdI	ζ-potential, mV	Colistin sulfate liposomal concentration, μg/mL	EE, %
untargeted	225±4	0.130±0.02	-11±10	49	98
LecA-targeted	230±2	0.161±0.01	-4±4	45	90
LecB-targeted	232±1	0.131±0.06	-5±2	42	84

2.4 Pathoblockers

Two pathoblockers were selected to investigate their encapsulation in liposomes. The first was HIPS2050 (Figure 5A), a *P. aeruginosa* quorum-sensing transcriptional regulator (PqsR) inhibitor, which was incorporated into the phospholipid bilayer due to its high hydrophobicity.[38] The second was DH181a (Figure 5B), a potent LecB inhibitor, which was encapsulated in the aqueous core of the liposome due to its hydrophilic properties.[39]

2.4.1 PqsR inhibitor HIPS2050

Due to its hydrophobic nature, HIPS2050 was dissolved in a $CHCl_3$:MeOH mixture along with DSPC and cholesterol for encapsulation within the phospholipid bilayer of liposomes. The resulting untargeted liposomal formulations had an average size of 196±3 nm, a PdI 0.28±0.08 and a ζ-potential -37±5 mV.

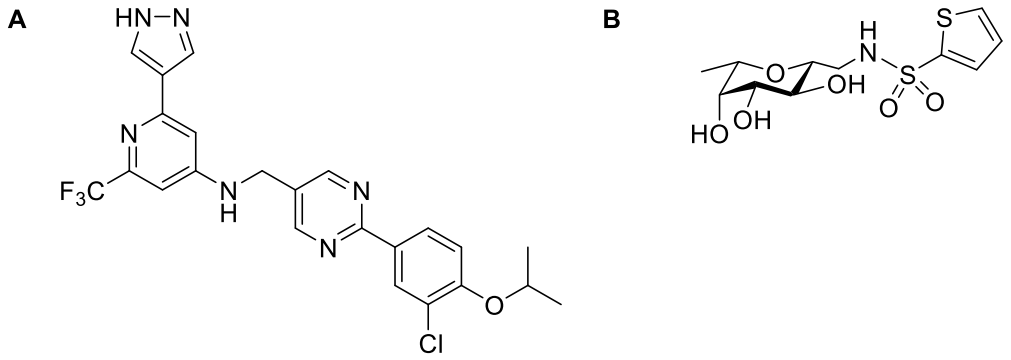

Figure 5. A) Structure of HIPS2050[38]; B) structure of DH181a.

Results showed that almost no release of HIPS2050 occurred even after 4 days of incubation at 37 °C in 10 mM sodium phosphate buffer, with 92% of the compound remaining encapsulated. These findings support the further use of the current formulation in potential in vitro studies, including the treatment of *P. aeruginosa* biofilm grown under flow conditions.

2.4.2. LecB-inhibitor DH181a

The ability to incorporate the LecB-inhibitor[40] into the aqueous core of the liposome was investigated via preparation of DH181a liposomal formulation. Obtained untargeted formulations had size 202±1 nm, PdI 0.2±0.05 and ζ-potential -32±2 mV. The release of DH181a at 37 °C in 10 mM sodium phosphate buffer pH 7.4 showed that over half of the encapsulated molecule was released within the first hour after formulation, leaving 47% encapsulated. After 24 h of incubation, only 21% of DH181a remained inside the liposomes, suggesting that further optimization of the liposomal formulation may be required for DH181a.

3. Materials and Methods

General protocol for preparation and characterization of liposomes[41]

For liposome preparation 20 mg phospholipids and 10 mg cholesterol were dissolved in a 5 mL mixture of $CHCl_3$/MeOH 2:1. LecA or LecB ligand-lipid conjugate (Figure 6) were added at 15 mol% to the corresponding lipid mixtures. After complete removal of organic solvents using a rotary evaporator under reduced pressure at 70 °C, the obtained thin lipid film was hydrated with 5 mL of the corresponding aqueous solution (see the information below) under rotation for 1 h at 65 °C followed by sonication for 30 sec at 65 °C. The resulting colloidal solution was extruded 10 times through a 0.2 μm pore size polycarbonate membrane (Polycarbonate track-etched membrane, Sartorius, Germany) at 70 °C via a Lipofast L-50 extruder (Avestin, Germany). The extrusion step was followed by centrifugation using Vivaspin® (Sartorius AG, Göttingen, Germany) at 2000 g at 23 °C for two intervals of 25 min each to remove unencapsulated small molecule. The volume of the liposome samples was then

restored to the initial one using a 10 mM sodium phosphate buffer pH 7.4, 2.7 mM KCl, 137 mM NaCl, 100 μM $CaCl_2$, after both rounds of centrifugation. The obtained liposomes were diluted 100-fold in MilliQ water to determine the size and PdI by DLS and measure the ζ-potential by electrophoretic light scattering via Zetasizer Nano ZS (Malvern Panalytical Ltd, UK). To measure the exact concentration of the LecA- or LecB-targeting ligands in the obtained solutions, liposomes were diluted 100-fold in MeOH and analyzed by LC-MS/MS using the solvent system A: iPrOH/MeOH/H_2O (5:4:1) + 0.05% HCOOH, B: iPrOH + 0.05% HCOOH and a gradient of 5 – 40% B.

Analytical HPLC-MS was performed on a Thermo Dionex Ultimate 3000 HPLC coupled to a Bruker amaZon SL mass spectrometer, with UV detection at 254 nm using a RP-18 column (100/2 Nucleoshell RP18plus, 2.7 μm from Macherey-Nagel, Germany) as stationary phase.

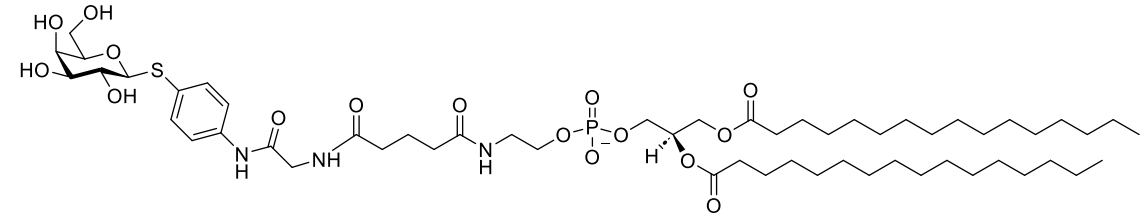

LecA-targeted lipid-ligand conjugate

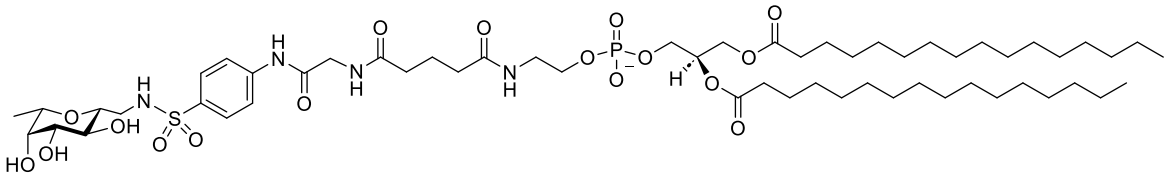

LecB-targeted lipid-ligand conjugate

Figure 6. Structures of LecA- and LecB-targeted lipid-ligand conjugates.

3.1 Preparation of liposomal ciprofloxacin

Liposomes were prepared according to the protocol described in section 1.2.1, where the lipid thin film was hydrated with 5 mL of a 120 mM solution of aqueous $(NH_4)_2SO_4$. The resulting liposomes were then dialyzed using a 5% (w/w) aqueous D-glucose solution, using a 25-fold volume relative to the liposomal suspension. This dialysis procedure involved three subsequent changes of the dialysis solution to ensure the complete removal of unencapsulated ammonium sulfate. Obtained liposomes were then incubated with 5 mL of 35 mg/mL aqueous ciprofloxacin hydrochloride solution at 65 °C for 30 min then equilibrated to 25 °C. The unencapsulated antibiotic was subsequently removed via centrifugation, utilizing a VivaSpin column, following the protocol described above.

3.1.1 HPLC method for ciprofloxacin concentration determination

To quantify drug loading, the ciprofloxacin content encapsulated within the liposomes was assessed by dissolving the loaded liposomes in methanol and subsequently quantifying the amount of the antibiotic present. Quantification of ciprofloxacin was performed using LC-MS/MS methods on a Thermo Dionex Ultimate 3000 HPLC coupled to a Bruker amaZon SL mass spectrometer, with UV detection at 275 nm using a RP-18 column (100/2 Nucleoshell RP18plus, 2.7 µm from Macherey-Nagel, Germany) as stationary phase. A standard curve was established for ciprofloxacin hydrochloride at a concentration range of 4 – 240 µg/mL in water (Figure 7).

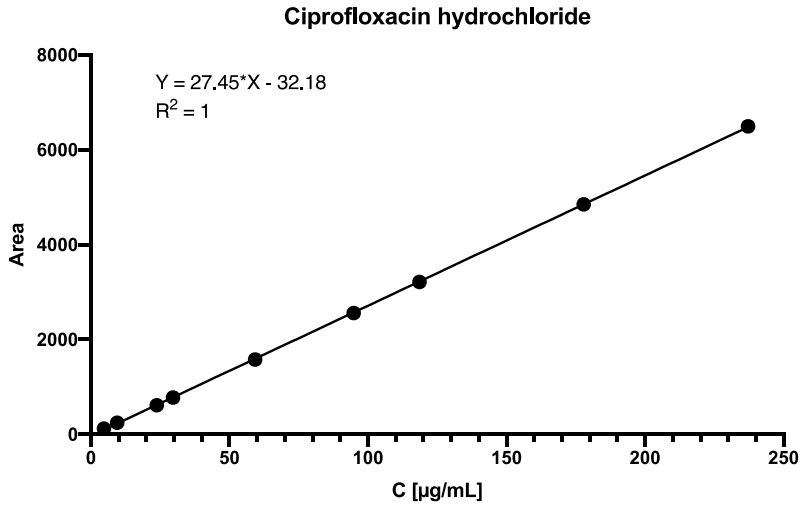

Figure 7. Calibration curve for determination of ciprofloxacin hydrochloride concentration.

3.1.2 Ciprofloxacin liposomal release

The liposomal samples were incubated at 37 °C under 300 rpm shaking conditions. After 4 h aliquots of the samples were taken and processed in similar way as described in section 2.1.2.3 for determination of concentration of encapsulated antibiotic.

3.2 Preparation of liposomal tobramycin

Liposomes were prepared according to the protocol described in section 1.2.1, where the lipid thin film was hydrated with 5 mL of tobramycin sulfate solution 40 mg/mL in 10 mM sodium phosphate buffer pH 7.4.

3.2.1 HPLC method for tobramycin concentration determination

To quantify the drug loading, the tobramycin content encapsulated within the liposomes was assessed by dissolving the loaded liposomes in methanol following the procedure developed by *Schütz et al.*[38] Quantification of tobramycin was achieved using liquid chromatography with tandem mass spectrometry (LC-MS/MS), utilizing the Xcalibur software

for system operation. A reverse phase C18 Accucore RP-MS column (150·2.1 mm) served as the stationary phase for tobramycin quantification at 30 °C. The mobile phase was a mixture of solvent A (water with 0.1% v/v formic acid, FA) and solvent B (acetonitrile with 0.1% v/v trifluoroacetic acid, TFA), with a solvent ratio of A:B set at 95:5. The flow rate, controlled by an Accela 1250 Pump, was 300 µL/min. A standard curve was established within the tobramycin concentration range of 6 – 100 µg/mL (Figure 8).[38]

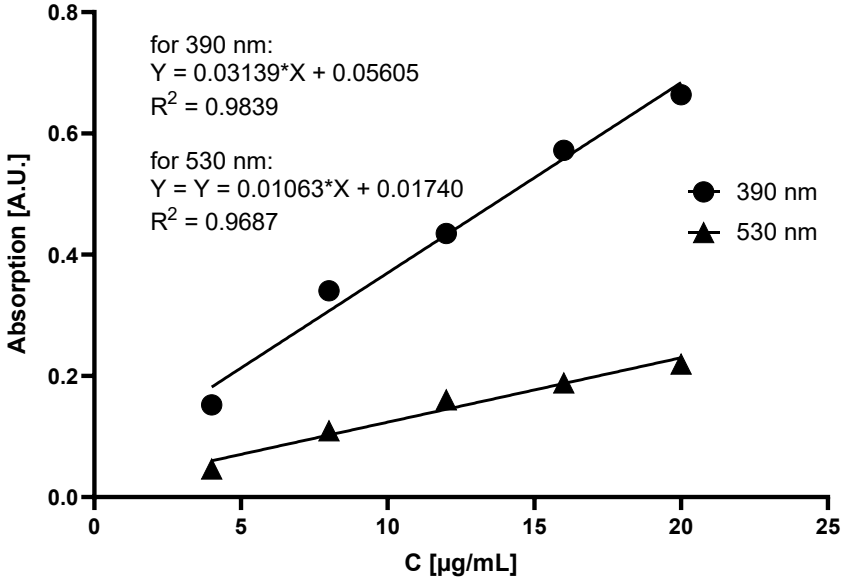

Figure 8. Calibration curves for determination of tobramycin concentration by HPLC method.

3.2.3 Tobramycin liposomal release

In vitro release studies of tobramycin from drug-loaded liposomes were conducted in 10 mM sodium phosphate buffer pH 7.4, maintained at 37 °C for a duration of 24 h. Loaded liposomes were diluted 10 times in sodium phosphate buffer and placed on a shaker at 300 rpm and incubated at 37 °C. Samples were collected from the supernatant at predefined time intervals spanning 24 h. After centrifugation using Vivaspin® (Sartorius AG, Göttingen, Germany) at 2000 g, the supernatant was discarded. The sample volume was then restored to its original value using 10 mM sodium phosphate buffer pH 7.4, and the concentration of the encapsulated tobramycin hydrochloride was determined. This quantification procedure required a 500-fold dilution of the liposomes in methanol, followed by the measurement of drug concentration using HPLC-MS described above.

3.3 Preparation of liposomal colistin

Liposomes were prepared according to the protocol described in section 1.2.1, where the lipid thin film was hydrated with 5 mL of colistin sulfate solution 50 mg/mL in 10 mM sodium phosphate buffer pH 7.4.

3.3.1 HPLC method for colistin concentration determination

To quantify the drug loading, the colistin content encapsulated within the liposomes was assessed by dissolving the loaded liposomes in methanol. Quantification of colistin was performed using liquid chromatography with tandem mass spectrometry (LC-MS/MS) methods on a Thermo Dionex Ultimate 3000 HPLC coupled to a Bruker amaZon SL mass spectrometer, with UV detection at 254 nm using a RP-18 column (100/2 Nucleoshell RP18plus, 2.7 µm from Macherey-Nagel, Germany) as stationary phase. A standard curve was established measuring absorbance at 254 nm within the colistin sulfate concentration range of 10 – 200 µg/mL in water (Figure 9).

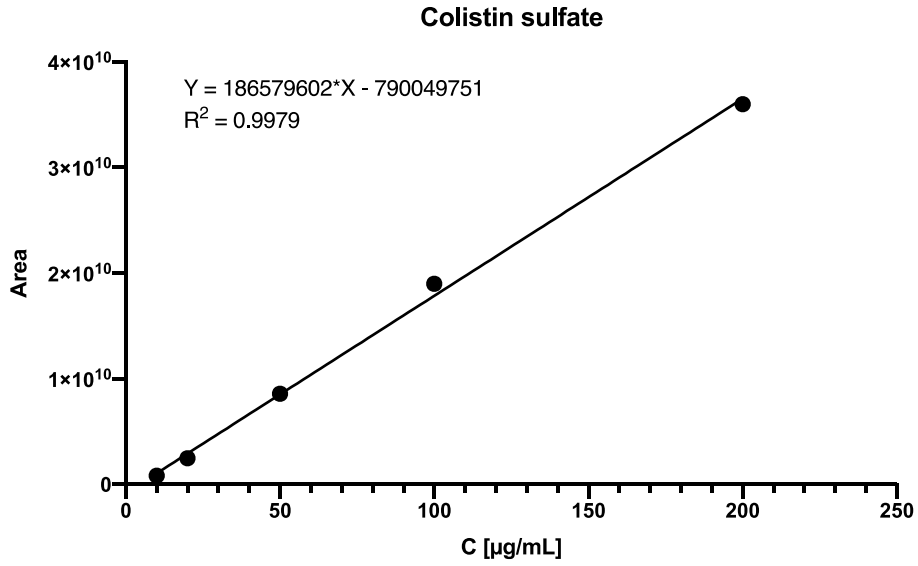

Figure 9. Calibration curves for determination of colistin sulfate concentration by HPLC method.

3.4 Preparation of liposomal HIPS2050

To prepare the liposomal formulation of HIPS2050 the protocol from section 1.2.1 was followed where 5 mmol HIPS2050, 30 mmol cholesterol and 30 mmol of DSPC were dissolved in 5 mL $CHCl_3$/MeOH 2:1 (v/v) and obtained thin film was rehydrated with 10 mM sodium phosphate buffer pH 7.4. The concentration of HIPS2050 remained in liposomes over time was determined via LC-MS/MS method using the solvent system A: iPrOH/MeOH/H_2O (5:4:1) + 0.05% HCOOH, B: iPrOH + 0.05% HCOOH and a gradient of 5 – 40% B. A standard curve

was established measuring absorbance at 254 nm within the HIPS2050 concentration range of 5 – 160 µg/mL in methanol (Figure 10A).

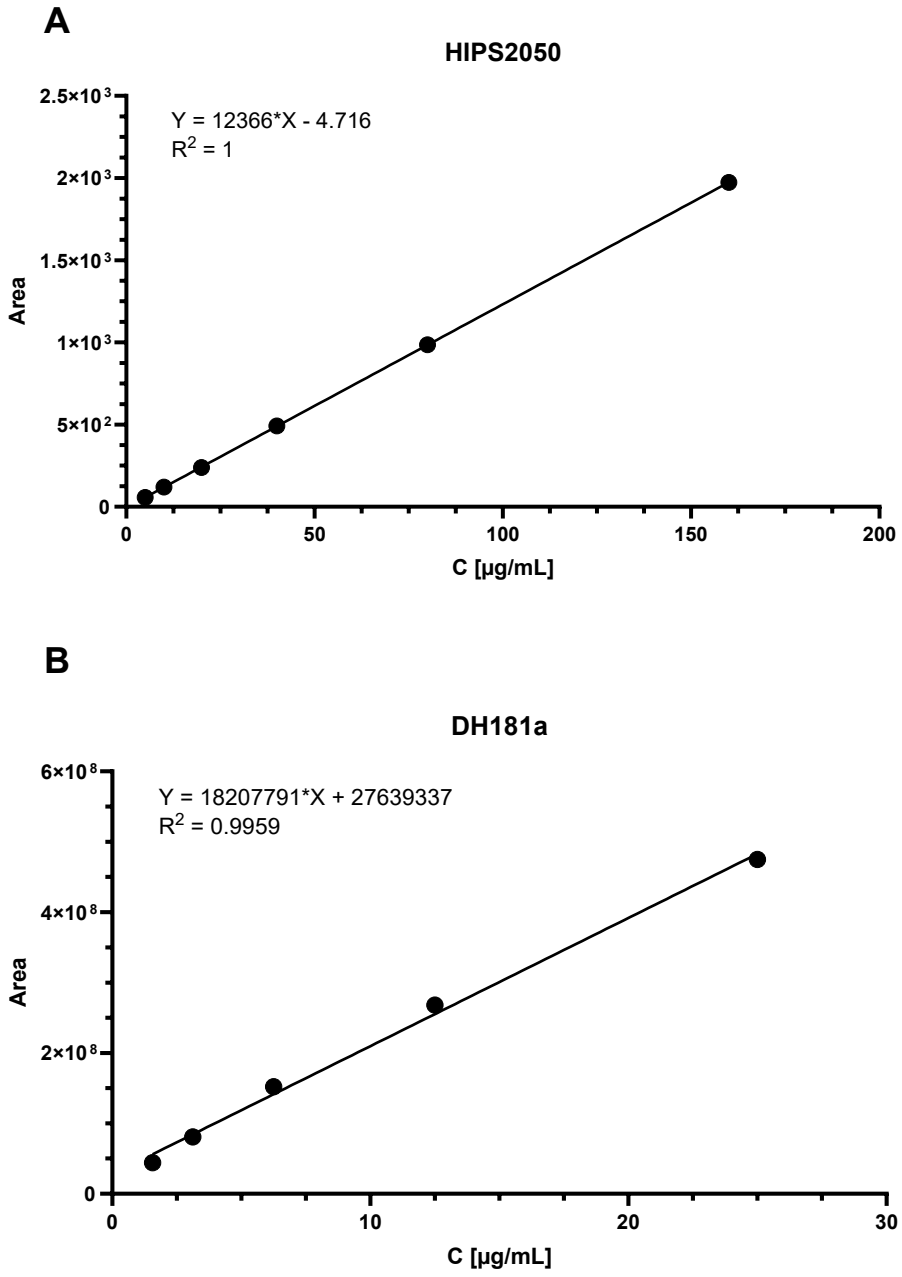

Figure 10. A) Calibration curves for determination of HIPS2050 concentration by HPLC method; B) Calibration curves for determination of DH181a concentration by HPLC method.

3.5 Preparation of liposomal DH181a

To prepare the liposomal formulation of DH181a the protocol from section 1.2.1 was followed using a 5 mM solution of DH181a in 10 mM sodium phosphate buffer pH 7.4 for the thin film hydration. The concentration of DH181a remained in liposomes over time was

determined via LC-MS/MS method using the solvent system A: iPrOH/MeOH/H_2O (5:4:1) + 0.05% HCOOH, B: iPrOH + 0.05% HCOOH and a gradient of 5 – 40% B. A standard curve was established within the DH181a concentration range of 1.5 – 25 µg/mL in water (Figure 10B).

Conclusions

Given that the high antibiotic resistance of *P. aeruginosa* is associated with its ability to form biofilms, preventing or reducing biofilm formation in combination with antibiotic treatment could enhance the effectiveness of infection therapy. The studies described above aimed to identify an optimal antibiotic candidate for liposomal encapsulation and explore its applicability for the potential treatment of *P. aeruginosa* infections. The glycofunctionalized liposomal formulations were designed to retain therapeutic molecules until it reaches the proximity of the in vitro-grown *P. aeruginosa* biofilm, where the drug is released upon interaction. The interaction with LecA and/or LecB can potentially initiate biofilm disruption, followed by bacterial killing due to the antibiotic presence, therefore enhancing the effectiveness of *P. aeruginosa* biofilm treatment. It was also demonstrated that incorporating lectin ligands did not significantly impact liposome formation, stability, or drug encapsulation efficiency. Based on the drug release profile and physicochemical properties of the liposomal formulations, colistin was selected over ciprofloxacin and tobramycin for potential application in in vitro studies.

Furthermore, the PqsR inhibitor HIPS2050 and the LecB ligand DH181a were successfully incorporated into liposomes, presenting an opportunity for non-antibiotic treatment of infection using liposomal formulations. The co-delivery of HIPS2050 within the glycosylated liposomes could reduce *P. aeruginosa* pathogenicity and host damage without impacting bacterial viability, potentially lowering the risk of resistance development. Encapsulating DH181a in lectin-targeted liposomes allows for a broader range of ligand concentrations compared to the lectin ligand-lipid conjugates incorporated into liposomes. However, further formulation optimization is required to improve its release profile.

Further studies will evaluate the efficacy of targeted liposomal formulations for in vitro treatment of *P. aeruginosa* biofilm. Additional formulation optimization may focus on liposomal composition and glycolipid structure, including the incorporation of a stealth linker between the ligand and the lipid tail.

[1] D. R. Stone, Sherwood. Gorbach, *Atlas of Infectious Diseases*, W.B. Saunders, London, **2000**.
[2] C. L. Ventola, *P T* **2015**, *40*, 277–283.
[3] M. Miethke, M. Pieroni, T. Weber, M. Brönstrup, P. Hammann, L. Halby, P. B. Arimondo, P. Glaser, B. Aigle, H. B. Bode, R. Moreira, Y. Li, A. Luzhetskyy, M. H. Medema, J.-L. Pernodet, M. Stadler, J. R. Tormo, O. Genilloud, A. W. Truman, K. J. Weissman, E. Takano, S. Sabatini, E. Stegmann, H. Brötz-Oesterhelt, W. Wohlleben, M. Seemann, M. Empting, A. K. H. Hirsch, B. Loretz, C.-M. Lehr, A. Titz, J. Herrmann, T. Jaeger, S. Alt, T. Hesterkamp, M. Winterhalter, A. Schiefer, K. Pfarr, A. Hoerauf, H. Graz, M. Graz, M. Lindvall, S. Ramurthy, A. Karlén, M. van Dongen, H. Petkovic, A. Keller, F. Peyrane, S. Donadio, L. Fraisse, L. J. V. Piddock, I. H. Gilbert, H. E. Moser, R. Müller, *Nature Reviews Chemistry* **2021**, *5*, 726–749.
[4] M. Ferreira, M. Ogren, J. N. R. Dias, M. Silva, S. Gil, L. Tavares, F. Aires-da-Silva, M. M. Gaspar, S. I. Aguiar, *Molecules* **2021**, *26*, DOI 10.3390/molecules26072047.
[5] A. Akbarzadeh, R. Rezaei-Sadabady, S. Davaran, S. W. Joo, N. Zarghami, Y. Hanifehpour, M. Samiei, M. Kouhi, K. Nejati-Koshki, *Nanoscale Res Lett* **2013**, *8*, 102.
[6] M.-L. Briuglia, C. Rotella, A. McFarlane, D. A. Lamprou, *Drug Deliv Transl Res* **2015**, *5*, 231–242.
[7] A. Gonzalez Gomez, S. Syed, K. Marshall, Z. Hosseinidoust, *ACS Omega* **2019**, *4*, 10866–10876.
[8] N. Maurer, K. F. Wong, M. J. Hope, P. R. Cullis, *Biochimica et Biophysica Acta (BBA) - Biomembranes* **1998**, *1374*, 9–20.
[9] M. C. Nacucchio, M. J. Bellora, D. O. Sordelli, M. D'Aquino, *Antimicrob Agents Chemother* **1985**, *27*, 137–139.
[10] R. Ghosh, M. De, *ACS Omega* **2023**, *8*, 35442–35451.
[11] Z. Du, M. M. Munye, A. D. Tagalakis, M. D. I. Manunta, S. L. Hart, *Sci Rep* **2014**, *4*, 7107.
[12] C. Mugabe, M. Halwani, A. O. Azghani, R. M. Lafrenie, A. Omri, *Antimicrob Agents Chemother* **2006**, *50*, 2016–2022.
[13] C. Oussoren, J. Zuidema, D. J. A. Crommelin, G. Storm, *Biochimica et Biophysica Acta (BBA) - Biomembranes* **1997**, *1328*, 261–272.
[14] H. Ren, Y. He, J. Liang, Z. Cheng, M. Zhang, Y. Zhu, C. Hong, J. Qin, X. Xu, J. Wang, *ACS Appl. Mater. Interfaces* **2019**, *11*, 20304–20315.
[15] F. Sakurai, R. Inoue, Y. Nishino, A. Okuda, O. Matsumoto, T. Taga, F. Yamashita, Y. Takakura, M. Hashida, *J Control Release* **2000**, *66*, 255–269.
[16] A. Elouahabi, J.-M. Ruysschaert, *Molecular Therapy* **2005**, *11*, 336–347.
[17] F. Maestrelli, M. L. González-Rodríguez, A. M. Rabasco, P. Mura, *International Journal of Pharmaceutics* **2006**, *312*, 53–60.
[18] K. Drlica, X. Zhao, *Microbiol Mol Biol Rev* **1997**, *61*, 377–392.
[19] D. C. Hooper, J. S. Wolfson, E. Y. Ng, M. N. Swartz, *Am J Med* **1987**, *82*, 12–20.
[20] A. Rehman, W. M. Patrick, I. L. Lamont, *J Med Microbiol* **2019**, *68*, 1–10.
[21] Santi Isabella, Manfredi Pablo, Maffei Enea, Egli Adrian, Jenal Urs, *mBio* **2021**, *12*, 10.1128/mbio.03482-20.
[22] Fournier Damien, Carrière Romain, Bour Maxime, Grisot Emilie, Triponney Pauline, Muller Cédric, Lemoine Jérôme, Jeannot Katy, Plésiat Patrick, *Antimicrobial Agents and Chemotherapy* **2021**, *65*, 10.1128/aac.01117-20.
[23] P. Laborda, F. Sanz-García, S. Hernando-Amado, J. L. Martínez, *Current Opinion in Microbiology* **2021**, *64*, 125–132.

[24] E. Sendra, A. Fernández-Muñoz, L. Zamorano, A. Oliver, J. P. Horcajada, C. Juan, S. Gómez-Zorrilla, *Infection* **2024**, *52*, 1235–1268.
[25] Bakker-Woudenberg Irma A. J. M., ten Kate Marian T., Guo Luke, Working Peter, Mouton Johan W., *Antimicrobial Agents and Chemotherapy* **2001**, *45*, 1487–1492.
[26] R. N. Brogden, R. M. Pinder, P. R. Sawyer, T. M. Speight, G. S. Avery, *Drugs* **1976**, *12*, 166–200.
[27] G. Yang, J. Trylska, Y. Tor, J. A. McCammon, *J. Med. Chem.* **2006**, *49*, 5478–5490.
[28] B. W. Ramsey, M. S. Pepe, J. M. Quan, K. L. Otto, A. B. Montgomery, J. Williams-Warren, M. Vasiljev-K, D. Borowitz, C. M. Bowman, B. C. Marshall, S. Marshall, A. L. Smith, *N Engl J Med* **1999**, *340*, 23–30.
[29] S. Smith, N. J. Rowbotham, K. H. Regan, *Cochrane Database Syst Rev* **2018**, *3*, CD001021.
[30] M. P. Mingeot-Leclercq, P. M. Tulkens, *Antimicrob Agents Chemother* **1999**, *43*, 1003–1012.
[31] E. E. Harruff, J. Kil, M. G. T. Ortiz, D. Dorgan, R. Jain, E. A. Poth, R. C. Fifer, Y. J. M. Kim, A. G. Shoup, P. A. Flume, *J Cyst Fibros* **2021**, *20*, 288–294.
[32] J. F. Marier, J. L. Brazier, J. Lavigne, M. P. Ducharme, *Journal of Antimicrobial Chemotherapy* **2003**, *52*, 247–252.
[33] K. Nakajima, J. Kawamata, *Biken J* **1966**, *9*, 115–123.
[34] M. Teuber, *Naturwissenschaften* **1967**, *54*, 71.
[35] S. Wagner, R. Sommer, S. Hinsberger, C. Lu, R. W. Hartmann, M. Empting, A. Titz, *J. Med. Chem.* **2016**, *59*, 5929–5969.
[36] G. Haran, R. Cohen, L. K. Bar, Y. Barenholz, *Biochim Biophys Acta* **1993**, *1151*, 201–215.
[37] P. C. Sharma, A. Jain, S. Jain, R. Pahwa, M. S. Yar, *Journal of Enzyme Inhibition and Medicinal Chemistry* **2010**, *25*, 577–589.
[38] C. Schütz, D.-K. Ho, M. M. Hamed, A. S. Abdelsamie, T. Röhrig, C. Herr, A. M. Kany, K. Rox, S. Schmelz, L. Siebenbürger, M. Wirth, C. Börger, S. Yahiaoui, R. Bals, A. Scrima, W. Blankenfeldt, J. C. Horstmann, R. Christmann, X. Murgia, M. Koch, A. Berwanger, B. Loretz, A. K. H. Hirsch, R. W. Hartmann, C.-M. Lehr, M. Empting, *Adv Sci (Weinh)* **2021**, *8*, e2004369.
[39] R. Sommer, S. Wagner, K. Rox, A. Varrot, D. Hauck, E.-C. Wamhoff, J. Schreiber, T. Ryckmans, T. Brunner, C. Rademacher, R. W. Hartmann, M. Brönstrup, A. Imberty, A. Titz, *J. Am. Chem. Soc.* **2018**, *140*, 2537–2545.
[40] Hauck, D., Jumde, V.R., Crawford, C.J., Titz, A., in *Carbohydrate Chmistry*, CRC Press, **2020**, p. 6.
[41] O. Metelkina, B. Huck, J. S. O'Connor, M. Koch, A. Manz, C.-M. Lehr, A. Titz, *J. Mater. Chem. B* **2022**, *10*, 537–548.

S1. Supporting information to "Dual inhibitors of *Pseudomonas aeruginosa* virulence factors LasB and LecA"

Olga Metelkina[▽a,b,c], Jelena Konstantinović[▽a], Andreas Klein[a,d], Roya Shafiei[a,d], Mario Fares[a,b,c], Alaa Alhayek[a], Samir Yahiaoui[a], Walid A. M. Elgaher[a], Jörg Haupenthal[a], Alexander Titz*[a,b,c], Anna K. H. Hirsch*[a,b,d]

[a]Helmholtz Institute for Pharmaceutical Research Saarland (HIPS) – Helmholtz Centre for Infection Research (HZI), 66123 Saarbrücken, Germany

[b]Deutsches Zentrum für Infektionsforschung (DZIF), Standort Hannover-Braunschweig, 38124 Braunschweig, Germany

[c]Saarland University, Department of Chemistry, 66123 Saarbrücken, Germany

[d]Saarland University, Department of Pharmacy, 66123 Saarbrücken, Germany

[▽]These authors contributed equally.

*corresponding authors: anna.hirsch@helmholtz-hips.de, alexander.titz@helmholtz-hips.de

General experimental details.

Commercial chemicals and solvents were used without further purification. Procedures were not optimized regarding yield. Thin layer chromatography (TLC) was performed using TLC Silica gel 60 F_{254} sheets (Merck KGaA, Darmstadt, Germany) and developed under UV light (254 nm) and using a cerium molybdate stain (0.02 M solution of $(NH_4)Ce(SO_4)_4 \cdot 2H_2O$ and $(NH_4)_6Mo_7O_{24} \cdot 4H_2O$ in aqueous 10% H_2SO_4) or a permanganate stain (3 g of $KMnO_4$, 20 g of K_2CO_3 in 5 mL of 5% NaOH and 300 mL of water) with heating. Medium pressure liquid chromatography (MPLC) was performed on a Combiflash Rf200 (Teledyne Isco) system using normal phase silica gel columns (60 Å, 400 mesh particle size, Fluka) or reversed-phase silica gel columns Chromabond Flash C_{18} ec (Macherey-Nagel, Düren, Germany). Preparative high-pressure liquid chromatography (HPLC) was performed on Waters 2545 Binary Gradient Module with a Waters 2489 UV/Vis detector using a RP-18 column (Nucleodur C18 Gravity SB, 5 µm, 250x21 mm from Macherey-Nagel, Germany) and DionexUltiMate 3000 UHPLC+ focused (Thermo Scientific, United States) using a reversed-phase C18 column (Hypersil gold, 5 µm, 250x10 mm from Macherey-Nagel, Germany). Analytical HPLC-MS was performed using: a) Thermo Dionex Ultimate 3000 HPLC (Thermo Scientific, United States) coupled to a Bruker amaZon SL mass spectrometer, with UV detection at 254 nm using a C18 column (Nucleoshell RP18plus, 2.7 µm, 100x2 mm from Macherey-Nagel, Germany) as stationary phase; b) ESI quadrupole MS (MSQ Plus or ISQ EC, Thermo Fisher Scientific, Dreieich, Germany) using C18 column (Hypersil gold, 3 µm, 100x2 mm from Thermo Scientific, United States) and c) Ultimate 3000 HPLC (Thermo Fisher) coupled to a TSQ Quantum Access Max triple quadrupole mass spectrometer (Thermo Fisher) using C18 column (Hypersil gold, 1.9 µm, 100x2 mm from Thermo Scientific, United States). Purity of the final compounds was determined by LC-MS using the UV trace recorded at a wavelength of 254 nm and found to be >95%. High resolution mass spectrometry (HRMS) was performed on an Ultimate 3000 UPLC system coupled to a Q Exactive Focus Orbitrap system with HESI source (Thermo Fisher, Dreieich, Germany). The UPLC was operated with a C18 column (EC 150/2 Nucleodur C18 Pyramid, 3 µm from Macherey-Nagel, Germany). ^{1}H- and ^{13}C-NMR spectra were recorded on a Bruker Avance III 500 UltraShield spectrometer at 500 MHz and 126 MHz, respectively. Chemical shifts (δ) are given in ppm and were calibrated on residual solvent peaks: $CHCl_3$-*d1* (^{1}H-NMR δ = 7.26 ppm, ^{13}C-NMR δ = 77.0 ppm), MeOH-*d4* (^{1}H-NMR δ = 3.31 ppm, ^{13}C -NMR δ = 49.0 ppm), DMSO-*d6* (^{1}H-NMR δ = 2.50 ppm, ^{13}C-NMR δ = 39.51 ppm). Deuterated solvents were purchased from Eurisotop (Saarbrücken, Germany). Multiplicities are specified

as s = singlet, bs = broad singlet, d = doublet, dd = doublet of doublets, t = triplet, td = triplet of doublets, q = quartet, m = multiplet. The spectra were assigned with the help of ^{1}H, ^{1}H-COSY and $^{1}H,^{13}C$-HSQC experiments.

Expression and purification of LasB and LecA

LecA was expressed recombinantly using *E. coli* pET25-pail, whereas LasB was isolated from *P. aeruginosa* PA14 culture supernatant as described previously.[1,2]

LecA labeling with fluorescein was performed in analogy to Sommer et al. [3] and Beshr et al.[4] To this end fluorescein isothiocyanate (FITC) was freshly dissolved in carbonate-bicarbonate buffer with pH of 9.3 at a concentration of 3 mg mL^{-1}. Subsequently, 66 µL of this FITC solution was combined with 1.4 mL of LecA at a concentration of 60 µM in carbonate-bicarbonate buffer, pH 9.3. The resulting mixture was then incubated at 25 °C with shaking at 500 rpm for 1 hour. Then, extensive washing with PBS/Ca^{2+} in a 5 kDa molecular weight cutoff centrifugal concentrator was performed to remove excess dye and buffer the labelled protein.

In vitro inhibition assay for LasB

The in vitro inhibition assay was performed as described previously,[2] using purified LasB (final concentration 0.3 nM), the fluorogenic substrate 2-aminobenzoyl-Ala-Gly-Leu-Ala-4-nitrobenzylamide (purchased from Peptides International (Louisville, KY, USA) or Vivitide, LLC (Gardner, MA, USA), final concentration 150 µM)) in assay buffer (50 mM Tris, pH 7.2, 2.5 mM $CaCl_2$, 0.075% Pluronic F-127, 5% DMSO). Fluorescence was measured using a CLARIOstar plate reader (BMG Labtech, Ortenberg, Germany). IC_{50} values were calculated using GraphPad Prism 8 (GraphPad Software, San Diego, CA, USA) from at least three independent experiments performed in duplicate.

Competitive binding assay for LecA

The procedure for the fluorescence polarization-based competitive binding assay for LecA was performed as reported by Joachim et al. with modifications.[1] The assay was performed in TBS/Ca^{2+} buffer (20 mM Tris, 137 mM NaCl, 2.6 mM KCl at pH 7.4 supplemented with 1 mM $CaCl_2$ and contained 5% DMSO). The final protein concentration in the assay was 5 µM for LecA. Fluorescence intensities were recorded on a PheraStar FS plate reader (BMG Labtech GmbH, Germany) and polarization was calculated using MARS Data Analysis (BMG Labtech). IC_{50} values were obtained from a four-parameter curve-fitting procedure. Averages

and standard deviations were calculated from at least three independent experiments of technical triplicates each.

Surface plasmon resonance direct LecA binding assay

SPR experiments were performed on a Reichert 2-channel SPR SR7500DC (Reichert Technologies Life Sciences, Buffalo, NY, USA) at 25 °C. For LecA immobilization, the surface of a HC1000M sensor chip (XanTec bioanalytics GmbH, Düsseldorf, Germany) was preequilibrated with borate buffer (1 M NaCl, 0.1 M sodium borate pH 9.0), followed by activation of the polycarboxylate hydrogel with 0.2 M *N*-hydroxysuccinimide (NHS) and 0.4 M 1-ethyl-3-(3-dimethylaminopropyl)carbodiimide hydrochloride (EDC·HCl) in MilliQ water in both channels for 240 s (flow rate 10 µL/min) until the binding response reached 1200 RU. Then, LecA (100 µg/mL) in 10 mM sodium acetate pH 3.6 was injected on the activated chip surface of one channel (injection time 420 s, flow rate 10 µL/min) and 6000 RU of LecA were immobilized. Unreacted NHS esters in both channels were blocked with 1 M ethanolamine hydrochloride in MilliQ water pH 8.5 (injection time 360 s, flow rate 10 µL/min).

Test compound stock solutions were prepared in DMSO (20 mM stocks for monovalent LecA inhibitors, 20 µM stocks for divalent LecA inhibitors) and were subsequently diluted in 10 mM phosphate buffer (pH 7.4, 2.7 mM KCl, 137 mM NaCl, 100 µM $CaCl_2$) to obtain solutions with 2% DMSO.

Monovalent inhibitors **17**, **18**, **24** and **25** were injected for 120 s (flow rate 50 µL/min) at concentrations ranging from 0.39–100 µM. Divalent inhibitors **26a**, **26b** and **27** were injected for 120 s (flow rate 50 µL/min) at concentrations 50–350 nM. The chip surface was regenerated after each inhibitor injection by one injection of 50 mM IPTG in running buffer (10 mM phosphate buffer, pH 7.4, 2.7 mM KCl, 137 mM NaCl, 100 µM $CaCl_2$, 2% DMSO) followed by one injection 20 mM EDTA disodium salt in MilliQ water, and then followed by three injections of the running buffer (injection time 120 s, flow rate 50 µL/min). 100 µM pNP-Gal (**1**) in running buffer was injected before each analyte to monitor and ensure chip regeneration and protein activity.

Affinity/equilibrium analysis was performed for **1** on the same chip. A stock solution of **1** (10 mM in PBS/$CaCl_2$ buffer) was prepared, then diluted to the required concentrations in running buffer and injected at 1.56–400 µM (injection time 60 s, flow rate 50 µL/min) without regeneration steps. Data analysis was performed using TraceDrawer software (Ridgeview Instruments) using a 1:1 binding model to fit the experimental data. Spikes at the end of the injections were removed in TraceDrawer during the data analysis.

Disulfide formation assay

The stability of two thiols **11** and **12** and their ability to form the corresponding disulfides was analyzed by HPLC-MS. Chemically synthesized disulfides **26** and **27** were used as references for the stability assay. 50 mM DMSO stocks of thiols **11** and **12** were diluted 40-fold with *P. aeruginosa* PA14 overnight LB medium culture supernatant (25% v/v, sterile filtered through 0.22 µm filters in 10 mM phosphate buffer, pH 7.4, 2.7 mM KCl, 137 mM NaCl, 100 µM $CaCl_2$) at 37 °C. Samples were drawn over 4.5 hours and analyzed by LC-MS using a RP-18 column 100/2 Nucleoshell RP18plus, 2.7 µm from Macherey-Nagel, Germany (H_2O/MeCN + 0.1% formic acid, 15 – 55% MeCN, retention time (t_R) 5.8 min (**11** or **12)**, 6.1 min and 6.3 min (disulfide products **26** or **27**) on a Thermo Dionex Ultimate 3000 HPLC coupled to a Bruker amaZon SL mass spectrometer, with UV detection at 254 nm). Thiol half-lives were determined by analysis of the obtained graphs and values of 80 min for **11** and 46 min for **12** were obtained (Figure 2).

Selectivity and toxicity assays

Human MMPs -1, -2, -3, -7, -8 and -14 along with the SensoLyte 520 Generic MMP Activity Kit*Fluorimetric* were purchased from AnaSpec (Fremont, CA, USA). The inhibition assay was performed according to the guidelines of the manufacturer and as described recently.[5]

Cytotoxicity on human liver (HepG2), kidney (HEK293) and lung (A549) cells were performed using MTT assay and measuring the optical density (OD) photometrically at 570 nm in a FLUOstar Omega plate reader (BMG labtech, Ortenberg, Germany) as described previously.[6]

Antimicrobial activity against *P. aeruginosa* PA14 was tested using ESCMID guidelines and details have been reported previously.[7]

***In vitro* evaluation of 12 and a combination of 1 and 2 using *P. aeruginosa* culture supernatant and A549 cells in a cell viability assay**

The A549 cell line, derived from human lung adenocarcinoma, was grown in Dulbecco's Modified Eagle Medium (DMEM) supplemented with 10% Fetal Bovine Serum (FBS) and 1% penicillin-streptomycin. The cells were cultured following standard protocols for cell maintenance.

To prepare the bacterial culture supernatant, individual flasks containing 15 mL of lysogeny broth (LB) culture medium were inoculated with PAO1 or PAO1 Δ*lasB* strains. Culture flasks were placed on a shaker and incubated at 37 °C and 180 rpm overnight for 18 hours. Following incubation, the bacterial cultures were subjected to centrifugation at 4 °C and 5000 rpm for

10 min, facilitating the separation of bacterial cells from the supernatant. The latter was filtered through a 0.22 µm sterile filter and stored at –80 °C until further use.

In a flat bottom 96-well plate (Corning™ Costar™), each well was seeded with 2.5–3.5*10^3 cells in 100 µL DMEM/FCS and then incubated at a temperature of 37 °C with 5% CO_2 for 24 hours. Then, compounds **12** and **1** combined with **2** in concentrations of 100 µM, 10 µM, and 1 µM were mixed with 10% (v/v) of culture supernatant of *P. aeruginosa* PAO1 (DSM 22644, ATCC 15692) in DMEM/FCS. To minimize the potential negative effect of DMSO, the compound was initially dissolved in 99.9% DMSO, and a final assay concentration of 0.5% DMSO was applied. Additionally, the cells were exposed to 10% (v/v) PAO1 Δ*lasB* culture supernatant to analyze the effect caused by LasB, while DMEM/FCS without any treatment served as a control. The plates were then incubated at 37 °C with 5% CO_2 for 24 hours before conducting the MTT assay.

MTT assay

To assess cell viability, the medium in the well plates was aspirated and a single wash was performed using 100 µL of phosphate buffered saline, pH 7.4 (PBS). A solution of 5 mg MTT (3-(4,5-dimethylthiazol-2-yl)-2,5-diphenyl tetrazolium bromide) per mL PBS was prepared and diluted to a concentration of 10% (v/v) in DMEM/FCS. Subsequently, 100 µL of this MTT solution was added to each well, and the plates were incubated at 37 °C for 3 hours with 5% CO_2. After incubation, the MTT solution was carefully removed, and the formazan crystals were dissolved by adding 150 µL of lysis solution (250 mL DMSO, 25 g SDS, and 1.25 mL AcOH) to each well. The plates were then incubated for an additional 30 min at 37 °C and then, the UV absorbance was measured using a PHERAstar microplate reader. The test samples were read at a wavelength of 550 nm, while the blank was read at 620 nm. At last, the data were statistically analyzed and presented graphically using GraphPad Prism 9 (Figure S4 and S5).

Evaluation of compounds 1, 2 and 12 in inhibiting LecA adhesion to A549 cells via fluorescence microscopy

The A549 cell line were cultured following the protocols for cell maintenance described above. In a flat-bottom cell culture black 96-well plate (Greiner Bio-One, #Cat 655090) each well was seeded with 1*10^4 cells in 100 µL DMEM/FCS and subsequently, incubated overnight at 37 °C with 5% CO_2. On the following day, concentrations of 100 µM, 10 µM, and 1 µM of the compounds **1**, **2**, the combination of **1** and **2**, or **12** were incubated for 30 min at room temperature with 10 µM FITC-labeled LecA. Each test sample comprises 100 µL solution of

10 µM FITC-labeled LecA in DMEM/FCS and varying concentrations of the test compound (ranging from 1 µM to 100 µM). This prepared mixture was then added after 30 min incubation at room temperature to the cell culture wells in duplicate. The compounds were initially dissolved in 99.9% DMSO, and a final assay concentration of 0.5% DMSO was used. Furthermore, the A549 cells were exposed to 10 µM FITC-labeled LecA both with or without DMSO to quantify staining efficacy of LecA on A549 cells and to ensure that DMSO did not have any negative effects. The plate was then incubated at 4 °C for 30 min and wells were washed 5 times with PBS prior to imaging via fluorescence microscopy.

Fluorescence image acquisition, processing, and quantification

Fluorescence images were captured using an inverted fluorescence microscope (Leica DMi8) equipped with a 20x objective (HC PL APO CS2 20x/0.75 IMM UV), an FITC filter cube (EX: 460-500 nm, DC: 505, EM: 512-542 nm) and a monochrome microscope camera (Leica DFC7000 GT). The Leica Application suite X (3.7.4.23463) software navigator was used to image the whole well at one plane. The same image settings were used for imaging all the conditions in each biological replicate.

From each of the three biological replicates, three representative images were selected, each originating from two technical duplicates. Background fluorescence was subtracted using the LasX image processing software with the slider value at 500. Background-subtracted images were then exported as TIFF files, lossless compression, and scale bar were ticked.

The fluorescence signal was quantified with ImageJ by selecting the whole background subtracted image and calculating its mean fluorescence intensity. Data were plotted and statistically analyzed using GraphPad Prism.

X-ray Crystallography of the complex of 11 with LasB.

LasB at a concentration of 3.6 mg/mL was mixed with the diastereomeric mixture of **11** to get a final concentration of 1 mM compound in a 10 mM Tris buffer containing 2 mM $CaCl_2$. Crystal-screens have been set up using the sitting drop method and commercially available PEGs and PEGs II screen solutions (NeXtal Biotechnologies, 6201 Trust Drive Holland, OH 43528). The crystal for the final data set was obtained from the PEG F6 condition, containing 0.2 M potassium nitrate and 20% (w/v) PEG 3350. For data collection, the crystals were cryoprotected with a final concentration of 25% glycerol. Diffraction data were collected at beamline ID30B (ESRF, Grenoble, France) at 100 K and a wavelength of 0.9763 Å. The data was processed using CCP4 Aimless,[8] and the structure was solved by molecular replacement using *P. aeruginosa* LasB (PDB ID 6FZX) without the ligand as a search model in PHASER.

The solution was rebuilt using AutoBuild. Refinement was done with phenix.refine (Phenix version 1.19.2-4158-000)[9] and manually with WinCOOT (0.9.6)[10]. Images were created using PyMOL (2.5.2)[11] (Figure S6).

Synthesis

General procedure A: Synthesis of *N*-aryl-2-bromo-2-alkyl(aryl)acetamide derivatives

2-Haloalkanoic acid (1.2 equiv.) and EDC·HCl (1.2 equiv.) were added to a solution of the corresponding aniline (1.0 equiv.) in DCM. The resultant mixture was stirred at r.t. for 4 h. The solution obtained was washed with 1 M HCl and saturated aqueous NaCl solution. The organic layer was dried over anhydrous Na_2SO_4, filtered and concentrated under reduced pressure to afford the crude product. The crude product was purified using column chromatography.

General procedure B: Synthesis of *N*-aryl-2-thioacetyl-2-alkyl(aryl)acetamide derivatives

N-Aryl-2-bromo-2-alkyl(aryl)acetamide derivative (1.0 equiv.) was dissolved in acetone, and potassium thioacetate (2.0 equiv.) was added to the solution. The resultant mixture was stirred at r.t. for 2 h. After concentration under vacuum, the resultant residue was diluted with H_2O and extracted with EtOAc. The organic layer was washed with saturated aqueous NaCl solution, dried over anhydrous Na_2SO_4, filtered and evaporated under reduced pressure. The crude residue was purified using column chromatography.

General procedure C: Synthesis of *N*-aryl-2-mercapto-2-alkyl(aryl)acetamide derivatives

N-aryl-2-thioacetyl-2-alkyl(aryl)acetamide derivatives were dissolved in MeOH under argon atmosphere and NaOMe (5.33 M in MeOH, 4.0–7.0 equiv.) was added to this solution. The reaction was stirred at r.t. for 45 min. pH was neutralized with Amberlite IR-120. After filtration and evaporation of the solvent, the product was obtained as pure material or purified using preparative HPLC.

General procedure D: Synthesis of disulfides

Thiols obtained as diastereomeric mixtures were dissolved in DMSO/H_2O 1:1 and 3% (v/v) H_2O_2 (2.5 equiv.) was added, and the reaction was stirred at r.t. for 4 h. The reaction mixture was diluted with ice-cold water and lyophilized. The product was purified by preparative HPLC.

***p*-Nitrophenyl 2,3,4,6-tetra-*O*-acetyl-β-D-thiogalactopyranoside (5)**.

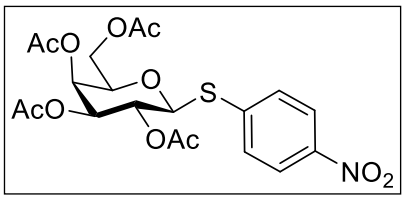

Penta-*O*-acetyl-β-D-galactose **4**[12] (2 g, 5.12 mmol) and *para*-nitro-thiophenol (1.59 g, 10.24 mmol) were dissolved in 20 mL dry dichloromethane with 200 mg 3 Å activated molecular sieves under nitrogen flow. The reaction mixture was cooled down to 0 °C on an ice bath, triflic acid (360 µL, 4.09 mmol) was added dropwise via a cannula and stirred for 30 min. The reaction was diluted with dichloromethane, filtered through celite and washed with sodium bicarbonate, water and saturated aqueous NaCl solution sequentially, then dried over anhydrous sodium sulfate. After filtration, the organic phase obtained was concentrated in vacuo and recrystallized twice from EtOAc to provide **5** as white crystals (1.65 g, 66%). The acquired ^{1}H and ^{13}C NMR spectra (500 MHz) were found in agreement with reported data of Escopy *et al*.[13]

***p*-Aminophenyl 2,3,4,6-tetra-*O*-acetyl-β-D-thiogalactopyranoside (6)**.

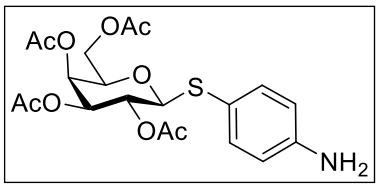

Compound **5** (900 mg, 1.86 mmol) was suspended in dry dichloromethane (40 mL), and palladium on activated charcoal (90 mg, 10% w/w) was added under a nitrogen atmosphere. The reaction flask was flushed with hydrogen and stirred at room temperature overnight under a hydrogen atmosphere. The reaction mixture was filtered through celite, and the solvent was removed *in vacuo.* The crude product was purified by normal phase MPLC (PhMe/EtOAc, 40–80% EtOAc). **6** was obtained as a pale pink solid (818 mg, 97%). The acquired ^{1}H and ^{13}C NMR spectra (500 MHz) were found in agreement with reported data of Casoni *et al*.[14]

(2*R*,3*S*,4*S*,5*R*,6*S*)-2-(Acetoxymethyl)-6-((4-(2-bromo-3-phenylpropanamido)phenyl)thio)tetrahydro-2*H*-pyran-3,4,5-triyl triacetate (7)

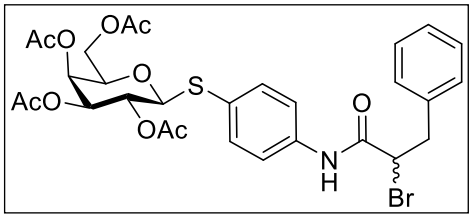

Compound **7** was synthesized according to the general procedure A, using 2-bromo-3-phenylpropanoic acid (72.5 mg, 0.32 mmol), compound **6** (120 mg, 0.26 mmol), EDC·HCl (60.4 mg, 0.32 mmol) and DCM (15 mL). The obtained crude product was purified using column chromatography (Hex/EtOAc = 6/4 to 1/1), to give compound **7** as a white solid (150.5 mg, 86%). ^{1}H NMR (500 MHz, $CDCl_3$) δ 7.85 (s, 1H), 7.53 – 7.49 (m, 2H), 7.47 – 7.43 (m, 2H), 7.35 – 7.25 (m, 5H), 5.40 (d, *J* = 3.2 Hz, 1H), 5.20 (td, *J* = 10.0, 2.2 Hz, 1H), 5.04 (dd, *J* = 9.9, 3.4 Hz, 1H), 4.64 (d, *J* = 9.9

Hz, 1H), 4.63 – 4.58 (m, 1H), 4.21 – 4.15 (m, 1H), 4.14 – 4.08 (m, 1H), 3.91 (t, *J* = 6.6 Hz, 1H), 3.61 (ddd, *J* = 14.3, 6.0, 2.1 Hz, 1H), 3.35 (ddd, *J* = 14.3, 7.5, 1.8 Hz, 1H), 2.11 (s, 3 H), 2.10 (s, 3 H), 2.05 (s, 3 H), 1.97 (s, 3 H). ^{13}C NMR (126 MHz, $CDCl_3$) δ 170.6, 170.4, 170.2, 169.6, 166.2, 137.4, 136.72, 136.69 (two signals at 136.7 due to diastereomeric mixture), 134.3, 129.6, 128.7, 128.1, 127.6, 120.4, 86.8, 74.6, 72.1, 67.34, 67.32, 61.7, 51.81, 51.76 (two signals at 51.8 due to diastereomeric mixture), 41.7, 21.0, 20.9, 20.8, 20.7. MS (ESI$^+$) m/z calculated for $[C_{29}H_{33}BrNO_{10}S]^+$ 666.10 $[M+H]^+$, found 665.97.

(2*R*,3*S*,4*S*,5*R*,6*S*)-2-(Acetoxymethyl)-6-((4-(2-bromo-4-methylpentanamido)phenyl)thio)tetrahydro-2*H*-pyran-3,4,5-triyl triacetate (8)

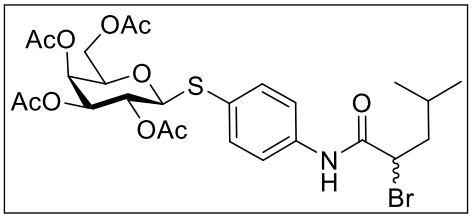

Compound **8** was synthesized according to the general procedure A, using 2-bromo-4-methylpentanoic acid (87.6 mg, 0.45 mmol), EDC·HCl (86.1 mg, 0.45 mmol), aniline **6** (170.5 mg, 0.37 mmol) and DCM (7.5 mL). The crude product obtained was purified using column chromatography (Hex/EtOAc = 1:1), to give compound **8** as a white solid (174.5 mg, 74%). ^{1}H NMR (500 MHz, $CDCl_3$) δ 8.04 (s, 1H), 7.51 (s, 4H), 5.41 (d, *J* = 2.6 Hz, 1H), 5.20 (t, *J* = 9.9 Hz, 1H), 5.03 (dd, *J* = 10.0, 3.3 Hz, 1H), 4.63 (d, *J* = 10.0 Hz, 1H), 4.43 (dd, *J* = 9.4, 5.5 Hz, 1H), 4.21 – 4.16 (m, 1H), 4.14 – 4.09 (m, 1H), 3.91 (t, *J* = 6.6 Hz, 1H), 2.12 (s, 3H), 2.10 (s, 3H), 2.05 (s, 3H), 2.03 – 1.95 (m, 2H), 1.97 (s, 3H), 1.95 – 1.85 (m, 1H), 1.00 (d, *J* = 6.6 Hz, 3H), 0.95 (d, *J* = 6.6 Hz, 3H). ^{13}C NMR (126 MHz, $CDCl_3$) δ 170.6, 170.4, 170.2, 169.6, 167.3, 137.7, 134.3, 127.8, 120.2, 86.8, 74.5, 72.1, 67.3 (2C), 61.7, 50.7, 44.6, 26.5, 22.8, 21.2, 21.0, 20.9, 20.8, 20.7. MS (ESI$^+$) m/z calculated for $[C_{26}H_{35}BrNO_{10}S]^+$ 632.12 $[M+H]^+$, found 632.00.

(2*R*,3*S*,4*S*,5*R*,6*S*)-2-(Acetoxymethyl)-6-((4-(2-(acetylthio)-3-phenylpropanamido)phenyl)thio)tetrahydro-2*H*-pyran-3,4,5-triyl triacetate (9)

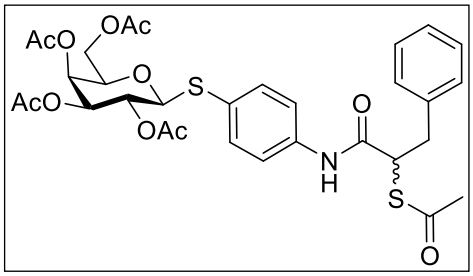

Compound **9** was synthesized according to the general procedure B, using compound **7** (147.7 mg, 0.22 mmol), potassium thioacetate (51 mg, 0.44 mmol) and acetone (5 mL). The crude product was purified using column chromatography (Hex/EtOAc = 1:1) to give compound **9** as a pale-yellow solid (106.2 mg, 72%). ^{1}H NMR (500 MHz, $CDCl_3$) δ 8.05 (bd, *J* = 4.4 Hz, 1H), 7.50 – 7.40 (m, 4H), 7.34 – 7.20 (m, 5H), 5.39 (bd, *J* = 3.4 Hz, 1H), 5.18 (td, *J* = 10.0, 2.8 Hz, 1H), 5.02 (dd, *J* = 9.9, 3.2 Hz, 1H), 4.60 (d, *J* = 9.9 Hz, 1H), 4.27 (dd, *J* = 8.3, 7.2 Hz, 1H),

4.20 – 4.05 (m, 2H), 3.89 (t, *J* = 6.6 Hz, 1H), 3.43 (dd, *J* = 14.1, 8.5 Hz, 1H), 2.99 (ddd, *J* = 14.2, 7.0, 1.8 Hz, 1H), 2.38 (s, 3H), 2.10 (s, 3H), 2.10 (s, 3H), 2.04 (s, 3H), 1.97 (s, 3H). ^{13}C NMR (126 MHz, $CDCl_3$) δ 197.70, 197.66 (two signals at 197.7 due to diastereomeric mixture), 170.6, 170.4, 170.2, 169.6, 168.6, 138.2, 137.6, 134.41, 134.37 (two signals at 134.4 due to diastereomeric mixture), 129.4, 128.8, 127.22, 127.17, 127.13 (two signals at 127.17 and 127.13 due to diastereomeric mixture), 120.17, 120.13 (two signals at 120.17 and 120.13 due to diastereomeric mixture), 87.0, 86.9 (two signals at 87.0 and 86.9 due to diastereomeric mixture), 74.6, 72.1, 67.4, 67.3, 61.7, 48.6, 48.5 (two signals at 48.6 and 48.5 due to diastereomeric mixture), 35.7, 30.6, 21.0, 20.86, 20.84 (two signals at 20.86 and 20.84 due to diastereomeric mixture), 20.81, 20.79 (two signals at 20.8 due to diastereomeric mixture), 20.73. MS (ESI$^+$) m/z calculated for $[C_{31}H_{36}NO_{11}S_2]^+$ 662.17 $[M+H]^+$, found 662.03.

(2*R*,3*S*,4*S*,5*R*,6*S*)-2-(Acetoxymethyl)-6-((4-(2-(acetylthio)-4-methylpentanamido)phenyl)thio)tetrahydro-2*H*-pyran-3,4,5-triyl triacetate (10)

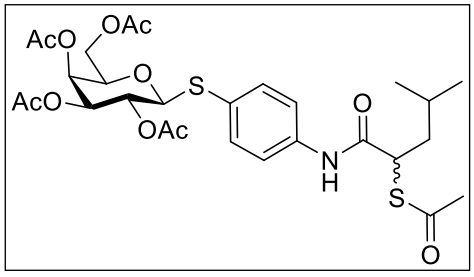

Compound **10** was synthesized according to the general procedure B, using compound **8** (152 mg, 0.24 mmol) and potassium thioacetate (55 mg, 0.48 mmol) in acetone (5 mL). The crude residue was purified using column chromatography (Hex/EtOAc = 8:2 to 6:4) to give compound **10** as a white solid (102 mg, 68%). ^{1}H NMR (500 MHz, $CDCl_3$) δ 8.23 (s, 1H), 7.53 – 7.44 (m, 4H), 5.40 (dd, *J* = 3.3, 0.8 Hz, 1H), 5.19 (t, *J* = 10.0 Hz, 1H), 5.02 (dd, *J* = 10.0, 3.3 Hz, 1H), 4.60 (d, *J* = 10.0 Hz, 1H), 4.20 – 4.14 (m, 1H), 4.12 – 4.06 (m, 2H), 3.91 – 3.86 (m, 1H), 2.41 (s, 3H), 2.12 (s, 3H), 2.10 (s, 3H), 2.05 (s, 3H), 2.01 – 1.94 (m, 1H), 1.98 (s, 3H), 1.73 (sep, *J* = 6.7 Hz, 1H), 1.59 – 1.54 (m, 1H), 0.96 (d, *J* = 6.6 Hz, 3H), 0.92 (d, *J* = 6.6 Hz, 3H). ^{13}C NMR (126 MHz, $CDCl_3$) δ 198.5, 170.6, 170.4, 170.2, 169.6, 169.3, 138.4, 134.4, 126.9, 120.0, 87.0, 74.5, 72.1, 67.3 (2C), 61.7, 45.2, 37.8, 30.5, 26.0, 22.5, 22.4, 21.0, 20.9, 20.84, 20.76. MS (ESI$^+$) m/z calculated for $[C_{28}H_{38}NO_{11}S_2]^+$ 628.19 $[M+H]^+$, found 628.06.

2-Mercapto-3-phenyl-*N*-(4-(((2*S*,3*R*,4*S*,5*R*,6*R*)-3,4,5-trihydroxy-6-(hydroxymethyl)tetrahydro-2*H*-pyran-2-yl)thio)phenyl)propanamide (11)

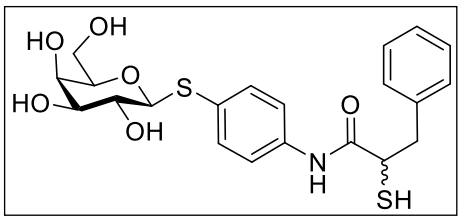

Compound **11** was synthesized according to the general procedure C, using compound **9** (102.7 mg, 0.16 mmol), sodium methoxide (175 µL, 5.33 M, 0.93 mmol) and MeOH (5 mL). The crude product was purified using preparative HPLC (CH_3CN (FA 0.05%)/H_2O (FA 0.05%) = 5:95 to 95:5), to give the compound **11** as a white solid (29.9 mg, 43%). ^{1}H NMR (500 MHz, DMSO-d_6) δ 10.05 (s, 1H), 7.51 – 7.44 (m, 2H), 7.39 (d, J = 8.6 Hz, 2H), 7.30 – 7.22 (m, 4H), 7.21 – 7.16 (m, 1H), 5.07 (d, J = 5.8 Hz, 1H), 4.83 (d, J = 5.6 Hz, 1H), 4.60 (t, J = 5.6 Hz, 1H), 4.45 (d, J = 9.3 Hz, 1H), 4.42 (d, J = 4.4 Hz, 1H), 3.76 – 3.70 (m, 1H), 3.68 (t, J = 3.7 Hz, 1H), 3.53 – 3.44 (m, 2H), 3.43 – 3.39 (m, 1H), 3.39 – 3.29 (m, 2H), 3.24 (dd, J = 13.6, 8.8 Hz, 1H), 3.12 (s, 1H), 2.93 (dd, J = 13.6, 6.4 Hz, 1H). ^{13}C NMR (126 MHz, DMSO-d_6) δ 170.4, 138.6, 137.6, 131.15, 131.13 (two signals at 131.15 and 131.13 due to diastereomeric mixture), 129.0, 128.9, 128.3, 126.5, 119.5, 88.27, 88.23 (two signals at 88.27 and 88.23 due to diastereomeric mixture), 79.2, 74.7, 69.2, 68.4, 60.6, 43.2, 41.2. HRMS (ESI$^-$) m/z calculated for $[C_{21}H_{24}NO_6S_2]^-$ 450.1051 $[M–H]^-$, found 450.1045.

2-Mercapto-4-methyl-*N*-(4-(((2*S*,3*R*,4*S*,5*R*,6*R*)-3,4,5-trihydroxy-6-(hydroxymethyl)tetrahydro-2*H*-pyran-2-yl)thio)phenyl)pentanamide (12).

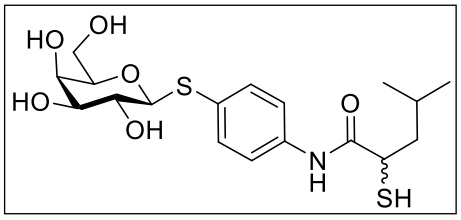

Compound **12** was synthesized according to the general procedure C, using compound **10** (97.4 mg, 0.16 mmol), sodium methoxide (175 µL, 5.33 M, 0.93 mmol) and MeOH (6 mL). The crude product was purified using preparative HPLC (CH_3CN (FA 0.05%)/H_2O (FA 0.05%) = 5:95 to 95:5), to give compound **12** as a white solid (38.9 mg, 60%). ^{1}H NMR (500 MHz, DMSO-d_6) δ 10.13 (s, 1H), 7.53 (d, J = 8.7 Hz, 2H), 7.42 (d, J = 8.7 Hz, 2H), 5.11 (d, J = 5.8, 1H), 4.88 (d, J = 5.5 Hz, 1H), 4.63 (t, J = 5.6 Hz, 1H), 4.48 – 4.44 (m, 2H), 3.68 (t, J = 3.7 Hz, 1H), 3.55 – 3.37 (m, 5H), 3.34 – 3.29 (m, 1H), 3.01 (s, 1H), 1.79 (ddd, J = 13.3, 8.5, 6.4 Hz, 1H), 1.62 (sep, J = 6.7 Hz, 1H), 1.50 (dt, J = 13.7, 7.0 Hz, 1H), 0.91 (d, J = 6.6 Hz, 3H), 0.86 (d, J = 6.6 Hz, 3H). ^{13}C NMR (126 MHz, DMSO-d_6) δ 171.2, 137.8, 131.2, 128.8, 119.5, 88.3, 79.2, 74.7, 69.2, 68.4, 60.6, 44.3, 40.1 (behind DMSO, based on HSQC), 25.8, 22.3, 22.1. HRMS (ESI$^+$) m/z calculated for $[C_{18}H_{28}NO_6S_2]^+$ 418.1353 $[M+H]^+$, found 418.1339.

(2*R*,3*S*,4*S*,5*R*,6*S*)-2-(Acetoxymethyl)-6-((4-((*S*)-2-bromo-3-phenylpropanamido)phenyl)thio)tetrahydro-2*H*-pyran-3,4,5-triyl triacetate (13)

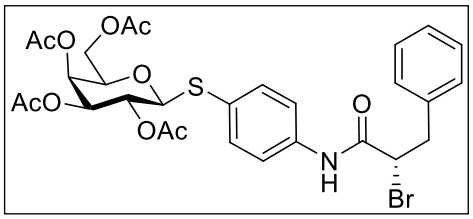

Compound **13** was synthesized according to the general procedure A, using (*S*)-2-bromo-3-phenylpropanoic acid (120.7 mg, 0.53 mmol), compound **6** (200 mg, 0.44 mmol), EDC·HCl (101.3 mg, 0.53 mmol) and DCM (15 mL). The obtained crude product was purified using column chromatography (Hex/EtOAc = 6:4 to 1:1), to give compound **13** as a white solid (246.9 mg, 84%). ^{1}H NMR (500 MHz, $CDCl_3$) δ 7.85 (s, 1H), 7.52 – 7.48 (m, 2H), 7.46 – 7.42 (m, 2H), 7.34 – 7.24 (m, 5H), 5.41 (d, *J* = 2.6 Hz, 1H), 5.20 (t, *J* = 10.0 Hz, 1H), 5.04 (dd, *J* = 9.9, 3.4 Hz, 1H), 4.64 (d, *J* = 9.9 Hz, 1H), 4.61 (dd, *J* = 7.5, 6.0 Hz, 1H), 4.21 – 4.15 (m, 1H), 4.13 – 4.08 (m, 1H), 3.91 (t, *J* = 6.6 Hz, 1H), 3.61 (dd, *J* = 14.3, 5.8 Hz, 1H), 3.35 (dd, *J* = 14.3, 7.5 Hz, 1H), 2.11 (s, 3 H), 2.10 (s, 3 H), 2.05 (s, 3 H), 1.97 (s, 3 H). ^{13}C NMR (126 MHz, $CDCl_3$) δ 170.5, 170.3, 170.2, 169.6, 166.2, 137.4, 136.7, 134.2, 129.6, 128.7, 128.1, 127.6, 120.4, 86.8, 74.6, 72.1, 67.33, 67.31, 61.7, 51.8, 41.7, 21.0, 20.9, 20.8, 20.7. MS (ESI$^+$) m/z calculated for $[C_{29}H_{33}BrNO_{10}S]^+$ 666.10 $[M+H]^+$, found 666.12.

(2*R*,3*S*,4*S*,5*R*,6*S*)-2-(Acetoxymethyl)-6-((4-((*S*)-2-bromo-4-methylpentanamido)phenyl)thio)tetrahydro-2*H*-pyran-3,4,5-triyl triacetate (14)

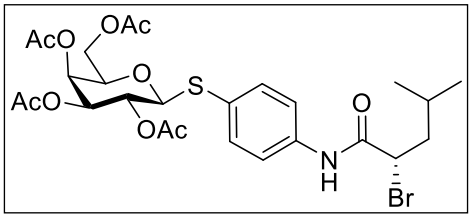

Compound **14** was synthesized according to the general procedure A, using (*S*)-2-bromo-4-methylpentanoic acid (103 mg, 0.53 mmol), EDC·HCl (101 mg, 0.53 mmol), aniline **6** (200 mg, 0.44 mmol) and DCM (20 mL). The crude product obtained was purified using column chromatography (Hex/EtOAc = 1:1), to give compound **14** as a white solid (232 mg, 84%). ^{1}H NMR (500 MHz, $CDCl_3$) δ 8.04 (s, 1H), 7.51 (s, 4H), 5.41 (d, *J* = 2.9 Hz, 1H), 5.20 (t, *J* = 10.0 Hz, 1H), 5.03 (dd, *J* = 9.9, 3.4 Hz, 1H), 4.63 (d, *J* = 9.9 Hz, 1H), 4.43 (dd, *J* = 9.5, 5.5 Hz, 1H), 4.21 – 4.15 (m, 1H), 4.13 – 4.08 (m, 1H), 3.91 (t, *J* = 6.6 Hz, 1H), 2.12 (s, 3H), 2.10 (s, 3H), 2.05 (s, 3H), 2.04 – 1.95 (m, 2H), 1.97 (s, 3H), 1.94 – 1.85 (m, 1H), 1.00 (d, *J* = 6.7 Hz, 3H), 0.94 (d, *J* = 6.6 Hz, 3H). ^{13}C NMR (126 MHz, $CDCl_3$) δ 170.6, 170.4, 170.2, 169.6, 167.2, 137.7, 134.3, 127.8, 120.2, 86.8, 74.5, 72.1, 67.27, 67.26, 61.7, 50.7, 44.6, 26.5, 22.8, 21.2, 21.0, 20.9, 20.83, 20.75. MS (ESI$^-$) m/z calculated for $[C_{26}H_{33}BrNO_{10}S]^-$ 630.10 $[M–H]^-$, found 630.28.

(2*R*,3*S*,4*S*,5*R*,6*S*)-2-(Acetoxymethyl)-6-((4-((*R*)-2-(acetylthio)-3-phenylpropanamido)phenyl)thio)tetrahydro-2*H*-pyran-3,4,5-triyl triacetate (15)

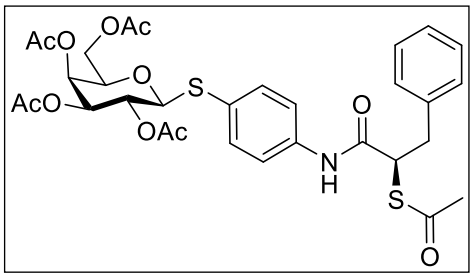

Compound **15** was synthesized according to the general procedure B, using compound **13** (239.3 mg, 0.36 mmol), potassium thioacetate (82 mg, 0.72 mmol) and acetone (7 mL). The crude product was purified using column chromatography (Hex/EtOAc = 1:1) to give compound **15** as a white solid (198.4 mg, 84%). ^{1}H NMR (500 MHz, $CDCl_3$) δ 8.06 (s, 1H), 7.48 – 7.40 (m, 4H), 7.32 – 7.20 (m, 5H), 5.40 (d, *J* = 2.9 Hz, 1H), 5.19 (t, *J* = 10.0 Hz, 1H), 5.02 (dd, *J* = 9.9, 3.4 Hz, 1H), 4.60 (d, *J* = 9.9 Hz, 1H), 4.27 (dd, *J* = 8.5, 7.1 Hz, 1H), 4.19 – 4.14 (m, 1H), 4.13 – 4.07 (m, 1H), 3.89 (t, *J* = 6.7 Hz, 1H), 3.43 (dd, *J* = 14.2, 8.5 Hz, 1H), 2.98 (dd, *J* = 14.1, 7.1 Hz, 1H), 2.38 (s, 3H), 2.11 (s, 3H), 2.10 (s, 3H), 2.04 (s, 3H), 1.97 (s, 3H). ^{13}C NMR (126 MHz, $CDCl_3$) δ 197.7, 170.5, 170.4, 170.2, 169.6, 168.5, 138.2, 137.6, 134.4, 129.4, 128.8, 127.2, 127.1, 120.1, 86.9, 74.6, 72.1, 67.4, 67.3, 61.7, 48.5, 35.7, 30.6, 21.0, 20.84, 20.80, 20.7. MS (ESI$^+$) m/z calculated for $[C_{31}H_{36}NO_{11}S_2]^+$ 662.17 $[M+H]^+$, found 662.23.

(2*R*,3*S*,4*S*,5*R*,6*S*)-2-(Acetoxymethyl)-6-((4-((*R*)-2-(acetylthio)-4-methylpentanamido)phenyl)thio)tetrahydro-2*H*-pyran-3,4,5-triyl triacetate (16)

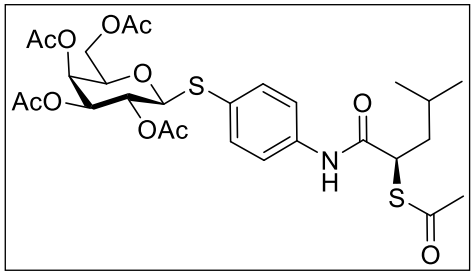

Compound **16** was synthesized according to the general procedure B, using compound **14** (225 mg, 0.36 mmol) and potassium thioacetate (81.2 mg, 0.71 mmol) in acetone (7 mL). The crude residue was purified using column chromatography (Hex/EtOAc = 8/2 to 6/4) to give compound **16** as a white solid (151 mg, 68%). ^{1}H NMR (500 MHz, $CDCl_3$) δ 8.23 (s, 1H), 7.52 – 7.45 (m, 4H), 5.40 (d, *J* = 2.7 Hz, 1H), 5.19 (t, *J* = 9.9 Hz, 1H), 5.02 (dd, *J* = 9.9, 3.4 Hz, 1H), 4.60 (d, *J* = 9.9 Hz, 1H), 4.20 – 4.14 (m, 1H), 4.13 – 4.06 (m, 2H), 3.91 – 3.87 (m, 1H), 2.41 (s, 3H), 2.12 (s, 3H), 2.10 (s, 3H), 2.05 (s, 3H), 2.00 – 1.95 (m, 1H), 1.98 (s, 3H), 1.74 (sep, *J* = 6.7 Hz, 1H), 1.60 – 1.54 (m, 1H), 0.96 (d, *J* = 6.6 Hz, 3H), 0.92 (d, *J* = 6.6 Hz, 3H). ^{13}C NMR (126 MHz, $CDCl_3$) δ 198.5, 170.6, 170.4, 170.2, 169.6, 169.3, 138.4, 134.4, 126.9, 120.0, 87.0, 74.5, 72.1, 67.3 (2C), 61.7, 45.2, 37.8, 30.5, 26.0, 22.5, 22.4, 21.0, 20.9, 20.84, 20.76. MS (ESI$^+$) m/z calculated for $[C_{28}H_{38}NO_{11}S_2]^+$ 628.19 $[M+H]^+$, found 628.13.

(*R*)-2-Mercapto-3-phenyl-*N*-(4-(((2*S*,3*R*,4*S*,5*R*,6*R*)-3,4,5-trihydroxy-6-(hydroxymethyl)tetrahydro-2*H*-pyran-2-yl)thio)phenyl)propanamide (17)

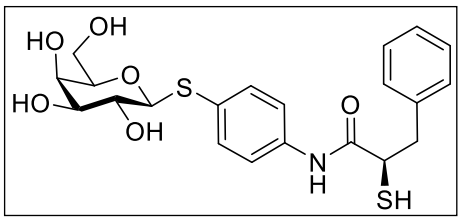

Compound **17** was synthesized according to the general procedure C, using compound **15** (184.3 mg, 0.28 mmol), sodium methoxide (210 µL, 5.33 M in MeOH, 1.11 mmol) and MeOH (6 mL). The crude product was purified using preparative HPLC (CH_3CN (FA 0.05%)/H_2O (FA 0.05%) = 5/95 to 95/5), to give the compound **17** as a white solid (47 mg, 37%). ^{1}H NMR (500 MHz, DMSO-d_6) δ 10.05 (s, 1H), 7.46 (d, J = 8.7 Hz, 2H), 7.39 (d, J = 8.7 Hz, 2H), 7.30 – 7.21 (m, 4H), 7.21 – 7.16 (m, 1H), 5.07 (d, J = 5.8 Hz, 1H), 4.83 (d, J = 5.6 Hz, 1H), 4.61 (t, J = 5.6 Hz, 1H), 4.45 (d, J = 9.3 Hz, 1H), 4.42 (d, J = 4.4 Hz, 1H), 3.75 – 3.71 (m, 1H), 3.68 (t, J = 3.7 Hz, 1H), 3.53 – 3.44 (m, 2H), 3.43 – 3.39 (m, 1H), 3.39 – 3.29 (m, 2H), 3.23 (dd, J = 13.6, 8.8 Hz, 1H), 3.12 (s, 1H), 2.93 (dd, J = 13.6, 6.4 Hz, 1H). ^{13}C NMR (126 MHz, DMSO-d_6) δ 170.5, 138.6, 137.6, 131.2, 129.0, 128.9, 128.3, 126.5, 119.5, 88.27, 79.2, 74.7, 69.2, 68.4, 60.6, 43.2, 41.2. HRMS (ESI$^-$) m/z calculated for $[C_{21}H_{24}NO_6S_2]^-$ 450.1051 $[M–H]^-$, found 450.1051.

(*R*)-2-Mercapto-4-methyl-*N*-(4-(((2*S*,3*R*,4*S*,5*R*,6*R*)-3,4,5-trihydroxy-6-(hydroxymethyl)tetrahydro-2*H*-pyran-2-yl)thio)phenyl)pentanamide (18).

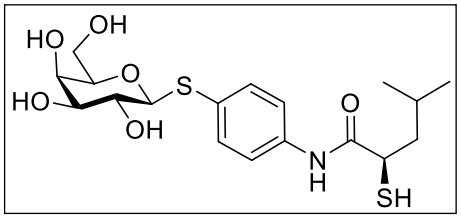

Compound **18** was synthesized according to the general procedure C, using compound **16** (136.8 mg, 0.22 mmol), sodium methoxide (245 µL, 5.33 M, 1.31 mmol) and MeOH (6 mL). The crude product was purified using preparative HPLC (CH_3CN (FA 0.05%)/H_2O (FA 0.05%) = 5:95 to 95:5), to give compound **18** as a white solid (44.3 mg, 49%). ^{1}H NMR (500 MHz, DMSO-d_6) δ 10.14 (s, 1H), 7.53 (d, J = 8.7 Hz, 2H), 7.42 (d, J = 8.7 Hz, 2H), 5.12 (d, J = 5.8 Hz, 1H), 4.88 (d, J = 5.5 Hz, 1H), 4.65 (t, J = 5.6 Hz, 1H), 4.48 – 4.44 (m, 2H), 3.68 (t, J = 3.7 Hz, 1H), 3.54 – 3.44 (m, 3H), 3.43 – 3.35 (m, 2H), 3.35 – 3.29 (m, 1H), 3.00 (s, 1H), 1.79 (ddd, J = 13.6, 8.4, 6.5 Hz, 1H), 1.61 (sep, J = 6.7 Hz, 1H), 1.50 (dt, J = 13.7, 7.0 Hz, 1H), 0.90 (d, J = 6.6 Hz, 3H), 0.85 (d, J = 6.6 Hz, 3H). ^{13}C NMR (126 MHz, DMSO-d_6) δ 171.2, 137.8, 131.3, 128.8, 119.5, 88.3, 79.2, 74.7, 69.2, 68.4, 60.6, 44.3, 40.1 (behind DMSO, based on HSQC), 25.8, 22.3, 22.2. HRMS (ESI$^-$) m/z calculated for $[C_{18}H_{26}NO_6S_2]^-$ 416.1207 $[M–H]^-$, found 416.1210.

(*R*)-2-Bromo-4-methylpentanoic acid (19´)

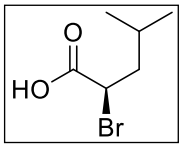

(*R*)-2-Bromo-4-methylpentanoic acid **19´** was synthesized according to the protocol reported in literature.[15] **19´** was obtained as colorless oil in quantitative yield and used in the next step without further purification.

(2*R*,3*S*,4*S*,5*R*,6*S*)-2-(Acetoxymethyl)-6-((4-((*R*)-2-bromo-3-phenylpropanamido)phenyl)thio)tetrahydro-2*H*-pyran-3,4,5-triyl triacetate (20)

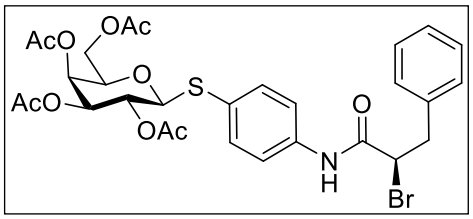

Compound **20** was synthesized according to the general procedure A, using (*R*)-2-bromo-3-phenylpropanoic acid **19** (120 mg, 0.52 mmol), compound **6** (197.4 mg, 0.43 mmol), EDC·HCl (100.1 mg, 0.52 mmol) and DCM (15 mL). The obtained crude product was purified using column chromatography (Hex/EtOAc = 6:4 to 1:1), to give compound **20** as a white solid (261.3 mg, 91%). ^{1}H NMR (500 MHz, $CDCl_3$) δ 7.85 (s, 1H), 7.52 – 7.48 (m, 2H), 7.46 – 7.42 (m, 2H), 7.34 – 7.24 (m, 5H), 5.41 (d, *J* = 2.9 Hz, 1H), 5.20 (t, *J* = 10.0 Hz, 1H), 5.04 (dd, *J* = 9.9, 3.4 Hz, 1H), 4.64 (d, *J* = 9.9 Hz, 1H), 4.60 (dd, *J* = 7.4, 6.0 Hz, 1H), 4.20 – 4.15 (m, 1H), 4.13 – 4.08 (m, 1H), 3.91 (t, *J* = 6.6 Hz, 1H), 3.61 (dd, *J* = 14.4, 5.9 Hz, 1H), 3.34 (dd, *J* = 14.3, 7.5 Hz, 1H), 2.11 (s, 3 H), 2.10 (s, 3 H), 2.05 (s, 3 H), 1.97 (s, 3 H). ^{13}C NMR (126 MHz, $CDCl_3$) δ 170.5, 170.3, 170.2, 169.6, 166.2, 137.4, 136.7, 134.2, 129.6, 128.7, 128.1, 127.6, 120.4, 86.8, 74.6, 72.1, 67.34, 67.31, 61.7, 51.8, 41.7, 21.0, 20.9, 20.8, 20.7. MS (ESI^+) m/z calculated for $[C_{29}H_{33}BrNO_{10}S]^+$ 666.10 $[M+H]^+$, found 666.11.

(2*R*,3*S*,4*S*,5*R*,6*S*)-2-(Acetoxymethyl)-6-((4-((*R*)-2-bromo-4-methylpentanamido)phenyl)thio)tetrahydro-2*H*-pyran-3,4,5-triyl triacetate (21)

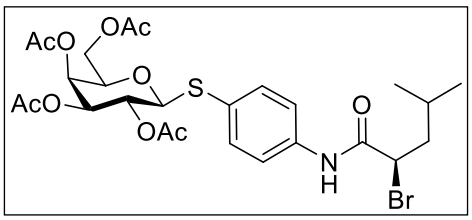

Compound **21** was synthesized according to the general procedure A, using (*R*)-2-bromo-4-methylpentanoic acid **19** (160.6 mg, 0.82 mmol), EDC·HCl (156.7 mg, 0.82 mmol), aniline **6** (250 mg, 0.55 mmol) and DCM (15 mL). The obtained crude product was purified using column chromatography (Hex/EtOAc = 1:1), to give compound **21** as a pale-yellow solid (240 mg, 69%). ^{1}H NMR (500 MHz, $CDCl_3$) δ 8.03 (s, 1H), 7.51 (s, 4H), 5.41 (d, *J* = 3.2 Hz, 1H), 5.20 (t, *J* = 9.9 Hz, 1H), 5.04 (dd, *J* = 10.0, 3.3 Hz, 1H), 4.64 (d, *J* = 9.9 Hz, 1H), 4.43 (dd, *J* = 9.4, 5.4 Hz, 1H), 4.20 – 4.15 (m, 1H), 4.14 – 4.08 (m, 1H), 3.91 (t, *J* = 6.6 Hz, 1H), 2.11 (s, 3H), 2.10 (s, 3H), 2.05 (s, 3H), 2.04 – 1.96 (m, 2H), 2.00 (s, 3H), 1.94 – 1.85 (m, 1H), 1.00 (d, *J* = 6.6 Hz, 3H), 0.95 (d, *J* = 6.6 Hz,

3H). ^{13}C NMR (126 MHz, $CDCl_3$) δ 170.5, 170.3, 170.2, 169.6, 167.2, 137.7, 134.4, 127.8, 120.2, 86.8, 74.6, 72.1, 67.33, 67.32, 61.7, 50.6, 44.6, 26.6, 22.8, 21.2, 21.0, 20.9, 20.8, 20.7. MS (ESI$^+$) m/z calculated for $[C_{26}H_{35}BrNO_{10}S]^+$ 632.12 $[M+H]^+$, found 632.12.

(2*R*,3*S*,4*S*,5*R*,6*S*)-2-(Acetoxymethyl)-6-((4-((*S*)-2-(acetylthio)-3-phenylpropanamido)phenyl)thio)tetrahydro-2*H*-pyran-3,4,5-triyl triacetate (22)

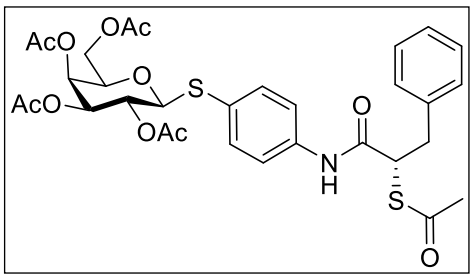

Compound **22** was synthesized according to the general procedure B, using compound **20** (246.5 mg, 0.37 mmol), potassium thioacetate (84.5 mg, 0.74 mmol) and acetone (6 mL). The crude product was purified using column chromatography (Hex/EtOAc = 1:1) to give compound **15** as a white solid (219.2 mg, 89%). ^{1}H NMR (500 MHz, $CDCl_3$) δ 8.03 (s, 1H), 7.48 – 7.40 (m, 4H), 7.32 – 7.22 (m, 5H), 5.39 (dd, *J* = 3.4, 0.8 Hz, 1H), 5.18 (t, *J* = 9.9 Hz, 1H), 5.02 (dd, *J* = 10.1, 3.4 Hz, 1H), 4.60 (d, *J* = 9.9 Hz, 1H), 4.27 (dd, *J* = 8.4, 7.2 Hz, 1H), 4.19 – 4.13 (m, 1H), 4.13 – 4.08 (m, 1H), 3.91 – 3.86 (m, 1H), 3.43 (dd, *J* = 14.2, 8.5 Hz, 1H), 2.99 (dd, *J* = 14.0, 7.0 Hz, 1H), 2.38 (s, 3H), 2.09 (s, 6H), 2.04 (s, 3H), 1.97 (s, 3H). ^{13}C NMR (126 MHz, $CDCl_3$) δ 197.6, 170.5, 170.3, 170.2, 169.6, 168.5, 138.2, 137.6, 134.4, 129.4, 128.8, 127.22, 127.17, 120.2, 87.0, 74.6, 72.1, 67.4, 67.3, 61.7, 48.5, 35.7, 30.6, 21.0, 20.9, 20.7, 20.7. MS (ESI$^+$) m/z calculated for $[C_{31}H_{36}NO_{11}S_2]^+$ 662.17 $[M+H]^+$, found 662.24.

(2*R*,3*S*,4*S*,5*R*,6*S*)-2-(Acetoxymethyl)-6-((4-((*S*)-2-(acetylthio)-4-methylpentanamido)phenyl)thio)tetrahydro-2*H*-pyran-3,4,5-triyl triacetate (23)

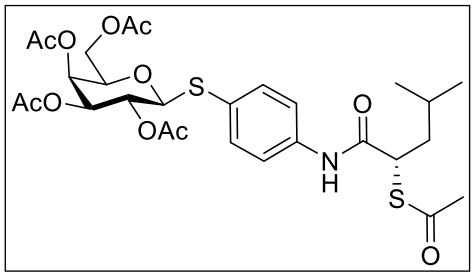

Compound **23** was synthesized according to the general procedure B, using compound **21** (227 mg, 0.36 mmol) and potassium thioacetate (81.8 mg, 0.72 mmol) in acetone (7 mL). The crude residue was purified using column chromatography (Hex/EtOAc = 8:2 to 6:4) to give compound **23** as a pale-yellow solid (188 mg, 84%). ^{1}H NMR (500 MHz, $CDCl_3$) δ 8.21 (s, 1H), 7.52 – 7.44 (m, 4H), 5.41 – 5.38 (m, 1H), 5.19 (t, *J* = 10.0 Hz, 1H), 5.03 (dd, *J* = 9.9, 3.4 Hz, 1H), 4.61 (d, *J* = 9.9 Hz, 1H), 4.20 – 4.14 (m, 1H), 4.13 – 4.06 (m, 2H), 3.91 – 3.87 (m, 1H), 2.41 (s, 3H), 2.11 (s, 3H), 2.10 (s, 3H), 2.05 (s, 3H), 2.02 – 1.94 (m, 1H), 1.97 (s, 3H), 1.74 (sep, *J* = 6.7 Hz, 1H), 1.62 – 1.54 (m, 1H), 0.97 (d, *J* = 6.6 Hz, 3H), 0.93 (d, *J* = 6.6 Hz, 3H). ^{13}C NMR (126 MHz, $CDCl_3$) δ 198.4, 170.6, 170.4, 170.2, 169.6, 169.3, 138.5, 134.5,

127.0, 120.0, 87.1, 74.6, 72.1, 67.4, 67.3, 61.7, 45.3, 37.9, 30.5, 26.0, 22.5, 22.4, 21.0, 20.9, 20.8, 20.7. MS (ESI$^+$) m/z calculated for $[C_{28}H_{38}NO_{11}S_2]^+$ 628.19 $[M+H]^+$, found 628.22.

(*S*)-2-Mercapto-3-phenyl-*N*-(4-(((2*S*,3*R*,4*S*,5*R*,6*R*)-3,4,5-trihydroxy-6-(hydroxymethyl)tetrahydro-2*H*-pyran-2-yl)thio)phenyl)propanamide (24)

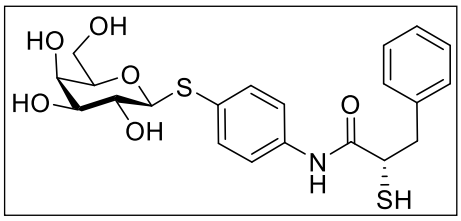

Compound **24** was synthesized according to the general procedure C, using compound **22** (201.8 mg, 0.30 mmol), sodium methoxide (230 µL, 5.33 M, 1.22 mmol) and MeOH (6 mL). After the workup with Amberlite, the mixture was evaporated, the obtained solid washed with MeOH and dried under high vacuum to afford the compound 24 as white solid (81 mg, 60%). ^{1}H NMR (500 MHz, DMSO-d_6) δ 10.04 (s, 1H), 7.47 (d, J = 8.7 Hz, 2H), 7.39 (d, J = 8.7 Hz, 2H), 7.30 – 7.22 (m, 4H), 7.21 – 7.17 (m, 1H), 5.07 (d, J = 5.8 Hz, 1H), 4.83 (d, J = 5.6 Hz, 1H), 4.60 (t, J = 5.6 Hz, 1H), 4.45 (d, J = 9.4 Hz, 1H), 4.42 (d, J = 4.4 Hz, 1H), 3.76 – 3.70 (m, 1H), 3.68 (t, J = 3.7 Hz, 1H), 3.53 – 3.44 (m, 2H), 3.43 – 3.39 (m, 1H), 3.39 – 3.34 (m, 1H), 3.32 – 3.29 (m, 1H), 3.24 (dd, J = 13.6, 8.8 Hz, 1H), 3.12 (s, 1H), 2.93 (dd, J = 13.6, 6.4 Hz, 1H). ^{13}C NMR (126 MHz, DMSO-d_6) δ 170.4, 138.6, 137.6, 131.1, 129.0, 128.8, 128.2, 126.5, 119.5, 88.23, 79.2, 74.7, 69.2, 68.3, 60.6, 43.2, 41.2. HRMS (ESI$^-$) m/z calculated for $[C_{21}H_{24}NO_6S_2]^-$ 450.1051 $[M–H]^-$, found 450.1044.

(*S*)-2-Mercapto-4-methyl-*N*-(4-(((2*S*,3*R*,4*S*,5*R*,6*R*)-3,4,5-trihydroxy-6-(hydroxymethyl)tetrahydro-2*H*-pyran-2-yl)thio)phenyl)pentanamide (25).

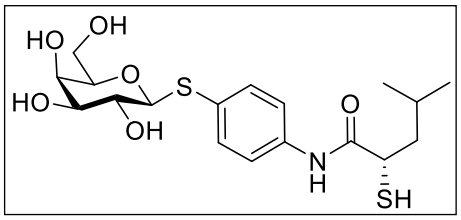

Compound **25** was synthesized according to the general procedure C, using compound **23** (183.8 mg, 0.29 mmol), sodium methoxide (220 µL, 5.33 M, 1.17 mmol) and MeOH (6 mL). The crude product was purified using preparative HPLC (CH_3CN (FA 0.05%)/H_2O (FA 0.05%) = 5:95 to 95:5), to give compound **25** as a white solid (82.3 mg, 68%). ^{1}H NMR (500 MHz, DMSO-d_6) δ 10.12 (s, 1H), 7.53 (d, J = 8.7 Hz, 2H), 7.42 (d, J = 8.7 Hz, 2H), 5.08 (d, J = 5.7, 1H), 4.84 (d, J = 5.5 Hz, 1H), 4.61 (t, J = 5.5 Hz, 1H), 4.48 – 4.42 (m, 2H), 3.69 (t, J = 3.6 Hz, 1H), 3.55 – 3.45 (m, 3H), 3.44 – 3.40 (m, 1H), 3.39 – 3.30 (m, 2H), 2.98 (s, 1H), 1.83 – 1.75 (m, 1H), 1.62 (sep, J = 6.7 Hz, 1H), 1.50 (dt, J = 13.7, 7.0 Hz, 1H), 0.91 (d, J = 6.6 Hz, 3H), 0.86 (d, J = 6.6 Hz, 3H). ^{13}C NMR (126 MHz, DMSO-d_6) δ 171.2, 137.8, 131.3, 128.8, 119.5,

88.3, 79.2, 74.7, 69.2, 68.4, 60.6, 44.3, 40.1 (behind DMSO, based on HSQC), 25.8, 22.2, 22.1. HRMS (ESI$^-$) m/z calculated for $[C_{18}H_{26}NO_6S_2]^-$ 416.1207 $[M–H]^-$, found 416.1198.

2,2'-Disulfanediylbis(3-phenyl-*N*-(4-(((2*S*,3*R*,4*S*,5*R*,6*R*)-3,4,5-trihydroxy-6-(hydroxymethyl)tetrahydro-2*H*-pyran-2-yl)thio)phenyl)propanamide) (26a and 26b)

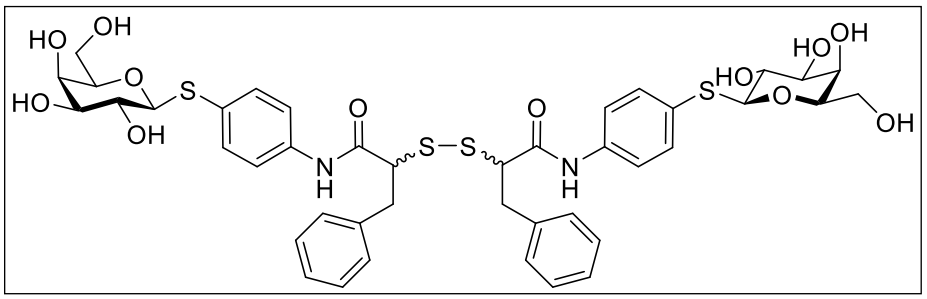

Compound **26** was synthesized according to the general procedure D, using thiol **11** (9.3 mg, 0.02 mmol), 3% (v/v) H_2O_2 (50 µL, 2.5 equiv., 0.05 mmol) and DMSO/H_2O 1:1 (500 µL). The product was purified by preparative HPLC (H_2O/MeCN + 0.1% formic acid, 30-60% MeCN) to result in two fractions **26a** (t_R 6.1 min) and **26b** (t_R 6.3 min). Both compounds were obtained as white solids (3.7 mg of **26a** and 4.1 mg of **26b**; 7.8 mg in total, 8.6 µmol, 86%). **26a:** ^{1}H NMR (500 MHz, DMSO-d_6) δ 10.16 (s, 1H), 10.10 (s, 1H), 7.52 – 7.36 (m, 8H), 7.31 – 7.10 (m, 10H), 5.09 (t, J = 5.6 Hz, 2H), 4.84 (dd, J = 5.7, 2.4 Hz, 2H), 4.60 (t, J = 5.5 Hz, 2H), 4.46 (d, J = 9.5 Hz, 2H), 4.45 – 4.43 (m, 2H), 4.00 – 3.94 (m, 2H), 3.69 (t, J = 3.7 Hz, 2H), 3.55 – 3.44 (m, 4H), 3.42 (d, J = 6.0 Hz, 2H), 3.40 – 3.34 (m, 2H), 3.31 – 3.29 (m, 2H), 3.28 – 3.18 (m, 2H), 3.12 (dd, J = 13.7, 5.5 Hz, 1H), 3.02 (dd, J = 13.7, 5.5 Hz, 1H). ^{13}C NMR (126 MHz, DMSO-d_6) δ 168.4, 168.3, 137.9, 137.8, 137.2, 137.1, 131.0, 130.9, 129.5, 129.2, 129.0, 128.9, 128.3, 126.6, 119.8, 119.7, 88.3, 79.2, 74.7, 69.2, 68.3, 60.5, 56.0, 55.2, 48.6, 37.1, 36.7. HRMS (ESI$^+$) m/z calculated for $[C_{42}H_{49}N_2O_{12}S_4]^+$ 901.2163 $[M+H]^+$, found 901.2157. **26b:** ^{1}H NMR (500 MHz, DMSO-d_6) δ 10.17 (s, 1H), 10.11 (s, 1H), 7.54 – 7.33 (m, 8H), 7.31 – 7.08 (m, 10H), 5.09 (t, J = 5.7 Hz, 2H), 4.84 (dd, J = 5.7, 2.5 Hz, 2H), 4.60 (t, J = 5.5 Hz, 2H), 4.46 (d, J = 9.5 Hz, 2H), 4.45 – 4.42 (m, 2H), 4.00 – 3.95 (m, 2H), 3.69 (t, J = 3.7 Hz, 2H), 3.55 – 3.44 (m, 4H), 3.42 (t, J = 6.4 Hz, 2H), 3.39 – 3.35 (m, 2H), 3.31 – 3.29 (m, 2H), 3.28 – 3.19 (m, 2H), 3.12 (dd, J = 13.7, 5.5 Hz, 1H), 3.02 (dd, J = 13.7, 5.5 Hz, 1H). ^{13}C NMR (126 MHz, DMSO-d_6) δ 168.4, 168.3, 137.9, 137.8, 137.2, 137.1, 131.0, 131.0, 129.5, 129.2, 129.0, 128.9, 128.3, 126.6, 119.8, 119.7, 88.3, 79.2, 74.7, 69.2, 68.3, 60.5, 56.0, 55.2, 48.6, 37.0, 36.7. HRMS (ESI$^+$) m/z calculated for $[C_{42}H_{49}N_2O_{12}S_4]^+$ 901.2163 $[M+H]^+$, found 901.2157.

2,2'-Disulfanediylbis(4-methyl-*N*-(4-(((2*S*,3*R*,4*S*,5*R*,6*R*)-3,4,5-trihydroxy-6-(hydroxymethyl)tetrahydro-2*H*-pyran-2-yl)thio)phenyl)pentanamide) (27).

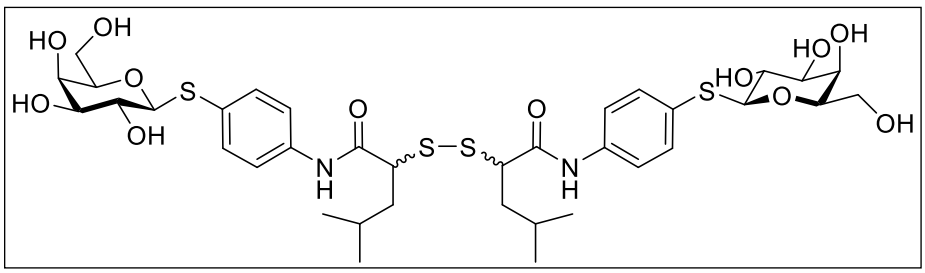

Compound **27** was synthesized according to the general procedure D, using thiol **12** (3.74 mg, 8.8 µmol), 3% (v/v) H_2O_2 (22 µL, 2.5 equiv., 22 µmol) and DMSO/H_2O 1:1 (200 µL). The product was purified by preparative HPLC (H_2O/MeCN + 0.1% formic acid, 15 - 55% MeCN) and **27** was obtained as a white solid (3 mg, 3.6 µmol, 82%). ^{1}H NMR (500 MHz, DMSO-d_6) δ 10.28 (s, 1H), 10.19 (s, 1H), 7.61 – 7.51 (m, 4H), 7.46 – 7.38 (m, 4H), 5.09 (dd, J = 5.9, 2.3 Hz, 2H), 4.84 (d, J = 5.6 Hz, 2H), 4.60 (t, J = 5.6 Hz, 2H), 4.46 (d, J = 9.5 Hz, 2H), 4.43 (d, J = 4.4 Hz, 2H), 3.78 – 3.71 (m, 2H), 3.69 (t, J = 3.9 Hz, 2H), 3.54 – 3.44 (m, 4H), 3.44 – 3.35 (m, 4H), 3.30 (s, 2H), 1.93 – 1.76 (m, 2H), 1.62 – 1.42 (m, 4H), 0.90 (d, J = 6.0 Hz, 3H), 0.87 (d, J = 6.0 Hz, 3H), 0.82 (d, J = 6.2 Hz, 3H), 0.80 (d, J = 6.2 Hz, 3H). ^{13}C NMR (126 MHz, DMSO-d_6) δ 169.3, 169.2, 137.5, 137.4, 131.1, 129.3, 129.0, 119.8, 119.7, 88.3, 79.2, 74.7, 69.2, 68.3, 60.5, 53.3, 48.6, 40.4, 40.2, 26.0, 25.9, 22.7, 22.6, 22.0, 21.8. HRMS (ESI$^+$) m/z calculated for $[C_{36}H_{53}N_2O_{12}S_4]^+$ 833.2476 $[M+H]^+$, found 833.2469.

Table S1. Inhibition of six human matrix metalloproteases (MMPs) in the presence of 100 μM of compounds **11** and **12***.

	Percent inhibition at 100 μM	
	11	**12**
MMP-1	10±5	n.i.
MMP-2	n.i.	19±3
MMP-3	n.i.	n.i.
MMP-7	n.i.	n.i.
MMP-8	n.i.	n.i.
MMP-14	n.i.	19±5

*Means and standard deviations from at least three independent experiments. n.i. = <10% inhibition

Table S2. Antibacterial activity of compounds **11** and **12** against *Pseudomonas aeruginosa* PA14.

	MIC (μM)	
	11	**12**
P. aeruginosa PA14	>100	>100

Table S3. Cytotoxicity of compounds **11** and **12** against HepG2, HEK293, and A549 cell lines*.

	IC_{50} (μM)	
	11	**12**
HepG2	>100	>100
HEK293	>100	>100
A549	>100	>100

*Means from at least three independent experiments

Table S4. Crystal structure of LasB in complex with 11: Data collection and refinement statistics.

LasB_11

PDB ID	**7Z68**
Data collection	
Space group	P 1 2_1 1
Cell dimension	
a, b, c (Å)	39.3, 92.5, 40.7
α, β, γ (°)	90.0, 114.2, 90
Wavelength (Å)	0.9763
Resolution	1.5 (1.53 – 1.50)
R_{sym} or R_{merge}	0.054 (0.318)
R_{pim}	0.031 (0.190)
CC (1/2)	0.999 (0.944)
$I/\sigma I$	18.1 (4.7)
Completeness (%)	99.9 (99.3)
Redundancy	7.1 (6.3)
Refinement	
Resolution (Å)	37.16 – 1.5
No. reflection	42387
R_{work} / R_{free}	0.157 / 0.195
No. atoms	2682
Protein	2317
Ligands	126
Solvent	297
Protein residues	298
B-factors	18.33
Protein	16.80
Ligands	29.83
Water	27.68
RMS deviations	
Bond length (Å)	0.011
Bond angles (°)	1.24

MolProbity score	1.39

*Statistics for the highest-resolution shell are shown in parentheses.

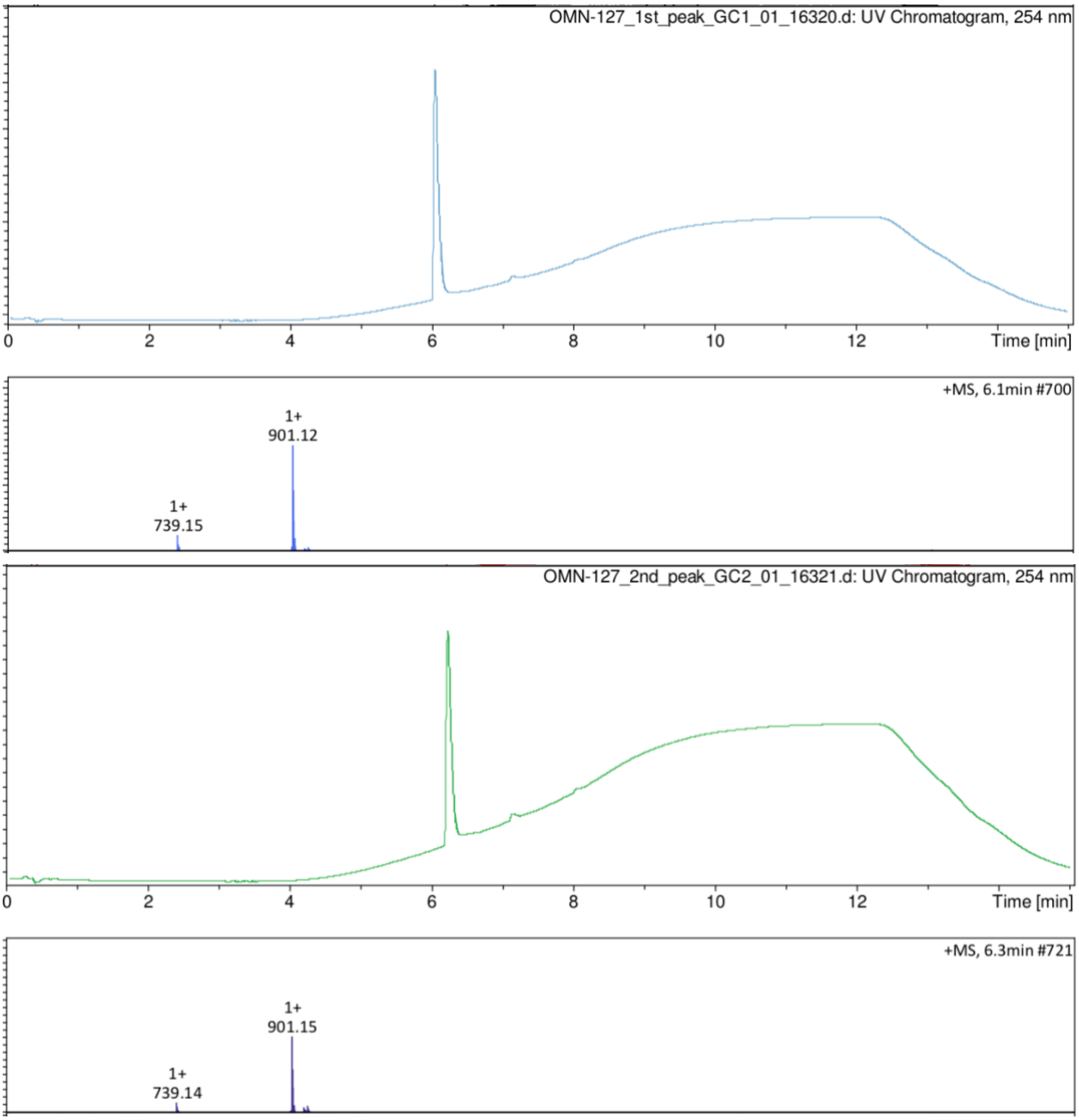

Figure S1. HPLC analysis of compounds **26a** (top) and **26b** (bottom).

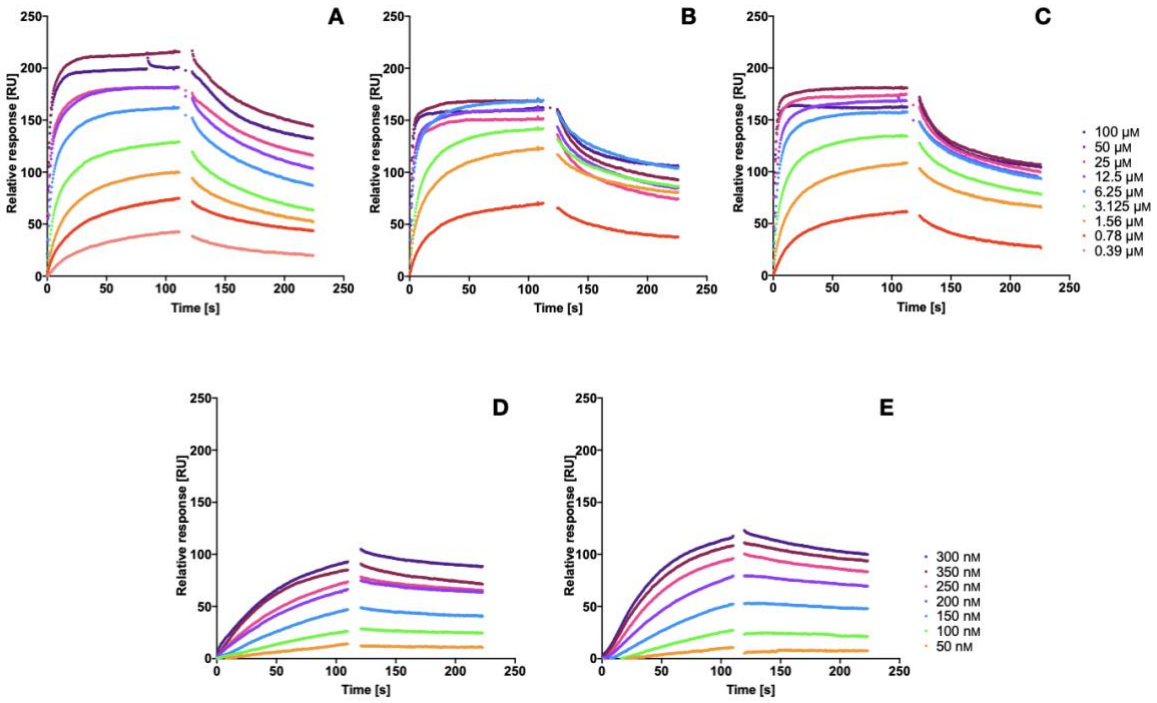

Figure S2. SPR binding curves of the interaction of dual inhibitors A) **24**, B) **18**, C) **25**, D) **27**, E) **26b** with LecA.

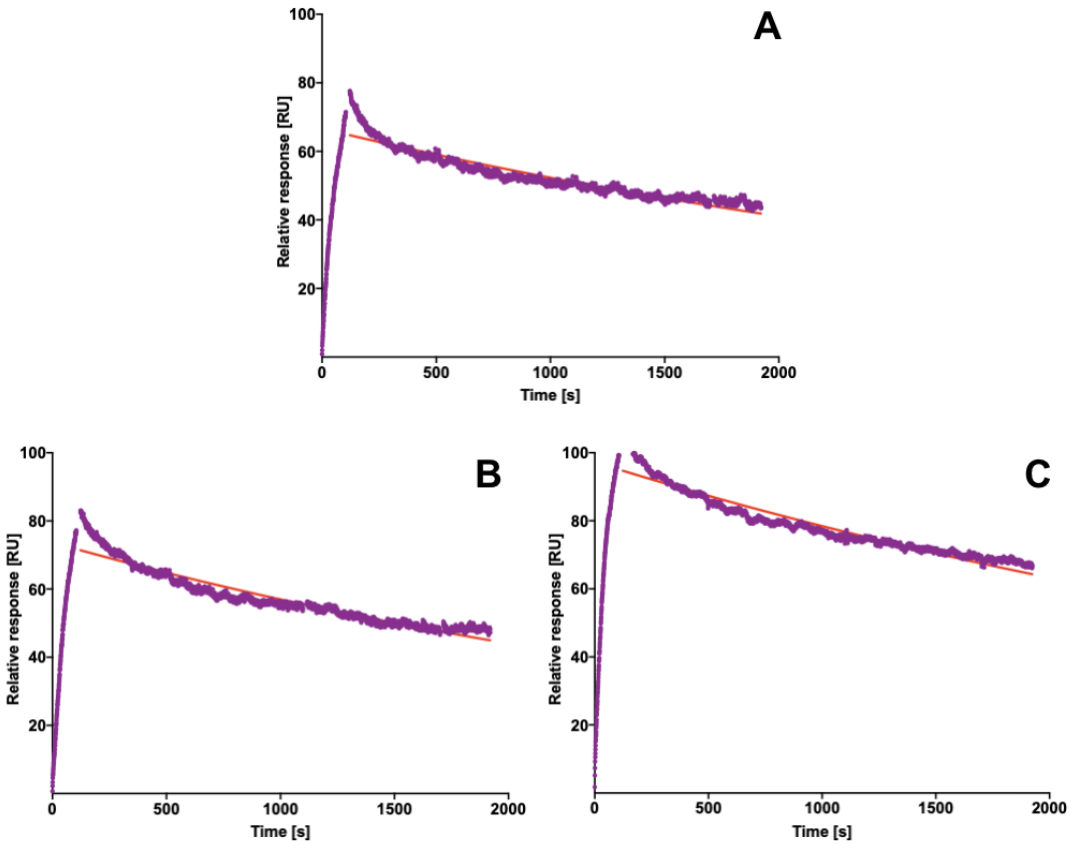

Figure S3. SPR dissociation kinetic analysis of the interaction of divalent LecA inhibitors A) **27**, B) **26a**, and C) **26b** with LecA.

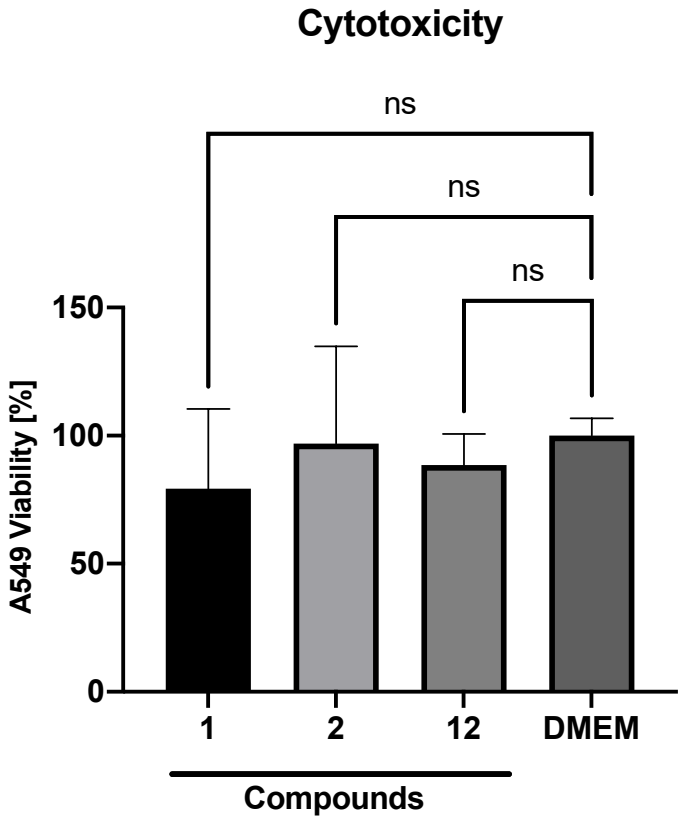

Figure S4. Evaluation of the cytotoxicity of compounds **1**, **2** and **12** at 100 µM. The graphs represent three independent experiments ± SD. One-way ANOVA statistical analysis was performed following Dunnett's multiple comparisons test, comparing the mean value of each concentration to the mean value of DMEM.

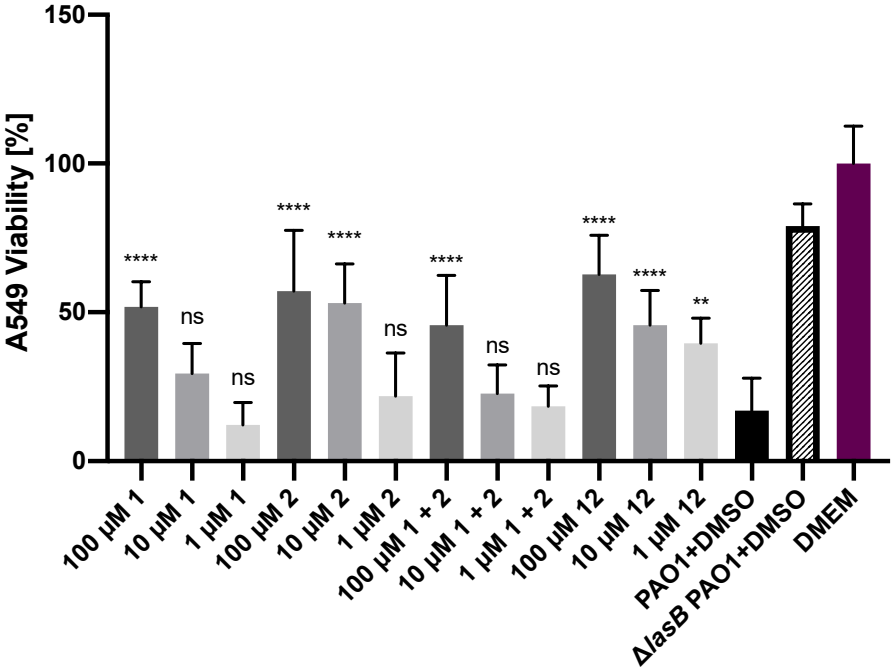

Figure S5. Inhibition of LasB-dependent cytotoxicity: The dose-response inhibitory effect of compounds **1**, **2** the combination of **1** and **2** and compound **12** against 10% (v/v) *P. aeruginosa* PAO1 culture supernatant. The graphs represent three independent experiments ± SD. One-way ANOVA statistical analysis was performed following Dunnett's multiple comparisons test, comparing the mean value of each concentration to the mean value of PAO1 without any treatment with compounds (**** $p \leq 0.0001$, ** $p \leq 0.01$).

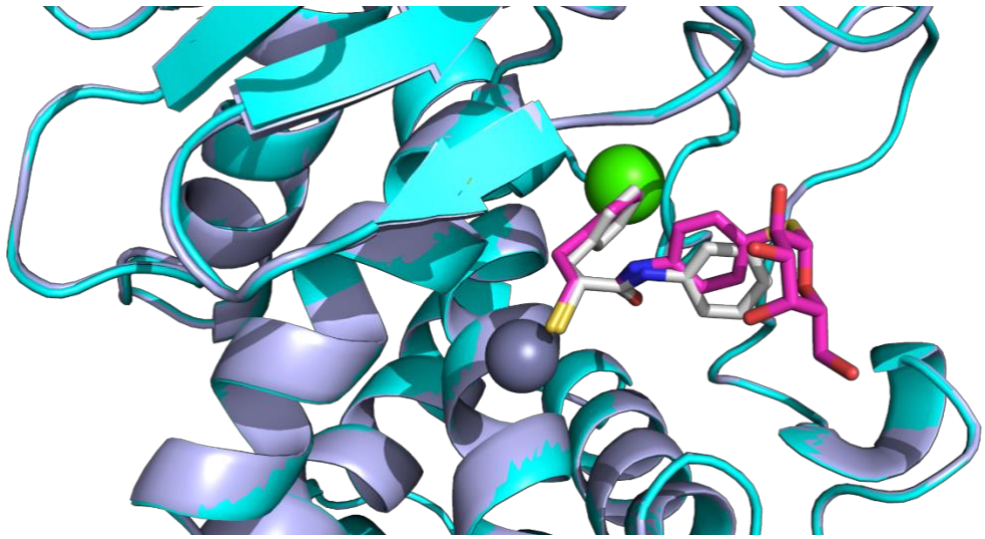

Figure S6. Superposition of the LasB-compound **11** (magenta) and LasB-α-alkyl-*N*-aryl mercaptoacetamide (gray; PDB 7OC7); Zn^{2+} is shown as a gray sphere; Ca^{2+} is shown as a green sphere; the protein structure demonstrates no major deviations between the two complexes

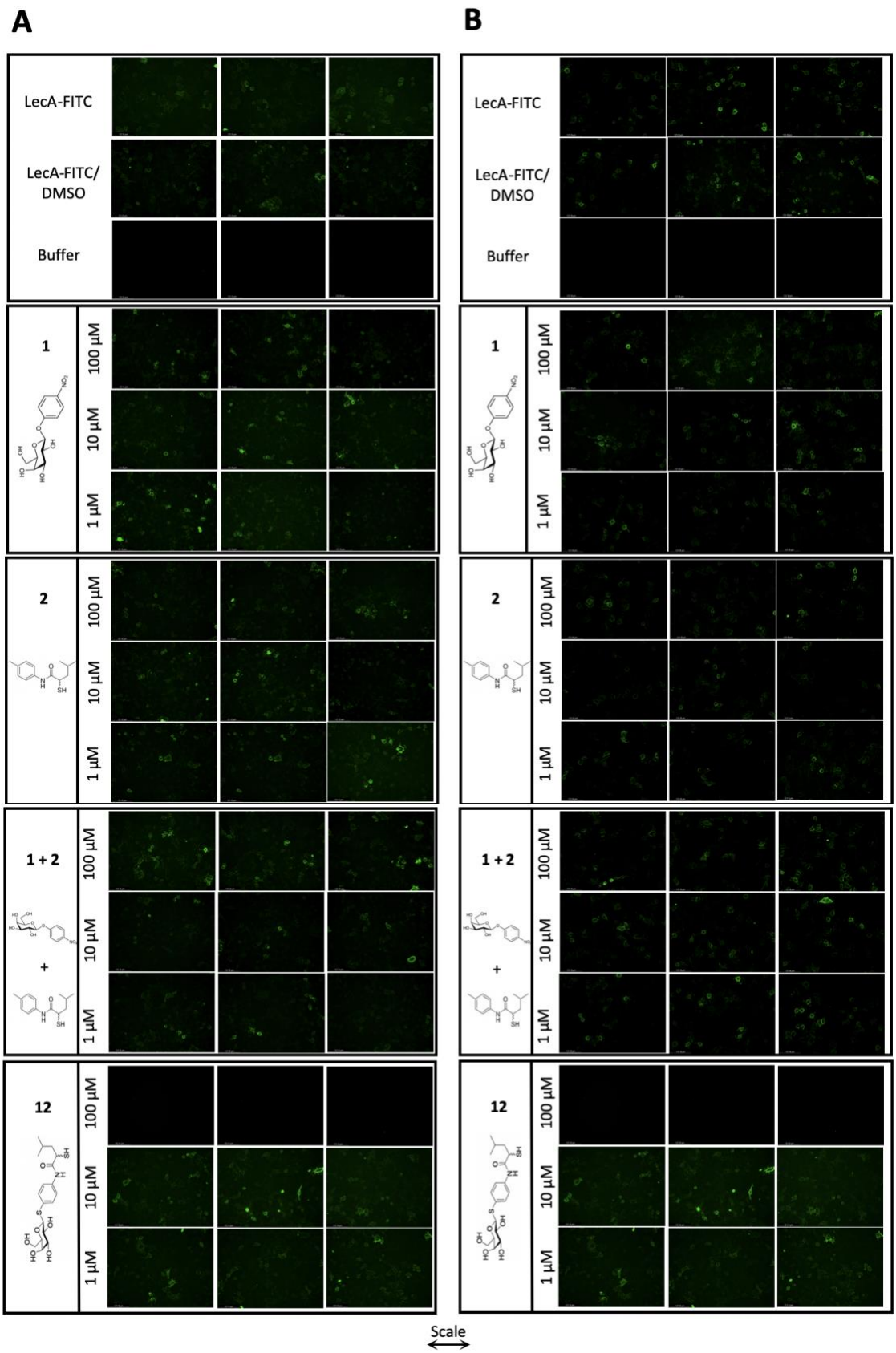
A
B
LecA-FITC
LecA-FITC/ DMSO
Buffer
1
2
1 + 2
12
100 µM
10 µM
1 µM
Scale

Figure S7. Fluorescence images of LecA-FITC bound to A549 cells in the presence of different concentrations of **1**, **2**, **1+2** and **12** (three representative images from two biological replicates (A, B). Scale bar corresponds to 250 µm

Supporting Information References

1 I. Joachim, S. Rikker, D. Hauck, D. Ponader, S. Boden, R. Sommer, L. Hartmann and A. Titz, *Org. Biomol. Chem.*, 2016, **14**, 7933–7948.

2 A. M. Kany, A. Sikandar, J. Haupenthal, S. Yahiaoui, C. K. Maurer, E. Proschak, J. Köhnke and R. W. Hartmann, *ACS Infect. Dis.*, 2018, **4**, 988–997.

3 R. Sommer, S. Wagner, A. Varrot, C. M. Nycholat, A. Khaledi, S. Häussler, J. C. Paulson, A. Imberty and A. Titz, *Chem. Sci.*, 2016, **7**, 4990–5001.

4 G. Beshr, A. Sikandar, E.-M. Jemiller, N. Klymiuk, D. Hauck, S. Wagner, E. Wolf, J. Koehnke and A. Titz, *Journal of Biological Chemistry*, 2017, **292**, 19935–19951.

5 E. Schönauer, A. M. Kany, J. Haupenthal, K. Hüsecken, I. J. Hoppe, K. Voos, S. Yahiaoui, B. Elsässer, C. Ducho, H. Brandstetter and R. W. Hartmann, *J. Am. Chem. Soc.*, 2017, **139**, 12696–12703.

6 J. Haupenthal, C. Baehr, S. Zeuzem and A. Piiper, *International Journal of Cancer*, 2007, **121**, 206–210.

7 W. A. M. Elgaher, M. Fruth, M. Groh, J. Haupenthal and R. W. Hartmann, *RSC Adv.*, 2014, **4**, 2177–2194.

8 M. D. Winn, C. C. Ballard, K. D. Cowtan, E. J. Dodson, P. Emsley, P. R. Evans, R. M. Keegan, E. B. Krissinel, A. G. W. Leslie, A. McCoy, S. J. McNicholas, G. N. Murshudov, N. S. Pannu, E. A. Potterton, H. R. Powell, R. J. Read, A. Vagin and K. S. Wilson, *Acta Crystallogr D Biol Crystallogr*, 2011, **67**, 235–242.

9 D. Liebschner, P. V. Afonine, M. L. Baker, G. Bunkóczi, V. B. Chen, T. I. Croll, B. Hintze, L. W. Hung, S. Jain, A. J. McCoy, N. W. Moriarty, R. D. Oeffner, B. K. Poon, M. G. Prisant, R. J. Read, J. S. Richardson, D. C. Richardson, M. D. Sammito, O. V. Sobolev, D. H. Stockwell, T. C. Terwilliger, A. G. Urzhumtsev, L. L. Videau, C. J. Williams and P. D. Adams, *Acta Crystallogr D Struct Biol*, 2019, **75**, 861–877.

10 P. Emsley and K. Cowtan, *Acta Crystallogr D Biol Crystallogr*, 2004, **60**, 2126–2132.

11 L. Schrödinger and W. DeLano, PyMOL 2020.

12 R. B. Cohen, S. H. Rutenburg, K.-C. Tsou, M. A. Woodbury and A. M. Seligman, *Journal of Biological Chemistry*, 1952, **195**, 607–614.

13 S. Escopy, Y. Singh and A. V. Demchenko, *Org. Biomol. Chem.*, 2019, **17**, 8379–8383.

14 F. Casoni, L. Dupin, G. Vergoten, A. Meyer, C. Ligeour, T. Géhin, O. Vidal, E. Souteyrand, J.-J. Vasseur, Y. Chevolot and F. Morvan, *Org Biomol Chem*, 2014, **12**, 9166–9179.

15 T. Fujisawa, K. Igeta, S. Odake, Y. Morita, J. Yasuda and T. Morikawa, *Bioorganic & Medicinal Chemistry*, 2002, **10**, 2569–2581.

S2. Supporting information to "Targeting extracellular lectins of *Pseudomonas aeruginosa* with glycomimetic liposomes"

Olga Metelkina[a,b,c], Benedikt Huck[d,e], Jonathan O'Connor[f,g], Marcus Koch[h], Andreas Manz[f,g], Claus Michael-Lehr[d,e], Alexander Titz[a,b,c,*]

[a]Chemical Biology of Carbohydrates, Helmholtz Institute for Pharmaceutical Research Saarland, Helmholtz Centre for Infection Research, 66123 Saarbrücken, Germany
[b]Deutsches Zentrum für Infektionsforschung (DZIF), Standort Hannover-Braunschweig, 38124 Braunschweig, Germany
[c]Department of Chemistry, Saarland University, 66123 Saarbrücken, Germany
[d]Drug Delivery, Helmholtz Institute for Pharmaceutical Research Saarland, Helmholtz Centre for Infection Research, 66123 Saarbrücken, Germany
[e]Department of Pharmacy, Saarland University, 66123 Saarbrücken, Germany
[f]KIST Europe, 66123 Saarbrücken, Germany
[g]Department of Systems Engineering, Saarland University, 66123 Saarbrücken, Germany
[h]INM - Leibniz Institute for New Materials, 66123 Saarbrücken, Germany

*corresponding author: alexander.titz@helmholtz-hzi.de

General experimental details.

Commercial chemicals and solvents were used without further purification.

DPPC, DSPC, DPPE and 16:0 Glutaryl PE (DPPE-GA) were purchased from Avanti Polar Lipids (Alabama, USA). All silicone tubing (ID x OD, 1/16 x 1/8 inch) was purchased from Sigma-Aldrich (produced by Saint-Gobain, MI, USA). Polylactic acid (PLA) filament, 2.85 mm diameter, was purchased from Formfutura (Nijmegen, Netherlands). Polydimethylsiloxane as Slygard 184, and black Slygard 170 (Dow Chemical Co., Michigen, USA) was purchased from Sigma-Aldrich. UHU plus endfest 90 min (UHU GmbH & Co. KG, Bühl, Germany) was purchased from a commercial supplier. HC polycarboxylate hydrogel, NHS-activated glass slides were purchased from XanTec bioanalytics GmbH (Düsseldorf, Germany).

Thin layer chromatography (TLC) was performed using silica gel 60 aluminum plates containing fluorescence indicator (Merck KGaA, Darmstadt, Germany) and developed under UV light (254 nm) and using a molybdate solution (0.02 M solution of $(NH_4)Ce(SO_4)_4 \cdot 2H_2O$ and $(NH_4)_6Mo_7O_{24} \cdot 4H_2O$ in aqueous 10% H_2SO_4) or a potassium permanganate solution (3 g of $KMnO_4$, 20 g of K_2CO_3 in 5 mL of 5% NaOH and 300 mL of water) with heating.

Medium pressure liquid chromatography (MPLC) was performed on a Teledyne Isco Combiflash Rf200 system using normal phase self-packed silica gel columns (60 Å, 400 mesh particle size, Fluka) or reversed-phase pre-packed silica gel 60 Å columns from Macherey-Nagel (C_{18} ec, endcapped). Preparative high-pressure liquid chromatography (HPLC) was performed on Waters 2545 Binary Gradient Module with a Waters 2489 UV/Vis detector using a RP-18 column (250/21 Nucleodur C18 Gravity SB, 5 µm from Macherey-Nagel, Germany).

Analytical HPLC-MS was performed on a Thermo Dionex Ultimate 3000 HPLC coupled to a Bruker amaZon SL mass spectrometer, with UV detection at 254 nm using a RP-18 column (100/2 Nucleoshell RP18plus, 2.7 µm from Macherey-Nagel, Germany) as stationary phase. High resolution mass spectrometry (HRMS) was performed on an Ultimate 3000 UPLC system coupled to a Q Exactive Focus Orbitrap system with HESI source (Thermo Fisher, Dreieich, Germany). The UPLC was operated with a C18 column (EC 150/2 Nucleodur C18 Pyramid, 3 µm from Macherey-Nagel, Germany).

^{1}H- and ^{13}C-NMR spectra were recorded on a Bruker Avance III 500 UltraShield spectrometer at 500 MHz and 126 MHz, respectively. Chemical shifts (δ) are given in ppm and were

calibrated on residual solvent peaks: $CHCl_3$-*d1* (^{1}H-NMR δ = 7.26 ppm, ^{13}C-NMR δ = 77.0 ppm), MeOH-*d4* (^{1}H -NMR δ = 3.31 ppm, ^{13}C -NMR δ = 49.0 ppm), DMSO-d_6 (^{1}H -NMR δ = 2.50 ppm, ^{13}C -NMR δ = 39.51 ppm). Deuterated solvents were purchased from Eurisotop (Saarbrücken, Germany). Multiplicities are specified as s = singlet, bs = broad singlet, d = doublet, dd = doublet of doublets, t = triplet, td = triplet of doublets, q = quartet, m = multiplet. The spectra were assigned with the help of ^{1}H,^{1}H-COSY and ^{1}H,^{13}C-HSQC experiments.

Compound synthesis

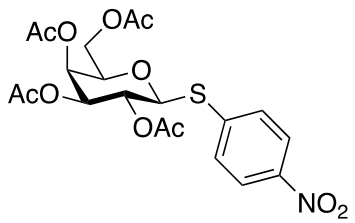

***p*-nitrophenyl 2,3,4,6-tetra-O-acetyl-β-D-thiogalactopyranoside (2)**.

Compound **2** was synthesized according to Escopy *et al.*[1]: Penta-*O*-acetyl-β-D-galactopyranose (**1**, 2 g, 5.1 mmol) and para-nitro-thiophenol (1.5 g, 2 equiv., 10.2 mmol) were dissolved in 20 mL dry dichloromethane with 200 mg 3 Å activated molecular sieves under nitrogen. The mixture was cooled to 0 °C, triflic acid (360 µL, 0.8 equiv., 4.09 mmol) was added dropwise and the reaction was stirred for 30 min. The reaction was diluted with DCM, filtrated through celite, washed with aqueous sodium bicarbonate, water and brine consequentially, and dried over anhydrous sodium sulfate. After filtration the obtained organic phase was concentrated *in vacuo* and the residue was recrystallized twice from EtOAc to provide **2** as white crystals (1.65 g, 3.4 mmol, 66%).

^{1}H NMR (500 MHz, $CHCl_3$-*d1*) δ 8.16 (d, *J* = 8.5 Hz, 2H, ArH), 7.60 (d, *J* = 8.5 Hz, 2H, ArH), 5.47 (d, *J* = 3.3 Hz, 1H, H-4), 5.29 (t, *J* = 9.9 Hz, 1H, H-2), 5.10 (dd, *J* = 9.9, 3.2 Hz, 1H, H-3), 4.86 (d, *J* = 10.0 Hz, 1H, H-1), 4.23 – 4.12 (m, 2H, H-6), 4.04 (t, *J* = 6.5 Hz, 1H, H-5), 2.15 (s, 3H, CH_3), 2.08 (d, *J* = 5.1 Hz, 6H, CH_3), 1.98 (s, 3H, CH_3).

^{13}C NMR (126 MHz, $CHCl_3$-*d1*) δ 170.33 ($CH_3\underline{C}(O)$), 170.04 ($CH_3\underline{C}(O)$), 169.97 ($CH_3\underline{C}(O)$), 169.39 ($CH_3\underline{C}(O)$), 146.85 (ArC), 142.41 (ArC), 130.41 (ArCH), 123.86 (ArCH), 84.85 (C-1), 74.86 (C-5), 71.73 (C-3), 67.08 (C-2), 66.72 (C-4), 61.68 (C-6), 20.76 (CH_3), 20.71 (CH_3), 20.66 (CH_3), 20.55 (CH_3).

HPLC-MS: $[C_{20}H_{23}NO_{11}S + Na]^+$ calcd. 508.09, found 508.08.
HRMS: $[C_{20}H_{23}NO_{11}S + Na]^+$ calcd. 508.0884, found 508.0873.

Spectroscopic data is in accordance with the literature[2].

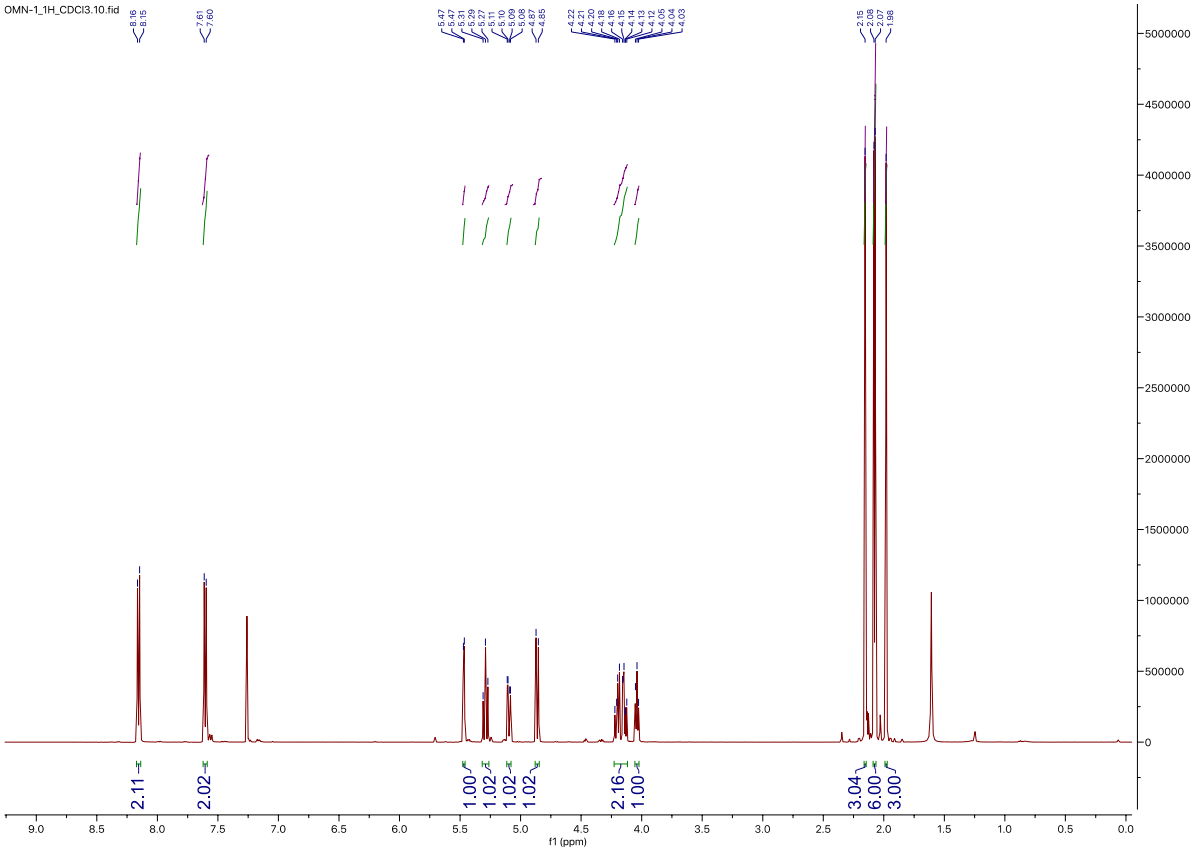
OMN-1_1H_CDCl3.10.fid
8.16
8.15
7.61
7.60
5.47
5.47
5.31
5.29
5.27
5.11
5.10
5.09
5.08
4.87
4.85
4.22
4.21
4.20
4.18
4.16
4.15
4.14
4.13
4.12
4.05
4.04
4.03
2.15
2.08
2.07
1.98
2.11
2.02
1.00
1.02
1.02
1.02
2.16
1.00
3.04
6.00
3.00
f1 (ppm)

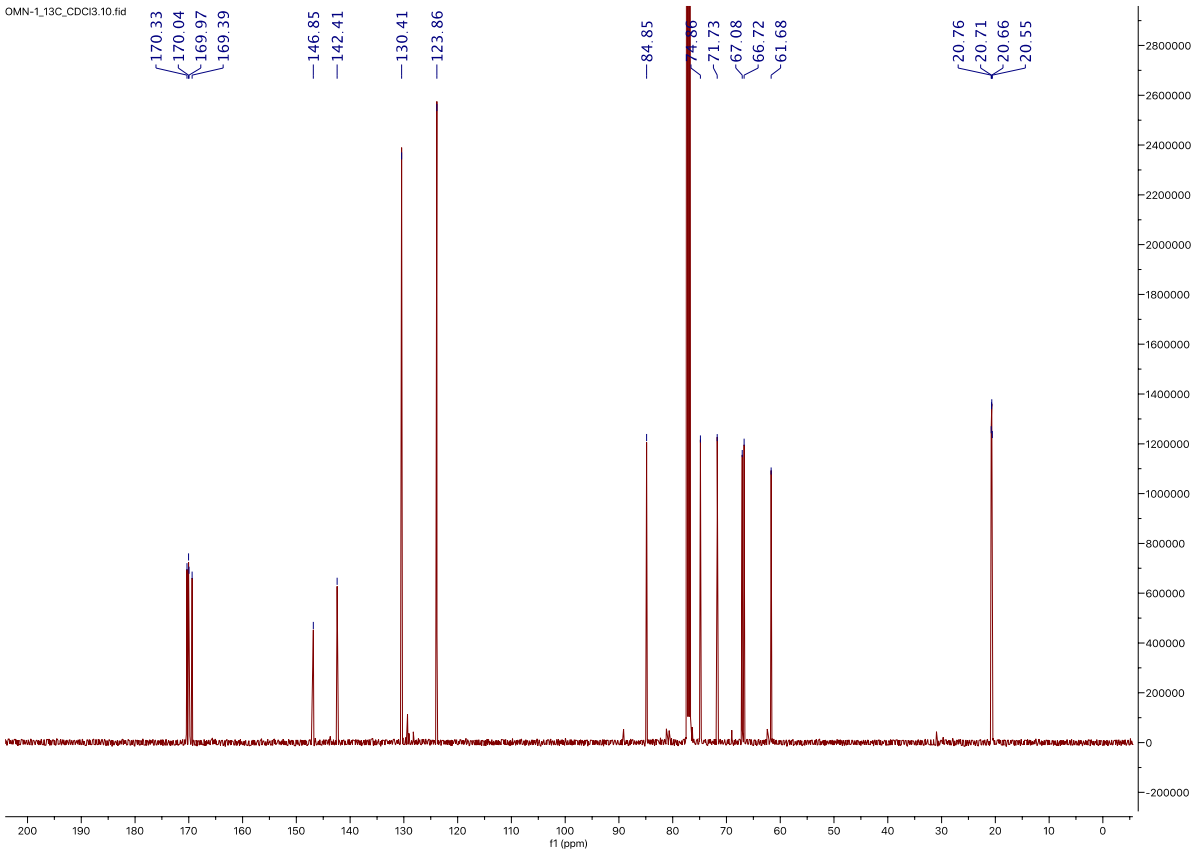
OMN-1_13C_CDCl3.10.fid
170.33
170.04
169.97
169.39
146.85
142.41
130.41
123.86
84.85
74.86
71.73
67.08
66.72
61.68
20.76
20.71
20.66
20.55
f1 (ppm)

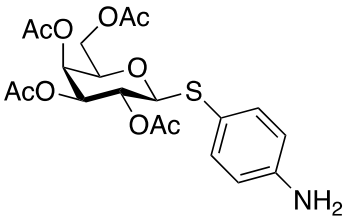

3

***p*-Aminophenyl 2,3,4,6-tetra-O-acetyl-β-D-thiogalactopyranoside (3)**.

Compound **3** was synthesized according to Casoni *et al.*[2]: **2** (900 mg, 1.85 mmol) was suspended in dry DCM (40 mL) and 90 mg palladium on activated charcoal (10% Pd basis) was added under nitrogen atmosphere. The reaction flask was flushed with hydrogen and stirred overnight at r.t. under hydrogen atmosphere. The reaction mixture was filtered through celite and the solvent was removed *in vacuo.* The crude product was purified by normal phase MPLC (Toluene/EtOAc, 40–80% EtOAc). **3** was obtained as a light-pink solid (818 mg, 1.8 mmol, 97%).

^{1}H NMR (500 MHz, Acetone-d_6) δ 7.29 – 7.23 (m, 2H, ArH), 6.68 – 6.61 (m, 2H, ArH), 5.38 (dd, J = 3.2, 0.9 Hz, 1H, H-4), 5.18 – 5.06 (m, 2H, H-2, H-3), 4.94 (br s, J = 10.9 Hz, NH_2), 4.73 (d, J = 9.3 Hz, 1H, H-1), 4.19 – 4.04 (m, 3H, H-5, H-6), 2.09 (s, 3H, CH_3), 2.04 (s, 3H, CH_3), 1.99 (s, 3H, CH_3), 1.90 (s, 3H, CH_3).

^{13}C NMR (126 MHz, Acetone-d_6) δ 170.81 ($CH_3\underline{C}$(O)), 170.60 ($CH_3\underline{C}$(O)), 170.26 ($CH_3\underline{C}$(O)), 169.88 ($CH_3\underline{C}$(O)), 150.39 (ArC), 150.34 (ArC), 136.71 (ArCH), 129.86 (Toluene contamination), 129.14 (Toluene contamination), 117.95 (ArC), 115.38 (ArCH), 115.35 (ArCH), 88.19 (C-1), 75.01 (C-5), 72.82 (C-3), 68.68 (C-2), 68.42 (C-4), 62.63 (C-6), 20.92 (CH_3), 20.73 (CH_3), 20.64 (CH_3), 20.63 (CH_3).

HPLC-MS: $[C_{20}H_{25}NO_9S + H]^+$ calcd. 456.13, found 456.09.
HRMS: $[C_{20}H_{25}NO_9S + H]^+$ calcd. 456.1323, found 456.1311.

Spectroscopic data is in accordance with the literature[2].

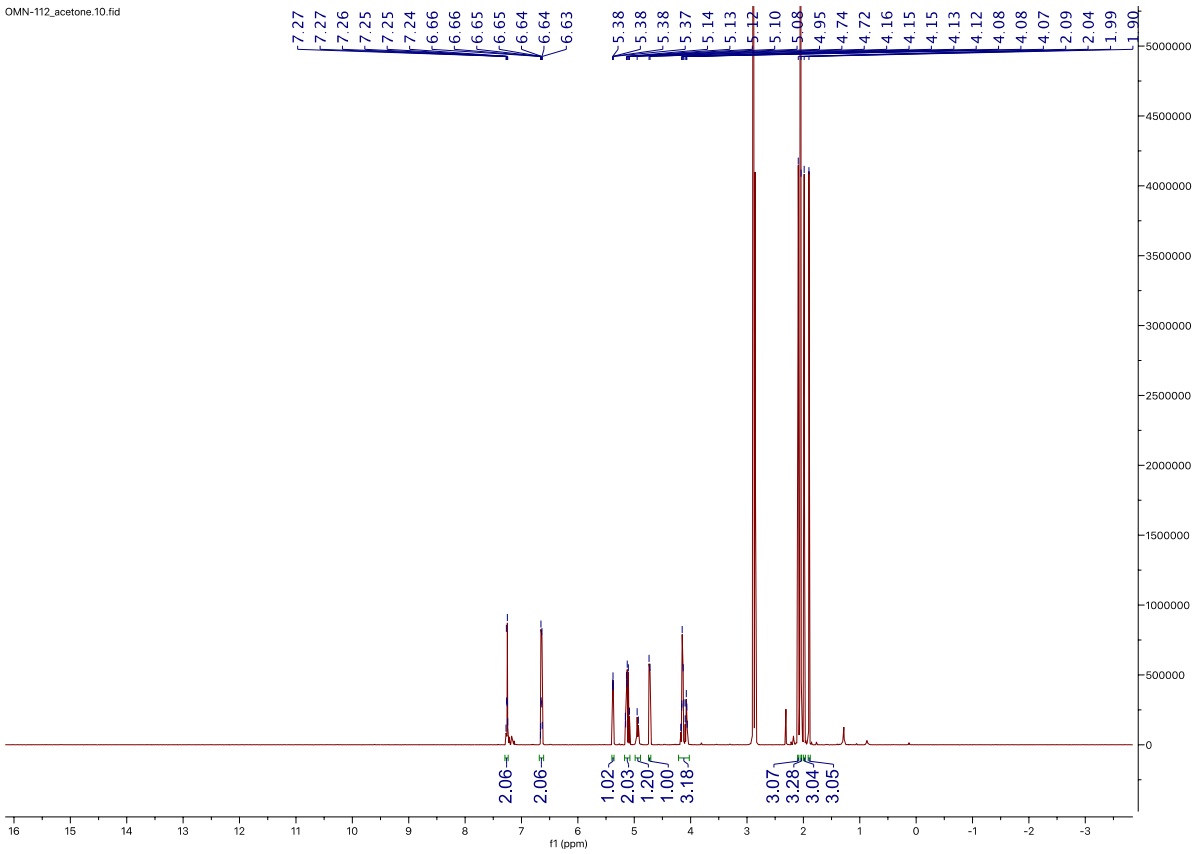
OMN-112_acetone.10.fid
7.27
7.27
7.26
7.25
7.25
7.24
6.66
6.66
6.65
6.65
6.64
6.64
6.63
5.38
5.38
5.38
5.37
5.14
5.13
5.12
5.10
5.08
4.95
4.74
4.72
4.16
4.15
4.13
4.12
4.08
4.08
4.07
2.09
2.04
1.99
1.90
2.06
2.06
1.02
2.03
1.20
1.00
3.18
3.07
3.28
3.04
3.05
f1 (ppm)

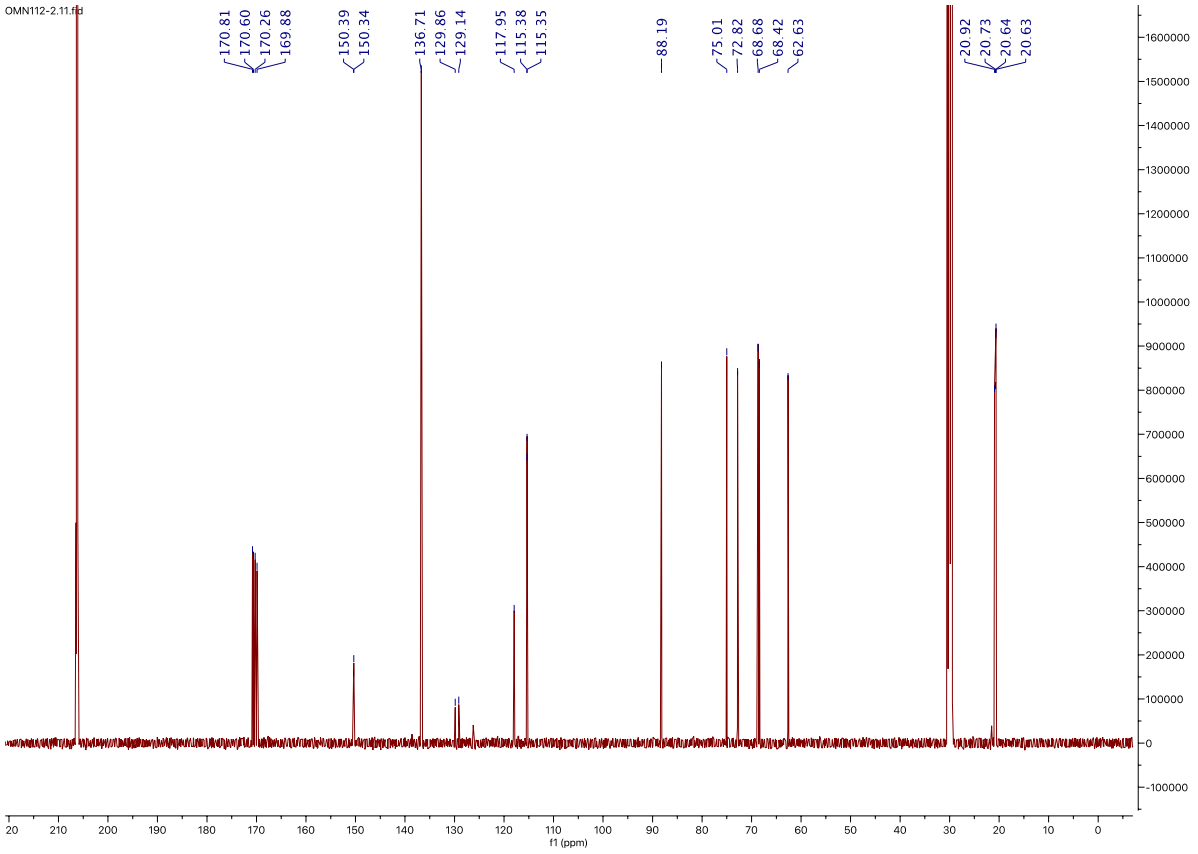
OMN112-2.11.fid
170.81
170.60
170.26
169.88
150.39
150.34
136.71
129.86
129.14
117.95
115.38
115.35
88.19
75.01
72.82
68.68
68.42
62.63
20.92
20.73
20.64
20.63
f1 (ppm)

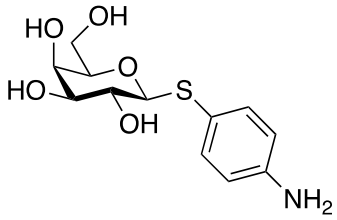

***p*-Aminophenyl β-D-thiogalactopyranoside (4)**.

Compound **3** (300 mg, 0.66 mmol) was suspended in dry MeOH (5 mL) and 5.3 M NaOMe in MeOH (62 µL, 0.5 equiv., 0.33 mmol) was added. The reaction mixture was stirred for 30 min at r.t., when 0.1 M HCl was added to neutralize the reaction mixture to pH 7. The solvent was removed *in vacuo* and the residue was purified by reverse phase MPLC (H_2O/MeCN + 0.1% formic acid, 5-15% MeCN) to give **4** as a white solid (178 mg, 0.62 mmol, quant.).

^{1}H NMR (500 MHz, D_2O) δ 7.48 – 7.42 (m, 2H, ArH), 6.93 – 6.88 (m, 2H, ArH), 4.56 (d, J = 9.8 Hz, 1H, H-1), 3.95 (d, J = 3.3 Hz, 1H, H-4), 3.78 – 3.62 (m, 4H, H-2, H-5, H-6), 3.55 (t, J = 9.6 Hz, 1H, H-3).

^{13}C NMR (126 MHz, D_2O) δ 144.74 (ArC), 134.54 (ArCH), 121.81 (ArC), 117.67 (ArCH), 88.83 (C-1), 78.93 (C-5), 73.96 (C-3), 69.08 (C-2), 68.67 (C-4), 60.91 (C-6).

HRMS: $[C_{12}H_{17}NO_5S + H]^+$ calcd. 288.0900, found 288.0891.

Spectroscopic data is in accordance with the literature[3].

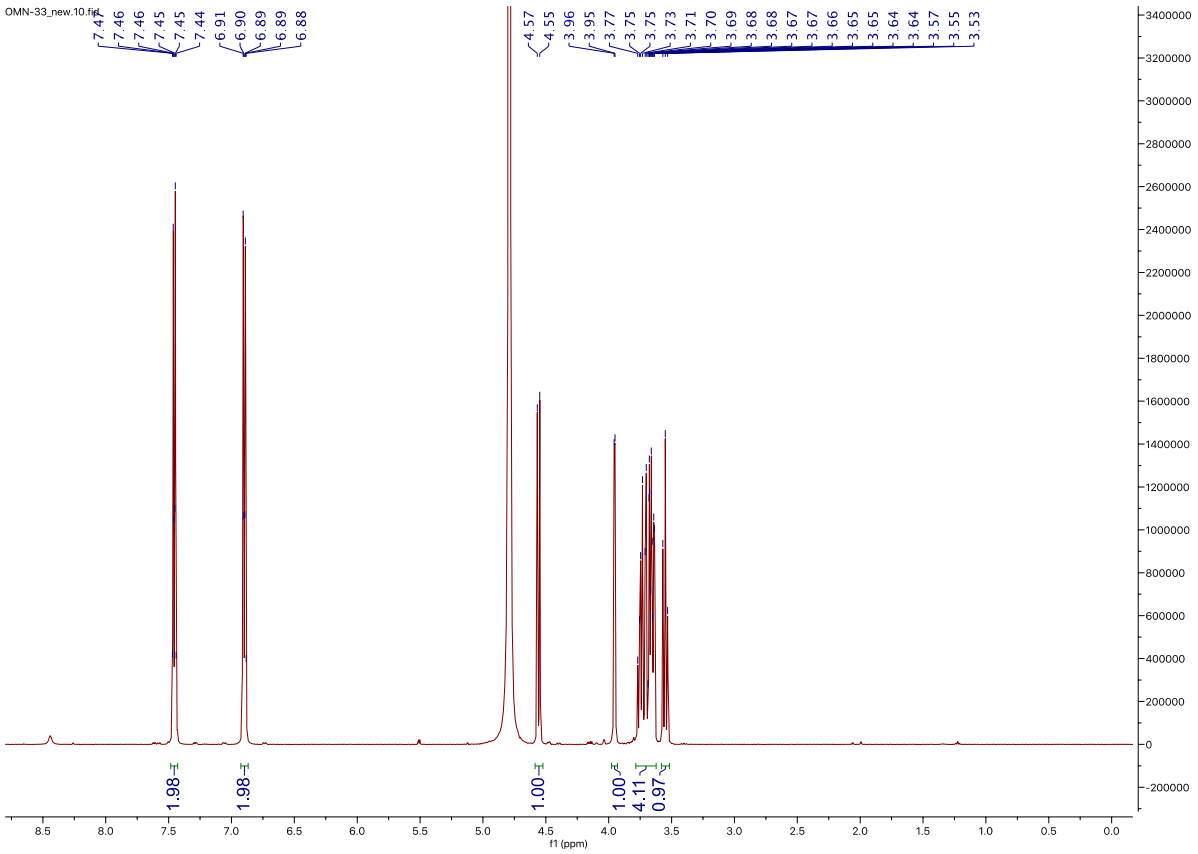
OMN-33_new.10.fid
7.47
7.46
7.46
7.45
7.45
7.44
6.91
6.90
6.89
6.89
6.88
4.57
4.55
3.96
3.95
3.77
3.75
3.75
3.73
3.71
3.70
3.69
3.68
3.68
3.67
3.67
3.66
3.65
3.65
3.64
3.64
3.57
3.55
3.53
1.98
1.98
1.00
1.00
4.11
0.97
f1 (ppm)

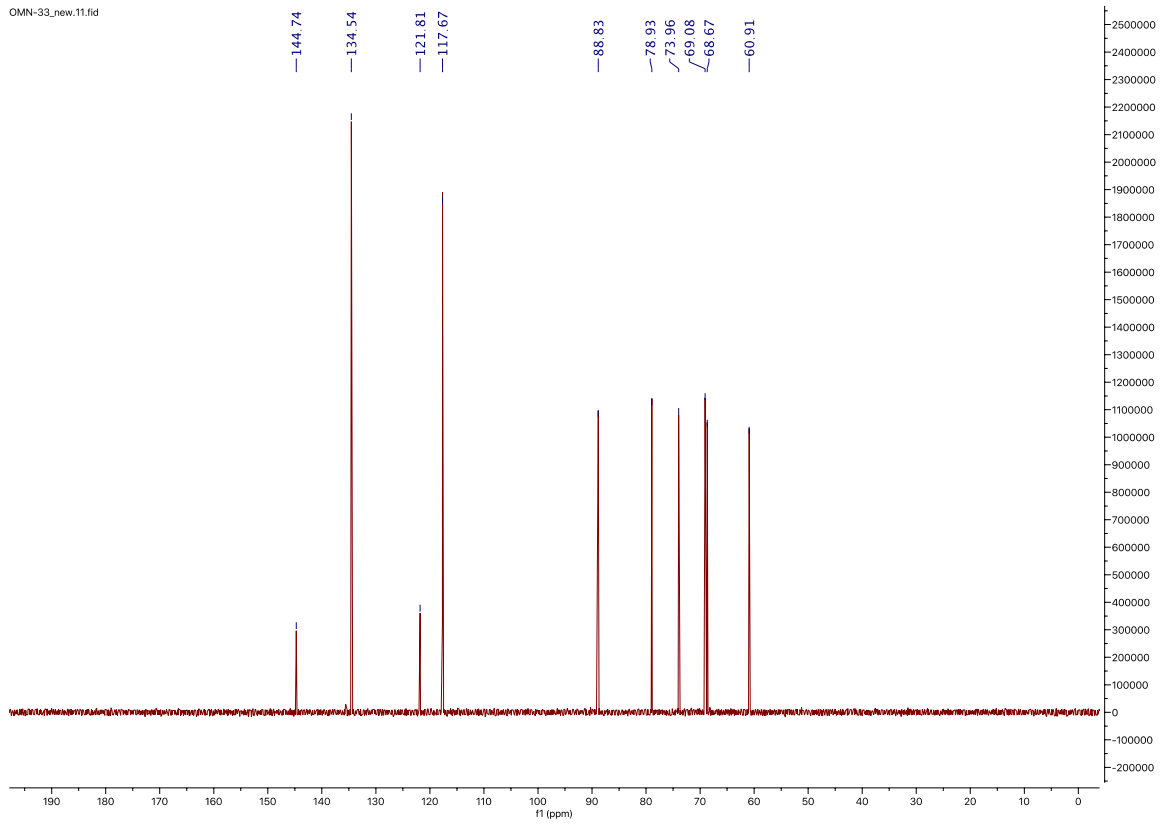
OMN-33_new.11.fid
144.74
134.54
121.81
117.67
88.83
78.93
73.96
69.08
68.67
60.91
f1 (ppm)

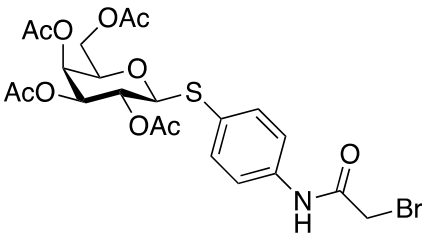

5

4-(2-Bromoacetamido)phenyl 2,3,4,6-tetra-O-acetyl-β-D-thiogalactopyranoside (5).

Compound **5** was synthesized according to Casoni *et al.*[2]: **3** (400 mg, 0.88 mmol) was dissolved in dry DCM (10 mL) and triethylamine (194 µL, 1.6 equiv., 1.4 mmol) was added under nitrogen atmosphere. The reaction flask was cooled to 0 °C and bromoacetyl bromide (115 µL, 1.5 equiv, 1.32 mmol) was added dropwise under vigorous stirring. The reaction mixture was warmed to r.t. and stirred for 2 h. Then, the reaction was diluted with DCM and washed with aqueous saturated ammonium chloride, water and brine consequentially, and dried over anhydrous sodium sulfate. After filtration, the solvent was removed *in vacuo.* Crude **5** (551 mg) was used for further modification without purification.

HPLC-MS: $[C_{22}H_{26}BrNO_{10}S + H]^+$ calcd. 576.05, found 576.00.

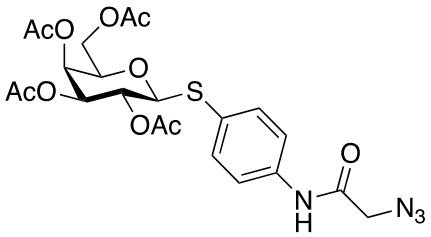

6, 73% over two steps

4-(2-Azidoacetamido)phenyl 2,3,4,6-tetra-O-acetyl-β-D-thiogalactopyranoside (6).

Compound **6** was synthesized according to Casoni *et al.*[2]: **5** (551 mg) was suspended in dry DMF (10 mL), sodium azide (285 mg, 5 equiv., 4.4 mmol) was added and the reaction was stirred for 3 h under nitrogen atmosphere. The reaction was diluted with water and extracted three times with EtOAc, combined organic phases were washed with water, brine and then dried over anhydrous sodium sulfate. After filtration, the solvent was removed *in vacuo*. The crude product was purified by normal phase MPLC (petroleum ether/EtOAc, 40–70% EtOAc). **6** was obtained as a white solid (341 mg, 0.64 mmol, 73% over two steps).

^{1}H NMR (500 MHz, $CHCl_3$-*d1*) δ 7.56 – 7.45 (m, 4H, ArH), 5.40 (dd, *J* = 3.4, 1.1 Hz, 1H, H-4), 5.19 (t, *J* = 10.0 Hz, 1H, H-2), 5.03 (dd, *J* = 9.9, 3.4 Hz, 1H, H-3), 4.64 (d, *J* = 9.9 Hz, 1H, H-1), 4.23 – 4.06 (m, 1H, H-6_a), 4.16 (s, 2H, CH_2) 3.95 – 3.86 (m, 1H, H-6_b), 2.11 (s, 3H, CH_3), 2.09 (s, 3H, CH_3), 2.05 (s, 3H, CH_3), 1.96 (s, 3H, CH_3).

^{13}C NMR (126 MHz, $CHCl_3$-*d1*) δ 170.53 ($CH_3\underline{C}$(O)), 170.33 ($CH_3\underline{C}$(O)), 170.19 ($CH_3\underline{C}$(O)), 169.55 ($CH_3\underline{C}$(O)), 164.68 (NHC(O)), 137.21 (ArC), 134.26 (ArCH), 128.03 (ArC), 120.34 (ArCH), 86.76 (C-1), 74.58 (C-5), 72.10 (C-3), 67.32 (C-4, C-2), 61.71 (C-6), 53.08 (CH_2), 20.99 (CH_3), 20.84 (CH_3), 20.79 (CH_3), 20.71 (CH_3).

HRMS: $[C_{22}H_{26}N_4O_{10}S + H]^+$ calcd. 539.1442, found 539.1436.

Spectroscopic data is in accordance with the literature[2].

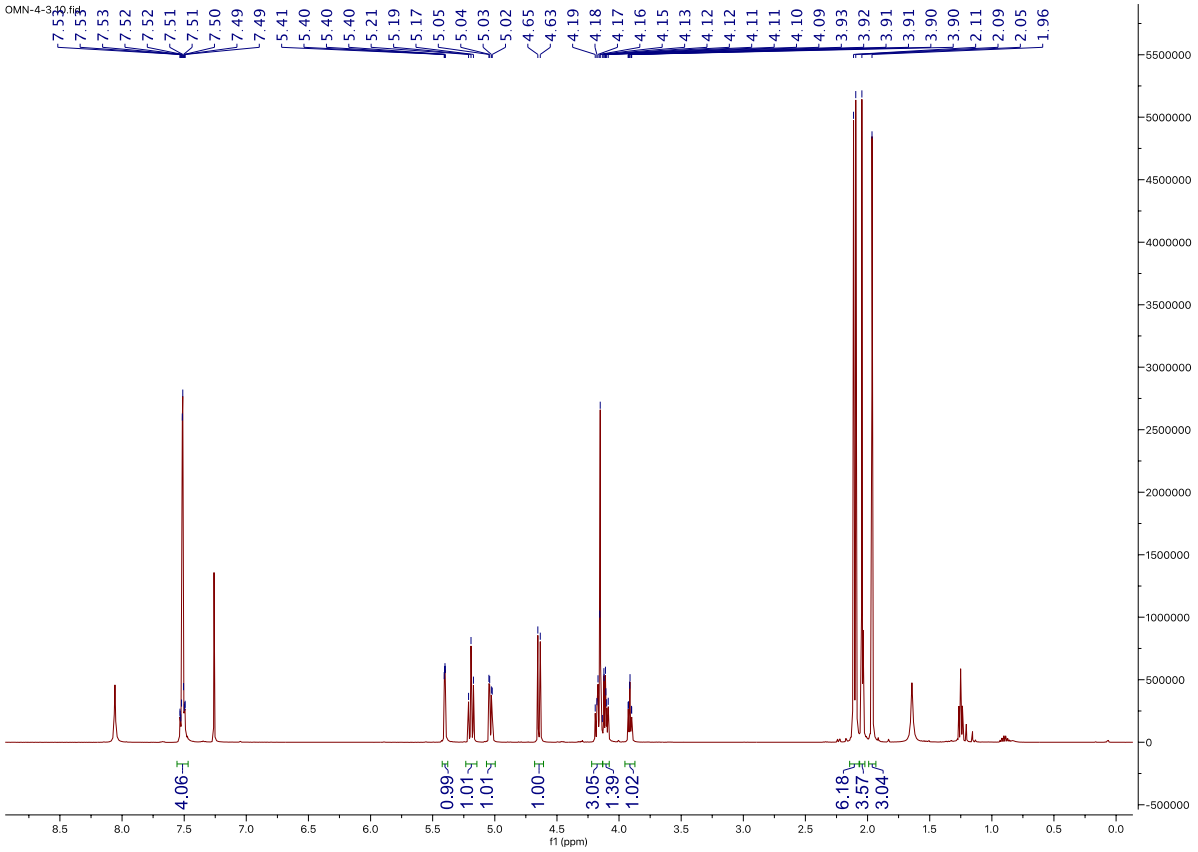
OMN-4-3.10.fid
7.53 7.53 7.53 7.52 7.52 7.51 7.51 7.50 7.49 7.49
5.41 5.40 5.40 5.40 5.21 5.19 5.17 5.05 5.04 5.03 5.02
4.65 4.63 4.19 4.18 4.17 4.16 4.15 4.13 4.12 4.12 4.11 4.11 4.10 4.09
3.93 3.92 3.91 3.91 3.90 3.90 2.11 2.09 2.05 1.96
4.06 0.99 1.01 1.01 1.00 3.05 1.39 1.02 6.18 3.57 3.04
f1 (ppm)

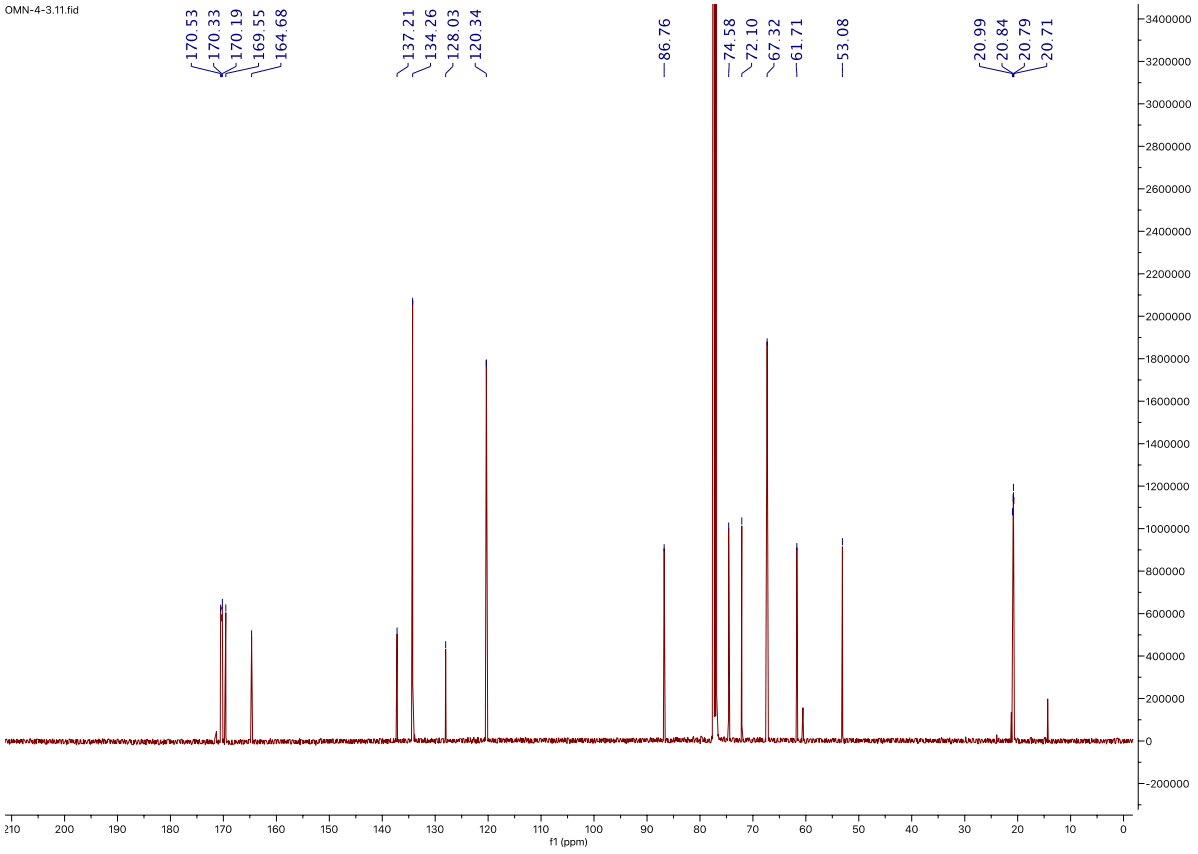
OMN-4-3.11.fid
170.53 170.33 170.19 169.55 164.68
137.21 134.26 128.03 120.34
86.76
74.58 72.10 67.32 61.71
53.08
20.99 20.84 20.79 20.71
f1 (ppm)

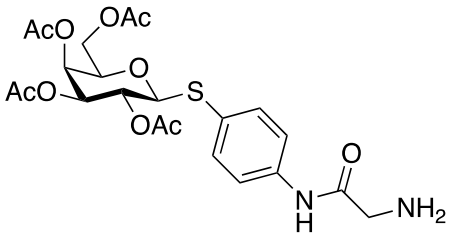

7, 97%

4-(2-Aminoacetamido)phenyl 2,3,4,6-tetra-O-acetyl-β-D-thiogalactopyranoside (7).

Compound **6** (320 mg, 0.6 mmol) was suspended in dry DCM (10 mL) and 32 mg palladium on activated charcoal (10% Pd basis) was added under nitrogen atmosphere. The flask was flushed with hydrogen and the reaction was stirred for 2 h at r.t. under hydrogen atmosphere. The reaction mixture was filtered through celite and the solvent was removed *in vacuo.* **7** was obtained as a white solid (308 mg, 1.8 mmol, 97%.).

^{1}H NMR (500 MHz, $CHCl_3$-*d1*) δ 9.55 (br s, 1H, NH_2), 7.56 (d, *J* = 8.2 Hz, 2H, ArH), 7.47 (d, *J* = 8.3 Hz, 2H, ArH), 5.40 (d, *J* = 3.4 Hz, 1H, H-4), 5.19 (t, *J* = 9.9 Hz, 1H, H-2), 5.04 (dd, *J* = 10.0, 3.4 Hz, 1H, H-3), 4.64 (d, *J* = 10.0 Hz, 1H), 4.17 (dd, *J* = 11.4, 6.6 Hz, 1H, H-6_a), 4.10 (dd, *J* = 11.4, 6.2 Hz, 1H, H-6_b), 3.91 (t, *J* = 6.7 Hz, 1H, H-5), 3.55 (s, 2H, CH_2), 2.11 (s, 3H, CH_3), 2.09 (s, 3H, CH_3), 2.03 (s, 3H, CH_3), 1.96 (s, 3H, CH_3).

^{13}C NMR (126 MHz, $CHCl_3$-*d1*) δ 170.61 ($CH_3\underline{C}$(O)), 170.38 ($CH_3\underline{C}$(O)), 170.20 ($CH_3\underline{C}$(O)), 169.61 (NHC(O)), 138.10 (ArC), 134.29 (ArCH), 126.93 (ArC), 119.86 (ArCH), 86.98 (C-1), 74.52 (C-5), 72.12 (C-3), 67.40 (C-2), 67.36 (C-4), 61.72 (C-6), 44.88 (CH_2), 21.01 (CH_3), 20.85 (CH_3), 20.80 (CH_3), 20.72 (CH_3).

HRMS: $[C_{22}H_{28}N_2O_{10}S + H]^+$ calcd. 513.1537, found 513.1535.

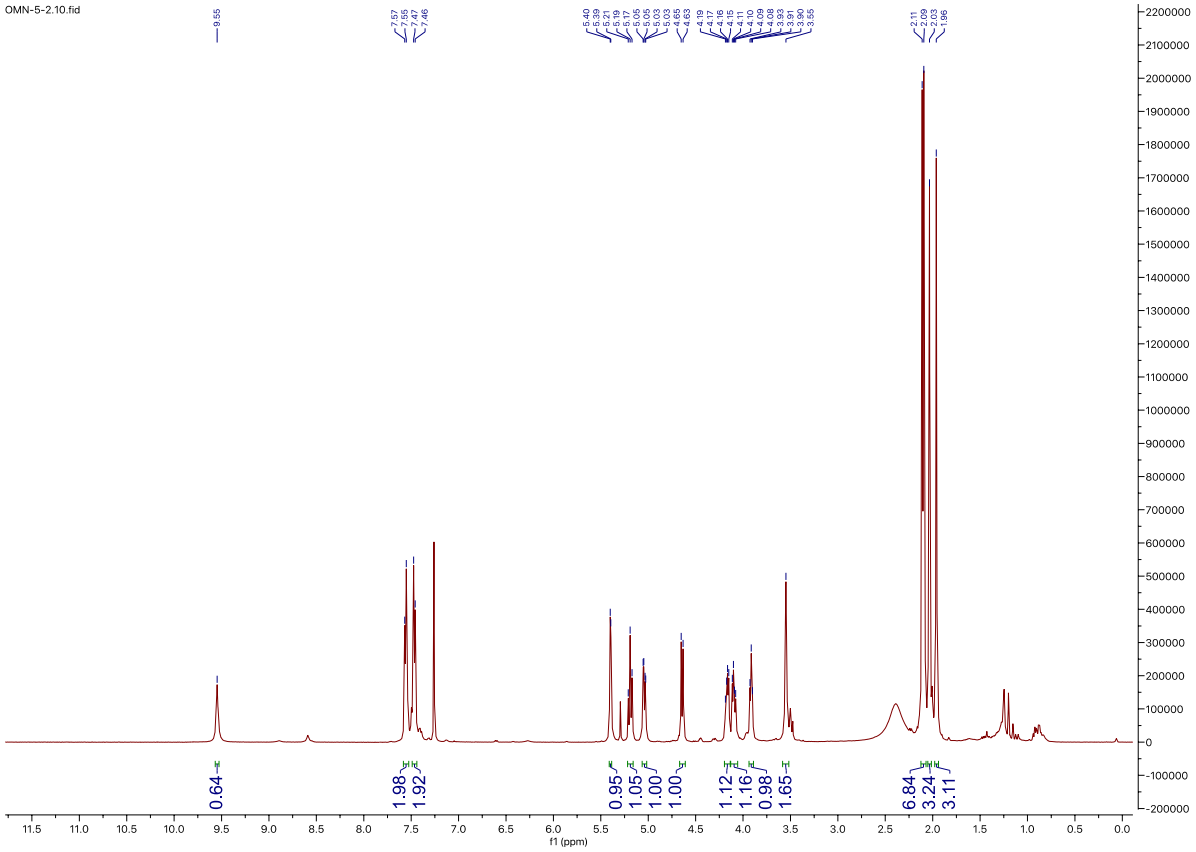
OMN-5-2.10.fid
9.55
7.57
7.55
7.47
7.46
5.40
5.39
5.21
5.19
5.17
5.07
5.05
5.03
5.03
4.65
4.63
4.19
4.17
4.16
4.15
4.11
4.10
4.09
4.08
3.93
3.91
3.90
3.55
2.11
2.09
2.03
1.98
0.64
1.98
1.92
0.95
1.05
1.00
1.00
1.12
1.16
0.98
1.65
6.84
3.24
3.11
f1 (ppm)

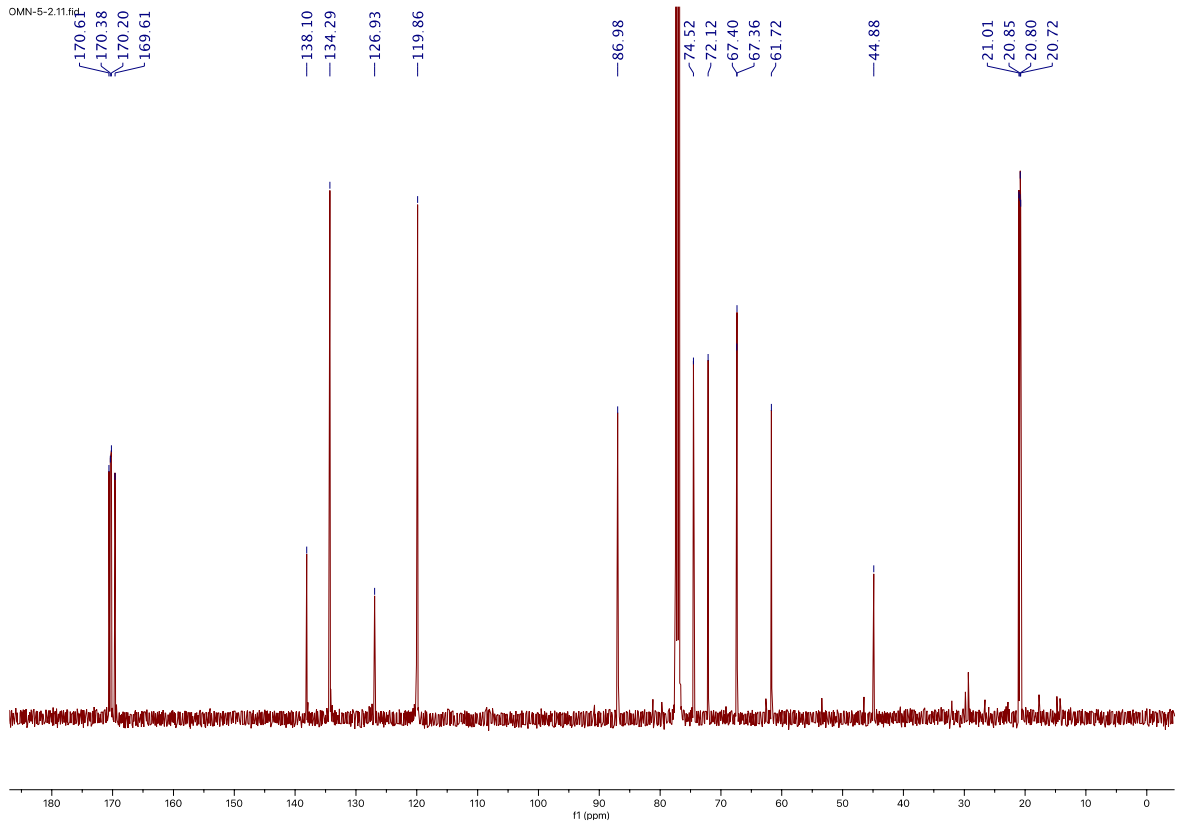
OMN-5-2.11.fid
170.61
170.38
170.20
169.61
138.10
134.29
126.93
119.86
86.98
74.52
72.12
67.40
67.36
61.72
44.88
21.01
20.85
20.80
20.72
f1 (ppm)

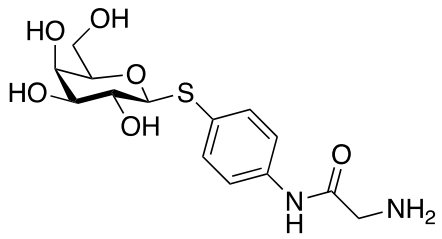

8, 96%

4-(2-Aminoacetamido)phenyl β-D-thiogalactopyranoside (8).

Compound **7** (220 mg, 0.429 mmol) was suspended in dry MeOH (3 mL) and 5.3 M NaOMe in MeOH (40 µL, 0.5 equiv., 0.214 mmol) was added. The reaction mixture was stirred for 15 min at r.t.. Then, 0.1 M HCl was added to neutralize the reaction mixture to pH 7. The solvent was removed *in vacuo* and crude product was purified by reverse phase MPLC (H_2O/MeCN + 0.1% formic acid, 5-20% MeCN) to give **8** as a white solid (148 mg, 4.28 mmol, quant.).

^{1}H NMR (500 MHz, D_2O) δ 7.59 (d, J = 8.3 Hz, 2H, ArH), 7.48 (d, J = 8.5 Hz, 2H, ArH), 4.73 (d, J = 9.7 Hz, 1H, H-1), 3.99 (m, 3H, H-4, CH_2), 3.81 – 3.66 (m, 4H, H-3, H-5, H-6), 3.61 (t, J = 9.6 Hz, 1H, H-2).

^{13}C NMR (126 MHz, D_2O) δ 165.43 (NHC(O)), 136.15 (ArC), 132.39 (ArCH), 128.96 (ArC), 121.69 (ArCH), 88.14 (C-1), 78.99 (C-5), 73.93 (C-3), 69.12 (C-2), 68.66 (C-4), 60.95 (C-6), 40.99 (CH_2).

HRMS: $[C_{14}H_{20}N_2O_6S + H]^+$ calcd. 345.1115, found 345.1105.

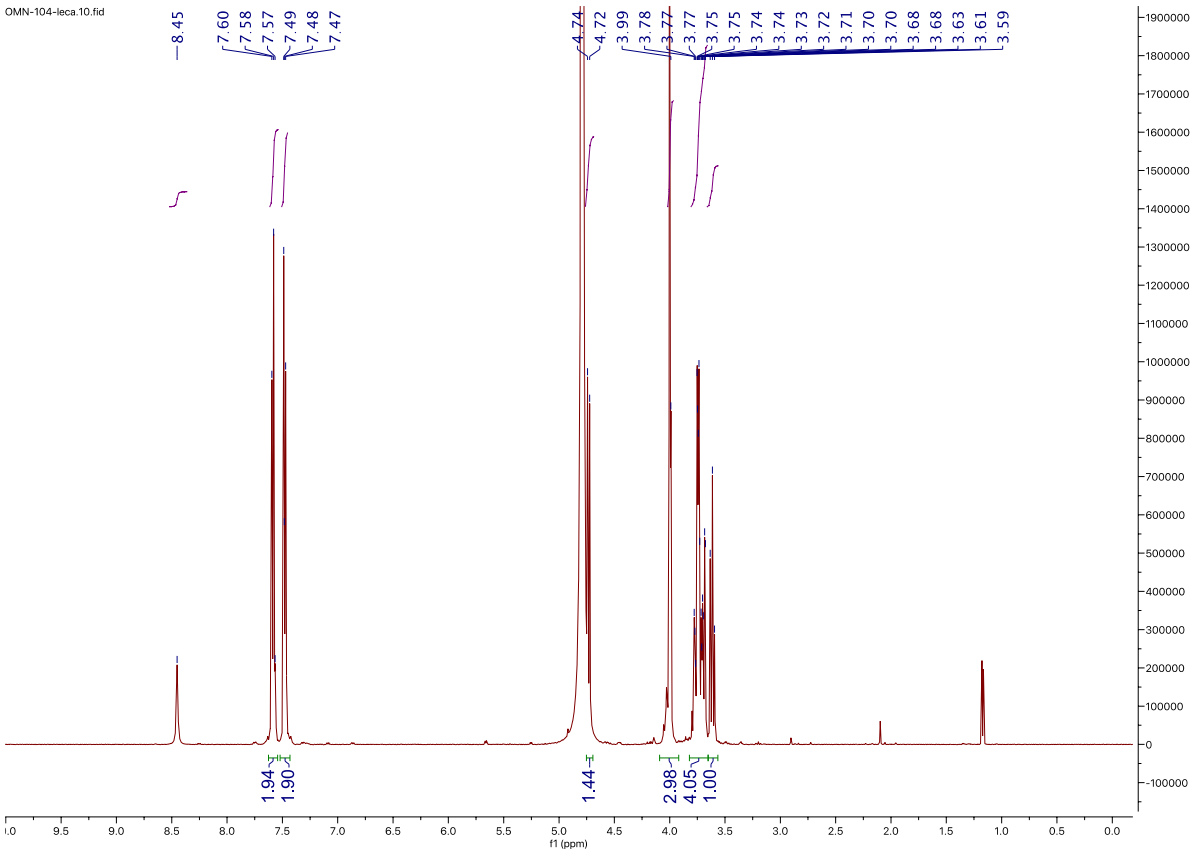
OMN-104-leca.10.fid
8.45
7.60
7.58
7.57
7.49
7.48
7.47
4.74
4.72
3.99
3.78
3.77
3.77
3.75
3.75
3.74
3.74
3.73
3.72
3.71
3.70
3.70
3.68
3.68
3.63
3.61
3.59
1.94
1.90
1.44
2.98
4.05
1.00
f1 (ppm)

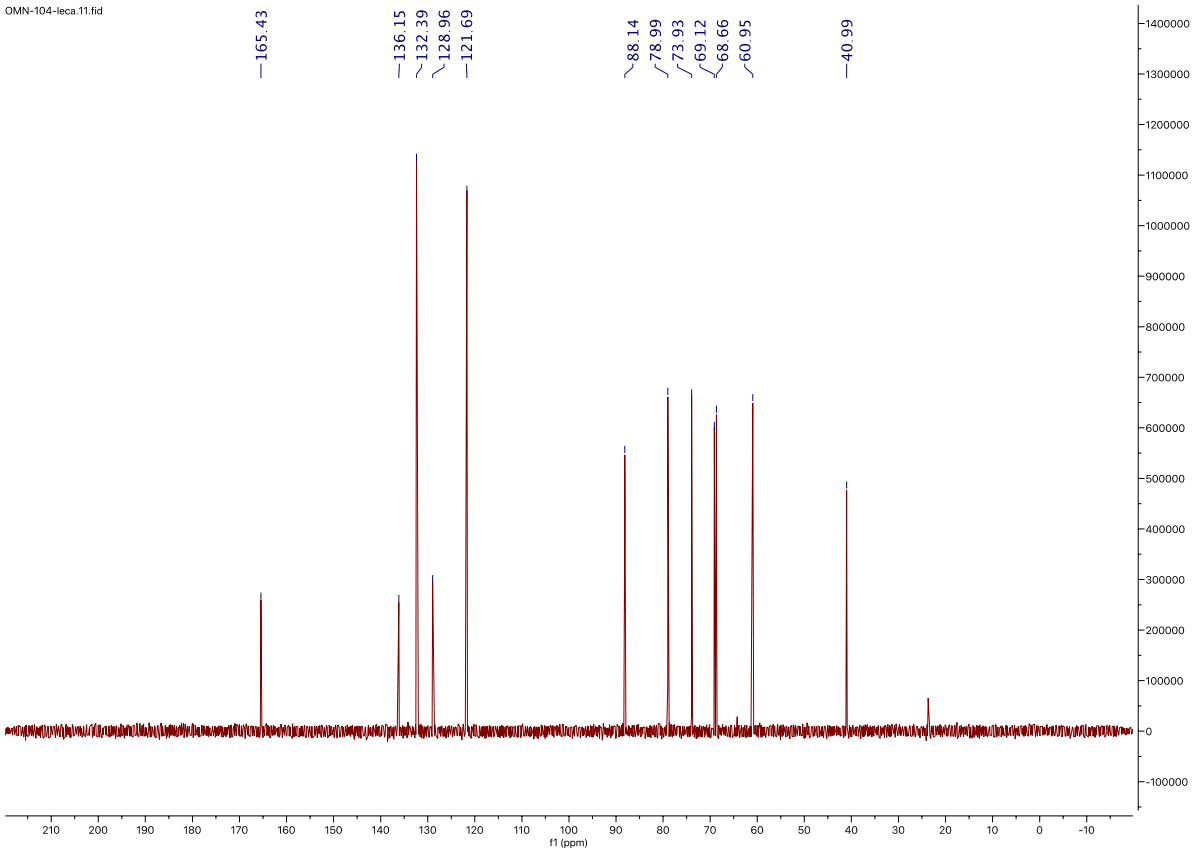
OMN-104-leca.11.fid
165.43
136.15
132.39
128.96
121.69
88.14
78.99
73.93
69.12
68.66
60.95
40.99
f1 (ppm)

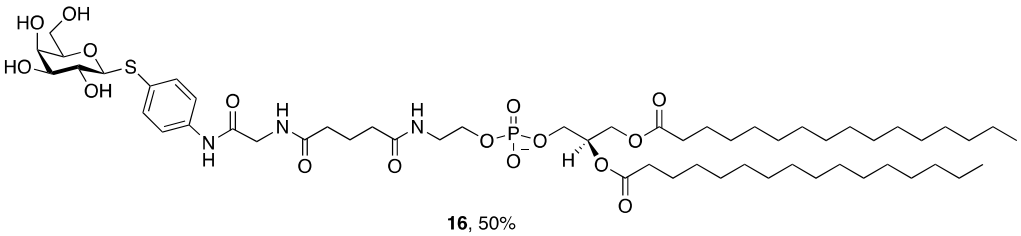

16, 50%

Glycolipid 16

16:0 Glutaryl PE (50 mg, 60 µmol) was suspended in a mixture of $CHCl_3$/DMF 1:1 (5 mL) and HBTU (28 mg, 1.2 equiv., 72 µmol), HOBt (8 mg, 1.2 equiv., 72 µmol) and Et_3N (42 µL, 5 equiv., 0.3 mmol) was added and stirred for 30 min under nitrogen atmosphere at 40 °C until phospholipid was completely dissolved. Then, **8** (32 mg, 1.55 equiv., 0.093 mmol) was added and the reaction was stirred at 40 °C for 48 h. The solvent was removed *in vacuo* and the crude product was purified by reverse phase MPLC (^{i}PrOH:H_2O:MeOH (5:4:1) / ^{i}PrOH + 0.2% formic acid, 10-50%). **16** was obtained as a beige solid (34 mg, 0.03 mmol, 50%).

^{1}H NMR (500 MHz, DMSO-d_6) δ 7.64 – 7.58 (m, 2H, ArH), 7.41 – 7.35 (m, 2H, ArH), 5.07 (ddd, J = 14.1, 7.5, 4.3 Hz, 1H, C(O)C<u>H</u>CH_2OPO_3), 4.82 (d, J = 5.7 Hz, 1H, NH), 4.65 (t, J = 5.7 Hz, 1H, NH), 4.44 (d, J = 9.4 Hz, 1H, H-1), 4.27 (dd, J = 12.0, 3.1 Hz, 1H, C(O)OC<u>H_{2a}</u>CH), 4.07 (dd, J = 12.1, 7.1 Hz, 1H, C(O)OC<u>H_{2b}</u>CH), 3.85 – 3.62 (m, 6H, C(O)C<u>H_2</u>NH, CH_2<u>C</u>H_2OPO_3, CH<u>C</u>H_2OPO_3), 3.55 – 3.44 (m, 2H, H-6), 3.18 (q, J = 5.2 Hz, 2H, C<u>H_2</u>CH_2OPO_3), 2.24 (t, J = 7.3 Hz, 4H, C<u>H_2</u>C(O)O), 2.17 (t, J = 7.4 Hz, 2H, CH_2CH_2C<u>H_2</u>C(O)NH), 2.03 (t, J = 6.6 Hz, 2H, NHC(O)C<u>H_2</u>CH_2CH_2), 1.79 – 1.69 (m, 2H, NHC(O)CH_2C<u>H_2</u>), 1.54 – 1.40 (m, 4H, C<u>H_2</u>CH_2C(O)O), 1.30 – 1.16 (m, 46H, CH_2), 1.08 – 0.98 (m, 2H, CH_2), 0.85 (t, J = 6.8 Hz, 6H).

^{13}C NMR (126 MHz, DMSO-d_6) δ 172.55 (OC(O)), 172.35 (OC(O)), 172.29 (NHC(O)), 171.77 (NHC(O)), 168.56 (NHC(O)), 138.01 (ArC), 131.06 (ArCH), 128.21 (ArC), 119.61 (ArCH), 88.36 (C-1), 79.14 (C-5), 74.75 (C-3), 70.45 (d, J = 8.1 Hz, C(O)C<u>H</u>CH_2OPO_3), 69.18 (C-2), 68.30 (C-4), 62.82 (d, J = 4.6 Hz, CH_2<u>C</u>H_2OPO_3), 62.55 (d, J = 5.4 Hz, CH<u>C</u>H_2OPO_3), 62.30 (C(O)O<u>C</u>H_2CH), 60.48 (C-6), 45.63, 43.45 (C(O)<u>C</u>H_2NH), 34.84 (NHC(O)<u>C</u>$H_2CH_2CH_2$), 33.92 (CH_2CH_2<u>C</u>H_2C(O)NH), 33.59 (<u>C</u>H_2C(O)O), 33.42 (<u>C</u>H_2C(O)O), 31.31, 29.08, 29.03, 28.95, 28.78, 28.76, 28.73, 28.45, 28.42, 24.48 (<u>C</u>H_2CH_2C(O)O), 24.43 (<u>C</u>H_2CH_2C(O)O), 22.11, 21.52 (NHC(O)CH_2<u>C</u>H_2), 13.95 (CH_3).

HRMS: $[C_{56}H_9N_3O_{16}PS + H]^+$ calcd. 1132.6478, found 1132.6442

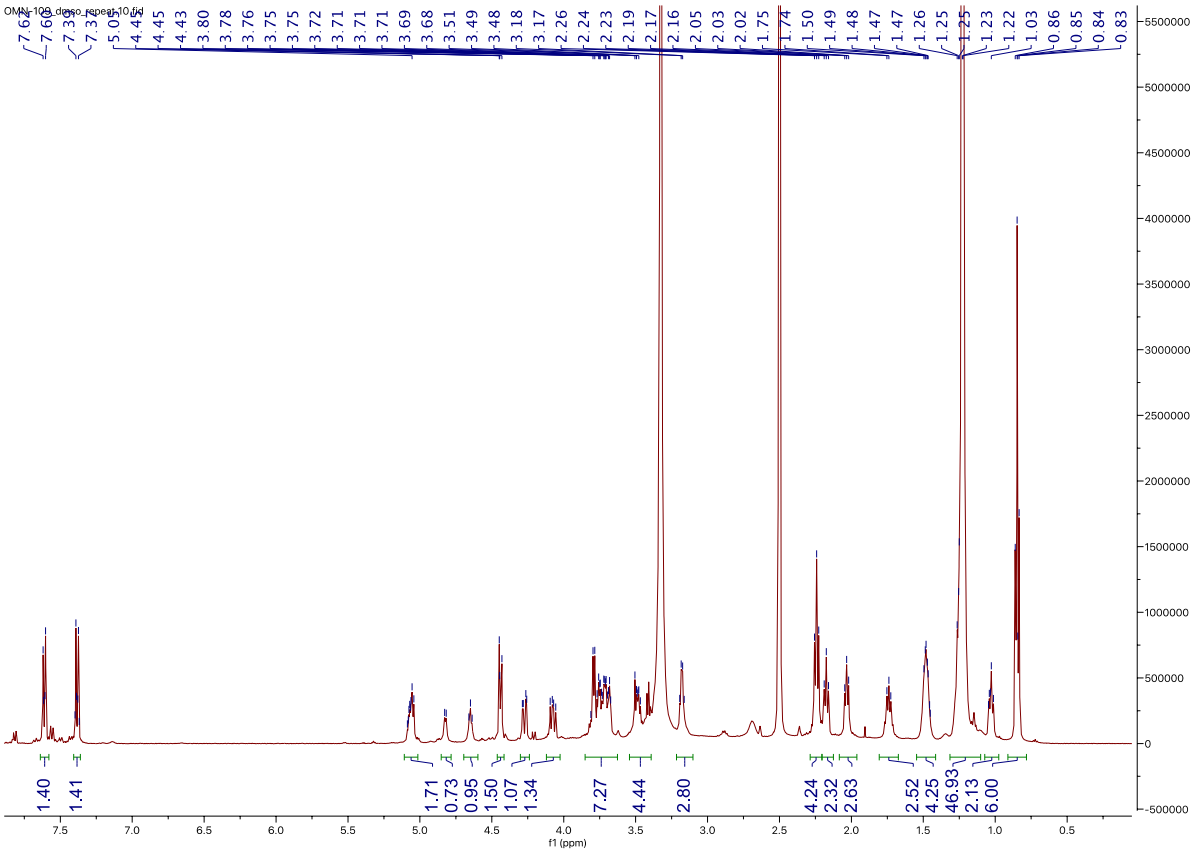

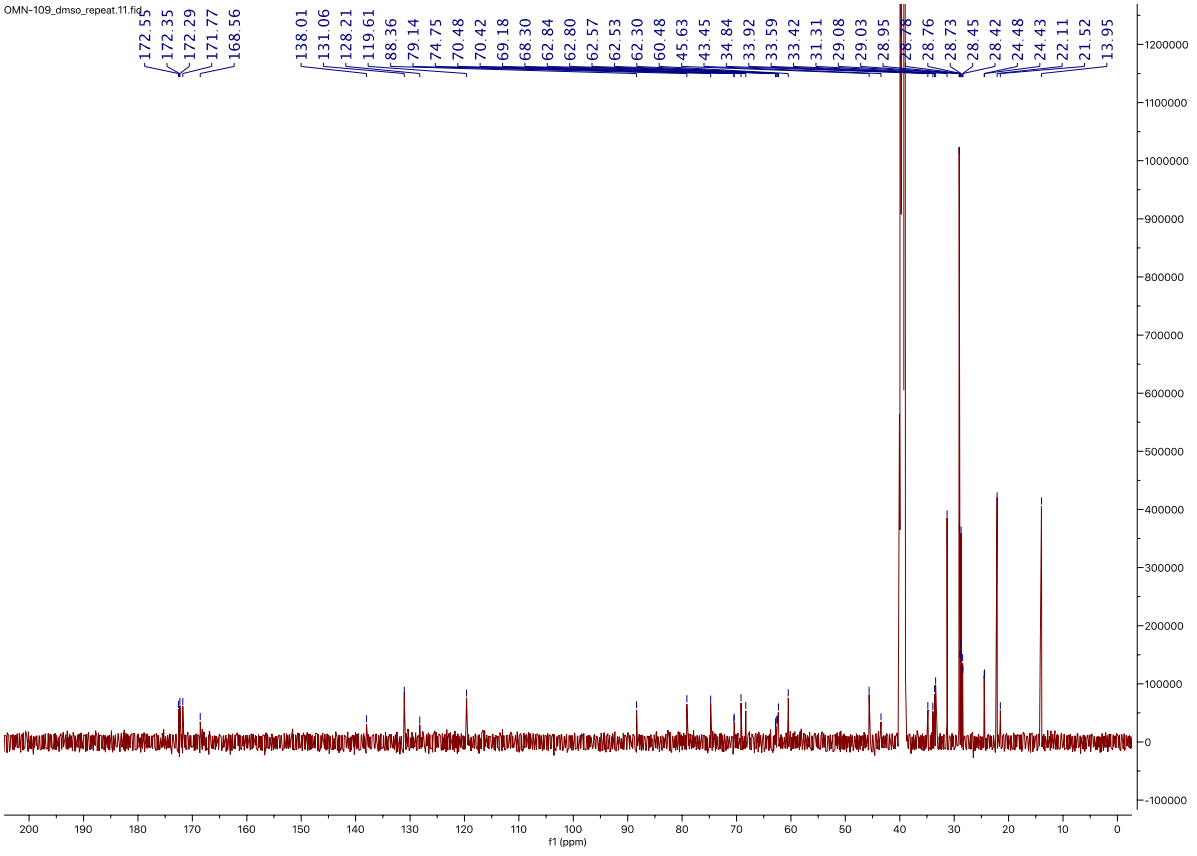

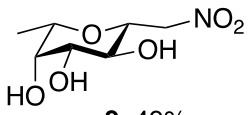

9, 49%

β-L-Fucopyranosyl nitromethane (9).

Compound **9** was synthesized according to Hauck *et al.*[4]: L-Fucose (2 g, 12.1 mmol) was dissolved in 12 mL dry DMSO and then nitromethane (8 mL, 12 equiv., 145.2 mmol) and 1 M sodium methoxide in MeOH (2.4 mL, 0.2 equiv., 2.4 mmol) were added under nitrogen dropwisely. The reaction mixture was stirred for 6 h and was then quenched by pouring the solution on ice-cold water premixed with 0.2 equiv. 1 M HCl. The obtained solution was adjusted to pH 4 by adding 1 M HCl and stirred o.n. under reflux. After cooling to r.t., the pH was adjusted to 6 by adding 1 M NaOH. The obtained solution was extracted with $CHCl_3$ to remove excess DMSO and then the aqueous phase was lyophilized. Crude product was purified by normal phase MPLC (DCM/MeOH, 0-15% MeOH) and then recrystallized from ethanol to give **9** (1268 mg, 6.12 mmol, 50%).

^{1}H NMR (500 MHz, MeOH-d_4) δ 4.84 (dd, J = 13.1, 2.3 Hz, 1H, CH_{2a}), 4.51 (dd, J = 13.1, 9.6 Hz, 1H, CH_{2b}), 3.91 (td, J = 9.6, 2.3 Hz, 1H, H-1), 3.67 (dd, J = 3.3, 1.1 Hz, 1H, H-4), 3.64 (dd, J = 6.4, 1.1 Hz, 1H, H-5), 3.51 (dd, J = 9.3, 3.2 Hz, 1H, H-3), 3.45 (t, J = 9.5 Hz, 1H, H-2), 1.22 (d, J = 6.5 Hz, 3H, CH_3).

^{13}C NMR (126 MHz, MeOH-d_4) δ 78.44 (C-1), 78.28 (CH_2), 76.24 (C-3), 75.72 (C-5), 73.42 (C-4), 69.27 (C-2), 16.92 (CH_3).

Spectroscopic data is in accordance with the literature[5].

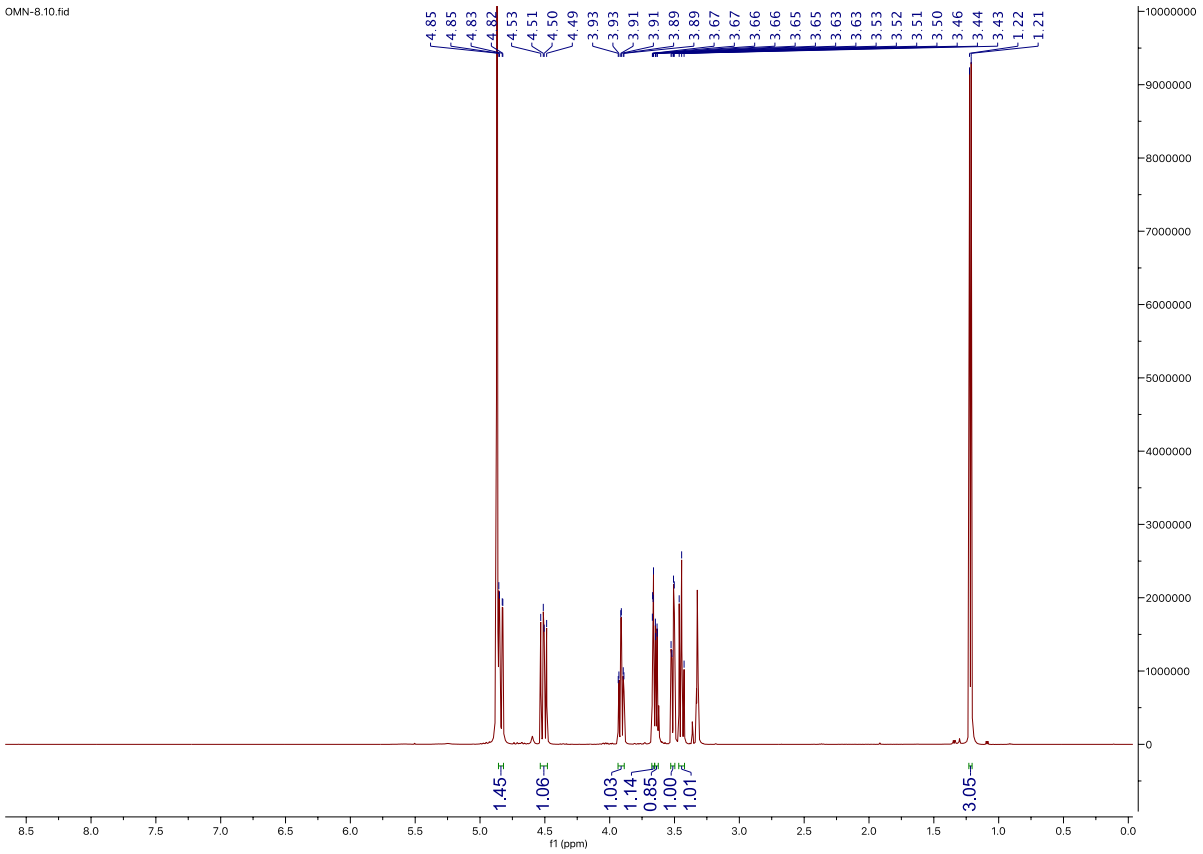
OMN-8.10.fid
4.85
4.85
4.83
4.82
4.53
4.51
4.50
4.49
3.93
3.93
3.91
3.91
3.89
3.89
3.67
3.67
3.66
3.66
3.65
3.65
3.63
3.63
3.53
3.52
3.51
3.50
3.46
3.44
3.43
1.22
1.21
1.45
1.06
1.03
1.14
0.85
1.00
1.01
3.05
f1 (ppm)

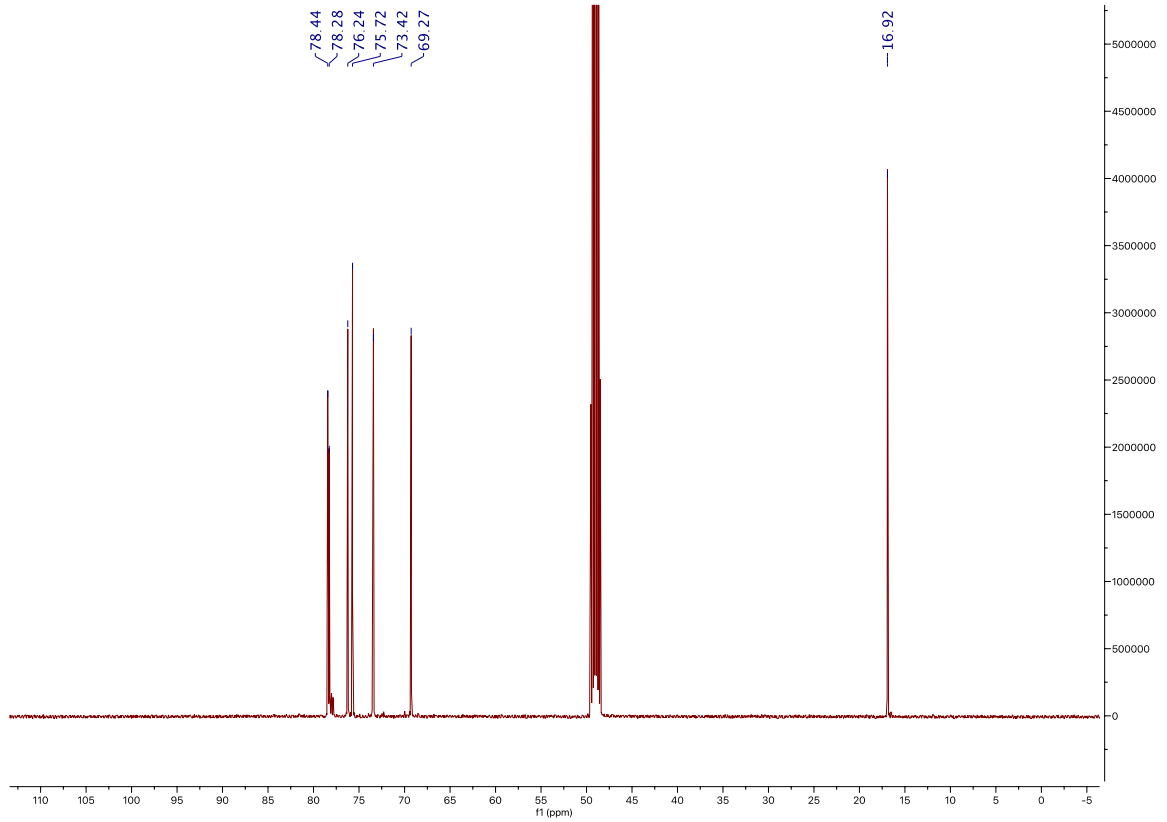
78.44
78.28
76.24
75.72
73.42
69.27
16.92
f1 (ppm)

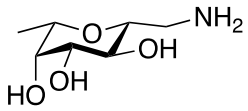

10, 98%

β-L-Fucopyranosyl methylamine (10).

Compound **10** was synthesized according to Sommer *et al.*[5]: Compound **9** (800 mg, 3.86 mmol) was suspended in dry MeOH (20 mL) and 80 mg palladium on activated charcoal (10% Pd basis) was added under nitrogen atmosphere. The reaction flask was flushed with hydrogen and stirred overnight at r.t. under hydrogen atmosphere. The reaction mixture was filtered through celite and the solvent was removed *in vacuo.* **10** was obtained as a white solid (682 mg, 3.85 mmol, quant.).

^{1}H NMR (500 MHz, MeOH-d_4) δ 3.66 (dd, J = 3.0, 1.1 Hz, 1H, H-4), 3.62 (qd, J = 6.4, 1.1 Hz, 1H, H-5), 3.48 – 3.41 (m, 2H, H-2, H-3), 3.16 (td, J = 8.0, 2.9 Hz, 1H, H-1), 3.05 (dd, J = 13.3, 3.0 Hz, 1H, CH_{2a}), 2.79 (dd, J = 13.3, 7.5 Hz, 1H, CH_{2b}), 1.26 (d, J = 6.5 Hz, 3H, CH_3).

^{13}C NMR (126 MHz, MeOH-d_4) δ 80.96 (C-1), 76.45 (C-3), 75.60 (C-5), 73.62 (C-4), 70.12 (C-2), 43.50 (CH_2), 17.13 (CH_3).

Spectroscopic data is in accordance with the literature[5].

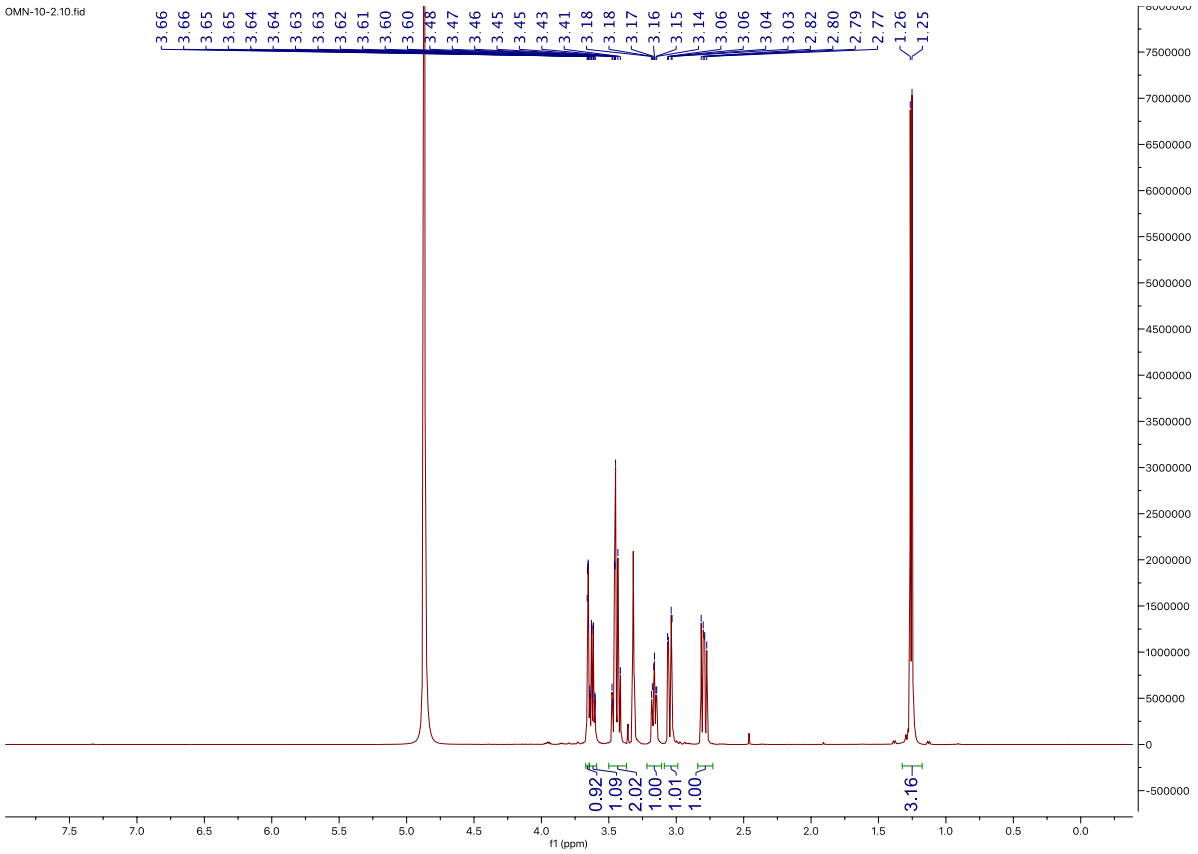
OMN-10-2.10.fid
3.66
3.66
3.65
3.65
3.64
3.64
3.63
3.63
3.62
3.61
3.60
3.60
3.48
3.47
3.46
3.45
3.45
3.43
3.41
3.18
3.18
3.17
3.16
3.15
3.14
3.06
3.06
3.04
3.03
2.82
2.80
2.79
2.77
1.26
1.25
0.92
1.09
2.02
1.00
1.01
1.00
3.16
f1 (ppm)

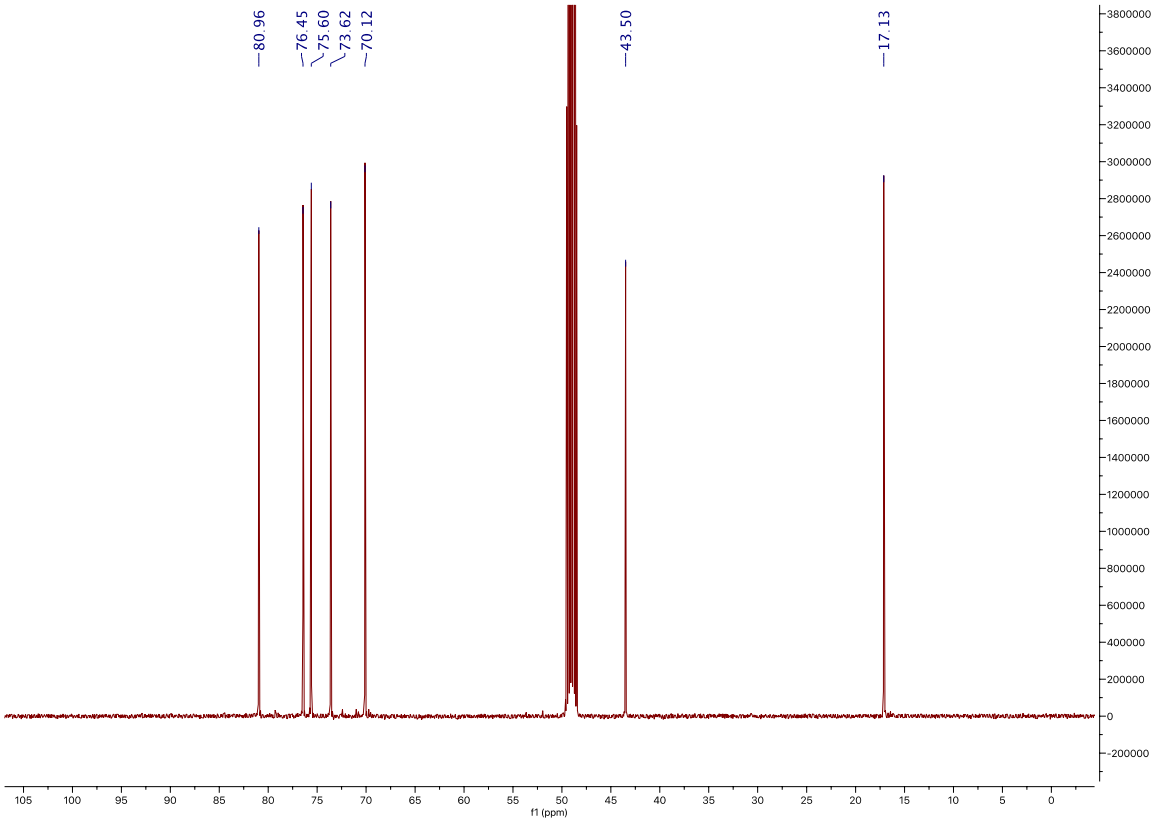
80.96
76.45
75.60
73.62
70.12
43.50
17.13
f1 (ppm)

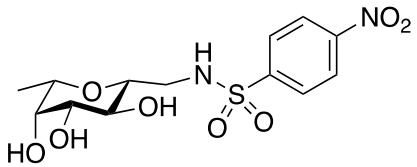

11, 62%

β-L-Fucopyranosylmethyl 4-nitrobenzenesulfonamide (11).

Amine **10** (480 mg, 2.24 mmol) was dissolved in dry DMF (10 mL) and triethylamine (465 µL, 1.5 equiv., 3.36 mmol) was added and stirred for 5 min under nitrogen atmosphere. The reaction flask was cooled down 0 °C and 4-nitro-benzenesulfonyl chloride (544 mg, 1.1 equiv, 2.46 mmol) in 10 mL of dry DMF was added dropwise under vigorous stirring. The reaction mixture was warmed to r.t. and stirred for 3 h. The reaction was quenched with ice-cold satd. sodium hydrogencarbonate, stirred for 5 min, then diluted with ice-cold water and lyophilized. Crude product was purified by reverse phase MPLC (H_2O/MeCN + 0.1% formic acid, 10-40% MeCN) to obtain **11** (502 mg, 1.38 mmol, 62%).

^{1}H NMR (500 MHz, D_2O) δ 8.44 – 8.32 (m, 2H, ArH), 8.09 – 7.99 (m, 2H, ArH), 3.64 (dd, *J* = 3.4, 1.0 Hz, 1H, H-4), 3.47 – 3.40 (m, 2H, H-3, H-5), 3.37 – 3.30 (m, 2H, H-2, CH_{2a}), 3.15 – 3.03 (m, 2H, H-1, CH_{2b}), 1.04 (d, *J* = 6.5 Hz, 3H, CH_3).

^{13}C NMR (126 MHz, D_2O) δ 150.04 (ArC), 144.57 (ArC), 128.04 (ArCH), 124.61 (ArCH), 77.44 (C-1), 74.06 (C-3), 73.81 (C-5), 71.56 (C-4), 67.84 (C-2), 43.80 (CH_2), 15.60 (CH_3).

HRMS: $[C_{13}H_{18}N_2O_8S + H]^+$ calcd. 363.0857, found 363.0844.

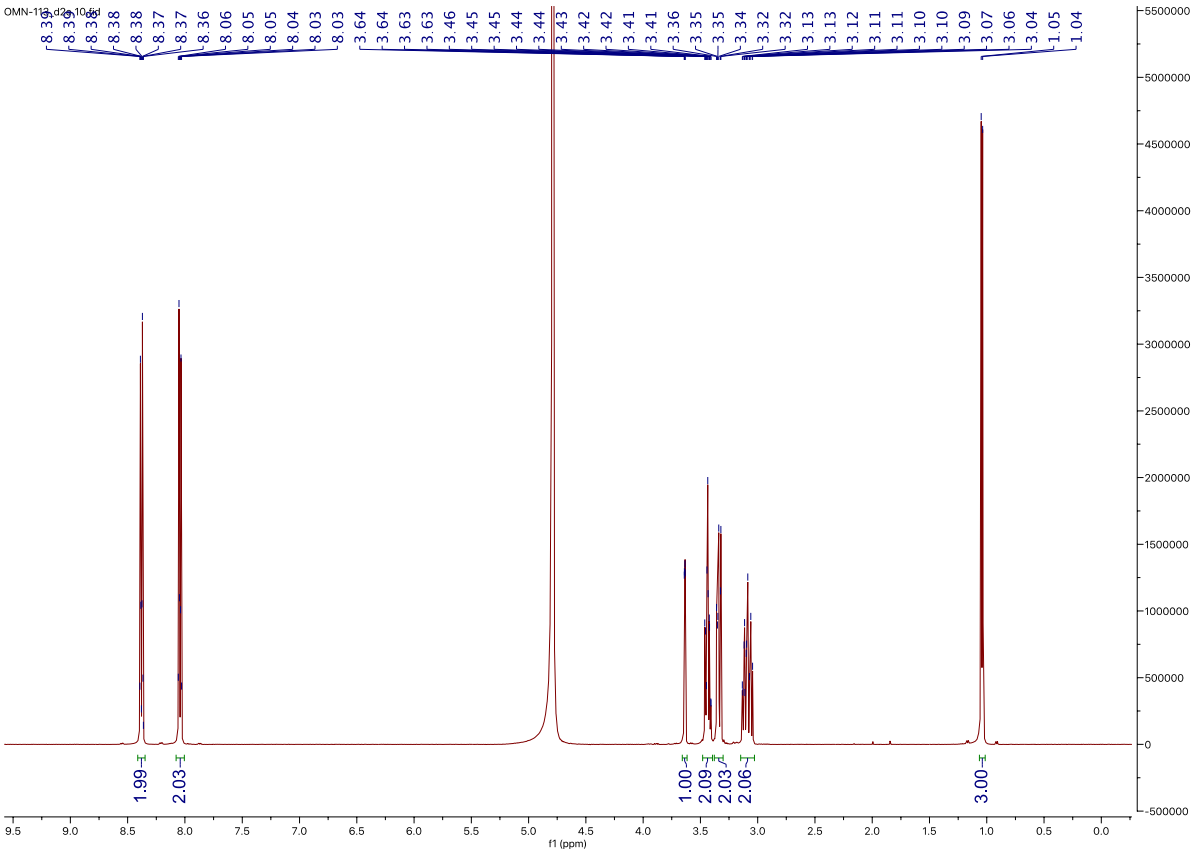
OMN-113_d2o.10.fid
8.39 8.39 8.38 8.38 8.38 8.37 8.37 8.36 8.06 8.05 8.05 8.04 8.03 8.03
3.64 3.64 3.63 3.63 3.46 3.45 3.45 3.44 3.44 3.43 3.42 3.42 3.41 3.41 3.36 3.35 3.35 3.34 3.32 3.32 3.13 3.13 3.12 3.11 3.11 3.10 3.10 3.09 3.07 3.06 3.04 1.05 1.04
1.99
2.03
1.00
2.09
2.03
2.06
3.00
f1 (ppm)

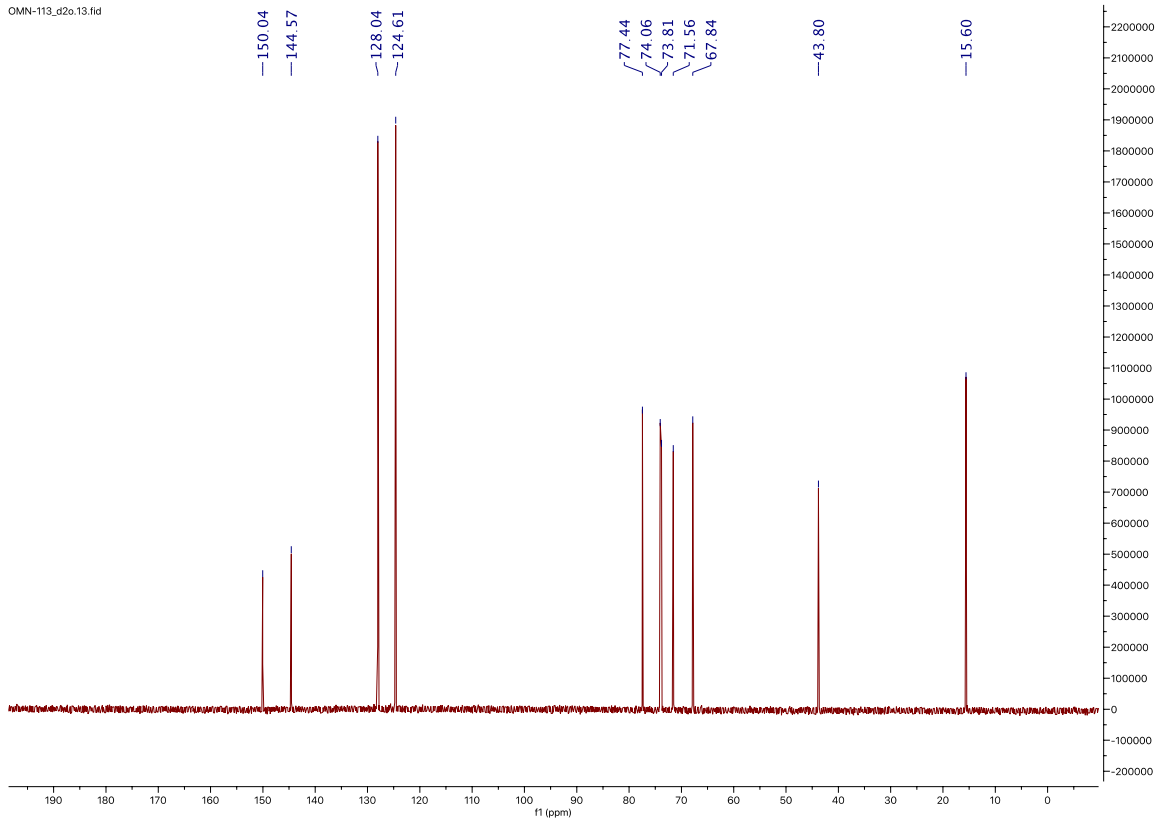
OMN-113_d2o.13.fid
150.04
144.57
128.04
124.61
77.44
74.06
73.81
71.56
67.84
43.80
15.60
f1 (ppm)

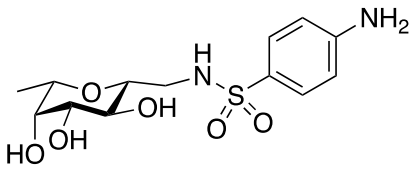

12, 98%

β-L-Fucopyranosylmethyl 4-aminobenzenesulfonamide (12).

Compound **11** (280 mg, 0.77 mmol) was suspended in dry MeOH (12 mL) and 9 mg palladium on activated charcoal (10% Pd basis) was added under nitrogen atmosphere. The reaction flask was flushed with hydrogen and stirred 2 h at r.t. under hydrogen atmosphere. The reaction mixture was filtered through celite and the solvent was removed *in vacuo.* **12** was obtained as a white solid (250 mg, 0.753 mmol, quant.).

^{1}H NMR (500 MHz, MeOH-d_4) δ 7.56 – 7.51 (m, 2H, ArH), 6.73 – 6.66 (m, 2H, ArH), 3.59 (dd, J = 3.0, 1.0 Hz, 1H, H-4), 3.47 (qd, J = 6.5, 1.1 Hz, 1H, H-5), 3.42 – 3.33 (m, 2H, H-3, H-2), 3.24 (dd, J = 12.9, 2.7 Hz, 1H, CH_{2a}), 3.12 (ddd, J = 8.9, 7.3, 2.7 Hz, 1H, H-1), 2.93 (dd, J = 12.9, 7.3 Hz, 1H, CH_{2b}), 1.19 (d, J = 6.5 Hz, 3H, CH_3).

^{13}C NMR (126 MHz, MeOH-d_4) δ 154.07 (ArC), 130.01 (ArCH), 127.39 (ArC), 114.39 (ArCH), 79.55 (C-1), 76.31 (C-3), 75.52 (C-5), 73.60 (C-4), 69.78 (C-2), 45.52 (CH_2), 17.06 (CH_3).

HRMS: $[C_{13}H_{20}N_2O_6S + H]^+$ calcd. 333.1115, found 333.1104.

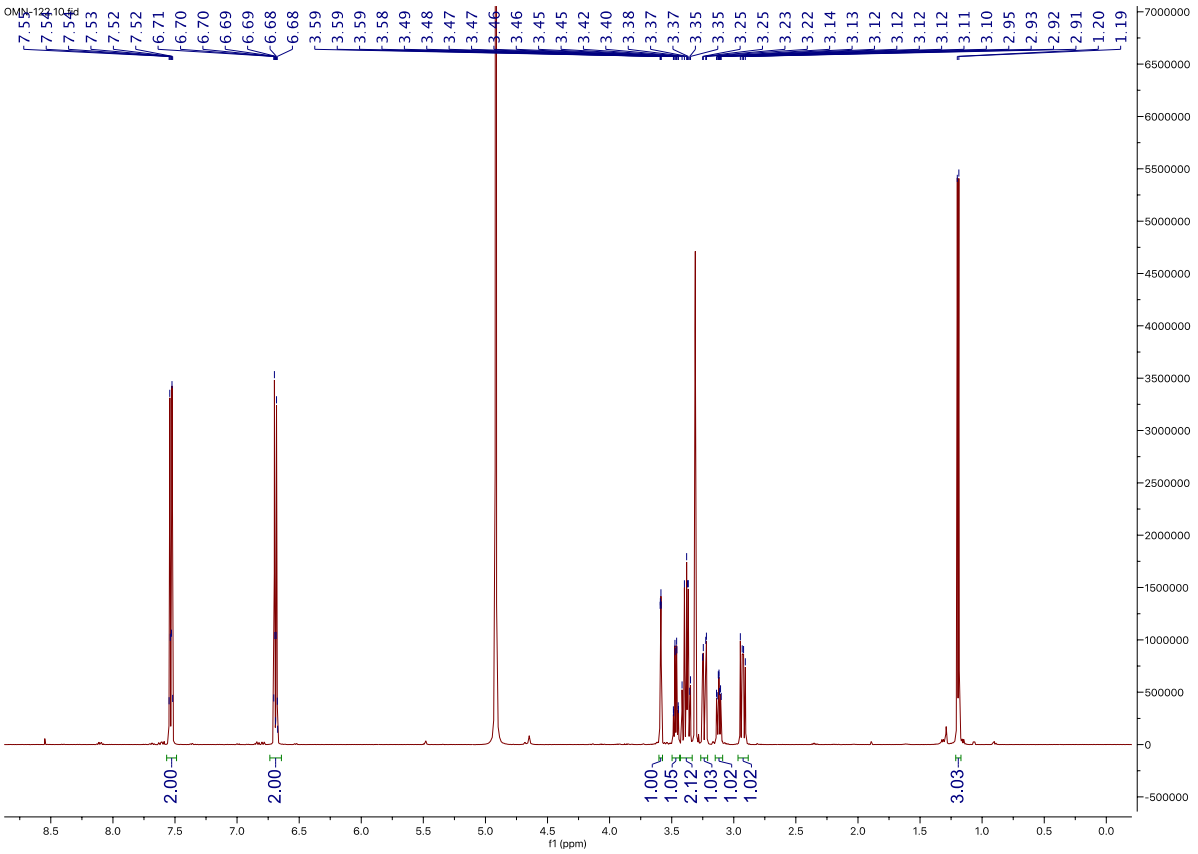
OMN-122.10.fid
7.54 7.54 7.54 7.53 7.52 7.52 6.71 6.70 6.70 6.69 6.69 6.68 6.68
3.59 3.59 3.59 3.58 3.49 3.48 3.47 3.47 3.46 3.46 3.45 3.45 3.42 3.40 3.38 3.37 3.37 3.35 3.35 3.25 3.23 3.22 3.14 3.13 3.12 3.12 3.12 3.12 3.11 3.10 2.95 2.93 2.92 2.91 1.20 1.19
2.00 2.00 1.00 1.05 2.12 1.03 1.02 1.02 3.03
f1 (ppm)

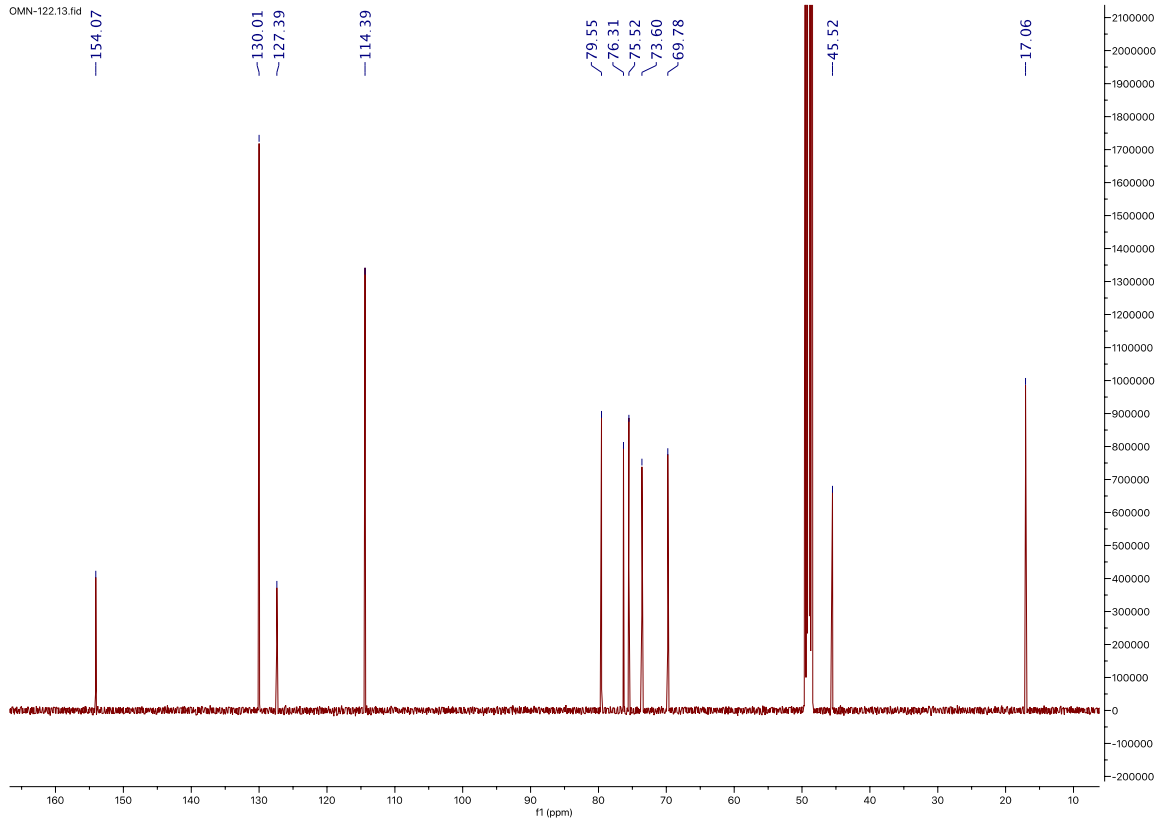
OMN-122.13.fid
154.07 130.01 127.39 114.39 79.55 76.31 75.52 73.60 69.78 45.52 17.06
f1 (ppm)

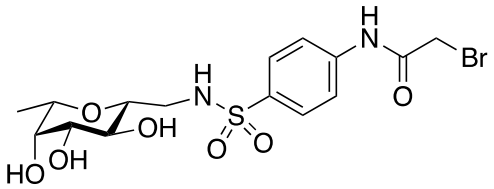

13

β-L-Fucopyranosylmethyl 4-(2-bromoacetamido)-benzenesulfonamide (13).

12 (275 mg, 0.83 mmol) was dissolved in dry DMF (5 mL) and triethylamine (252 µL, 2.2 equiv., 1.82 mmol) was added and stirred for 5 min under nitrogen atmosphere. The reaction flask was cooled down 0 °C and bromoacetyl bromide (48 µL, 1.1 equiv, 0.91 mmol) was added dropwise under vigorous stirring. The reaction mixture was warmed to r.t. and stirred for 4 h. The reaction was diluted with EtOAc and washed with satd. ammonium chloride, water and brine sequentially, then dried over anhydrous sodium sulfate. After filtration, the solvent was removed *in vacuo.* The crude product was purified by reverse phase MPLC (H_2O/MeCN + 0.1% formic acid, 15-50% MeCN). **13** was obtained as a white solid (293 mg, 0.645 mmol, 78%)

^{1}H NMR (500 MHz, MeOH-d_4) δ 7.86 – 7.81 (m, 2H, ArH), 7.80 – 7.75 (m, 2H, ArH), 4.00 (s, 2H, CH_2Br), 3.58 (dd, J = 2.9, 1.1 Hz, 1H, H-4), 3.44 (qd, J = 6.4, 1.1 Hz, 1H, H-5), 3.41 – 3.33 (m, 2H, H-2, H-3), 3.29 (d, J = 2.6 Hz, 1H, CH_{2a}), 3.11 (dddd, J = 8.2, 7.3, 2.6, 1.0 Hz, 1H, H-1), 2.98 (dd, J = 13.0, 7.3 Hz, 1H, CH_{2b}), 1.18 (d, J = 6.5 Hz, 3H, CH_3).

^{13}C NMR (126 MHz, MeOH-d_4) δ 167.95 NHC(O)), 143.45 (ArC), 137.08 (ArC), 129.22 (ArCH), 120.63 (ArCH), 79.59 (C-1), 76.32 (C-2), 75.52 (C-5), 73.58 (C-4), 69.73 (C-3), 45.57 (CH_2N_3), 29.55 (CH_2), 17.06 (CH_3).

HRMS: $[C_{15}H_{21}BrN_2O_7S + H]^+$ calcd. 455.0305, found 455.0292.

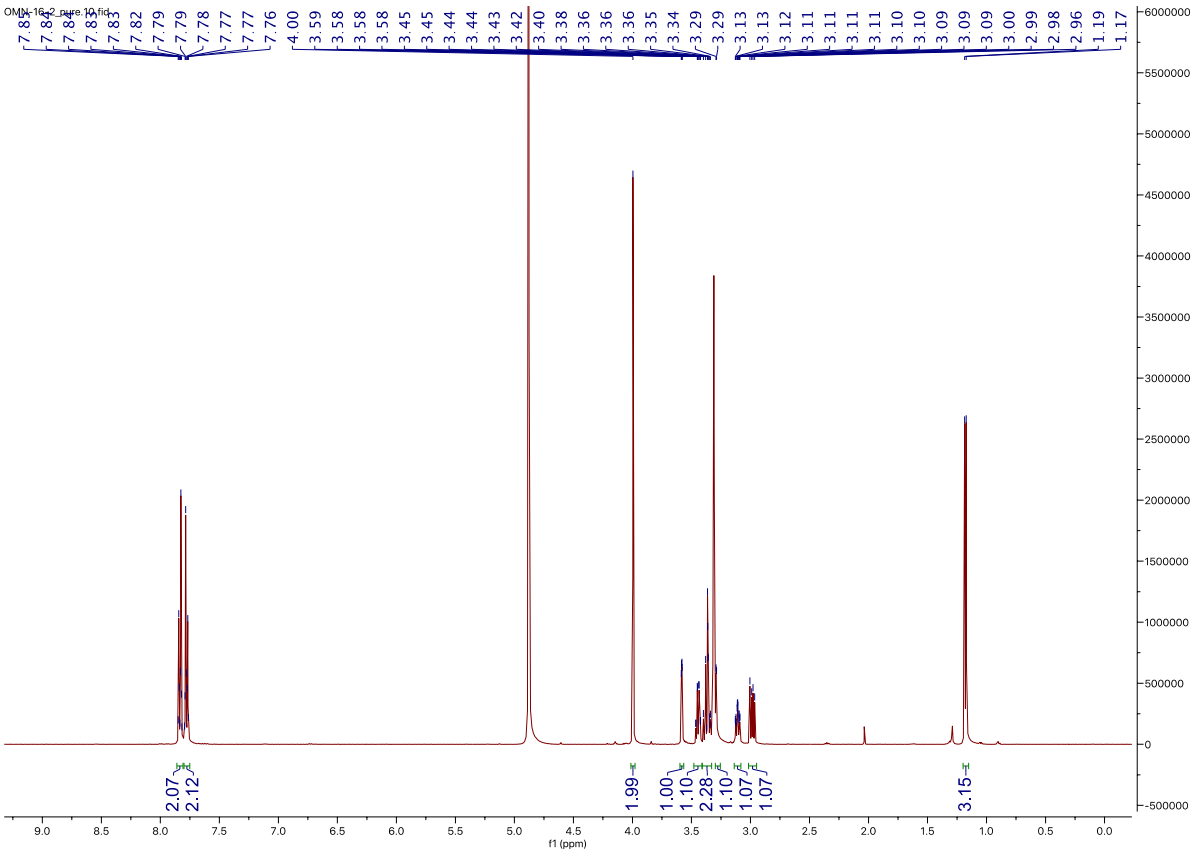
OMN-162_pure-10.fid
7.84 7.84 7.83 7.83 7.82 7.79 7.79 7.78 7.77 7.77 7.76
4.00 3.59 3.58 3.58 3.58 3.45 3.44 3.44 3.43 3.42 3.40 3.38 3.36 3.36 3.35 3.34 3.29 3.29
3.13 3.13 3.12 3.11 3.11 3.11 3.11 3.10 3.10 3.09 3.09 3.09 3.00 2.99 2.98 2.96 1.19 1.17
2.07 2.12 1.99 1.00 1.10 2.28 1.10 1.07 1.07 3.15
f1 (ppm)

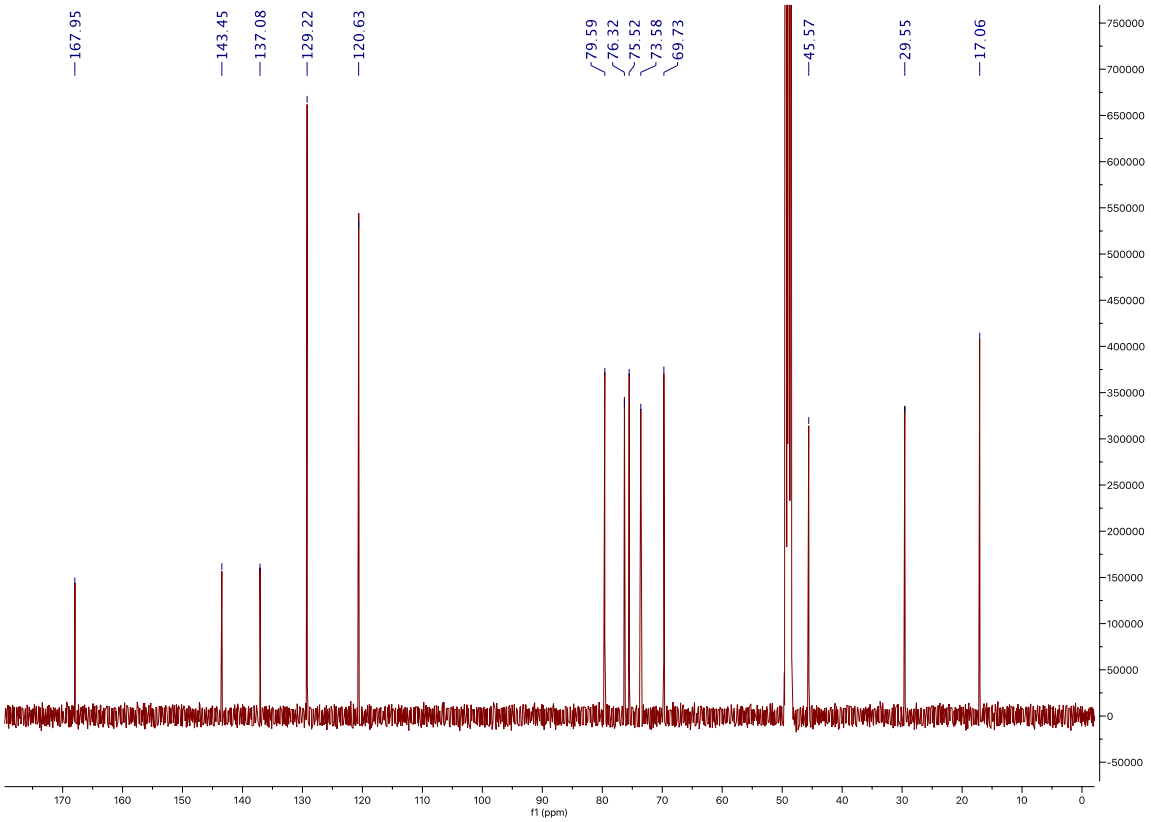
167.95 143.45 137.08 129.22 120.63
79.59 76.32 75.52 73.58 69.73
45.57 29.55 17.06
f1 (ppm)

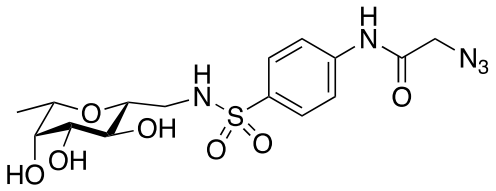

14, 56% over two steps

β-L-Fucopyranosylmethyl 4-(2-azidoacetamido)-benzenesulfonamide (14).

13 (262 mg, 0.58 mmol) was suspended in dry DMF (15 mL), sodium azide (114 mg, 3 equiv., 1.74 mmol) was added and the mixture was stirred for 2 h under nitrogen atmosphere. The reaction was diluted with water and extracted three times with EtOAc, combined organic phases were washed with satd. ammonium chloride, water, brine and then dried over anhydrous sodium sulfate. After filtration, the solvent was removed *in vacuo.* The crude product was purified by normal phase MPLC (DCM/MeOH, 10–45% EtOAc). **6** was obtained as a white solid (173 mg, 0.42 mmol, 72%).

^{1}H NMR (500 MHz, MeOH-d_4) δ 7.90 – 7.52 (m, 4H, ArH), 4.03 (s, 2H, CH_2N_3), 3.63 – 3.55 (m, 2H, NH, H-4), 3.43 (q, J = 6.4 Hz, 1H, H-5), 3.39 – 3.31 (m, 2H, H-2, H-3), 3.28 (dd, J = 8.1, 2.1 Hz, 1H, CH_{2a}), 3.10 (td, J = 8.5, 8.0, 2.5 Hz, 1H, H-1), 2.97 (dd, J = 13.0, 7.2 Hz, 1H, CH_{2b}), 1.16 (d, J = 2.3 Hz, 3H, CH_3).

^{13}C NMR (126 MHz, MeOH-d_4) δ 168.86 (NHC(O)), 143.18 (ArC), 136.85 (ArC), 129.17 (ArCH), 120.76 (ArCH), 79.52 (C-1), 76.27 (C-2), 75.48 (C-5), 73.54 (C-4), 69.70 (C-3), 53.20 (CH_2N_3), 45.53 (CH_2), 17.05 (CH_3).

HRMS: $[C_{15}H_{23}N_5O_7S + H]^+$ calcd. 416.1234, found 416.1223.

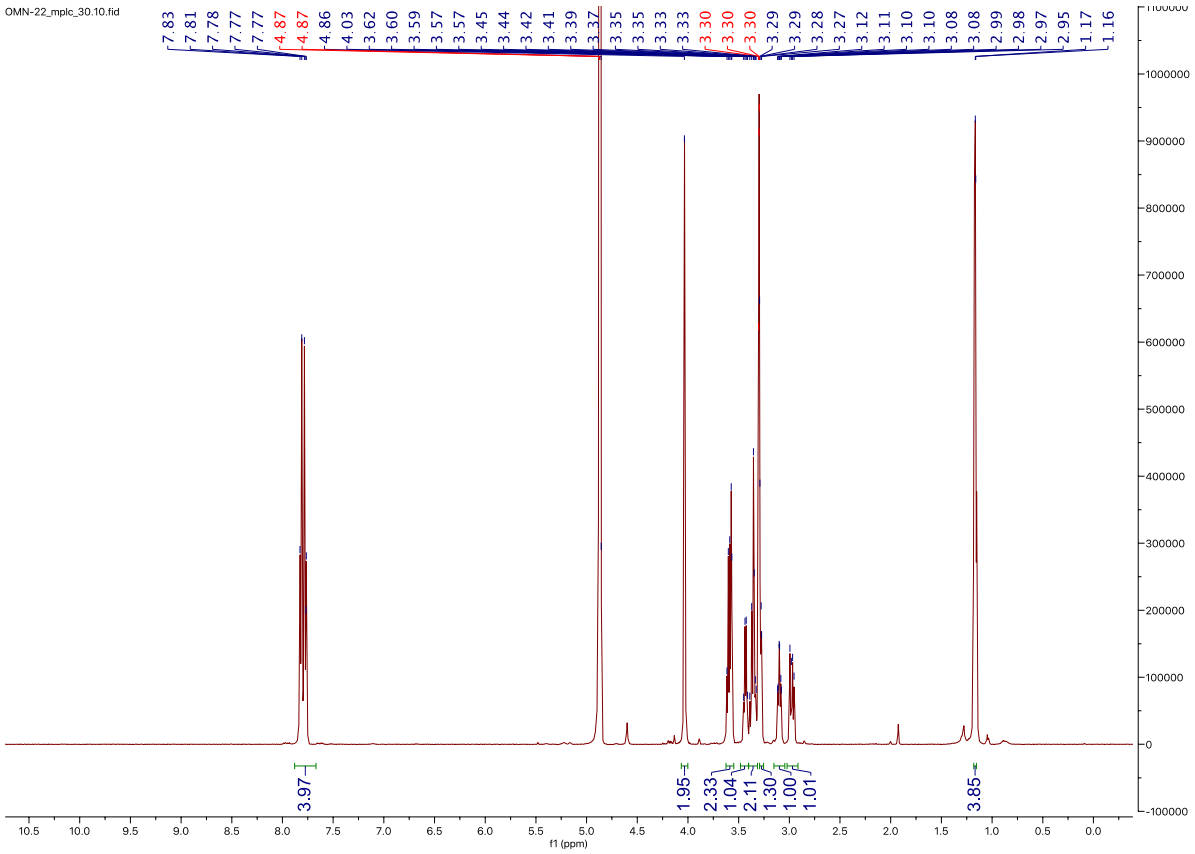
OMN-22_mplc_30.10.fid
7.83
7.81
7.78
7.77
7.77
4.87
4.87
4.86
4.03
3.62
3.60
3.59
3.57
3.57
3.45
3.44
3.42
3.41
3.39
3.37
3.35
3.35
3.33
3.33
3.30
3.30
3.30
3.29
3.29
3.28
3.27
3.12
3.11
3.10
3.10
3.08
3.08
2.99
2.98
2.97
2.95
1.17
1.16
3.97
1.95
2.33
1.04
2.11
1.30
1.00
1.01
3.85
f1 (ppm)

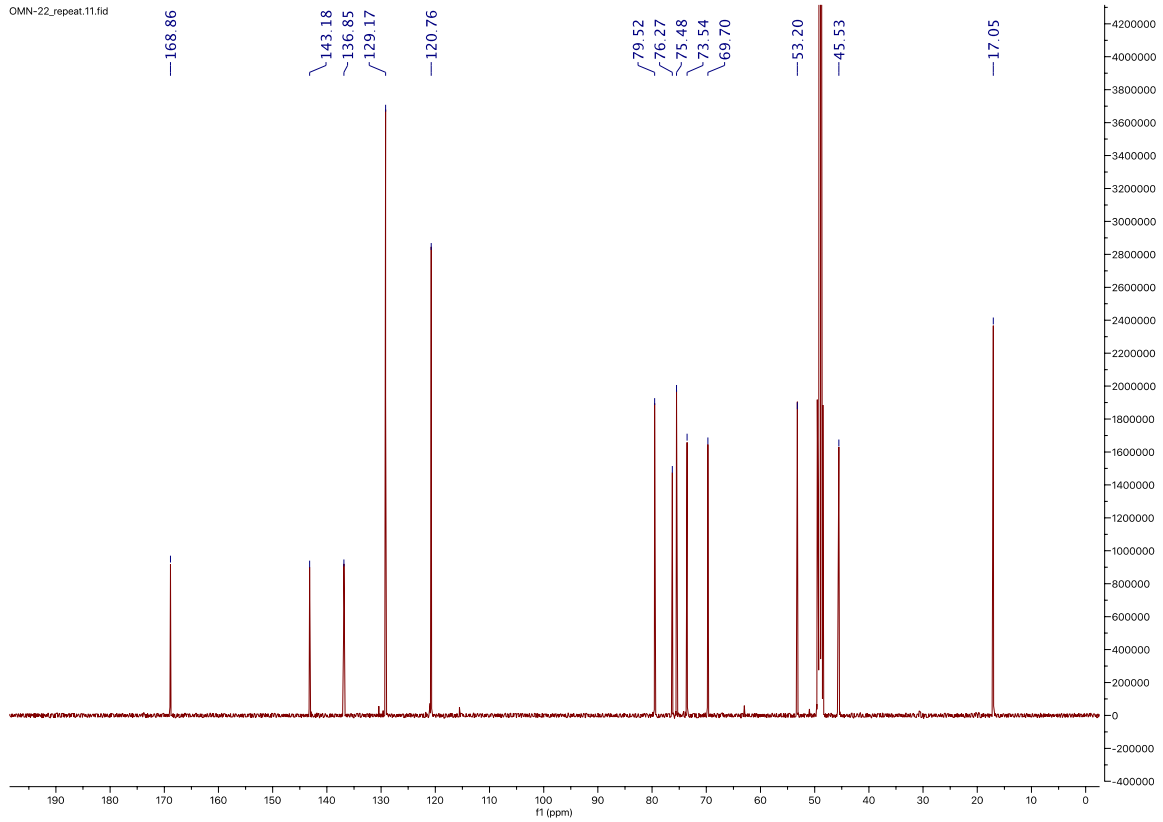
OMN-22_repeat.11.fid
168.86
143.18
136.85
129.17
120.76
79.52
76.27
75.48
73.54
69.70
53.20
45.53
17.05
f1 (ppm)

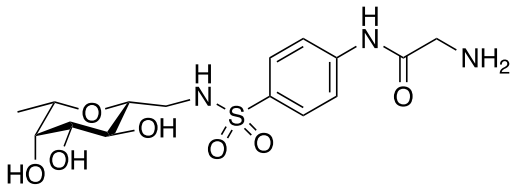

15, 97%

β-L-Fucopyranosylmethyl 4-(2-aminoacetamido)-benzenesulfonamide (15).

Compound **14** (150 mg, 0.36 mmol) was suspended in dry MeOH (5 mL) and 15 mg palladium on activated charcoal (10% Pd basis) was added under a nitrogen atmosphere. The reaction flask was flushed with hydrogen and stirred overnight at r.t. under hydrogen. The reaction mixture was filtered through celite and the solvent was removed *in vacuo.* **15** was obtained as a white solid (135 mg, 0.347 mmol, quant.).

^{1}H NMR (500 MHz, MeOH-d_4) δ 8.51 (s, 2H, NH_2), 7.87 – 7.76 (m, 4H, ArH), 3.87 (s, 2H, CH_2), 3.59 (d, J = 2.7 Hz, 1H, H-4), 3.45 (q, J = 6.4 Hz, 1H, H-5), 3.41 – 3.34 (m, 2H, H-2, H-3), 3.30 – 3.27 (m, 1H, CH_{2a}), 3.12 (ddd, J = 9.1, 7.6, 2.5 Hz, 1H, H-1), 2.98 (dd, J = 12.9, 7.3 Hz, 1H, CH_{2b}), 1.18 (d, J = 6.4 Hz, 3H, CH_3).

^{13}C NMR (126 MHz, MeOH-d_4) δ 166.64 (NHC(O)), 143.10 (ArC), 136.93 (ArC), 129.30 (ArCH), 120.41 (ArCH), 79.60 (C-1), 76.29 (C-2), 75.50 (C-5), 73.56 (C-4), 69.68 (C-3), 45.54 (CH_2NH), 42.51 (CH_2NH_2), 17.08 (CH_3).

HRMS: $[C_{15}H_{23}N_3O_7S + H]^+$ calcd. 390.1329, found 390.1327.

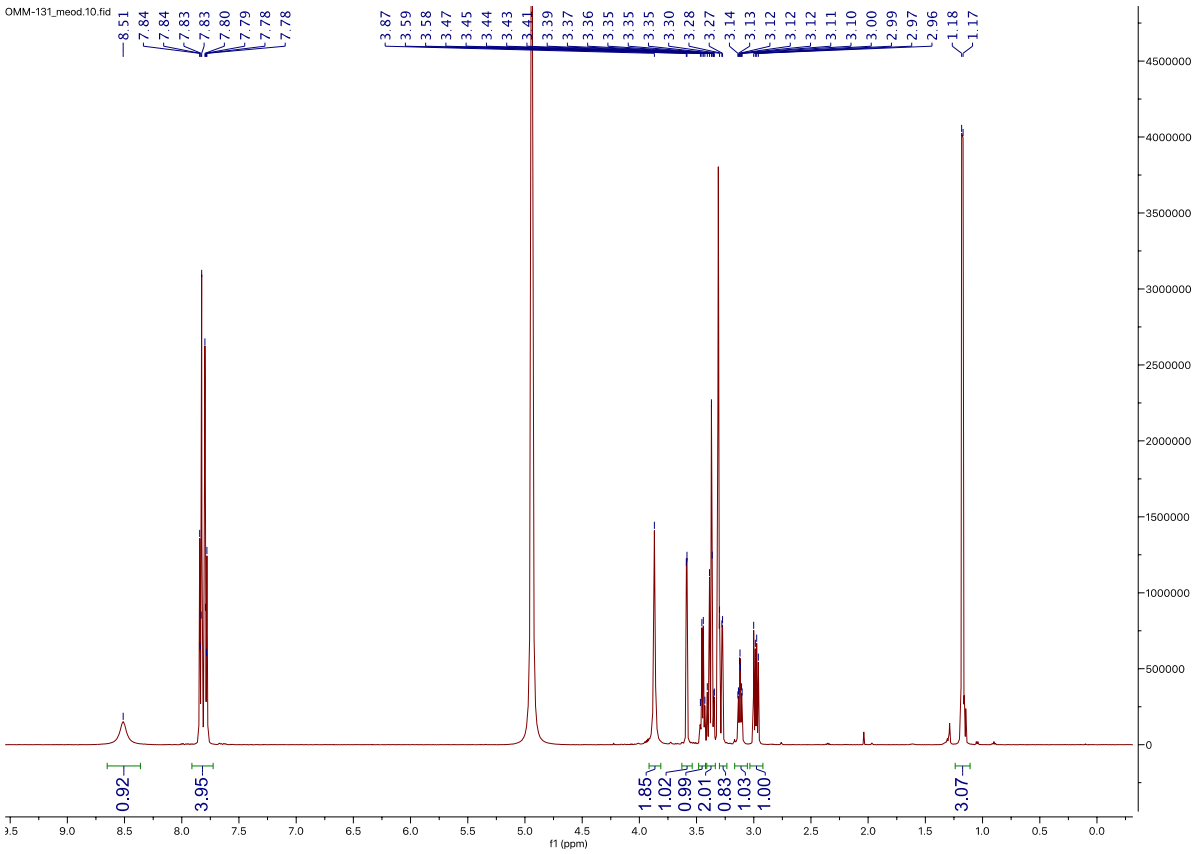
OMM-131_meod.10.fid
8.51
7.84
7.84
7.83
7.83
7.80
7.79
7.78
7.78
3.87
3.59
3.58
3.47
3.45
3.44
3.43
3.41
3.39
3.37
3.36
3.35
3.35
3.35
3.30
3.28
3.27
3.14
3.13
3.12
3.12
3.12
3.11
3.10
3.00
2.99
2.97
2.96
1.18
1.17
0.92
3.95
1.85
1.02
0.99
2.01
0.83
1.03
1.00
3.07
f1 (ppm)

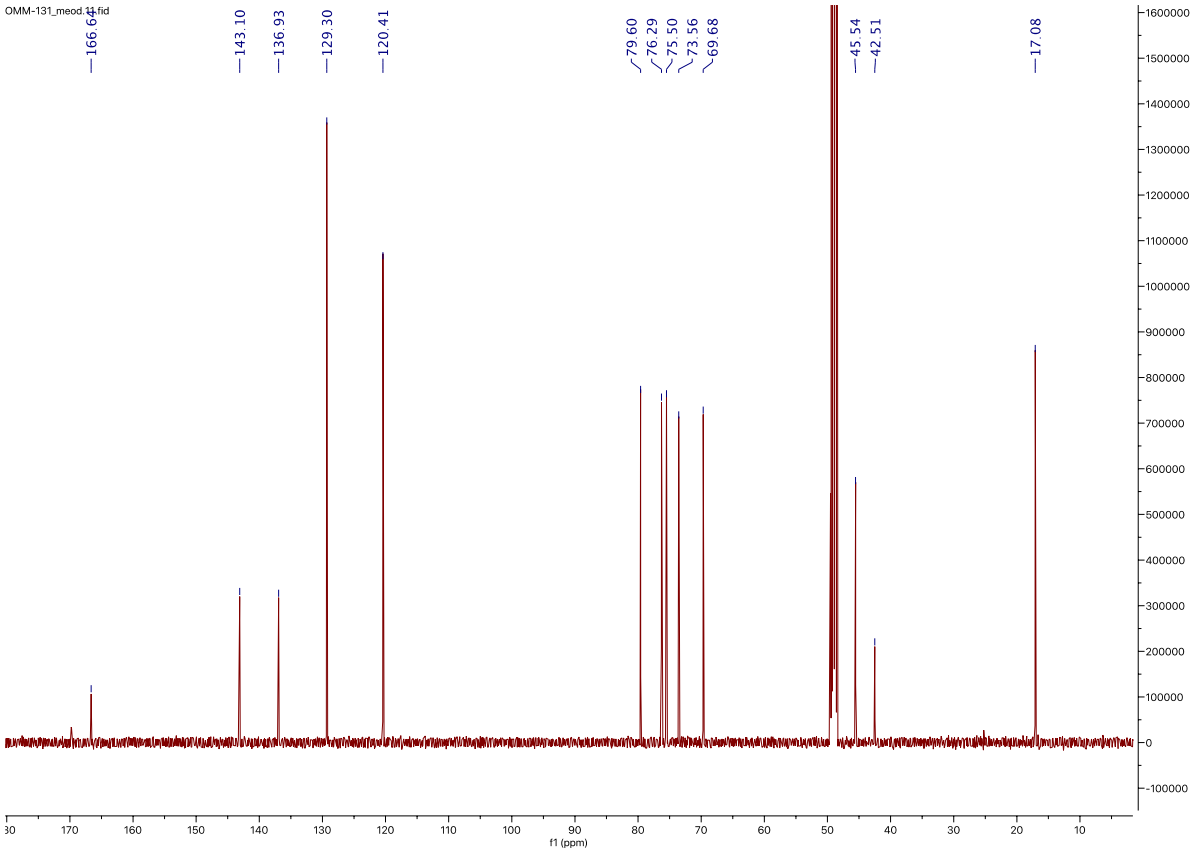
166.66
143.10
136.93
129.30
120.41
79.60
76.29
75.50
73.56
69.68
45.54
42.51
17.08
f1 (ppm)

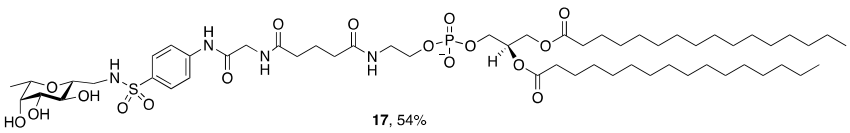

17, 54%

Glycolipid 17.

16:0 Glutaryl PE (50 mg, 60 µmol) was suspended in mixture $CHCl_3$/DMF 1:1 (5 mL) and HBTU (28 mg, 1.2 equiv., 72 µmol), HOBt (8 mg, 1.2 equiv., 72 µmol) and Et_3N (42 µL, 5 equiv., 0.3 mmol) was added and stirred for 30 min under a nitrogen atmosphere at 40 °C until the phospholipid was completely dissolved. Then, **8** (32 mg, 1.55 equiv., 93 µmol) was added and reaction was stirred at 40 °C for 48 h. The solvent was removed *in vacuo* and the crude product was purified by reverse phase MPLC (^{i}PrOH:H_2O:MeOH (5:4:1) / ^{i}PrOH + 0.2% formic acid, 10-50%). **17** was obtained as a white solid (39 mg, 33 µmol, 54%).

^{1}H NMR (500 MHz, DMSO-d_6) δ 7.87 – 7.68 (m, 4H, ArH), 5.16 – 5.05 (m, 1H, C(O)C<u>H</u>CH_2OPO_3), 4.86 – 4.71 (m, 1H, NH), 4.60 (br s, 1H, NH), 4.28 (dd, J = 12.0, 3.1 Hz, 1H, C(O)OC<u>H_{2a}</u>CH), 4.09 (dd, J = 12.0, 7.1 Hz, 1H, C(O)OC<u>H_{2b}</u>CH), 3.84 (m, 3H, C(O)OCHC<u>H_{2a}</u>OPO_3, CH_2C<u>H_2</u>OPO_3), 3.78 – 3.71 (m, 2H, CHC<u>H_2</u>OPO_3), 3.39 – 3.37 (m, H-4, H-5, HDO), 3.24 – 3.15 (m, 4H, H-2, C<u>H_{2a}</u>$NHSO_2$, C<u>H_2</u>CH_2OPO_3), 3.15 – 3.09 (m, 3H, H-3, CH_2), 3.06 – 2.94 (m, 3H, H-1, CH_2), 2.74 (s, 2H, C(O)<u>C</u>H_2NH), 2.71 – 2.62 (m, 1H, C<u>H_{2b}</u>$NHSO_2$), 2.25 (m, 4H, C<u>H_2</u>C(O)O), 2.17 (t, J = 7.5 Hz, 2H, NHC(O)C<u>H_2</u>CH_2), 2.05 (m, 2H, NHC(O)C<u>H_2</u>CH_2), 1.78 – 1.69 (m, 2H, NHC(O)CH_2C<u>H_2</u>), 1.29 – 1.18 (m, 40H), 1.06 (d, J = 6.4 Hz, 3H, C<u>H_3</u>CHO), 0.85 (t, J = 6.9 Hz, 6H, CH_3)

^{13}C NMR (126 MHz, DMSO-d_6) δ 172.54 (OC(O)), 172.41 (OC(O)), 172.30 (NHC(O)), 171.87 (NHC(O)), 169.04 (NHC(O)), 158.45, 142.44 (ArC), 134.52 (ArC), 127.54 (ArCH), 118.83 (ArCH), 78.32 (C-1), 74.64 (C-2), 73.61 (C-5), 71.55 (C-4), 70.19 (d, J = 5.0 Hz, C(O)O<u>C</u>HCH_2OPO_3), 68.29 (C-3), 63.36 (d, J = 5.5 Hz, CH_2<u>C</u>H_2OPO_3), 63.02 (d, J = 7.1 Hz, CH<u>C</u>H_2OPO_3), 62.13 (C(O)O<u>C</u>H_2CH), 54.55, 44.52 (CH_2NHSO_2), 43.34, 42.15 (C(O)<u>C</u>H_2NH), 39.95 (m, <u>C</u>$H_2CH_2OPO_3$), 34.78 (NHC(O)C<u>H_2</u>CH_2), 34.11 (d, J = 11.1 Hz, CH_2<u>C</u>H_2OPO_3), 33.57 (<u>C</u>H_2C(O)O), 33.40 (<u>C</u>H_2C(O)O), 31.31, 29.08 (CH_2), 29.04, 28.96, 28.95, 28.79, 28.76, 28.73, 28.45, 28.42, 24.47 (<u>C</u>H_2CH_2C(O)O), 24.42 (<u>C</u>H_2CH_2C(O)O), 22.11, 21.46 (NHC(O)CH_2C<u>H_2</u>), 16.91 (<u>C</u>H_3CHO), 15.64, 13.95 (CH_3).

HRMS: $[C_{57}H_{101}N_4O_{17}PS + H]^+$ calcd. 1177.6693, found 1177.6654.

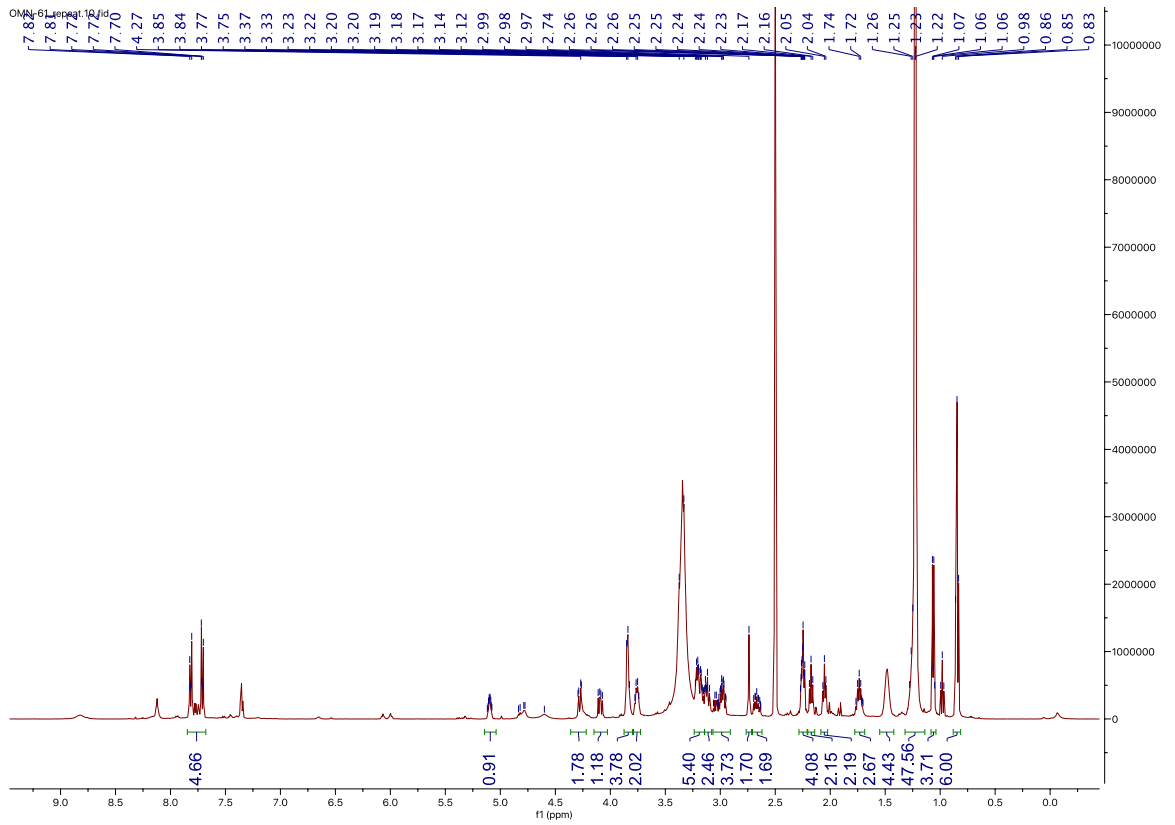
OMN-61_repeat.10.fid
7.83 7.81 7.77 7.77 7.72 7.70 4.27 3.85 3.84 3.77 3.75 3.37 3.33 3.23 3.22 3.20 3.20 3.19 3.18 3.17 3.14 3.12 2.99 2.98 2.97 2.74 2.26 2.26 2.25 2.25 2.24 2.24 2.23 2.17 2.16 2.05 2.04 1.74 1.72 1.26 1.25 1.23 1.22 1.07 1.06 1.06 0.98 0.86 0.85 0.83
4.66 0.91 1.78 1.18 3.78 2.02 5.40 2.46 3.73 1.70 1.69 4.08 2.15 2.19 2.67 4.43 47.56 3.71 6.00
f1 (ppm)

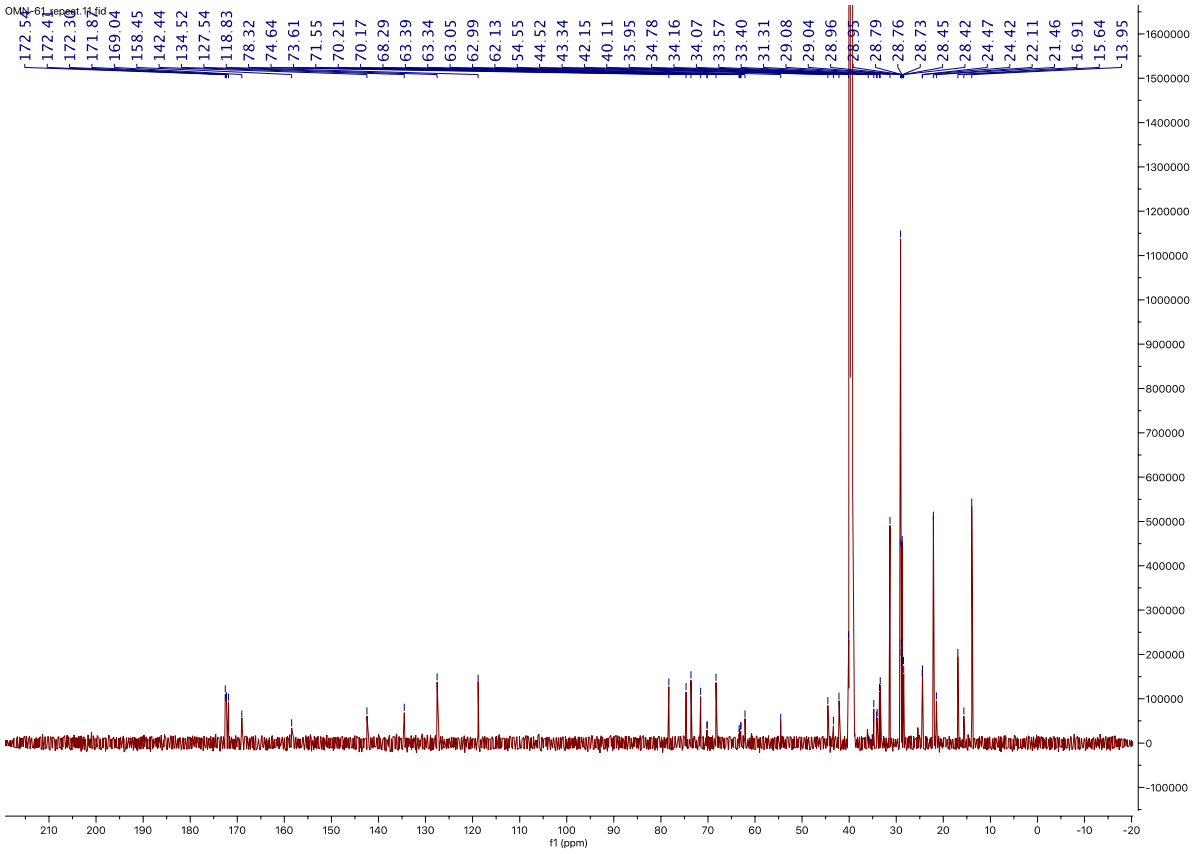
OMN-61_repeat.11.fid
172.54 172.41 172.30 171.82 169.04 158.45 142.44 134.52 127.54 118.83 78.32 74.64 73.61 71.55 70.21 70.17 68.29 63.39 63.34 63.05 62.99 62.13 54.55 44.52 43.34 42.15 40.11 35.95 34.78 34.16 34.07 33.57 33.40 31.31 29.08 29.04 28.96 28.95 28.79 28.76 28.73 28.45 28.42 24.47 24.42 22.11 21.46 16.91 15.64 13.95
f1 (ppm)

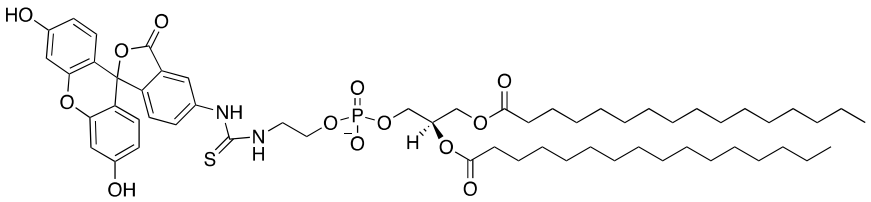

Fluorescein-conjugated DPPE (18).

DPPE (30 mg, 1.1 equiv., 43 µmol) was suspended in mixture $CHCl_3$/DMF 1:1 (5 mL) and FITC (15 mg, 39 µmol) and Et_3N (18 µL, 3 equiv., 123 µmol) were added and stirred overnight under nitrogen atmosphere at 40 °C. Then, **8** (32 mg, 1.55 equiv., 93 µmol) was added and reaction was stirred at 40 °C for 48 h. The solvent was removed *in vacuo* and the crude product was purified by reverse phase MPLC (iPrOH:H_2O:MeOH (5:4:1) + 0.2% formic acid/ iPrOH + 0.2% formic acid, 10-80% PrOH + 0.2% formic acid). **18** was obtained as an orange solid (33 mg, 0.03 mmol, 72%).

^{1}H NMR (500 MHz, MeOH-d_4) δ 8.14 (s, 1H, ArH), 7.90 (d, J = 8.2 Hz, 1H, ArH), 7.16 (d, J = 8.3 Hz, 1H, ArH), 6.90 (d, J = 8.9 Hz, 2H, ArH), 6.67 (s, 2H, ArH), 6.60 (m, 2H, ArH), 5.22 (s, 1H, CHOC(O)), 4.44 (dd, J = 11.8, 3.1 Hz, 1H, C(O)OC$\underline{H}_{2a}$CH), 4.18 (dd, J = 12.1, 6.5 Hz, 1H, C(O)OC$\underline{H}_{2b}$CH), 4.04 (dt, J = 30.1, 5.8 Hz, 4H, $CH_2C\underline{H}_2OPO_3$, $CHC\underline{H}_2OPO_3$), 3.88 (s, 2H, NH), 3.12 (q, J = 7.4 Hz, 6H, CH_2), 2.32 (dq, J = 14.9, 7.4 Hz, 4H, $C\underline{H}_2CH_2OPO_3$, $C\underline{H}_2C(O)O$), 1.66 – 1.51 (m, 4H, $C\underline{H}_2CH_2C(O)O$), 1.28 (m, 42 H, CH_2,), 0.89 (t, J = 6.1 Hz, 6H, CH_3).

^{13}C NMR (126 MHz, MeOH-d_4) δ 181.76 (CS), 174.52 (C(O)O), 174.19 (C(O)O), 169.41 (C(O)O), 152.89 (ArCOH), 130.87, 119.88, 112.25, 103.21, 87.28, 78.11, 70.94, 63.04, 34.67, 34.50, 32.34, 30.11, 30.09, 30.07, 29.96, 29.94, 29.77, 29.74, 29.56, 29.54, 25.35, 25.29, 23.07, 14.28 (CH_3).

HPLC-MS: $[C_{58}H_{85}N_2O_{13}PS + H]^+$ calcd. 1081.5583, found 1081.5540.

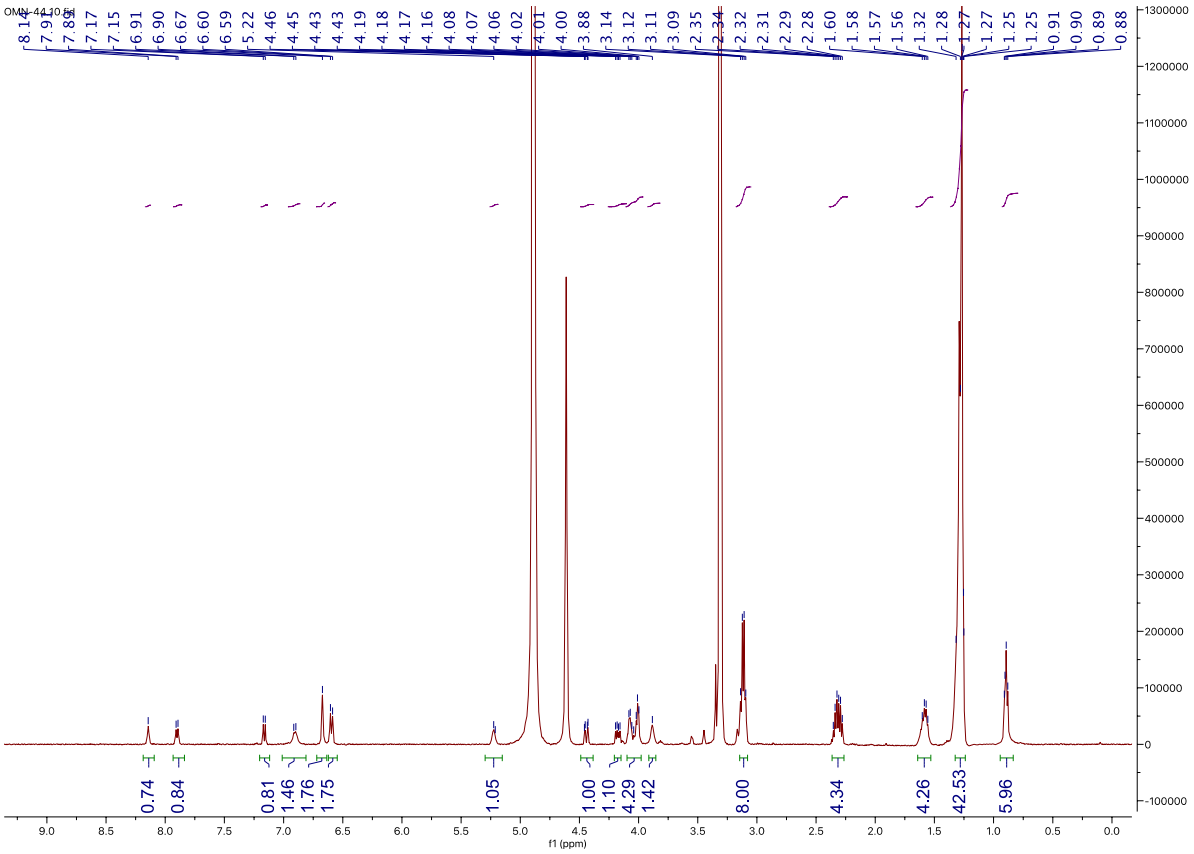
OMN-44-10.fid
8.14 7.91 7.89 7.17 7.15 6.91 6.90 6.67 6.60 6.59 5.22 4.46 4.45 4.43 4.43 4.19 4.18 4.17 4.16 4.08 4.07 4.06 4.02 4.01 4.00 3.88 3.14 3.12 3.11 3.09 2.35 2.34 2.32 2.31 2.29 2.28 1.60 1.58 1.57 1.56 1.32 1.28 1.27 1.27 1.25 1.25 0.91 0.90 0.89 0.88
0.74 0.84 0.81 1.46 1.76 1.75 1.05 1.00 1.10 4.29 1.42 8.00 4.34 4.26 42.53 5.96
f1 (ppm)

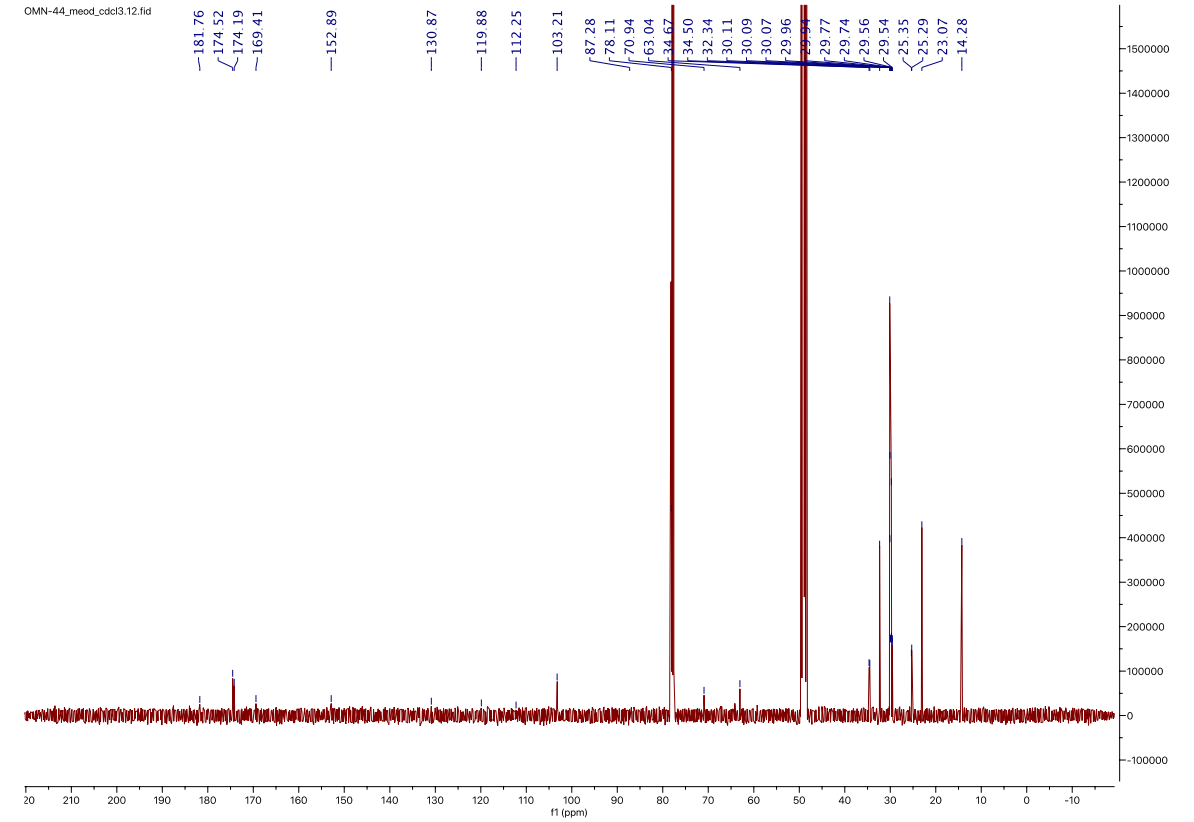
OMN-44_meod_cdcl3.12.fid
181.76 174.52 174.19 169.41 152.89 130.87 119.88 112.25 103.21 87.28 78.11 70.94 63.04 34.67 34.50 32.34 30.11 30.09 30.07 29.96 29.91 29.77 29.74 29.56 29.54 25.35 25.29 23.07 14.28
f1 (ppm)

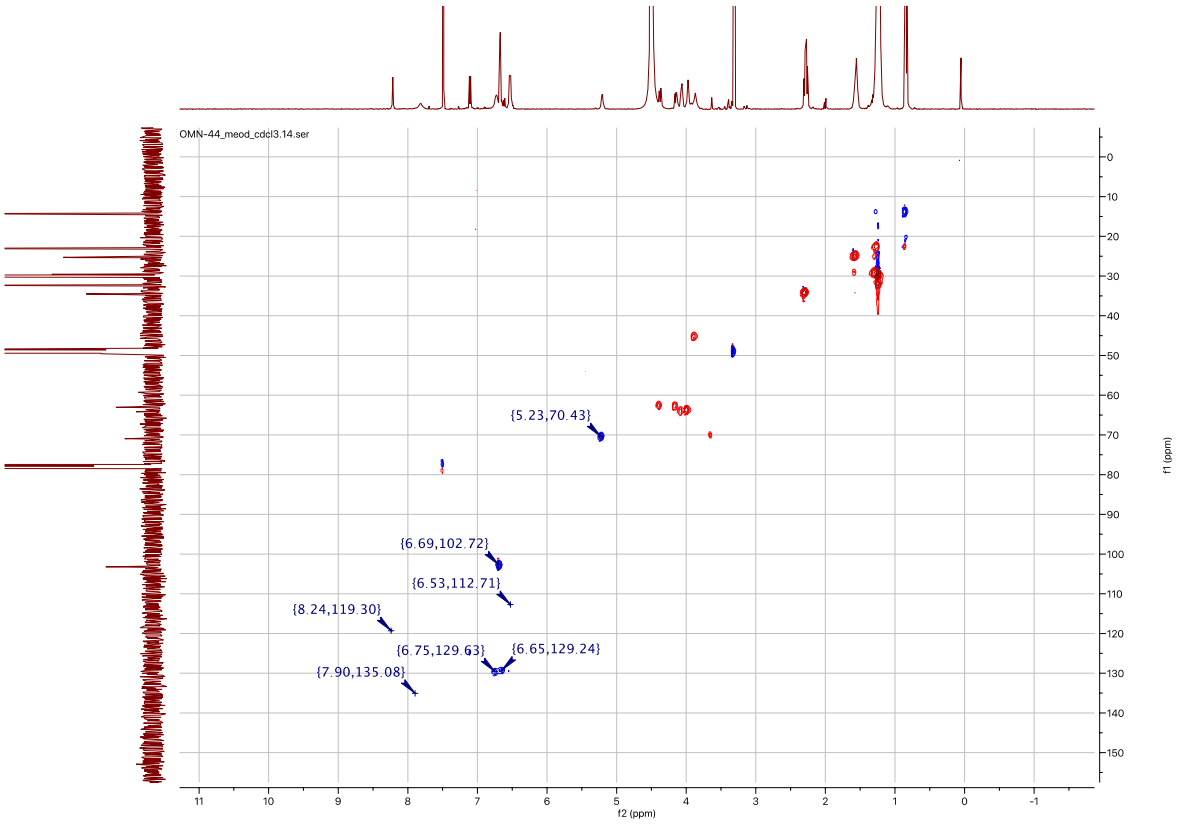
OMN-44_meod_cdcl3.14.ser
{5.23,70.43}
{6.69,102.72}
{6.53,112.71}
{8.24,119.30}
{6.75,129.63}
{6.65,129.24}
{7.90,135.08}
f2 (ppm)
f1 (ppm)

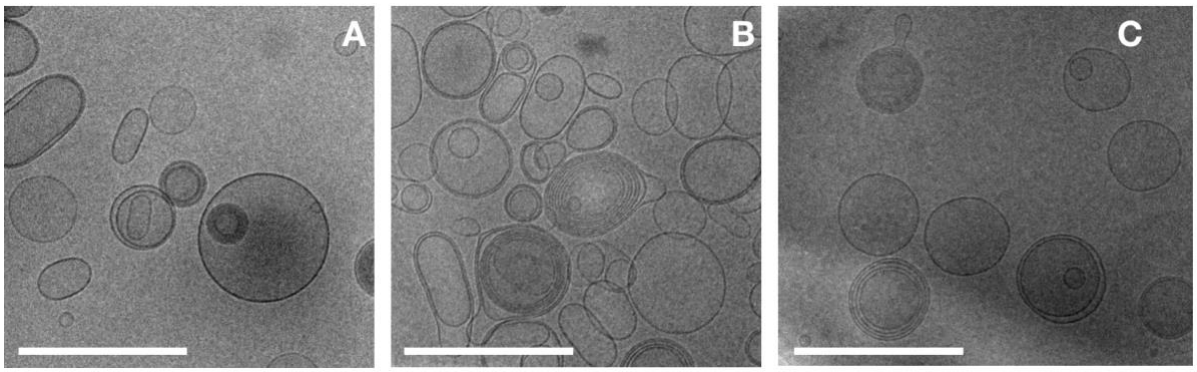

Figure S1. Transmission electron micrograph for the fluorescent liposomes produced by extrusion: plain liposomes (A), 15%-LecA-targeted ligand **16** (B), 15%-LecB-targeted ligand **17** (C).

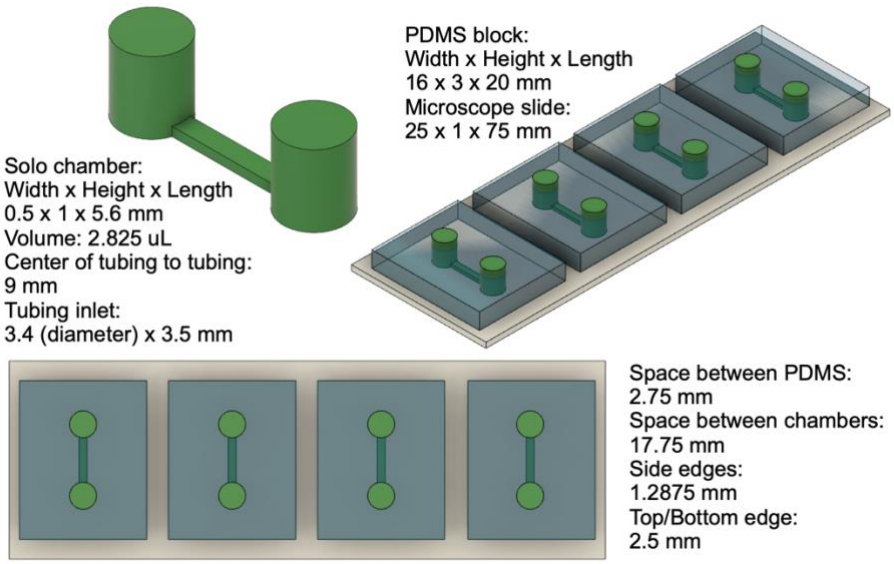

Figure S2. Detailed representation of the flow chamber.

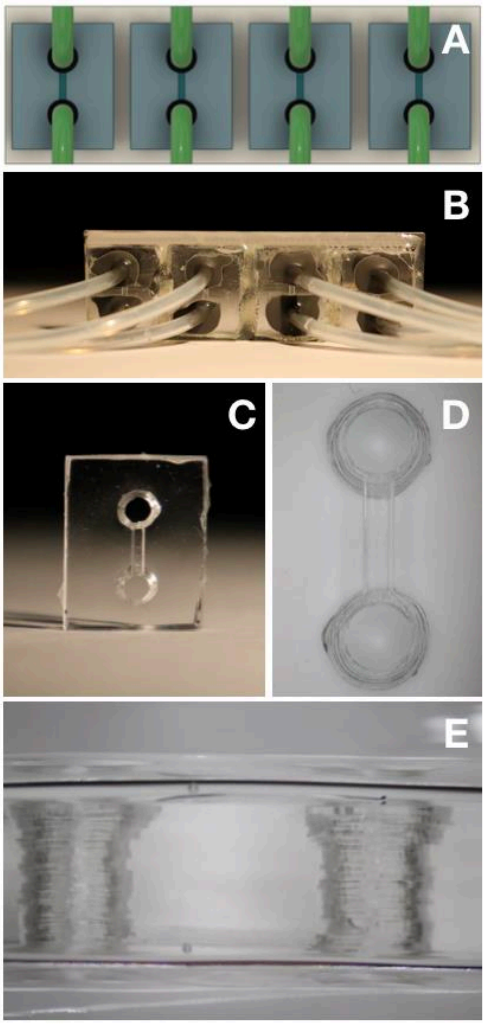

Figure S3. Flow chamber. Tube side: graphic representation (A) and photo (B); single flow chamber (C and D); profile of the outlet (E).

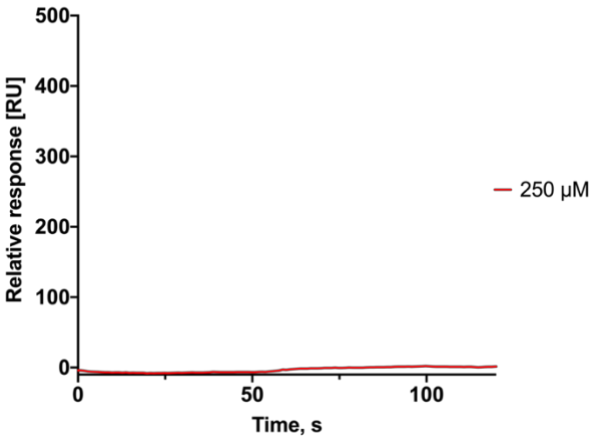

Figure S4: SPR sensorgram for LecB-targeted liposomes injected on the LecA-coupled chip demonstrates lectin-specificity of binding.

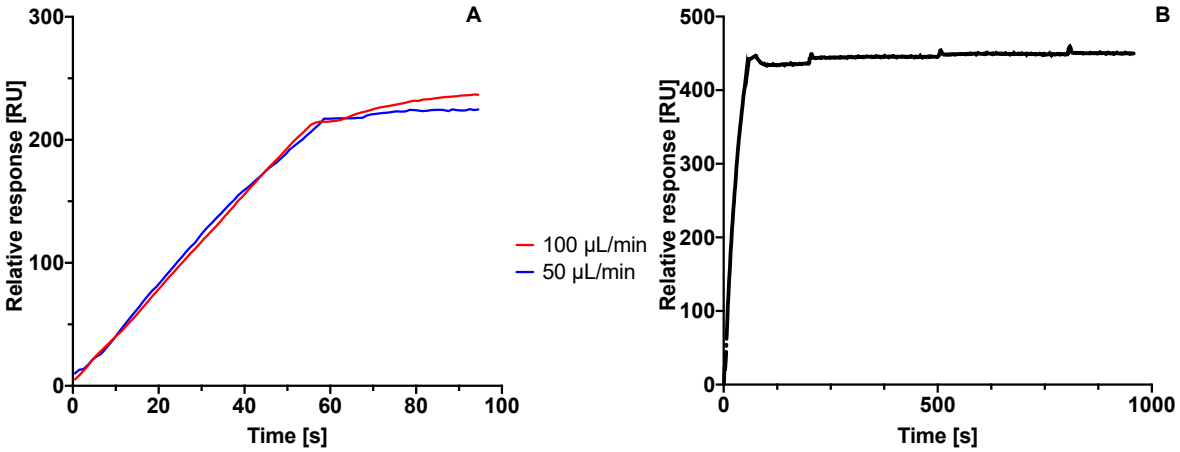

Figure S5. Sensograms of LecA interactions with: 15% LecA-targeted non-fluorescent liposomes (32 µM of LecA-ligand **16**) at different flow rates to reveal an impact of mass transfer effect (A), 15% LecA-targeted non-fluorescent liposomes (250 µM of LecA-ligand **16**) with 15 min dissociation time (B).

Supporting Information References

1. S. Escopy, Y. Singh and A. V. Demchenko, *Org Biomol Chem*, 2019, **17**, 8379–8383.
2 F. Casoni, L. Dupin, G. Vergoten, A. Meyer, C. Ligeour, T. Géhin, O. Vidal, E. Souteyrand, J.-J. Vasseur, Y. Chevolot and F. Morvan, *Org. Biomol. Chem.*, 2014, **12**, 9166–9179.
3 S. Chipowsky and C. L. Yuan, *Carbohydr. Res.*, 1973, **31**, 339–346.
4 D. Hauck, V. R. Jumde, C. J. Crawford and A. Titz, in *Carbohydrate Chemistry*, CRC Press, 2021, pp. 17–22.
5 R. Sommer, T. E. Exner and A. Titz, *PLoS ONE*, 2014, **9**, e112822.
6 R. Sommer, K. Rox, S. Wagner, D. Hauck, S. S. Henrikus, S. Newsad, T. Arnold, T. Ryckmans, M. Brönstrup, A. Imberty, A. Varrot, R. W. Hartmann and A. Titz, *J. Med. Chem.*, 2019, **62**, 9201–9216.

Overarching conclusion and outlook

In this study, the potential of ligands targeting *P. aeruginosa* lectins LecA and LecB to serve both as targeting moieties for drug delivery and as small-molecule therapeutics was investigated.

The first dual-function inhibitors targeting *P. aeruginosa* virulence factors LecA and LasB were discovered, demonstrating significantly enhanced potency with binding affinities of 220 nM for LasB and 18 μM for LecA, outperforming previously reported single-target inhibitors. The in situ formation of divalent disulfides led to a 200-fold improvement in LecA inhibition reaching KDs <8 nM measured via SPR. Structural studies confirmed the binding mechanism of the dual inhibitor **11** with LasB, while biological evaluations demonstrated strong selectivity, with no off-target effects on six human MMPs and no observed cytotoxicity. Moreover, dual inhibitor **12** effectively reduced the cytotoxic effects of *P. aeruginosa* supernatant on A549 cells and inhibited LecA-mediated adhesion, outperforming individual LecA or LasB inhibitors and their combinations.

As a next step, the molecular structures of LasB/LecA inhibitors can be further optimized to enhance their therapeutic potency, including improved pharmacokinetic and pharmacodynamic properties, based on in vivo studies. For the further development of dual inhibitors, their impact on biofilm growth in vitro, as well as their ability to completely eradicate bacteria when combined with antibiotic treatment, should be thoroughly investigated.

Another part of this study was focused on the functionalization of the liposome surface with LecA- and LecB-specific ligands, enabling highly specific interactions between the nanocarriers and their corresponding lectins. The lectin ligands, represented by glycomimetics whose structures were previously optimized for binding to LecA and LecB, were conjugated with phospholipids, and the resulting glycolipids were incorporated in liposome formulations. Although these ligands possess limited binding efficiency towards their targets and arrangement of the lectin ligands on the surface of the particle in a multivalent fashion allowed to drastically improve their binding. Additionally, a microfluidic platform was established for microscopic analysis of targeted fluorescent liposomes to evaluate their targeting efficiency and potential for imaging applications. Characterization of the obtained liposomes using various biophysical techniques confirmed the high affinity and specificity of the interactions between the glycofunctionalized nanoparticles and the lectins.

To assess the ability of glycosylated liposomes to encapsulate drug molecules, three antibiotics from different classes—ciprofloxacin, tobramycin, and colistin—as well as the

LecB ligand DH181a and the PqsR inhibitor HIPS2050 were loaded into the nanocarriers. The resulting formulations were analyzed for their physicochemical properties, encapsulation efficiency, and drug release profiles. The data showed that, under the tested conditions, colistin exhibited the lowest release rate among the three antibiotics, making it the most suitable candidate for further in vitro studies. Glycosylation of the liposomes had no significant impact on drug release profiles or encapsulation efficiency, allowing for the further application of glyco-targeted formulations in drug delivery.

Future research will focus on the application of both dual inhibitors and targeted liposomes to combat antimicrobial resistance via interaction with biofilm-associated LecA and LecB and providing site-specific infection treatment. For targeted liposomes, the developed delivery system should first be investigated in vitro in a biofilm model under flow conditions to optimize several parameters, such as the overall carbohydrate ligand density on the liposome surface, the molar ratio between LecA- and LecB-targeting ligands, and the concentration of the liposomal antibiotic required for effective biofilm elimination. Additionally, the implementation of a PEG spacer between the lipid anchor (e.g., DSPE) and the lectin ligand should be evaluated in this in vitro setup to determine the impact of PEGylation on both targeting efficiency and liposome–biofilm interactions. In this context, both the PEG chain length and polymer density can be systematically assessed. Moreover, the incorporation of a stealth lipid can be explored independently, providing the opportunity to fine-tune the PEG content and carbohydrate moiety separately. Another important parameter to investigate in vitro is the combination of the antibiotic with a pathoblocker at various ratios, co-encapsulated in targeted liposomes, to maximize therapeutic efficacy against *P. aeruginosa* infections. Following in vitro optimization of the formulation, the next step is to conduct in vivo studies to assess nanoparticle potency and biodistribution and further optimize of the lipid composition if needed. For example, modification of the lipid anchor in the glycolipid molecule or of the stealth lipid, if used, can significantly influence the rate of lipid shedding from the liposome, thereby affecting nanoparticle circulation time and tissue distribution. Additionally, the ζ-potential of the liposomes may also impact biodistribution and can potentially be modulated by adjusting the lipid composition.

Overall, evaluating both dual inhibitors and targeted LNPs in advanced in vitro and in vivo models will guide further development by enabling structural and compositional optimization of LecA- and LecB-specific therapies for clinical translation.